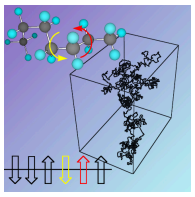

A concise

Introduction to Polymer Physics

- Theoretical Concepts and Applications

Reinhard Hentschke*

This text is intended for students, predominantly in physics and with a one-semester background in statistical mechanics, who are about to start their bachelor thesis project or who are past this stage already. These students may be interested in polymer physics, because they pursue research projects overlapping with this area of science or because they want to broaden their knowledge in condensed matter physics in general. If they have followed the regular physics curriculum up to this point, it is unlikely that they had much exposure to polymer physics. Hence they may be interested in an overview, without becoming overwhelmed, providing a basis from which to explore more detailed or advanced textbooks, research papers, and talks.

1 Introductory Remarks

Why should you be interested in polymer physics? One reason is that polymer materials are ubiquitous and have countless applications. Hence, a significant amount of research and development goes into polymer related products, which in turn means that there are well paid jobs and not only for chemists! Many physics student don't know this, because they believe that polymers are an exclusive domain for chemists. Another reason why polymer physics is interesting is that problems in polymer physics require a broad background in physics, including both classical and quantum physics. There are virtually countless intellectually challenging questions and answering them never gets boring. Polymer physics overlaps with the physics of liquids, colloids and with the physics of surfaces and interfaces. Note that polymer materials are complex and may contain many components which are not polymers - like nanoparticles. There is of course overlap with chemistry in general and physical chemistry in particular. Can one make big discoveries in polymer physics? Most physics students, at least initially, have this dream. Well, Nobel prizes have been awarded for work in polymer science. However, since there is not just ´one big mystery´ (like what is Dark Matter), progress and discoveries are achieved in smaller increments. But this usually means that earnest intelligent work will be rewarded with success and recognition - which cannot be said about the work on ´big questions´.

Virtually all the material compiled in these notes was worked out long ago and thus can be found in numerous textbooks. However, all textbooks, and these notes are no exception, present a subset of the 'total polymer knowledge'. Sometimes the subset is larger and sometimes it is more focussed ('less' sometimes is indeed 'more'!). But always there is a certain bias due to the author's feel at the time of writing of what a student should know. A serious difficulty when teaching polymer physics are the many variables, e.g. polymer type and mass, environments like melts, solvents (good, bad, θ-), gels, networks, etc., temperature, frequency and so on and so forth. This gives rise to a host of results for numerous combinations of system parameters, mostly power laws, which can be very confusing for the beginner since no Ariadne thread appears to exist in this maze. Clearly, the challenge is to avoid this confusion without omitting too much important information.

The current standard textbook on polymer physics is M. Rubinstein and R. H. Colby *Polymer Physics*, Oxford University Press. This book focusses on the theoretical concepts, which does not mean that there are no experimental results to which the theory is compared. The opposite is true. However, these well defined experiments are designed specifically to test abstract theory. In practice, polymer materials are designed for complex applications requiring likewise complex materials. This in turn means that experimental measurements are less 'clear' and usually less 'clean'. Understanding an application polymer material on the molecular level is a very demanding task! It is therefore interesting to contrast Rubinstein and Colby with another book written by an application scientist. C. Wrana's *Introduction to Polymer Physics*, Lanxess Company (unfortunately, the english version is not widely available; there is also a similar, somewhat older text, by U. Eisele) focusses on the practical side - albeit for elastomers. Elastomers, the polymer ingredients of rubber materials, are arguably the 'most physical' of all polymers. Wrana concentrates on the viscoelastic properties of elastomer materials

* *School of Mathematics and Natural Sciences, Bergische Universität Wuppertal, e-mail: hentschk@uni-wuppertal.de*
https://constanze.materials.uni-wuppertal.de/fileadmin/physik/theochemphysik/Skripten/rsc-polymerphysics.pdf

and their nonlinear deformation behavior from the point of view of someone working in the elastomer industry. He also includes a discussion of nano-fillers and their effects on the mechanics of elastomers. These notes are an attempt to cover and combine key sections in both texts - nevertheless, bits and pieces from many other literature sources are included as well (and referenced throughout the notes). Here I briefly want to mention a mere few. Two older general textbooks on polymer physics are G. Strobl *The Physics of Polymers*, Springer and R. J. Young and P. A. Lovell *Introduction to Polymers*. Strobl discusses in particular many of the basic key measurements. The book by Young and Lovell is less mathematical and focusses more on synthesis and polymer characterization as well as on the description of numerous standard techniques used for characterization. And then there is one book that every person seriously working in polymer physics had and probably still has in reach - P.-G. de Gennes *Scaling Concepts in Polymer Physics*, Cornell University Press. The book was first published in 1979, but its elegant style and timeless ingenuity makes it a valuable source of insight even to this day. However, I do not recommend it for beginners. Pretty much the same comment, minus the elegance perhaps, applies to M. Doi and S. F. Edwards *The Theory of Polymer Dynamics*, Oxford Science Publications. However, this book contains most, if not all, the details, which makes it very valuable to the advanced student of the subject. There is a less formidable text by M. Doi alone (*Introduction to Polymer Physics*, Oxford Science Publications), which, even though it still is not a text for beginners, is much easier to read. Written at about the same time as Doi's book, *Statistical Physics of Macromolecules* by A. Y. Grossberg and A. R. Khokhlov also is not a beginner's text. Again, it is of interest for polymer students at a more advanced stage (e.g., its extensive discussion of phase transitions in polymer systems). Finally, going still back in time to the 1950s and 1960s, there are the books by Paul Flory *Principles of Polymer Chemistry* and *Statistical Mechanics of Chain Molecules*. Reading these notes you will recognise his wide ranging impact on the field. Like the previous books, I do not recommend them for beginners. But Flory explains many important aspects of theoretical approaches in polymer physical chemistry, which the subsequent literature does not explain with the same amount of detail and insight. You may want to keep this in mind and when you seem to be missing a piece of information, hampering your understanding of a problem in polymer physical chemistry, you should consult Flory's books. Both Flory (1974) and de Gennes (1991), by the way, have received Nobel prizes (Flory in Chemistry and de Gennes in Physics) for their work on the physical properties of polymers.

The computer simulation of polymers has made and will continue to contribute important insights. However, it is very difficult to develop this aspect of polymer research in notes like these including a sensible amount of detail. Therefore no such attempt has been made. Nevertheless, I want to mention some references. *Computer Simulation of Liquids* by M. P. Allen and D. J. Tildesley (Oxford University Press: Oxford (1990)), in my opinion, still ranks among the best books on the subject of computer simulation for beginners. If somebody wants to try out some basic simulations fast, then I can offer my *Computer Simulation Laboratory* (https://constanze.materials.uni-wuppertal.de/fileadmin/physik/theochemphysik/Skripten/SimTutorial.pdf). Specifically for polymer simulations one can find a number of texts. One example is *Simulation Methods for Polymers* edited by M. Kotelyanskii and D. N. Theodorou (Marcel Dekker: New York (2004)). The advanced reader will benefit from *Monte Carlo Simulations in Statistical Physics* by D. P. Landau & K. Binder (Cambridge University Press:Cambridge (2000)). Especially the second author and his group have made numerous important contributions to the simulation of polymers, which is reflected in the book.

A number of colleagues and students have supported my efforts to present this material in useful fashion - either by providing general encouragement or by improving specific points or by correcting my mistakes. These people, to whom I am very grateful, are Nils Hojdis, Frack Fleck, Michael Karbach, Jan Weilert, Lena Tarrach, ...

Contents

2 Polymers - Microstructure, Classification, and Mass

2.1 Polymer Microstructure and Classification

The simplest type of polymer is a linear covalent chain containing one type of monomer i.e. -A-A-A-A-A-A-A-A-. This is a **homopolymer**. A few example are compiled in Tab. 1. Not obvious from -A-A-A-A-A-A-A-A- is that there are possible differences between this -A-A-A-A-A-A-A-A- and another -A-A-A-A-A-A-A-A- due to stereoisomerism or structural isomerism. The former is depicted in Fig.1. An example of structural isomerism is shown in Fig. 2. Since rotation around the double bond is not possible polyisoprene, for instance, can locally exist as *cis* or *trans*. How much *cis* or *trans* there is depends on how the polymer was polymerized. Naturally produced PI from rubber trees (hevea brasiliensis) is almost completely cis-1,4-polyisoprene. Even though these stereoisomers or structural isomers do not 'look' very different, there physical properties are usually quite distinct. For instance, isotactic homopolymers show the tendency to form helical structures, whereas their atactic variants do not. Another example is cis-1,4-polyisoprene, which is used in large quantities in automobile and particularly in truck tires, whereas trans-1,4-polyisoprene (gutta-percha) has a strong tendency to crystallize and today only has a few specialized uses.

Table 1 A few common homopolymers

monomers	polymer	comments
Ethylene $CH_2 = CH_2$	Polyethylene (PE) -[CH_2- CH_2]$_n$-	moulded objects, tubing, films, insulation
Propylene $CH_2 = C(CH_3)H$	Polypropylene (PP) -[CH_2- $C(CH_3)H$]$_n$-	similar uses to PE
Styrene $CH_2 = C(C_6H_5)H$	Polystyrene (PS) -[CH_2- $C(C_6H_5)H$]$_n$-	cheap moulded objects
Vinyl chloride $CH_2 = C(Cl)H$	Poly(vinyl chloride) (PVC) -[CH_2- $C(Cl)H_2$]$_n$-	pipes, hoses, sheathing on electrical cables
Isoprene $CH_2 = C(CH_3)$-CH=CH_2	cis-1,4-polyisoprene (PI) -[CH_2 - $C(CH_3)$=CH-CH_2]$_n$-	tires, latex products sheathing on electrical cables

The combination of several different monomers, as shown in Fig. 3, yields so called **heteropolymers**. If the heteropolymer contains two monomer types it is called a **copolymer**. Copolymers can be alternating, random, block or graft. Polymers containing two blocks are called diblock copolymers; with three blocks they become triblock copolymers and then multiblock copolymers. Polymers containing three types of monomers are called **terpolymers**. An example of a biopolymer with four different types of monomers (nucleotides) is DNA.

Another distinguishing feature is the polymer architecture. Fig. 4 shows sketches of (a) linear, (b) ring, (c) star-branched, (d) H-branched, (c) comb, (d) ladder, (g) dendrimer and (h) randomly branched polymer architectures. In this text our sole focus is case (a), linear polymers.

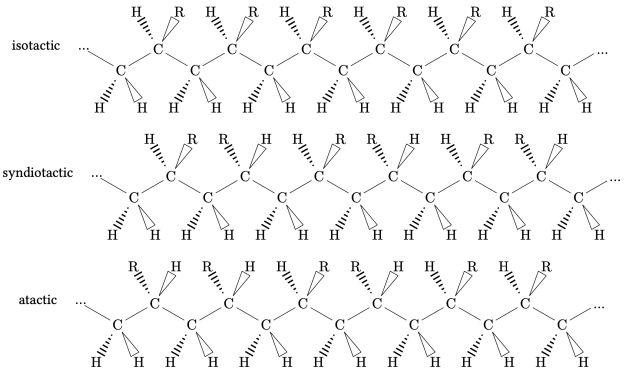

Fig. 1 Tacticities of vinyl polymers. The carbon atoms are in the same plane, whereas the hydrogens and the R-moieties lie below or above, respectively.

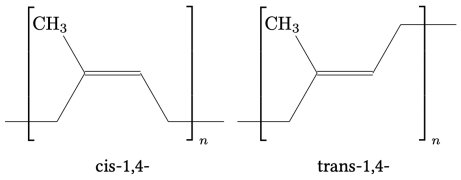

Fig. 2 Two structural isomers of polyisoprene.

Commonly technical polymers are classified into three groups as depicted in Fig. 5:

Thermoplastics are linear or branched polymers which can melt when heated. They can be moulded and remoulded using processing techniques like injection moulding and extrusion. They constitute the largest fraction of industrial polymers. Many thermoplastics are amorphous and are incapable of crystallization. Amorphous polymers are characterized by their **glass transition temperature** T_g, the temperature at which they transform from a hard or glassy state to a soft or rubbery state.

If the polymers crystallize this occurs between the glass transition, T_g and the melting temperature T_m. In this temperature range, there is sufficient molecular movement for crystalline domains to form. This process can take place during heating or during cooling from the melt. The main characteristics of crystalline polymers is that are normally semi-crstalline. The size, shape and percentage of crystals depend on the heating and cooling of the material. The change from the amorphous-liquid state of the melt to the crystalline state is a kinetically controlled process and depends primarily on nucleation. This is why the crystallization temperature T_c is always below the thermodynamically controlled melting temperature (for a detailed discussion see chapter 4 of R. J. Young, P. A. Lovell *Introduction to Polymers* (1991)).

Elastomers are polymer whose response to large deformations is mostly elastic over a wide range of temperatures. This range

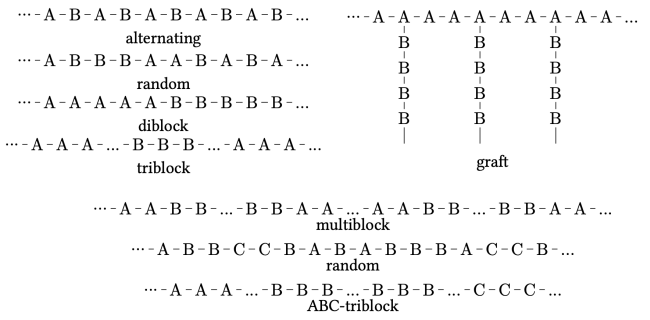

Fig. 3 Different types of polymers. Figure adopted from Rubinstein and Colby.

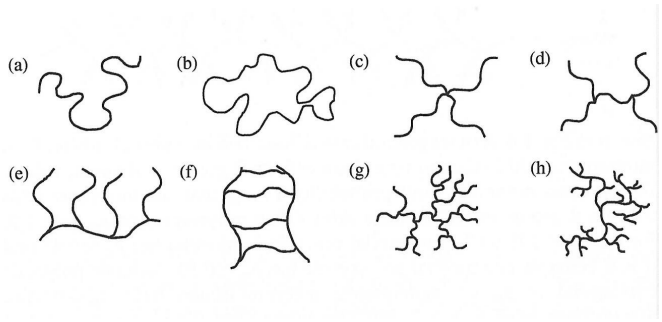

Fig. 4 Examples of polymer architectures ((a) linear, (b) ring, (c) star-branched, (d) H-branched, (c) comb, (d) ladder, (g) dendrimer and (h) randomly branched). Figure 1.5 from Rubinstein and Colby.

is bracketed by T_g on the low side and the thermal degradation on the high side. Elastic response to deformations is greatly enhanced by cross-linking of the polymers, which largely prevents them from 'flowing' in response to the deformation. Such materials are commonly known as rubbers.

Since we just mentioned 'cross-linking'. What is a **cross-link**? A **chemical cross-link** consists of a certain number -usually in the single digits- of covalent bonds joining two polymer chains or, since polymers are flexible and long, form a link within one and the same polymer chain. A famous example is the formation of sulfur (atom) bridges in a reaction called **vulcanisation**. The second type of cross-link is the **physical cross-link**. Polymers are mostly like 'entangled ropes'. These entanglements are hairpin-style curves of one polymer around another or one polymer section around another section of the same polymer. The density and the nature of the cross-links is one of the most important parameters determining the physical behavior of polymer systems.

Thermosets normally are rigid materials and are highly cross-linked polymers. Like elastomers they are intractable once formed and degrade rather than melt when heated.

This classification schema is not absolute and possess a certain degree of overlap between the three groups.

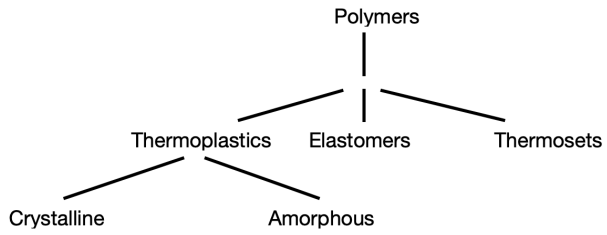

Fig. 5 Polymer classification.

When we look at polymers from the perspective of statistical thermodynamics, they possess one particular feature - conformation entropy, distinguishing them from simple liquids or solids. A chain of monomers, even a short one between cross-links or other branch or terminal points, can have many different shapes. The number of possible shapes or 'paths' give rise to the conformation entropy of the chain. This entropy wants to be a large as possible. A constraint imposed on the number of possible chain conformations reduces the conformation entropy and produces forces acting along the entire chain and beyond. This long range effect in conjunction with liquid-like interactions produces unique structural and dynamic material properties.

2.2 Molecular Mass Distribution

When discussing the polymer microstructure we had stated that two chemically identical polymers can still be very different when they are isomers. Another distinguishing parameter is mass. Nature can make biopolymers with a specific mass. Technical polymers, however, are more or less **polydisperse**, i.e. they possess a certain mass distribution. The **number-average molar mass** $\bar{M}_n$ is defined via

$$\bar{M}_n = \sum_i x_i M_i \, . \tag{1}$$

The index i indicates the fraction of polymers in the sample containing N_i molecules of molar mass M_i. The quantity x_i is the mole fraction of these polymers, i.e.

$$x_i = N_i / \sum_j N_j \, . \tag{2}$$

A related quantity is the **weight-average molar mass** $\bar{M}_w$ defined via

$$\bar{M}_w = \sum_i w_i M_i \, , \tag{3}$$

where

$$w_i = N_i M_i / \sum_j N_j M_j \, . \tag{4}$$

There are still other average masses - but just $\bar{M}_n$ and $\bar{M}_w$ alone may be confusing. What is the difference between them?

Note that x_i is the probability to pick any polymer from group i at random, whereas w_i is the probability to pick any monomer from within any polymer in this group. These probabilities can be very different. Imagine 3 identical light and one heavy polymer all made of the same type monomer. If $i = 1$ stands for the light polymer then $x_1 = 3/4$. If we now cut the light polymers in half and add the monomers which we have cut off to the heavy polymer - what changes? Well, x_1 is still 3/4, but w_1 is only half of what it was before (Note: Even though x_i does not change, $\bar{M}_n$ changes during this 'experiment'.). The only time $x_i = w_i$ is when there is only one group or one term in $\sum_i$, i.e. all polymers possess the same mass, i.e. they are **monodisperse**. In this case $\bar{M}_w/\bar{M}_n = 1.0$. Hence, we introduce x_i and w_i as a means to determine polydispersity. We can see this more clearly via the following equation

$$\bar{M}_w = \bar{M}_n + \frac{\delta\bar{M^2}_n}{\bar{M}_n} \,. \tag{5}$$

Here $\delta\bar{M^2}_n = \bar{M^2}_n - (\bar{M}_n)^2$ is the variance of the mass computed with the distribution (2) (the derivation is left to the reader as an exerecise). Typically $\bar{M}_w/\bar{M}_n$ is in the range 1.5-2.0. But how do we measure these different molar masses?

The osmotic pressure Π of polymers in solution in the limit of vanishing polymer concentration c (usually in g/volume) is given by van't Hoff's law:

$$\frac{\Pi}{c} = \frac{RT}{\bar{M}_n} \,. \tag{6}$$

A formula for Π in polymer solutions will be discussed in chapter 4. However, we can already see that Π involves $\bar{M}_n$ rather than $\bar{M}_w$. Had we performed the above 'thought experiment', which does not alter the number of polymers, in the polymer solution, it would not have altered Π, since the osmotic pressure in van't Hoff's law depends only on the polymer concentration and not on the distribution of monomers across the polymer population. Figure 6 shows the concentration dependence of the osmotic pressure of poly(α-methyl styrene) for different molecular weights in toluene. Based on the figure estimate $\bar{M}_n$ for the three upmost curves. Note that the unit of osmotic pressure in this case is g cm^{-2}. Compare your numbers to the numbers in table 1 of I. Noda et al. *Thermodynamic Properties of Moderately Concentrated Solutions of Linear Polymers* Macromolecules *16*, 668 (1981).

And how do we measure $\bar{M}_w$? One good method is static light scattering. Why is this? Let us assume that unpolarized light, possessing the wavelength λ, interacts with an isolated isotropically polarizable molecule. Within the molecule a dipole moment $\vec{p} = \alpha\vec{E}(\omega)$ is induced by the local $\vec{E}$-field. Here α is the isotropic polarizability of the molecules, $\omega = 2\pi c/\lambda$, and c is the speed of light. Remember now the discussion of dipole radiation from your E&M-lecture. The pointing vector $\vec{S}$, measuring electromagnetic energy per area and time in a certain direction, which essentially is our scattered intensity, is given by

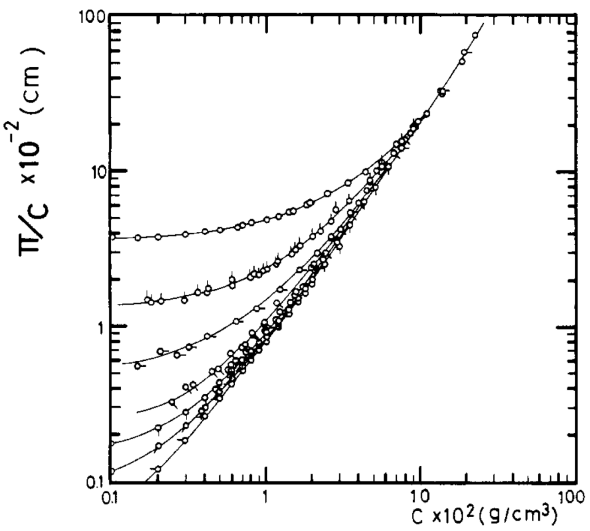

Fig. 6 Concentration dependence of the osmotic pressure of poly(α-methyl styrene) for different molecular weights in toluene at $T = 25^o$C from I. Noda, N. Kato, T. Kitano, M. Nagasawa *Thermodynamic Properties of Moderately Concentrated Solutions of Linear Polymers.* Macromolecules *16*, 668 (1981).

$$\vec{S} = \frac{1}{4\pi r^2 c^3}(\ddot{\vec{p}} \times \vec{n})^2\vec{n} \tag{7}$$

in the case of dipole radiation. Here r is the distance between the dipole and the detector and $\vec{n}$ is a unit vector in the direction from the dipole to the detector. The double dot indicates time derivatives. We also remember that the magnitude of the Pointing vector (at the position of the molecule) is $S_{in} = cE^2/(4\pi)$. Now we can write down the **Rayleigh ratio** R_θ, which is the scattered intensity times r^2 divided by the incident intensity, i.e.

$$R_\theta = \frac{16\pi^4}{\lambda^4}\alpha^2\rho P(\theta) \,, \tag{8}$$

where

$$P(\theta) = \langle(\vec{e}_p \times \vec{n})^2\rangle_{\vec{e}_p} \,. \tag{9}$$

The quantity $\vec{e}_p$ is a unit vector in $\vec{p}$-direction. In addition, $\langle\ldots\rangle_{\vec{e}_p}$ is an orientation average of the dipole vector and we have used $\ddot{E} = \omega^2 E$. The factor ρ is an average number density of isolated molecules, which we insert here since we want to collect intensity from $\langle N\rangle$ molecules per volume V, i.e. $\rho = \langle N\rangle/V$. Here $\langle\ldots\rangle$ is a thermodynamic average of the (in principle) fluctuating number of molecules.

If we define the direction of the incident light as our z-direction, then $\vec{e}_p = (\cos\varphi, \sin\varphi, 0)$, i.e. $\vec{e}_p$ is in the xy-plane. Note that the components of the $\vec{E}$-field, and therefore the components of the induced dipole, are perpendicular to the direction in which the light travels. In the same coordinate system $\vec{n} = (\cos\phi\sin\theta, \sin\phi\sin\theta, \cos\theta)$. With this we find

$$P(\theta) = (\cos^2\theta + 1)/2\,. \tag{10}$$

However, we are not so much interested in isolated molecules. Instead we are interested in a dilute solution of our polymers in a solvent. If ε_o is the dielectric constant of the pure solvent and ε_1 is the dielectric constant of the solution we have $(\varepsilon_o - 1)/(4\pi)\vec{E} = \vec{P}_o$ and $(\varepsilon_1 - 1)/(4\pi)\vec{E} = \vec{P}_1$, where $\vec{E}$ is the average electric field and the polarization $\vec{P}$ is the local dipole moment per unit volume. Subtracting the two equations yields $(4\pi)^{-1}(\varepsilon_1 - \varepsilon_o)\,\vec{E} = \Delta\vec{P}$. Note that $V\Delta\vec{P}$ replaces or previous $\vec{p}$ when the molecules were isolated (cf. Debye's 1947 cited below!). We now write

$$\frac{\varepsilon_1 - \varepsilon_o}{4\pi} = \frac{n_1^2 - n_o^2}{4\pi} \approx \frac{1}{4\pi} 2 n_o \frac{dn}{dc_w}\Big|_o c_w\,. \tag{11}$$

The quantities n_1 and n_o are the refractive indices of the solution and the solvent, respectively. Note that we expand $n_1 (c_w)^2$, where c_w is the solute weight concentration, in terms of c_w around n_o. With this the Rayleigh ratio becomes

$$R_\theta = \left(\frac{2\pi}{\lambda}\right)^4 \frac{1}{(4\pi)^2}\frac{1}{V}\left(2 n_o \frac{dn}{dc_w}\Big|_o\right)^2 c_w^2 V^2 P(\theta)\,. \tag{12}$$

Aside from the above replacement of the molecular dipole moment $\vec{p}$ by $V\Delta P$ we have also replaced ρ by $1/V$. The average number of molecules $\langle N\rangle$ now becomes the average number of polymers in the system $\langle \nu_1\rangle$ and, as we shall see, $\langle \nu_1\rangle$ is contributed by a new version of $P(\theta)$.

The overall solute mass density c_w can be rewritten in terms of an integral over the local solute mass densities $c_w(\vec{r})$ throughout the system, i.e.

$$c_w = \frac{1}{V}\int_V d^3 r\, c_w(\vec{r})\,. \tag{13}$$

Thus far $P(\theta)$ only accounts for radiation without interference of radiation from the different volume elements of the system. This means we need another substitution, i.e.

$$c_w^2 P(\theta) \to \langle c_w\rangle^2 P_i(\theta) \equiv \frac{\langle c_w\rangle^2}{V^2}\int_V d^3 r\, d^3 r'\, e^{i\vec{q}\cdot(\vec{r}-\vec{r}')}\,\frac{\langle c_w(\vec{r}) c_w(\vec{r}')\rangle}{\langle c_w\rangle^2}\,. \tag{14}$$

Here $\vec{q} = \vec{k}_{out} - \vec{k}_{in}$ is the momentum transfer from the incoming wave vector $\vec{k}_{in}$ to the scattered one $\vec{k}_{out}$, i.e. we keep the phases of $\vec{E}_{in}(\vec{r})$ and $\vec{E}_{out}(\vec{r})$ and let them interfere. The above corresponds to the 1^{st} Born approximation in quantum scattering theory. Note that we collect scattering intensity from many thermodynamically identical copies of our system of interest. Hence our final R_θ is a thermal average over such systems, i.e.

$$R_\theta = K\langle c_w\rangle M P_i(\theta)\langle \nu_1\rangle\,, \tag{15}$$

where M is the polymer mass, i.e. $\langle c_w\rangle = M\langle\nu_1\rangle/V$, and

$$K = \frac{4\pi^2 n_o^2}{\lambda^4}\left(\frac{dn}{dc_w}\Big|_o\right)^2\,. \tag{16}$$

These expressions for R_θ and K go back to work by Einstein (*Theorie der Opalenszenz homogener Flüssigkeitsgemischen in der Nähe des kritischen Zustandes* Annalen der Physik *33* 1275 (1910)) and Debye (*Molecular weight determination by light scattering* J. Phys. Chem. *51* 18 (1947)). The derivation of K is not trivial -the above is a mere sketch!- and initially there was even controversy regarding the exact form of the factor $n_o^2\left(\frac{dn}{dc_w}\big|_o\right)^2$ (see P. M. Doty, B. H. Zimm, H. Mark *An investigation of the determination of molecular weights of high polymers by light scattering* J. Chem. Phys. *13*, 159 (1945); first column on page 160).

Thus far we have considered monodisperse molecules. What happens if the molecules are polydisperse? In this case $c_w M$ is replaced by $\sum_i c_{w,i} M_i$, i.e.

$$c_w M \to \sum_i c_{w,i} M_i = \frac{\sum_i c_{w,i} M_i}{\sum c_{w,i}} c_w = \bar{M}_w c_w\,, \tag{17}$$

where $c_i = N_i M_i/V$ and $c_w = \sum_i c_{w,i}$. Hence,

$$R_\theta = K\langle c_w\rangle \bar{M}_w P_i(\theta)\langle \nu_1\rangle\,, \tag{18}$$

relates the light scattering intensity to the weight-average (molar) mass (note that there is no mass dependence left in $P_i(\theta)$). We shall come back to scattering and to Eq. (18) in chapter 2. In particular we shall discuss the evaluation of $P_i(\theta)$ in detail.

Of course there are other techniques for measuring molar masses as well, which we must bypass at this point. A overview is the paper by S. E. Harding et al. *Molecular weight determination of polysaccharides.* Advances in Carbohydrate Analysis *1*, 63 (1991). Another nice review covering light scattering is P. J. Wyatt *Light scattering and the absolute characterization of macromolecules.* Analytica Chimica Acta *272*, 1 (1993). Remark: If you want information regarding a particular technique, e.g. light scattering, it is often a good idea to check out the webpages of the companies selling this particular experimental equipment. Typically you can find 'technical glossaries', learning pages', etc. containing very good, albeit simplified, explanations of the method and the underlying theory.

We shall also skip over the shape of the mass distribution since it depends on the polymerization mechanism - a topic we do not cover here.

3 Equilibrium Conformation of Single Chains

3.1 Flexibility Mechanism and Polymer Dimension

A quantity used to characterise the linear dimension of a polymer chain is its **end-to-end vector** $\vec{R}$, which is the sum over monomer end-to-end vectors $\vec{b}$ (cf. Fig. 7). The monomer end-to-end vector may itself be a sum over a number of shorter vectors within the flexible monomer as shown in the example in Fig. 8. Having

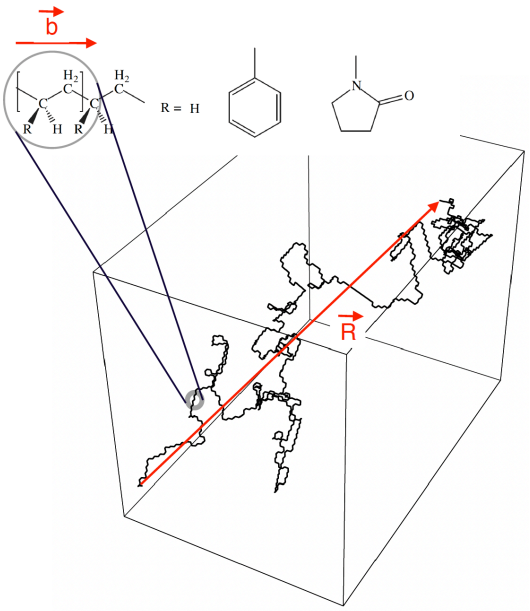

Fig. 7 Examples (cartoon!) of a linear homopolymer chain based on the monomer unit -CH_2-CHR, where R stands for different moities (three examples are shown: polyethylene, polystyrene and polyvinylpyrrolidone). Note that $\vec{R}$ (not to be confused with the previous letter R) is the end-to-end vector, which itself is a sum over monomer vectors $\vec{b}$.

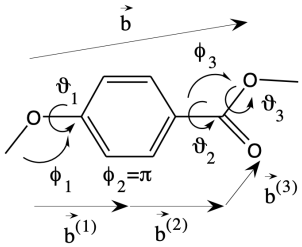

Fig. 8 Monomer unit of p-PHB (poly(4-hydroxybenzoic acid)). The ϕ_i are valence angles, whereas the ϑ_i are torsion angles.

said this we want to concentrate on the simplest case, i.e. in the following the mathematical realization of a polymer chain is merely a sum over bond vectors $\vec{b}_i$ of constant magnitude b as depicted in Fig. 9

But what do we mean by 'flexibility' in this context? Fig. 10 shows four covalently bonded atoms i, j, k, and l. The bond lengths are pretty much constant and so are the valence angles, i.e. the angles between the bonds ij and jk or jk and kl. But when the bond jk is a single bond, then the angle ϑ, which is called torsion angle, is variable. A polymer contains a large number of these torsion angles, which allow the polymer chain to assume many different conformations. Loosely speaking flexibility is a measure for the decrease of orientation correlation of two vectors $\vec{b}_i$ and $\vec{b}_{i+s}$ along a polymer chain as function of their separation s. In other words, rotational freedom of the torsion angles diminishes orientational correlation between $\vec{b}$-vectors and thus increases chain flexibility.

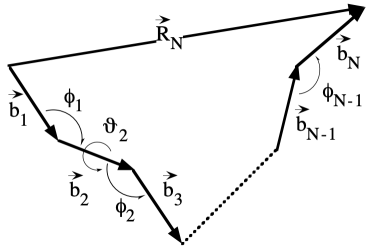

Fig. 9 Cartoon of a linear polymer consisting of N units.

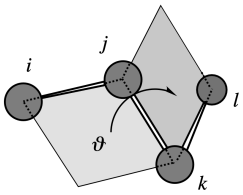

Fig. 10 Definition of a torsion angle via four successive atoms.

Under these conditions, i.e. fixed bond lengths and fixed valence angles while the torsion angles can freely vary, what is the largest end-to-end distance R_{max}? Let's look at Fig. 9 and assume that all bond lengths b_i and valence angles ϕ_i are constant, i.e. $b_i = b$ and $\phi_i = \phi \ \forall$ i. If we flatten our polymer onto a planar surface, we obtain the largest end-to-end distance for a straight zig-zag line. The projection of each bond onto the direction defined by this zig-zag line is $b\cos((\pi-\phi)/2)$ and the overall length of the zig-zag line therefore is

$$R_{max} = b\cos((\pi-\phi)/2)N = b\sin(\phi/2)N\,. \qquad (19)$$

This length, i.e. the maximum magnitude of the end-to-end vector, is also called the **contour length** L of the polymer, i.e. $L = R_{max}$.

In these notes contour length is defined dependent on the type of flexibility mechanism. In the present case this means that measuring contour length along the bonds of the polymer backbone yields a greater length, i.e. bN.

While a polymer only has one contour length, it can assume many different conformations and consequently the magnitude (and direction) of its end-to-end vector varies. Therefore we focus on statistical averages of the powers of $\vec{R}$. Obviously

$$\langle\vec{R}\rangle = 0\,, \qquad (20)$$

i.e. this average does not tell us much. However, $\langle\vec{R}^2\rangle \neq 0$ and since $\sqrt{\langle\vec{R}^2\rangle}$ possess the unit of length we are going to use it as measure for the linear dimension of a polymer in space.

So let's study the end-to-end vector depicted in Fig. 9 in more detail, i.e.

$$\vec{R}_N = \sum_{i=1}^{N} \vec{b}_i = b \sum_{i=1}^{N} \vec{e}_i \, . \tag{21}$$

Note that the $\vec{e}_i$ are unit vectors. The quantity we are most interested in is the average of the square of $\vec{R}_N$. It essentially describes the spatial extension of a polymer chain. Hence

$$\langle \vec{R}_N^2 \rangle = b^2 \sum_{i=1}^{N} \sum_{j=1}^{N} \langle \vec{e}_i \cdot \vec{e}_j \rangle = b^2 \Big(1 + \frac{2}{N} \sum_{i>j}^{N} \langle \vec{e}_i \cdot \vec{e}_j \rangle \Big) N \, . \tag{22}$$

The correlation function $\langle \vec{e}_i \cdot \vec{e}_j \rangle$ is quite difficult to calculate in general. It depends not only on $i-j$ but on i and j explicitly, since the middle of a polymer is different from its ends.

Let's therefore consider two simple approximations. The first one is $\langle \vec{e}_i \cdot \vec{e}_j \rangle = 0$ $(i \neq j)$, i.e. the orientation of $\vec{e}_i$ does not influence $\vec{e}_j$ in the slightest. This defines a **freely jointed chain**. In this case

$$\langle \vec{R}_N^2 \rangle = b^2 N \, . \tag{23}$$

This result has the familiar form of the **Einstein law of diffusion**

$$\langle \vec{R}(t)^2 \rangle = 6Dt \, . \tag{24}$$

Here $\vec{R}(t)$ is the vector connecting the starting and the end point of a random walk in three dimensions (3D) measured at time t after the walker has started and D is the (long time) diffusion coefficient. Note that the time t is the equivalent of N. In other words, a polymer chain is just a random walk.

The second approximation is the straight zig-zag chain which we used to calculate R_{max}. Here $\langle \vec{e}_i \cdot \vec{e}_j \rangle = 1$ if $i-j$ is even and $\langle \vec{e}_i \cdot \vec{e}_j \rangle = \cos(\pi - \phi)$ if $i-j$ is odd. Hence $\sum_{i>j}^{N} \langle \vec{e}_i \cdot \vec{e}_j \rangle = N(N-1)/2 \cdot (1-\cos\phi)/2$ and thus

$$\langle \vec{R}_N^2 \rangle = b^2 \sin^2(\phi/2) N^2 \, , \tag{25}$$

where we assume that N is large. Note that (25) is consistent with (19).

A generalization of Eq. (23) is

$$\langle \vec{R}_N^2 \rangle = C_N b^2 N^{2\nu} \, . \tag{26}$$

In Eq. (23) the coefficient C_N equals 1 and the exponent ν equals 1/2. This value of ν characterizes an **ideal chain**. When we do not make the above approximation $\langle \vec{e}_i \cdot \vec{e}_j \rangle = 0$ the coefficient C_N will be larger than one, because non-vanishing correlations make the chain locally stiffer and therefore the volume of the 'coil', i.e. $\langle \vec{R}_N^2 \rangle^{3/2}$, larger. In this context C_N is called **characteristic ratio** - even though in most cases this refers to the limit $N \to \infty$. However, since N does not have to be larger than $O(10)$ in order for C_N to be close to C_∞ this is not important for most practical purposes. Whether or not the exponent ν also changes depends on the range of the correlation function $\langle \vec{e}_i \cdot \vec{e}_j \rangle$. We shall return to this point below.

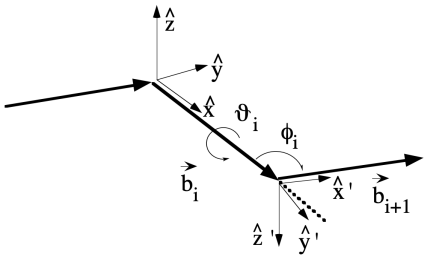

Fig. 11 Coordinate systems of two successive bonds.

The leading approximation of $\langle \vec{R}_N^2 \rangle$ which takes the angles ϕ_1, ϑ_1, ϕ_2, ϑ_2, ... (cf. Fig. 9) into consideration is the following:

$$\begin{aligned} \langle \vec{e}_i \cdot \vec{e}_j \rangle &= \langle \begin{pmatrix} 1 \\ 0 \\ 0 \end{pmatrix} \Pi_{k=0}^{i-1-j} \mathbf{T}_{j+k \to j+k+1} \begin{pmatrix} 1 \\ 0 \\ 0 \end{pmatrix} \rangle \\ &\approx \begin{pmatrix} 1 \\ 0 \\ 0 \end{pmatrix} \langle \mathbf{t} \rangle^{i-j} \begin{pmatrix} 1 \\ 0 \\ 0 \end{pmatrix} \, . \end{aligned} \tag{27}$$

What does this mean? In the first equation each of the two unit vectors $\vec{e}_i$ and $\vec{e}_j$ are considered unit vectors along the respective x-axes of their own 'private' coordinate systems. The projection of $\vec{e}_j$ onto the direction of $\vec{e}_i$ is then handled in a series of $i-j$ steps or rotations of the coordinate system of $\vec{e}_j$ onto the coordinate system of $\vec{e}_i$. The average is over a matrix $\mathbf{T}$ that contains all angle ϕ and ϑ between monomers i and j. The second equation assumes that all steps are statistically independent, i.e. the average of a product of rotation matrices becomes the product of $i-j$ identical average single step rotation matrices $\mathbf{t}$. This is a strong approximation - but it simplifies matters considerably. Note that different monomers may be correlated despite this approximation. This is because a monomer's orientation is coupled to the orientation of its predecessor if for instance either the bond angle ϕ or the torsion angle ϑ (or both) is fixed or limited to a sector of the full solid angle. Nevertheless, for an 'observer' on the predecessor monomer, any average involving functions of ϕ and ϑ, defining the orientation of the following monomer, are independent of the position of the predecessor along the chain. This also implies that monomers in the middle of the chain are no different from those near the chain ends.

So how do we find $\mathbf{t}$? Fig. 11 shows two successive vectors $\vec{b}_i$ and $\vec{b}_{i+1}$ along the x-axes of their coordinate systems. Let's say we are looking at this from within the xyz-system and we want to rotate $\vec{b}_{i+1}$ so that it becomes parallel to the x-axis. Thus we first (1) rotate $\vec{b}_{i+1}$ with respect to the x-axis by the angle $-\vartheta$ (omitting the index i) and then (2) we rotate the resulting $\vec{b}_{i+1}$ with respect to the z-axis until it is aligned with the x-axis. This angle of rotation is $\pi - \phi$ (also omitting the index i). Mathematically this is accomplished by the the product of two rotation matrices:

$$\underbrace{\begin{pmatrix} -\cos\phi & \sin\phi & 0 \\ -\sin\phi & -\cos\phi & 0 \\ 0 & 0 & 1 \end{pmatrix}}_{(2)} \underbrace{\begin{pmatrix} 1 & 0 & 0 \\ 0 & \cos\vartheta & -\sin\vartheta \\ 0 & \sin\vartheta & \cos\vartheta \end{pmatrix}}_{(1)} \tag{28}$$

Note that this is not yet **t**. Two things must be done. First, what we want is the inverse the above matrix. In addition, we want to rotate coordinate systems rather than vectors within them. This mean we must replace ϑ by $-\vartheta$ and ϕ by $-\phi$. The resulting **t** is given by

$$\mathbf{t} = \begin{pmatrix} -\cos\phi & \sin\phi & 0 \\ -\sin\phi\cos\vartheta & -\cos\phi\cos\vartheta & -\sin\vartheta \\ -\sin\phi\sin\vartheta & -\cos\phi\sin\vartheta & \cos\vartheta \end{pmatrix} . \tag{29}$$

The average $\langle\mathbf{t}\rangle$ is given by

$$\langle\mathbf{t}\rangle = \begin{pmatrix} -\cos\phi & \sin\phi & 0 \\ -\sin\phi\langle\cos\vartheta\rangle & -\cos\phi\langle\cos\vartheta\rangle & -\langle\sin\vartheta\rangle \\ -\sin\phi\langle\sin\vartheta\rangle & -\cos\phi\langle\sin\vartheta\rangle & \langle\cos\vartheta\rangle \end{pmatrix} , \tag{30}$$

where we assume that ϕ is a constant angle.

Next we insert the approximation (27) into Eq. (22) and evaluate $\sum_{i>j}\langle\mathbf{t}\rangle^{i-j}$:

$$\begin{aligned} \sum_{i>j}\langle\mathbf{t}\rangle^{i-j} &= (N-1)\langle\mathbf{t}\rangle + (N-2)\langle\mathbf{t}\rangle^2 + \cdots + (N-N)\langle\mathbf{t}\rangle^N \\ &= N\sum_{i=1}^{N}\langle\mathbf{t}\rangle^i - \sum_{i=1}^{N} i\langle\mathbf{t}\rangle^i \\ &= N\langle\mathbf{t}\rangle(\mathbf{I}-\langle\mathbf{t}\rangle)^{-1} - \langle\mathbf{t}\rangle(\mathbf{I}-\langle\mathbf{t}\rangle^N)(\mathbf{I}-\langle\mathbf{t}\rangle)^{-2} \\ &\approx N\langle\mathbf{t}\rangle(\mathbf{I}-\langle\mathbf{t}\rangle)^{-1} (\text{for large } N) . \end{aligned} \tag{31}$$

In the limit of large N the final result is

$$\langle\vec{R}_\infty^2\rangle = C_\infty b^2 N \tag{32}$$

with

$$C_\infty = \left.\frac{\mathbf{I}+\langle\mathbf{t}\rangle}{\mathbf{I}-\langle\mathbf{t}\rangle}\right|_{11} , \tag{33}$$

where the subscript 11 indicates the matrix element. When $\langle\sin\vartheta\rangle = 0$, i.e. the torsion potential is symmetric, this expression simplifies to

$$C_\infty = \frac{(1-\cos\phi)(1-\langle\cos\vartheta\rangle)}{(1+\cos\phi)(1+\langle\cos\vartheta\rangle)} . \tag{34}$$

Fig. 12 shows a number of examples for C_N and C_∞ calculated at various levels of approximation. The dotted line in the top panel is the freely jointed chain for which, according to Eq. (23), $C_N = 1$. The dashed line in the same panel is for a freely rotating chain for which the angle between bonds is $\phi = 112^o$ (corresponding to the C-C-C valence bond in polyethylene (PE)). Since $\langle\cos\varphi\rangle = 0$ in this case, Eq. (34) yields $C_\infty \approx 2.2$. However, the figure also shows that C_N increases with N. The N-dependence shown here follows if we include the correction terms in the summation (31) and not just the limit $N \to \infty$. The solid lines in the two panels are calculated using

$$\langle\cos\vartheta\rangle = \frac{\int_0^{2\pi} d\vartheta\cos\vartheta\exp[-\beta u_{torsion}(\vartheta)]}{\int_0^{2\pi} d\vartheta\exp[-\beta u_{torsion}(\vartheta)]} . \tag{35}$$

Here $\beta = 1/(k_B T)$. The torsion potential $u_{torsion}$ is modelled via an empirical potential energy describing butane (W.L. Jorgensen, J.D. Madura, C.J. Swenson JACS *106*, 6638 (1984)), i.e.

$$\begin{aligned} u_{torsion} \equiv u^B &= 355.1(\cos(\vartheta)+1) \\ &\quad -68.21(1-\cos(2\vartheta)) + 791.6(\cos(3\vartheta)+1) . \end{aligned} \tag{36}$$

As before $\phi = 112^o$. The potential (36) is depicted in Fig. 13. Note the three pronounced minima. The one in the middle (trans) occurs when the C-Atoms form a flat zig-zag in the plane. The other two minima are called gauche minus und gauche plus. Note that for this type of hindered rotation C_∞ is significantly larger than before. However, this depends on temperature. Increasing T let the PE models approach the limit of the freely rotating chain. There is one more line, the long-dashed line, in the bottom panel of Fig. 12. Its calculation is based on an approximation which takes into account the coupling between successive torsion angles. We shall discuss this approximation below.

Aside from the contour length L and the mean square end-to-end distance $\langle R_N^2\rangle$ there are two additional lengths, which are mentioned with equal frequency in the context of polymer chain conformations. The first is the **Kuhn length** κ, which is defined via

$$\kappa n = L = b\sin(\phi/2)N \tag{37}$$

and

$$\kappa^2 n = \langle R^2\rangle = C_\infty b^2 N . \tag{38}$$

This means that a chain is made of n freely jointed (i.e. $\langle\vec{e}_i\cdot\vec{e}_j\rangle = 0$) straight elements, each one Kuhn length long, which possess the same contour length and the same mean-square end-to-end distance than our polymer chain consisting of N monomers of length b. Note that N is considered large and thus C_N is replaced by C_∞. Hence

$$\kappa = \frac{C_\infty}{\sin(\phi/2)} b . \tag{39}$$

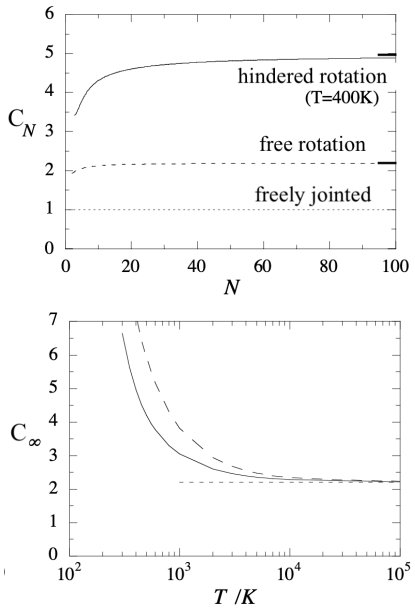

Fig. 12 Top: C_N vs. N for various chain models. Bottom: Temperature dependence of C_∞.

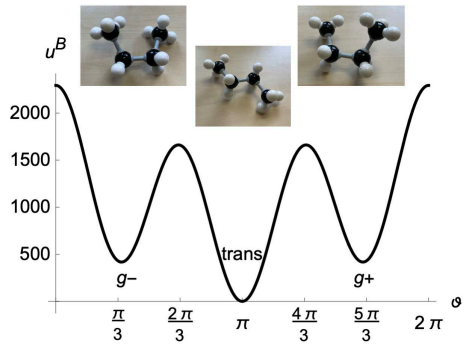

Fig. 13 The torsion potential u^B (in units of Kelvin) modelled on the basis of the butane molecule.

Since C_∞ usually is between 5 to 10 and $\sin(\phi/2)$ is between 0.8 and 1, κ corresponds to several monomers.

The second length is the **persistence length** P. There are polymers, for instance helical ones (like DNA), whose flexibility cannot be described by rotations around bonds. Their conformations are better described by homogeneous bending of the helical backbone as illustrated by the example in Fig. 14. The polymer is described as a smooth curve in space whose local orientation is defined by tangent vectors $\vec{t}$ along this curve. The correlation function $\langle \vec{t}(i)\cdot\vec{t}(j)\rangle$ is given by

$$\langle \vec{t}(i)\cdot\vec{t}(j)\rangle = \exp(-b|i-j|/P)\,, \tag{40}$$

which defines P (we shall return to this equation and its derivation in section 6.3). Here b is a certain suitable unit of length, e.g. the rise of the helix per turn, and i and j are integers, enumerating the turns of the helix. The contour length of such polymer is $L = bN$, where N is the number of turns of the helix.

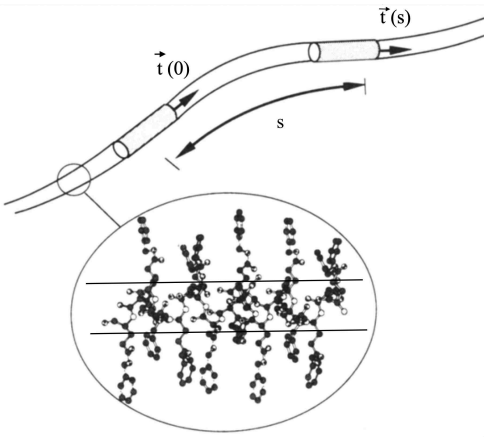

Fig. 14 Illustration of a poly(γ-bebzyl-L-glutamate) (PBLG) molecule as a homogeneously bend-elastic rod. PBLG is a helical polypeptide enveloped in benzene-terminated side chains for better solubility. Here $\vec{t}(0)$ and $\vec{t}(s)$ are unit tangent vectors, separated by the distance s, along the helical backbone of PBLG.

Note that (40) is a special case of (27). Again $\mathbf{t}$ is given by (29). But now $\langle\sin\vartheta\rangle = \langle\cos\vartheta\rangle = 0$. In addition, the angle θ defined via $\vec{t}(i)\cdot\vec{t}(i+1) = \cos\theta$ is related to ϕ via $\theta = \pi - \phi$. Since θ is very small we use the approximations $\langle\sin\phi\rangle = \langle\sin\theta\rangle \approx 0$ and $-\langle\cos\phi\rangle = \langle\cos\theta\rangle \approx 1 - \frac{1}{2}\langle\theta^2\rangle$. Hence

$$\langle\mathbf{t}\rangle \approx \begin{pmatrix} 1-\frac{1}{2}\langle\theta^2\rangle & 0 & 0 \\ 0 & 0 & 0 \\ 0 & 0 & 0 \end{pmatrix} \tag{41}$$

and

$$\langle \vec{t}(i)\cdot\vec{t}(j)\rangle = \left(1-\frac{1}{2}\langle\theta^2\rangle\right)^{|i-j|} = \exp(-b|i-j|/P)\,, \tag{42}$$

where

$$P = 2b/\langle\theta^2\rangle\,. \tag{43}$$

Let's compute $\langle\vec{R}_N^2\rangle$ via Eq. (22) replacing $\langle\vec{e}_i\cdot\vec{e}_j\rangle$ with $\langle\vec{t}(i)\cdot\vec{t}(j)\rangle$. The double sum becomes

$$\sum_{i>j}\langle\vec{t}(i)\cdot\vec{t}(j)\rangle = \sum_{i>j}^{N} q^{i-j} = N\frac{q}{1-q} - q\frac{1-q^N}{(1-q)^2}\,, \tag{44}$$

where $q \equiv \exp(-b/P) < 1$. If we concentrate on the large N limit, i.e. we neglect the second term on the right, then

$$\langle\vec{R}_N^2\rangle = b^2\frac{1+q}{1-q} \approx 2LP\,. \tag{45}$$

Note that $b \ll P$ and therefore $q \approx 1 - b/P$. Since in the case of the Kuhn length our result was $\langle\vec{R}^2\rangle = L\kappa$, we may conclude

$$\kappa = 2P\,. \tag{46}$$

This result is not really a deep interconnection between the Kuhn

length and the persistence length. It merely reflects the fact that independent of the flexibility mechanism, i.e. rotation around bonds or continuous bending, an ideal chain becomes a random path if its contour length is much longer than a certain characteristic length - and different characteristic length are related.

The above type of chain usually is referred to as **wormlike chain** and sometimes as **persistent flexible polymers**. Contrary to the freely jointed chain, however, which ceases to be useful in the limit $L \sim \kappa$, i.e. when it is so short that its contour length is roughly its Kuhn length, the wormlike chain, which is then called **semi-flexible** rather than wormlike, has numerous applications in the corresponding limit $L \sim P$. This is because persistent flexible polymers in solution may undergo orientation phase transitions, e.g. from an isotropic phase to a nematic phase, dependent on concentration. How this particular **lyotropic liquid crystalline phase transitions** depends on the ratio L/P is discussed in a nice paper by T. Odijk [*Macromolecules*, 1986, **18**, 2313]. In addition it is worth mentioning that there are important classes of such polymers which are not helical polypeptides. Examples are non-covalent assemblies of globular proteins like sickle cell haemoglobin or actin into superstructures. Tobacco mosaic virus is another such assembly. These self-assembled polymers are rod-like, i.e. their persistence length is comparable or larger than their contour length. We shall discuss lyotropic liquid crystalline polymers in section 6.3.

3.2 Statistical Thermodynamics of Single Chains

The conformational partition function of a polymer chain is given by

$$Q = \sum_p \exp[-\beta U(p)] \,. \tag{47}$$

Here p is an index identifying a particular chain conformation, i.e. the sum extends over all possible conformations of the chain. In practice p is replaced by the cartesian coordinates of the chain's atoms or by the internal coordinates (bonds lengths, valence and torsion angles. U is the potential energy of the chain and $\beta = (k_B T)^{-1}$. For an arbitrary potential energy the evaluation of the sum is very difficult. Here we focus on two summation methods, each of which is based on certain approximations of U. The first method, the **transfer matrix method**, is mainly used to calculate chain properties like its characteristic ratio or its scattering structure factor based on a chemically realistic representation of the monomer units. The second method, **the self consistent field method**, is useful for the computation of the configurational chain properties if the chain is interacting with an external field (e.g. the density profile of an adsorbed chain) or if the field represents self-interaction of the chain.

Rotational Isomeric State Model and Transfer Matrix Method:

The transfer matrix method assumes that U includes the internal potential energy of the monomers individually plus the coupling of neighboring monomers. It is also assumed that the relative orientation of a monomer with respect to its neighbors is well described by a small number of discrete (torsion) angles. We discuss the method based on the simple example of the polyethylene (PE) chain with fixed bond lengths and fixed valence angles, i.e. different conformations are entirely due to the variable C-C-torsion angles ϑ. The conformation potential energy in this case is

$$U = \sum_{i=1}^{N} u(\vartheta_i, \vartheta_{i+1}) = \sum_{i=1}^{N} \left(u^B(\vartheta_i) + u^P(\vartheta_i, \vartheta_{i+1}) \right) \,. \tag{48}$$

The meaning of this is explained in Fig. 15. Each monomer is defined via a torsion angle ϑ, which in turn is defined by four C atoms or four methylene units respectively (cf. Fig. 10). Note that n-butane contains four carbons bonded like this and thus the superscript B. u_B is the same as $u_{torsion}$ in Eq. (36). The coupling of adjacent monomers arises due to the interaction of the methylene units 1 and 5 in the figure, possessing the separation R_4. This coupling often is referred to as pentane effect and thus the superscript P. Here the **rotational isomeric state (RIS) approximation** is the assertion that every torsion angle assumes one of three discrete values called g_- (gauche minus), t (trans), and g_+ (gauche plus). For the moment this is sufficient.

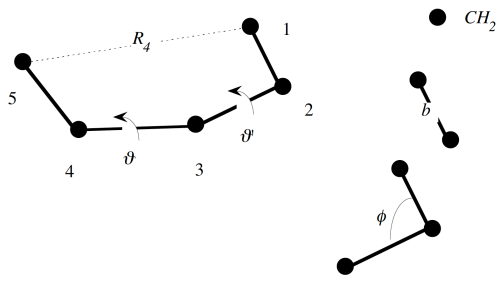

Fig. 15 PE model

Figure 16 illustrates how we can use the three torsion angle values to express each conformation as a path on a lattice whose rows are ϑ_{g_-}, ϑ_t, and ϑ_{g_+} and whose columns are numbered according to the torsion angles along the chain. By translating each line connecting two dots into a Boltzmann factor we obtain a product of N Boltzmann factors for each conformation, where N is the number of torsion angles along the chain. The subsequent summation over all distinct paths, i.e. products, yields Q.

However, there is a much simpler method. This method is illustrated in Fig. 17. For the sake of transparency we assume that every torsion angle can be in one of two states, i.e. 1 and 2 (e.g. ϑ_{g_-} and ϑ_{g_+}). In addition the current chain consists of three monomers only. Now consider two 2×2 **'transfer matrices' a** and **b**. For instance, the element a_{11} means that this matrix element takes us from the first monomer/torsion angle in the chain, which is in state 1, to the second monomer/torsion angle in the chain, which is in state 1 also. Analogous, the element b_{12} means that this matrix element takes us from the second monomer/torsion angle in the chain, which is in state 1 again, to the third monomer/torsion angle in the chain, which is in state 2.

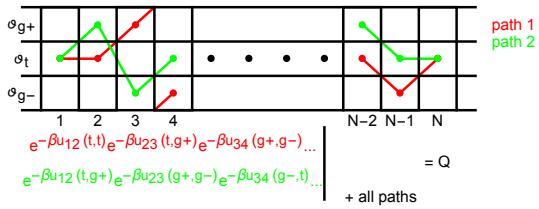

Fig. 16 Q as a sum over different paths defined by the torsion angles along the chain. Two paths, one green and one red, are shown. At the bottom we see their (partial) representation as Boltzmann factors in the partition function.

This particular path is the upper one of the two red paths starting both in state 1 and ending both in state 2. Thus, every element of the product matrix $\mathbf{a}\,\mathbf{b}$ is the mathematical representation of two paths starting at one particular state and ending in the same or in the other state (cf. the diagrams depicted in the lower right of Fig. 17). Thus, we need to figure out what the transfer matrices are in the case of PE, take their N-product, and then add up the elements of this matrix. This does not sound like a real simplification - or does it?

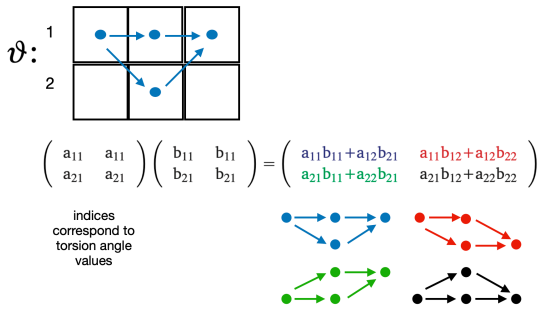

Fig. 17 Paths expressed via products of two 2×2 'transfer matrices' $\mathbf{a}$ and $\mathbf{b}$.

We begin by rewriting Q as follows

$$\begin{aligned} Q &= \sum_{\vartheta_1,\vartheta_2,\ldots,\vartheta_N} \exp\left[-\beta\sum_{i=1}^{N}\left(u^B(\vartheta_i)+u^P(\vartheta_i,\vartheta_{i+1})\right)\right] \\ &= \sum_{\vartheta_1,\vartheta_2,\ldots,\vartheta_N} \exp\left[-\beta\left(\frac{1}{2}u^B(\vartheta_1)+u^P(\vartheta_1,\vartheta_2)+\frac{1}{2}u^B(\vartheta_2)\right)\right] \\ &\quad\times\exp\left[-\beta\left(\frac{1}{2}u^B(\vartheta_2)+u^P(\vartheta_2,\vartheta_3)+\frac{1}{2}u^B(\vartheta_3)\right)\right] \\ &\quad\ldots \\ &\quad\times\exp\left[-\beta\left(\frac{1}{2}u^B(\vartheta_{N-1})+u^P(\vartheta_{N-1},\vartheta_N)+\frac{1}{2}u^B(\vartheta_N)\right)\right] \\ &\quad\times\exp\left[-\beta\left(\frac{1}{2}u^B(\vartheta_N)+\frac{1}{2}u^B(\vartheta_1)\right)\right]. \end{aligned}$$

Note that all factors, save for the last one, are of the form

$$T_{ij} = \exp\left[-\beta\left(\frac{1}{2}u^B(\vartheta_i)+u^P(\vartheta_i,\vartheta_j)+\frac{1}{2}u^B(\vartheta_j)\right)\right]. \tag{49}$$

The last factor contains no coupling term (If it did, the chain would form a loop as depicted in Fig. 4 (b).) and thus has the form

$$T_{o,ij} = \exp\left[-\beta\left(\frac{1}{2}u^B(\vartheta_i)+\frac{1}{2}u^B(\vartheta_j)\right)\right]. \tag{50}$$

The indices i and j label the isomeric states g_i, t, and g_+ in the two neighboring monomers. Hence the corresponding matrix $\mathbf{T}$ has the same meaning as the above matrices $\mathbf{a}$ and $\mathbf{b}$. The meaning of $\mathbf{T_o}$ is analogous - except for one peculiar twist.

The example in Fig. 17 taught us to work out the product $\mathbf{T}^{N-1}\mathbf{T_o}$ and then compute the sum over all elements to obtain Q. But the example also included paths which start in one state and end in another. This is not true now. Due to the specific way in which we have rewritten Q, specifically the splitting of the factor $\exp\left[-\beta u^B(\vartheta_1)\right]$, every path ends in the same state from which it started! If we only include such paths in the example in Fig. 17 this mean that instead of summing over all elements of $\mathbf{a}\,\mathbf{b}$ we only sum over the elements along the diagonal of $\mathbf{a}\,\mathbf{b}$, i.e. we calculate the trace $\mathrm{Tr}(\mathbf{a}\,\mathbf{b})$ - and the trace has very useful properties. Here this means

$$Q = \mathrm{Tr}(\mathbf{T}^{N-1}\mathbf{T_o}), \tag{51}$$

which actually is quite easy to calculate.

Let us assume that $\mathbf{T}$ can be diagonalized, i.e.

$$\mathbf{S}^{-1}\mathbf{T}\mathbf{S} = \begin{pmatrix} \lambda_> & 0 & 0 \\ 0 & \lambda_< & 0 \\ 0 & 0 & \lambda_{<<} \end{pmatrix} \equiv \mathbf{D}, \tag{52}$$

where $\mathbf{S}\mathbf{S}^{-1} = \mathbf{I}$ and $\mathbf{I}$ is the unit matrix. Hence

$$\begin{aligned} Q &= \mathrm{Tr}(\mathbf{T}^{N-1}\mathbf{T_o}) = \mathrm{Tr}(\mathbf{T}\mathbf{S}\mathbf{S}^{-1}\mathbf{T}\mathbf{S}\mathbf{S}^{-1}\ldots\mathbf{S}\mathbf{S}^{-1}\mathbf{T_o}\mathbf{S}\mathbf{S}^{-1}) \\ &= \mathrm{Tr}(\mathbf{S}^{-1}\mathbf{T}\mathbf{S}\mathbf{S}^{-1}\mathbf{T}\mathbf{S}\mathbf{S}^{-1}\ldots\mathbf{S}\mathbf{S}^{-1}\mathbf{T_o}\mathbf{S}) \\ &= \mathrm{Tr}(\mathbf{D}^{N-1}\tilde{\mathbf{T}}_\mathbf{o}) \\ Q &= \lambda_>^{N-1}\tilde{T}_{o,11} + \lambda_<^{N-1}\tilde{T}_{o,22} + \lambda_{<<}^{N-1}\tilde{T}_{o,33}, \end{aligned} \tag{53}$$

where

$$\tilde{\mathbf{T}}_\mathbf{o} = \mathbf{S}^{-1}\mathbf{T_o}\mathbf{S}. \tag{54}$$

Note that the second equation follows via the cyclic permutation of $\mathbf{S}^{-1}$ from left to right, which is one of the useful properties of the trace. With this the (reduced) conformation free energy $\beta F = -\ln Q$ of the chain becomes

$$\beta F = -\ln\left(\lambda_>^{N-1}\tilde{T}_{o,11} + \lambda_<^{N-1}\tilde{T}_{o,22} + \lambda_{<<}^{N-1}\tilde{T}_{o,33}\right). \tag{55}$$

Let's briefly discuss our notation, i.e. the subscripts $>$, $<$ and $<<$. There is a mathematical theorem, the theorem by Perron-Frobenius, which states the following: Let $\mathbf{A}$ be positive N×N matrix, i.e. $A_{ij} > 0 \; \forall \; i,j$. This $\mathbf{A}$ possess a real, non-degenerate eigenvalue $\lambda_>$ and $\lambda_> > |\lambda_k|$, where the index k enumerates all other eigenvalues. Here $k = <, <<$, without implying any particular order of these eigenvalues.

Hence we may write the free energy as a sum over three contributions (for sufficiently large N)

$$\beta F = -N \ln \lambda_> - \ln \frac{\tilde{T}_{o,11}}{\lambda_>} + O(e^{-(N-1)/\xi}) \; . \tag{56}$$

The first term on the right hand side is the bulk limit dominating for large N. The next term is the surface contribution of the ends. The third term is another finite size contribution, which vanishes in the limit $N \to \infty$. The quantity ξ is a correlation lengths defined via

$$\xi \equiv -\frac{1}{\ln |\lambda_< / \lambda_>|} \; . \tag{57}$$

ξ essentially is a measure for how far from the chain ends the latter will have an effect. It also is a measure for the decay of pair-correlations along the chain, e.g. $\langle \vartheta_t(i) \vartheta_t(j) \rangle$, where i and j are two monomers separated by the distance $|i-j|$. However, this is all good and well, but how do we calculate quantities like C_∞?

We start with $p(\vartheta_t;k)$, the probability that the k^{th} torsion angle along the chain is in the trans-state. This quantity is

$$p(\vartheta_t;k) = \frac{Q(\vartheta_t;k)}{Q} = \frac{\sum \text{ paths passing through } \vartheta_t \text{ at } k}{\sum \text{ all paths}} \; . \tag{58}$$

We do know Q, i.e. the (Boltzmann weighted) sum over all paths. But how do we force a polymer conformation (or path) to be in the trans-state at position k? The answer is that we calculate the partition function as before, except that we insert the matrix

$$\mathbf{I}_{\vartheta_t} = \begin{pmatrix} 0 & 0 & 0 \\ 0 & 1 & 0 \\ 0 & 0 & 0 \end{pmatrix}$$

before the k^{th} transfer matrix in the trace. The result is

$$\begin{pmatrix} 0 & 0 & 0 \\ 0 & 1 & 0 \\ 0 & 0 & 0 \end{pmatrix} \begin{pmatrix} g_- \leftarrow g_- & g_- \leftarrow t & g_- \leftarrow g_+ \\ t \leftarrow g_- & t \leftarrow t & t \leftarrow g_+ \\ g_+ \leftarrow g_- & g_+ \leftarrow t & g_+ \leftarrow g_+ \end{pmatrix} = \begin{pmatrix} 0 & 0 & 0 \\ t \leftarrow g_- & t \leftarrow t & t \leftarrow g_+ \\ 0 & 0 & 0 \end{pmatrix} ,$$

i.e. we force the path through the trans state at this torsion angle along the chain. Note that here we use the notation $i \leftarrow j$ compared to Eqs. (49) and (50). The analogous matrices for the other two probabilities, $p(\vartheta_{g_-};k)$ and $p(\vartheta_{g_+};k)$ are

$$\mathbf{I}_{\vartheta_{g_-}} = \begin{pmatrix} 1 & 0 & 0 \\ 0 & 0 & 0 \\ 0 & 0 & 0 \end{pmatrix} \quad \text{and} \quad \mathbf{I}_{\vartheta_{g_+}} = \begin{pmatrix} 0 & 0 & 0 \\ 0 & 0 & 0 \\ 0 & 0 & 1 \end{pmatrix} .$$

Hence

$$\begin{aligned} p(\vartheta\alpha;k) &= \frac{Tr(\mathbf{T}^{k-1}\mathbf{I}_{\vartheta_\alpha}\mathbf{T}^{N-k}\mathbf{T_o})}{Tr(\mathbf{T}^{N-1}\mathbf{T_o})} \\ &= \frac{Tr(\mathbf{D}^{k-1}\tilde{\mathbf{I}}_{\vartheta_\alpha}\mathbf{D}^{N-k}\tilde{\mathbf{T}}_\mathbf{o})}{Tr(\mathbf{D}^{N-1}\tilde{\mathbf{T}}_\mathbf{o})} \overset{N\to\infty}{=} \tilde{I}_{\vartheta_\alpha,11} \; . \end{aligned} \tag{59}$$

Here α stands for either t, g_-, or g_+ and $\tilde{\mathbf{I}}_{\vartheta_\alpha} = \mathbf{S}^{-1}\mathbf{I}_{\vartheta_\alpha}\mathbf{S}$. We also assume that the larges eigenvalue, $\lambda_>$, is the element D_{11}.

Let us now attempt to compute C_∞ for PE with this method. First we need to work out the transfer matrix elements according to Eq. (49). This means that we need an expression for $u^P(\vartheta,\vartheta')$, since we already have $u_B(\vartheta)$ (cf. Eq. (36)). $u^P(\vartheta,\vartheta')$ is modelled via

$$u^P(\vartheta,\vartheta') = 4\varepsilon_{CC}\left[\left(\frac{\sigma_{CC}}{R_4}\right)^{12} - \left(\frac{\sigma_{CC}}{R_4}\right)^{6}\right] \tag{60}$$

and

$$\begin{aligned} R_4^2 &= 4b^2 + 2b^2\Big\{ -\cos\phi\left(3 - 2\cos\phi + \cos^2\phi - \sin^2\phi cos\vartheta\right) \\ &\quad - \sin^2\phi\left(\cos\vartheta + \cos\vartheta' - \sin\vartheta\sin\vartheta'\right) \\ &\quad + \sin\phi\sin(2\phi)\cos^2\frac{\vartheta}{2}\cos\vartheta'\Big\} \; . \end{aligned}$$

Note that $b = 1.53$ Å for the C-C bond length, $\phi = 112^o$, $\varepsilon_{CC}/k_B = 3.725\ K$ und $\sigma_{CC} = 4$ Å. This is a steric interaction in the form of a Lennard-Jones potential of C-atoms which are separated by four bonds along the chain. The direct separation (after some trigonometry) between these atoms is R_4. Note that we never mention any of the hydrogen atoms. This is because this is a so-called *united atom*-model and hydrogens are fused with their carbon atom into one effective carbon atom.

Table 2 lists the minima of u^B defining our RIS angles. The next table, Tab. 3, shows R_4/σ_{CC}, for the different combination of two successive RIS angles. Values less than unity mean that u^P adds an extra repulsion. Otherwise u^P tends to make this particular combination of torsion angles more favourable. Note that the pairs $\vartheta_{g_-}\ \vartheta_{g_+}$ and $\vartheta_{g_+}\ \vartheta_{g_-}$ give rise to a pronounced steric hinderance, which in turn suppresses the likelihood of this pairing. Finally, Eq. (61) is the transfer matrix based on these values of the RIS angles. At $T = 400$ K it possess the eigenvalues 1.59, 0.32, −0.22. Note that in this case $\xi \approx 1$, i.e. the effect of the chain ends or the extend of correlations along the chain are short-ranged.

Table 2 Minima of u^B defining our RIS angles

		$u^B[K]$
ϑ_{g_-}	1.107	417.5
ϑ_t	π	0
ϑ_{g_+}	5.176	417.5

Table 3 R_4/σ_{CC} for the different combination of two successive RIS angles

	ϑ_{g_-}	ϑ_t	ϑ_{g_+}
ϑ_{g_-}	0.94	1.12	0.70
ϑ_t	1.12	1.27	1.12
ϑ_{g_+}	0.70	1.12	0.94

$$\mathbf{T} = \begin{pmatrix} e^{-427/T} & e^{-205/T} & e^{-1468/T} \\ e^{-205/T} & e^{2.72/T} & e^{-205/T} \\ e^{-1468/T} & e^{-205/T} & e^{-427/T} \end{pmatrix} \tag{61}$$

Figure 18 shows a comparison of $p(\vartheta_{g_-})$ vs. T with $u^P = 0$ (solid line) and with $u^P \neq 0$ (dashed line). Here $p(\vartheta_{g_-})$ is computed according to Eq. (59) for $N = \infty$. Note that we do not need to also show $p(\vartheta_{g_+})$ and $p(\vartheta_t)$ because $p(\vartheta_{g_-}) = p(\vartheta_{g_+})$ and $p(\vartheta_t) + p(\vartheta_{g_-}) + p(\vartheta_{g_+}) = 1$. We can see that including the u^P-interaction between neighboring monomers makes 'kinks' less likely and therefore we expect that it increases C_∞. We obtain C_∞ using $\langle f(\vartheta)\rangle = \sum_\alpha f(\vartheta_\alpha)p(\vartheta_\alpha)$, where $f(\vartheta)$ stands for $\sin(\vartheta)$ or $\cos(\vartheta)$. Thus in this particular case $\langle\cos\vartheta\rangle = 2(\cos\vartheta_{g_-} + 1)p(\vartheta_{g_-}) - 1$ and $\langle\sin\vartheta\rangle) = 0$. Therefore we may use Eq. (34) and obtain

$$C_\infty = \frac{1-\cos\phi}{1+\cos\phi}\left(\frac{1}{(\cos\vartheta_{g_-}+1)p(\vartheta_{g_-})} - 1\right), \tag{62}$$

which is plotted in Fig. 19 (selected values: $T = 100$ K, $C_\infty = 101$; $T = 400$ K, $C_\infty = 7.2$; $T = 450$ K, $C_\infty = 6.6$). Apparently this result is very close to what is shown in the bottom panel of Fig. 12. However, a couple of points are worth commenting on. (i) The solid line Fig. 12 is computed by averaging $\cos\vartheta$ over the full interval $0 \leq \vartheta \leq 2\pi$, whereas the solid line in 19 is computed by averaging $\cos\vartheta$ over only the three RIS angles. In principle, we may view this as confirmation of the quality of this approximation. (ii) the calculation of the RIS-transfer matrix result in Fig. 12 deviates in some (minor) aspects from our above calculation (for details see R. Hentschke, Statistische Mechanik). Finally we may ask whether our calculation of C_∞ can be verified by experiments? This is indeed possible, using for instance small angle X-ray or neutron scattering. We shall come to this.

Before leaving this topic, we briefly want to comment on correlations between the RIS torsion angles. Fig. 20 shows the probabilities of pairs of trosion angles $h_s^{(\alpha\beta)} \propto \langle\vartheta_\alpha(0)\vartheta_\alpha(s)\rangle$ as function of the separation s. Here α and β stand for g_-, t, and g_+. These calculation were done in the bulk part of the chain, i.e. the chain ends do not affect the results. Technically the calculation is very

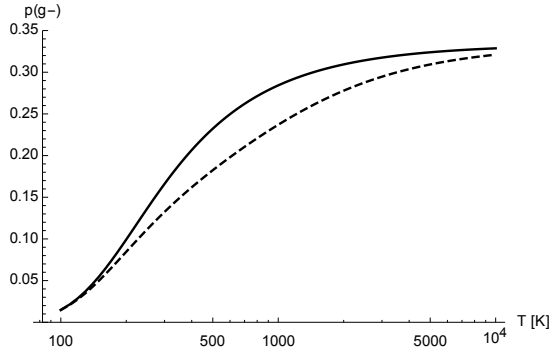

Fig. 18 Comparison of $p(\vartheta_{g_-})$ vs. T with $u^P = 0$ (solid line) and with $u^P \neq 0$ (dashed line).

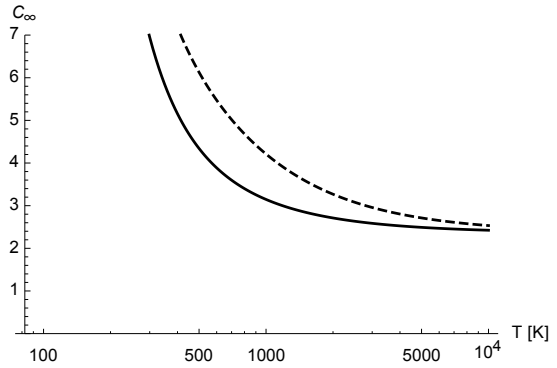

Fig. 19 Comparison of C_∞ vs. T with $u^P = 0$ (solid line) and with $u^P \neq 0$ (dashed line).

similar to our above calculation of $p(\vartheta_\alpha)$. We only need to insert two matrices $\mathbf{I}_{\vartheta_\alpha}$ and $\mathbf{I}_{\vartheta_\beta}$ in the proper positions within the product of transfer matrixes - instead just one. The resulting correlations possess a short range. Already after two monomers the result is $h_s^{(\alpha\beta)} = p(\vartheta_\alpha)p(\vartheta_\beta)$. Note that $h_s^{(g_+g_-)} = 0$ for $s = 0$, because one and the same torsion angle cannot be in two different RIS states. The details of this calculation can be found in 'Molekulares Modellieren mit Kraftfeldern' (Chapter IX).

The RIS/transfer matrix method has been applied to almost every polymer. Much of this work was done by Paul Flory and/or his coworkers. Most of the sometimes complicated details are described in his classic book *Statistical Mechanics of Chain Molecules*, Interscience: New York (1969). The first hint I have found that the transfer matrix method is useful for polymers is footnote 5 (referencing work by Mr. E. Montroll) in a classic paper in the context of the solution of the two-dimensional Ising model with this method (H. A. Kramers, G. H. Wannier Phys. Rev. *60*, 263 (1941)).

Self-Consistent Field Method:

This method applies to polymers whose partition function factorises as in the case of the transfer matrix method. For the sake of simplicity we consider a one-dimensional polymer chain depicted in Fig. 21. Each Kuhn segment has length b (I sometimes

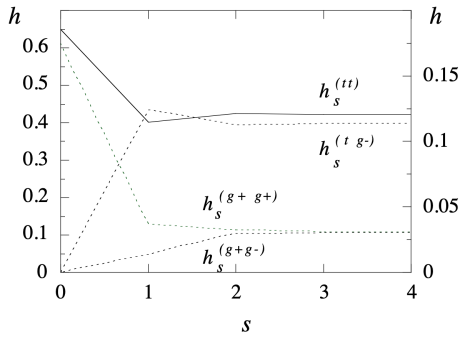

Fig. 20 Probability of pairs tt, tg_-, g_-g_+ and g_+g_+ as function of the distance s at $T = 400$ K. The left axis is for the solid lines, while the right axis is for the dashed lines.

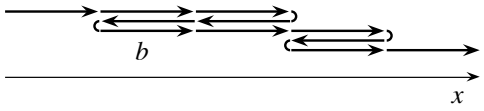

Fig. 21 A one-dimensional polymer path along the x-axis.

prefer b for the Kuhn length even though b is also used for the monomer length. However, the meaning of b should always be clear from the context.) and can be oriented in either x or $-x$ direction. Therefore there are 2^n possible conformations for a polymer consisting of n Kuhn segments. Let $Q_n(x_1,x_n)$ be the partition function of such polymer starting at x_1 and ending at x_n. The factor 2^n is introduced as a normalization. The Kuhn segments 'feel' the external potential $u(x_i)\,(i=1,...,n)$. Hence

$$Q_{n+1}(x_1,x_{n+1}) = \frac{1}{2}\sum_{x_n}{}' Q_n(x_1,x_n) e^{-\beta u(x_{n+1})} \,. \tag{63}$$

$\sum'_{x_n}$ is the sum over all x_n from where we can reach the $(n+1)^{th}$ segment at position x_{n+1} .

At this point we assume the following: (i) $\beta u(x_i) \ll 1 \;\forall\; i$; (ii) $u(x)$ varies little on the scale of one Kuhn segment. These assumptions allow us to expand the right hand side of Eq. (63) at x_{n+1}, i.e.

$$\begin{aligned} Q_{n+1}(x_1,x_{n+1}) &= \frac{1}{2}\sum_{x_n}{}' \Big\{ Q_n(x_1,x_{n+1}) \\ &\quad + (x_n - x_{n+1}) \left.\frac{\partial Q_n(x_1,x)}{\partial x}\right|_{x_{n+1}} \\ &\quad + \frac{1}{2}(x_n - x_{n+1})^2 \left.\frac{\partial^2 Q_n(x_1,x)}{\partial x^2}\right|_{x_{n+1}} + ... \Big\} \\ &\times \Big\{ 1 - \beta u(x_{n+1}) + ... \Big\} \,. \end{aligned} \tag{64}$$

Using $\sum'_{x_n}(x_n - x_{n+1}) = 0$ and keeping the leading terms only yields

$$Q_{n+1}(x_1,x_{n+1}) - Q_n(x_1,x_{n+1}) \cong \frac{1}{2} b^2 \left.\frac{\partial^2 Q_n(x_1,x)}{\partial x^2}\right|_{x_{n+1}} - \beta u(x_{n+1}) Q_n(x_1,x_{n+1}) \,. \tag{65}$$

Large n allow us to simply continue in the continuum limit, i.e.

$$\frac{\partial}{\partial n} Q_n(x',x) = \frac{b^2}{2}\frac{\partial^2}{\partial x^2} Q_n(x',x) - \beta u(x) Q_n(x',x) \,. \tag{66}$$

We solve this partial differential equation employing the ansatz

$$Q_n(x',x) \cong e^{-n\mu_0} \psi_0(x') \psi_0(x) \,. \tag{67}$$

This can be justified in various ways. First note that (66) looks a lot like Schrödinger's equation in quantum mechanics if n is replaced by a complex time. From this angle (67) looks much like the step that takes us from the time-dependent Schrödinger equation to the stationary Schrödinger equation. Eq. (67) can also be understood as the leading term in an expansion in eigenfunctions. Using only the first term is equivalent to the assumption of ground state dominance for large n. Another angle is this: (i) the free energy and therefore $-k_BT \ln Q_n$ must be extensive in n; (ii) segments at x' and x are to good approximation independent and their contributions should therefore factorise. Hence we see that

$$\frac{\Delta F_{conf}}{n k_B T} \cong -\frac{1}{n} \ln\left[e^{-n\mu_0}\right] = \mu_0 \tag{68}$$

for large n, where $\Delta F_{conf} = F_{conf} - F_{conf}^{(ideal)}$ with $F_{konf}^{(ideal)}/(nk_BT) = -\ln 2$.

In any case, inserting (67) into (66) yields

$$\frac{b^2}{2}\frac{d^2}{dx^2}\psi_0(x) + \Big(\mu_0 - \beta u(x)\Big)\psi_0(x) = 0 \,, \tag{69}$$

from which we obtain $\psi_0(x)$. But what is the meaning of $\psi_0(x)$? This becomes clear if we write down the probability for finding a polymer segment at x in terms of the partition function, i.e.

$$c(x) = \frac{1}{n}\frac{\sum_{x',x'',n'} Q_{n'}(x',x) Q_{n-n'}(x,x'')}{\sum_{x',x''} Q_n(x',x'')} \,. \tag{70}$$

Here the numerator is the number of paths or polymer conformations starting from (all possible) x', then reaching x in (all possible) n' steps or segments and then continue in $n-n'$ steps to (all possible) x''. The denominator counts all possible paths of length n connecting (all possible) x' with (all possible) x''. Note that $c(x)$ also is a measure for the polymer concentration at x. Inserting Eq. (67) into (70) yields

$$c(x) \cong \psi_0^2(x) \,. \tag{71}$$

In the following we want to demonstrate the use of Eqs. (68),

(69) and (71) via two examples:

• A polymer near a sticky wall

We assume that a polymer sticks to a wall at position $x = 0$. However, the interaction range is short (on the order of one segment length) and polymer segments outside this distance from the wall are free. Here we are interested in the polymer concentration outside the range of the direct interaction with the wall, which means that we must solve

$$\frac{b^2}{2}\frac{d^2}{dx^2}\psi_0(x) + \mu_0\psi_0(x) = 0$$

for $\psi_0(x)$. Since we consider a bound state, $\mu_0 < 0$ and the solution far from the wall is given by

$$\psi_0(x) \propto \exp[-\kappa x] \ ,$$

where

$$\kappa^2 = -\frac{2\mu_0}{b^2} \ .$$

The attendant change in free energy of the chain due to the adsorption is

$$\frac{\Delta F_{conf}}{nk_BT} = -\frac{(b\kappa)^2}{2} \ . \tag{72}$$

• A polymer confined inside a one-dimensional slit

The polymer is confined between two hard walls inside a slit whose width is D. This problem is analogous to a quantum particle in an infinite potential well. As before we assume ground state dominance. For ψ_0 we easily find

$$\psi_0 \propto \sin(\pi x/D)$$

and for ΔF_{conf}

$$\frac{\Delta F_{conf}}{nk_BT} = \frac{1}{2}\frac{\pi^2 b^2}{D^2} \ . \tag{73}$$

We shall return to the results of the these two examples, when we solve the same or similar problems using other methods .

Remark 1: What does this method have to do with 'self-consistency'? Thus far we have treated the segment potential $u(x)$ as a purely external potential. However, we can assume that segments interact with each other, i.e.

$$u(x) \propto c(x) = \psi_0^2(x) \ . \tag{74}$$

Eq. (69) then becomes a non-linear eigenvalue problem

$$-\frac{b^2}{2}\frac{d^2}{dx^2}\psi_0(x) + \beta\upsilon(T)\psi_0^3(x) = \mu_0\psi_0(x) \ . \tag{75}$$

Here $\upsilon(T)$ is a function of temperature.

Remark 2: It is easy to generalize this approach to three dimensions. On a cubic lattice Eq. (66) becomes

$$\frac{\partial}{\partial n}Q_n(\vec{r}\,',\vec{r}) = \frac{b^2}{6}\vec{\nabla}_{\vec{r}}^2 Q_n(\vec{r}\,',\vec{r}) - \beta u(\vec{r})Q_n(\vec{r}\,',\vec{r}) \ . \tag{76}$$

Counting Paths for Different R_N - the Conformation Entropy:

When discussing the mean square end-to-end distance $\langle R^2\rangle$ we have not stated what the underlying probability distribution of $\vec{R}$ looks like. In this section we want to obtain this distribution as well as the conformation entropy of a polymer chain. We want to base the discussion on the convenient and popular polymer model depicted in Fig. 22, which is a chain of Kuhn segments of length b on a cubic lattice. The question whether there is a significant reduction of generality implied by the lattice we shall address at the end of this section.

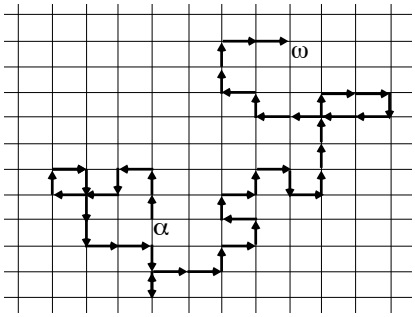

Fig. 22 A polymer chain on a lattice.

Here we ask the question: What is the probability $p(R)$ that the two ends, labeled α and ω, do have the separation R? The answer is $p(R) = \Omega(R)/\sum_R \Omega(R)$. The quantity $\Omega(R)$ is the number of different paths of length n originating from the same lattice point and ending at a distance R from this lattice point. The denominator is the sum over all possible paths of length n originating from the same lattice point without constraining the distance between α and ω. Using Boltzmann's famous entropy formula $S = k_B \ln\Omega$ we have

$$S(R) - S = k_B \ln p(R) \ , \tag{77}$$

where $S(R) = k_B \ln\Omega(R)$ and $S = k_B \ln\sum_R \Omega(R)$. The end-to-end vector $\vec{R}$ is given by

$$\vec{R} = \sum_{i=1}^{n}(x_i, y_i, z_i) = \left(\sum_{i=1}^{n} x_i, \sum_{i=1}^{n} y_i, \sum_{i=1}^{n} z_i\right) \ , \tag{78}$$

where x_i, y_i, and z_i are random variables. Each of these may assume the values $\{-b,0,0,0,0,b\}$ with equal likelihood. Here b is the lattice spacing and the six values correspond to the six possible orientations of the links (in Fig. 22) along the main axes of the cubic lattice.

We obtain $p(R)$ via an important mathematical theorem - the **central limit theorem**. This theorem states that if the s_i are random variables with the average μ_s and the mean square fluctuation σ_s^2 then the new random variable

$$S_n = \frac{\sum_{i=1}^{n} s_i - n\mu_s}{\sigma_s \sqrt{n}} \tag{79}$$

possesses the probability density

$$f(S_n) = \frac{1}{\sqrt{2\pi}} \exp[-S_n^2/2] \tag{80}$$

in the limit of infinite n. However, this is a very good approximation even if n is not very large (The reader may confirm this by generating S_5 from random numbers $s_i \in (0,1)$ (i.e. $\mu_s = 1/2$ and $\sigma_s = 1/\sqrt{12}$). Construction of a distribution histogram based on 10^4 S_5-values generated in this fashion closely approximates a Gaussian distribution with zero mean and standard deviation equal to unity.). Based on the central limit theorem we immediately conclude

$$p(R) \approx \left(\frac{3}{2\pi n b^2}\right)^{1/2} \exp\left[-\frac{3}{2}\frac{R_x^2}{nb^2}\right] \times \left(\frac{3}{2\pi n b^2}\right)^{1/2} \exp\left[-\frac{3}{2}\frac{R_y^2}{nb^2}\right] \times \left(\frac{3}{2\pi n b^2}\right)^{1/2} \exp\left[-\frac{3}{2}\frac{R_z^2}{nb^2}\right] ,$$

i.e.

$$p(R) = \left(\frac{3}{2\pi n b^2}\right)^{3/2} \exp\left[-\frac{3}{2}\frac{R^2}{nb^2}\right] , \tag{81}$$

where $\mu_x = \mu_y = \mu_z = 0$, $\sigma_x^2 = \sigma_y^2 = \sigma_z^2 = b^2/3$, and $4\pi \int_0^\infty dR R^2 p(R) = 1$. Using this expression in Eq. (77) we obtain

$$S(R) = S(0) - \frac{3k_B R^2}{2nb^2} . \tag{82}$$

Note that the conformation entropy decreases when the separation of the ends of the chain is increased. This is because stretching a chain reduces the number of paths along which it can join the two two endpoints.

Equation (81) is the limiting form of $p(R)$ when the polymer chain is purely a random walk and molecular details are not important. Note also that the above results are independent of the constraint of the Kuhn segments to a cubic lattice. Finally, it is worth pointing out that (81) as well as (82) are frequent building blocks in the various construction schemes for the free energy of polymer systems in the subsequent sections.

3.3 Flory's Calculation of the Exponent ν

We had introduced the exponent ν in Eq. (26) - the general expression for the mean square end-to-end distance in terms of the chain length. For an ideal chain $\nu = 1/2$. But what is the value of ν when the chain is not ideal - and what does 'not ideal' mean? 'Ideal' meant that chain conformations, on a certain length scale, are random walks. An ideal chain does not interact with itself (beyond short-ranged interactions of the monomers in close proximity) - or other chains for that matter. An intuitive and rather simple calculation, which allows us to study the influence of 'interaction' on ν and thus on the mean square end-to-end distance is this:

Consider a polymer chain occupying a certain volume R^d, where d is the dimension of space. Here R is the same quantity as in Eq. (82). The free energy of the chain in units of $k_B T$ may be expressed as the sum of two contributions, i.e.

$$f(R) = f^{el}(R) + f^{i}(R) . \tag{83}$$

The contribution $f^{el}(R)$ is due to our chain entropy in Eq. (82), i.e.

$$f^{el}(R) = \frac{3R^2}{2C_\infty b^2 N} + \text{const} . \tag{84}$$

Here we substitute $C_\infty b^2 N$ for $b^2 n$.

The interaction term is modelled in analogy to the free energy (per $k_B T$) of a dilute real gas of small molecules, i.e. $f \approx f_{ideal} + N\rho B_2(T)$. Here f_{ideal} is the free energy of an ideal gas of N molecules, whose number density is ρ. The quantity $B_2(T)$ is the second virial coefficient. Hence

$$f^{i}(R) = N\rho\upsilon(T) , \tag{85}$$

where $\rho = N/R^d$ and $\upsilon(T)$, like $B_2(T)$, is a function of T. In other word, the N monomers of the chain are treated as entities analogous to the N molecules in the dilute gas.

Combination of Eqs. (83), (84) and (85) yields

$$f(R) = \frac{3R^2}{2C_\infty b^2 N} + \upsilon(T)\frac{N^2}{R^d} + \text{const} . \tag{86}$$

According to the second law of thermodynamics the free energy wants to be at its minimum. This means that the polymer size R is adjusted to an equilibrium value R_o following from $df(R)/dR|_{R_o} = 0$, i.e.

$$\frac{3R_o}{C_\infty b^2 N} - d\upsilon(T)\frac{N^2}{R_o^{d+1}} = 0$$

or

$$R_o^{d+2} \propto N^3 \; .$$

Since $R_o \propto N^\nu$ we conclude

$$\nu = \frac{3}{d+2} \; . \tag{87}$$

The ν-values for different d are compiled in Tab. 4. The value for $d = 1$ is without doubt correct. The values for $d = 2$ and $d = 3$ we cannot confirm at the moment. However, 0.6 for $d = 3$ is larger than 0.5, the value of the ideal chain. This is reasonable, because interaction should prevent the chain overlap and thus enlarge the linear chain dimension. We shall return to this point shortly. For $d \geq 4$ we obtain the ideal value, $\nu = 0.5$. For $d = 4$ this is easy to see, at least from (87), but what about $d > 4$?

Table 4 Dimension dependence of ν.

d	ν
1	1
2	3/4=0.75
3	3/5=0.6
≥ 4	1/2=0.5

We expect $R_o \geq R_{ideal}$ and thus

$$f^i \leq \upsilon(T) \frac{N^2}{R_{ideal}^d} \propto \upsilon(T) N^{2-d/2} \overset{N\to\infty}{\longrightarrow} 0$$

for $d > 4$! Since f^{el} does not vanish equally quick, we conclude that the chain is ideal for $d > 4$.

Our above interaction term is based on the notion of a dilute gas. But when does a polymer chain resemble a dilute gas? The situation in which the monomers inside a polymer chain can be compared to a dilute gas arises when the polymer is in a solvent. This means that the above interaction term $\upsilon(T)$ effectively includes the solvent but it is still modelled according to the second virial coefficient of a gas. The simplest theory, which nevertheless contains all important ingredients, is the van der Waals theory in which $B_2(T) = b - a/(k_B T)$. Here b and a describe the (excluded) volume of the gas molecules and their long-range attraction, respectively (van der Waals equation: $P = \rho k_B T/(1-\rho b) - a\rho^2$ where $\rho = N/V$). It is customary to distinguish different types of solvent in terms of the effective quantities a and b:

• Athermal solvents: In an athermal solvent there is only hard-body repulsion. Here this is the limit of the above $B_2(T)$ when T becomes infinite (or $a = 0$) and the molecules are hard bodies. Even though this is never quite realized in nature, the concept use useful due to its simplicity.

• Good solvent: In a good solvent there is a small attraction which reduces the repulsion and thus the polymer appears 'fluffy'.

• θ-solvent: Note that both b and a are positive and thus we can adjust T so that $B_2(T)$, or $\upsilon(T)$ for that matter, is zero. This temperature is the Boyle temperature in a gas. What does it mean for our above calculation if $\upsilon(T_\theta) = 0$? It means we must look at the next term in the expansion in powers of the density when we model f^i. Hence

$$f^i(R) \sim R^d \rho^3 \upsilon'(T) \propto \frac{N^3}{R^{2d}} \; . \tag{88}$$

This leads to

$$\nu = \frac{2}{d+1} \; . \tag{89}$$

In $d = 3$ we now have $\nu = 1/2$, i.e. the chains are ideal under θ-conditions.

• Poor solvent: The second virial coefficient becomes negative when T is below the Boyle temperature. Analogously we expect that for $T < T_\theta$ the attractions overwelm the repulsion, which would yield very compact conformations. Of course, we must proceed with caution here, because we are looking at just one term in an expansion. But nevertheless, it is plausible that at the polymer chain will collapse at some point and essentially will fall out of solution. In this case the monomers are densely packed like molecules inside a liquid droplet.

An experiment in which the temperature is varied across the θ-temperature is shown in Fig. 23. The figure depicts the temperature dependence of the radius of gyration (S) and the hydrodynamic radius (R_H), both quantities are measures for the size of a polymer chain akin to the mean square end-to-end distance, for polystyrene ($M_w = 2.6 \cdot 10^7$) in cyclohexane. The phenomenon is called **coil-globule transition**.

The relation between R_o and N for these solvents in three dimensions is summarized in Tab. 5

Table 5 Size of polymer chain in different solvents.

	$R_o \sim$
athermal solvent	$N^{3/5}$
good solvent	$N^{3/5}$
θ-solvent	$N^{1/2}$
poor solvent	$N^{1/3}$

3.4 The Scaling Concept

Most of you are familiar with simple examples of **dimensional analysis**. One such example is the time period T_p of a pendulum. In step one of the dimensional analysis approach to this problem we compile a list of all physical quantities which might have something to do with T_p. These quantities include m, the mass of the weight at the end of the string, l, the length of the string

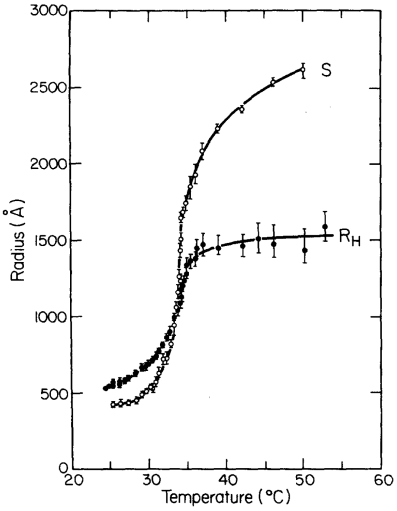

Fig. 23 Temperature dependence of the radius of gyration (S) and the hydrodynamic radius (R_H) for polystyrene ($M_w = 2.6 \cdot 10^7$) in cyclohexane. This is Fig. 2 in S.-T. Sun, I. Nishio, G. Swislow, T. Tanaka *The coil–globule transition: Radius of gyration of polystyrene in cyclohexane* J. Chem. Phys. *73*, 5971 (1980).

(which is assumed to have no mass), and g is the acceleration of gravitation. In a second step we write down these quantities including their physical dimension (cf. Table 6).

Table 6 Quantities potentially affecting the period of a mathematical pendulum including their physical dimensions.

T_p	s
m	kg
l	m
g	m s^{-2}

Next we construct dimensionless expressions based the quantities in Table 6. Here there is only one

$$\frac{T_p^2 g}{l} \sim 1\,. \tag{90}$$

The notation ~ 1 means that $T_p^2 g/l$ is (most likely) on the order of one. Note that m does not appear, because the unit kg is not cancelled by any of the other units. Hence we find

$$T_p \sim \sqrt{l/g}\,, \tag{91}$$

which is correct except for a factor 2π on the rhs.

'Scaling' is based on essentially the same idea, i.e. identification of the 'basic' quantities in a physical problem and using them to construct dimensionless expressions. The difference is that basic quantities are not merely quantities like b or N. Instead they are slightly more complex. So what are they?

Let's assume we are interested in a polymer's free energy F, which is the equivalent to T_p in the above example. Here F of course is a piece of the polymer's total free energy only. This piece depends on the specific problem. What we always exclude are contributions to the total free energy from the many atomic degrees of freedom (manly vibrational modes). Now let's talk about the basic quantities F may depend upon.

Figure 24 shows a polyethylene chain constructed via an algorithm based on the transfer matrix approach. We shall explain the algorithm in the next section. Here we merely remark that this chain consists of 10^4 monomers. The key observation is that it appears divided into 'blobs' - highlighted by the red circles. Another chain of similar length, for which the same observation can be made, is the one in the figure on the title page of this document (A note of caution: Not everything that looks like a blob may in fact be one. Some blobs disappear when we look at the chain from a different direction.). So let's assume these blobs all have roughly the same diameter ξ and that within each blob there are roughly N_ξ monomers. The two quantities should be connected via

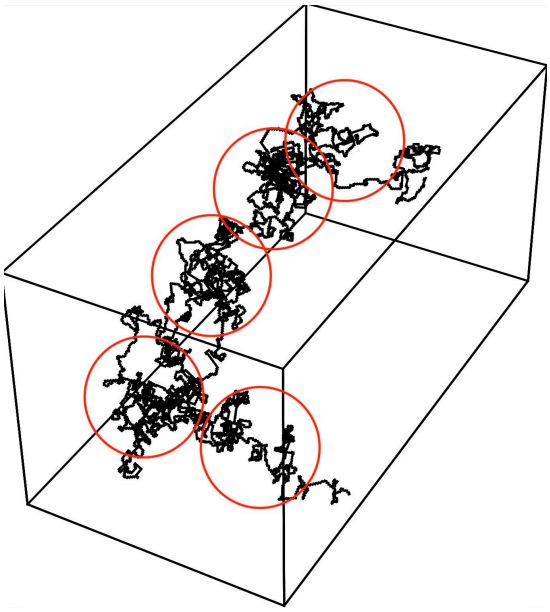

Fig. 24 Polyethylene chain consisting of 'blobs'.

$$\xi \sim b N_\xi^\nu\,. \tag{92}$$

This means that ξ is likely one of the aforementioned basic quantities.

Another basic quantity is the typical 'thermal blob energy', which we assume is $k_B T$. In principle a rotation with respect to a single bond, corresponding to energies on the order of $k_B T$, is sufficient to significantly alter the shape of a blob. Note again that this does not include the 'many $k_B T$s' from the atomic degrees of freedom, since those presumably do not affect the piece of F we are interested in.

The equivalent to (90) therefore is

$$\frac{F}{k_B T} \sim \frac{N}{N_\xi}\,. \tag{93}$$

Here we assert that F is extensive in the number of blobs which is N/N_ξ. At this point it is useful to study (93) in three examples.

• Conformation free energy of polymers in dilute solution

Relation (93) by itself does not tell us much, because we do not know N_ξ or if we replace N_ξ with ξ/b via (92) we do not know ξ. In essence we need one extra equation or relation, allowing to eliminate N_ξ in (93). Here this relation is

$$R \sim \xi \frac{N}{N_\xi} \,. \tag{94}$$

The quantity R of course is the end-to-end distance in the polymer. Note that (94) is reasonably well supported by Fig. 24.

Using (94) in conjunction with (92) and (93) yields the configuration free energy of the chain as

$$F \sim k_B T \left(\frac{R}{bN^\nu}\right)^{1/(1-\nu)} \,. \tag{95}$$

Setting $\nu = 1/2$, i.e. the polymer chain is ideal, we find that the result is in complete accord with Eq. (82). This is important since it confirms that our intuition thus far is correct. It also strengthens our confidence in a new result which we obtain with $\nu = 3/5$, i.e. the real chain-result!

Remark: If we pull on the ends of the chain, we can calculate the magnitude of the restoring force $f^{(el)}$ via $f^{(el)} = dF/dR$, which yields

$$f^{(el)} \sim k_B T \left(\frac{R}{b^{1/\nu} N}\right)^{\nu/(1-\nu)} \,. \tag{96}$$

This force will be linear (Hook's law) for an ideal chain. But in the case of a real chain it will increase with a larger power, i.e. $(R/N)^{3/2}$ for Flory's ν-value in three dimensions. Eventually, however, (96) must break down when R approaches the contour length. The finite extensibility of the chain, which here is not included, leads to a rapid divergence of the force.

• Weakly adsorbed chain

In this example we estimate the free energy of a weakly adsorbed chain. As before we utilize the blob-picture as shown in Fig. 25. The size of the absorbed blobs is once again given by (92) and the free energy of adsorption F_{ad} of the weakly adsorbed chain is once again given by (93). The only modification is that $k_B T$ is replaced by $-k_B T$, since this is the (negative) blob adsorption energy. And as in the previous example we need one extra relation to eliminate N_ξ, which here involves δ, the fraction of adsorption energy (in units of $k_B T$) of a single polymer segment inside a layer of thickness b above the surface (i.e. we assume that the range of the interaction with the surface has this short range).

We obtain the number of monomers in contact with the surface, i.e. the monomers inside a layer of thickness b, via multiplication of the number density of monomers inside the blob, N_ξ/ξ^3, with the volume of the layer $\xi^2 b$:

$$\frac{N_\xi}{\xi^3}\xi^2 b \sim \left(\frac{b}{\xi}\right)^{1-1/\nu} \,. \tag{97}$$

Every monomer in this layer has a small fraction δ of the blobs total adsorption energy. Hence

$$\left(\frac{b}{\xi}\right)^{1-1/\nu} \delta \sim 1 \,, \tag{98}$$

which yields the desired additional equation

$$\xi \sim b\delta^{\nu/(\nu-1)} \,. \tag{99}$$

We conclude that the free energy of adsorption of the chain is

$$\begin{aligned} F \sim -k_B T \frac{N}{N_\xi} \quad &\approx -k_B T N \delta^{1/(1-\nu)} \\ &= -k_B T N \begin{cases} \delta^2 & (\nu = 1/2) \\ \delta^{5/2} & (\nu = 3/5) \end{cases} \,. \end{aligned} \tag{100}$$

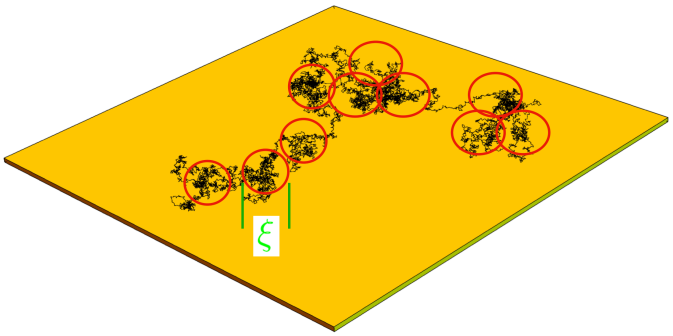

Fig. 25 Weakly adsorbed chain in the 'blob'-picture.

Note that the ideal chain result agrees with the result (72) obtained using the self-consistent field approach.

• A polymer confined inside a tube

In this example we study a polymer confined inside a tube of diameter D. The situation is depicted in Fig. 26. This is very similar to the polymer in a one-dimensional slit discussed previously using the self-consistent field approach.

We are interested in the D-dependence of the polymer's configurational free energy. As in the previous two examples we rely on the blob-picture and on equations (92) and (93). Here our extra equation is

$$\xi \approx D \,, \tag{101}$$

i.e. the blob-size is constraint by the tube diameter. Hence

$$F_{conf}(D) \sim k_B T \frac{N}{N_\xi} \approx k_B T N \begin{cases} \left(\frac{b}{D}\right)^2 & (\nu = 1/2) \\ \left(\frac{b}{D}\right)^{5/3} & (\nu = 3/5) \end{cases} . \quad (102)$$

Note that F_{conf} for $\nu = 1/2$ agrees with our previous result (73) obtained using the self-consistent field approach to within a factor. This difference is not surprising, since (i) the scaling approach (usually) does not yield numerical factors and (ii) Eq. (73) was obtained in 1D.

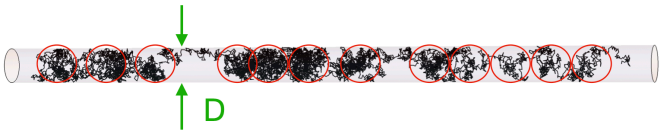

Fig. 26 Polymer confined to a tube.

Remark: There is one detail here which should not escape our attention. By starting from (101) we assume that the condition $bN^\nu \gg D$ is satisfied, or $bN^{1/2} \gg D$ in the case of the ideal chain. In the opposite limit the chain is not constraint by the tube and we cannot expect the above results for $F_{conf}(D)$ to hold. Since we successfully compared $F_{conf}^{(ideal)}(D)$ with the self-consistent field result (73), we should wonder where the condition $bN^{1/2} \gg D$ is hidden in this calculation! The answer is that it is hidden in Eq. (67). The right hand side of (67) is the first term in a sum over terms $\exp[-n\mu_i]\psi_i(x')\psi_i(x)]$, where $i = 0, 1, \ldots$ indicates the eigenvalues and eigenfunctions. Ground state dominance, i.e. the first term is sufficient, here implies $n(\mu_1 - \mu_0) \gg 1$. If we compare Eq. (66) with Schrödinger's equation for the infinite potential well of width D (e.g. R. Hentschke *Introductory Quantum Theory*, section 1.3) we find that the eigenvalues μ_i are given by $\mu_i \sim (b/D)^2(i+1)^2$. Hence, $n(\mu_1 - \mu_0) \gg 1$ implies $nb^2/D^2 \gg 1$!

In summary, the scaling approach involves a certain amount of sound physical observation and intuition. Here the observation is that longer chains appear to form chains of blobs. Therefore the blob's linear dimension ξ becomes the basic length. How the chain of blobs behaves under given circumstances is where the intuition comes in. Using k_BT as the basic energy unit is another important ingredient. Yet another is that the free energy is extensive. Scaling allows to obtain significant results quickly. However, there is the risk that an observation was not sound or the intuition was not good, which produces incorrect results. Therefore it is always good if a comparison with the results obtained by other methods, like the ideal chain results in the above examples, is possible. This then inspires confidence in the new results for real chains.

3.5 Measuring Size and More by Scattering

We have invested considerable effort into the computation of C_∞ (for PE). Therefore we should try and verify our results. This can be done via small angle scattering experiments - for instance using X-rays or neutrons. Visible light also is an option. Note that the 'object's' size here can be quite large, i.e. $\sqrt{\langle R_N^2 \rangle} = \sqrt{C_\infty b^2 N^{2\nu}} \sim 10$ nm (assuming $C_\infty \sim 10$, $b \sim 5$ Å, $N \sim 10^5$, and $\nu = 3/5$)).

Before we begin our discussion of scattering, we take a moment to introduce another measure of size. Even though we had introduced the mean-square end-to-end distance $\langle R_N \rangle$ as being a good measure for 'size' or 'linear dimension', this is not strictly true. For instance, how would we apply this to a branched polymer, which may have many ends? A more general measure for 'size' or 'linear dimension' can be defined via the mean-square **radius of gyration**

$$\langle R_g^2 \rangle = \frac{1}{N} \sum_{i=1}^{N} \langle (\vec{r}_i - \vec{r}_{cm})^2 \rangle \stackrel{*}{=} \frac{1}{N^2} \sum_{i>j}^{N} \langle r_{ij}^2 \rangle , \quad (103)$$

where $\vec{r}_{cm} = N^{-1} \sum_{j=1}^{N} \vec{r}_j$ is the center of mass of the polymer. We leave * as an exercise to the reader. If we use once again $\langle r_{ij}^2 \rangle = b^2|i-j|$, we can easily obtain

$$\langle R_g^2 \rangle = \frac{1}{6} \langle R_N^2 \rangle \quad (104)$$

for ideal linear chains (note: $\sum_{i>j}^{N} |i-j| = (N-1)1 + (N-2)2 + \cdots = \frac{1}{6}(N^2-1)N \approx \frac{1}{6}N^3$).

Now let us turn to scattering. The sketch 27 illustrates the general setup of such experiments. Incoming radiation with momentum $\vec{k}_{in}$ is scattered (elastically) into $\vec{k}_{out}$ by the sample. The momentum transfer or magnitude of the scattering vector $\vec{q}$ is

$$q = \frac{4\pi}{\lambda} \sin(\theta/2) . \quad (105)$$

λ is the wavelength of the the radiation (note: $k_{in} = k_{out} = 2\pi/\lambda$).

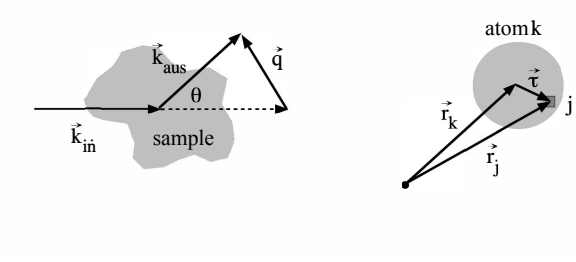

Fig. 27 Left: The scattering vector q resulting from the wave vectors of incoming and outgoing radiation/particles. Right: Definition of the vectors $\vec{r}_i$ and $\vec{r}_j$ and $\vec{\tau}$ in relation to the scattering center (an atom in this case).

When we discussed light scattering in chapter 2 we arrived at Eq. (14) and in particular at

$$P_i(\theta) = \frac{1}{V^2} \int_V d^3r d^3r' e^{i\vec{q}\cdot(\vec{r}-\vec{r}')} \frac{\langle c_w(\vec{r}) c_w(\vec{r}') \rangle}{\langle c_w \rangle^2} . \quad (106)$$

While we arrived at $P_i(\theta)$ by considering the scattering of visible light, this expression also can be used to obtain the angular distribution of scattered intensity for other types of radiation like X-rays or neutrons. There are still other probes like low-energy electron diffraction (LEED), which is used to study solid surfaces under vacuum conditions. In this case (106) is not sufficient, because we must include multiple scattering, i.e. we must go beyond the 1^{st} Born approximation. But fortunately this is not relevant for the study of polymers with electromagnetic radiation or neutrons.

Let's assume we want to calculate the scattering amplitude collected over a volume element ΔV. In the example on the right hand side in Fig. 27 the volume element i at the position $\vec{r}_i$ is occupied by an atom but the same concept can be applied to a molecule or a monomer or even a group of neighboring monomers within a polymer. In any case the scattering amplitude is given by

$$\int_{\Delta V} d^3r\, e^{i\vec{q}\cdot\vec{r}} c(\vec{r}) = \int_{\Delta V} d^3\tau\, e^{i\vec{q}\cdot(\vec{r}_i+\vec{\tau})} c(\vec{\tau}) = e^{i\vec{q}\cdot\vec{r}_i} m f(\vec{q})\,, \qquad (107)$$

where

$$f_i(\vec{q}) = \frac{1}{m}\int_{\Delta V} d^3\tau\, e^{i\vec{\tau}\cdot\vec{q}} c(\vec{\tau}) \qquad (108)$$

is a so called **form factor**. The mass m is given by $m = \int_{\Delta V} d^3\tau\, c(\vec{\tau})$. The form factor sums over the scattering amplitudes from within ΔV. In general $c(\vec{\tau})$ is not merely a mass density as in our case -we developed (106) based on our discussion of light scattering - but it will be a function of the interaction between the probing radiation/particle beam and the atom, monomer etc. with which the radiation/particle beam interacts. Nevertheless, this interaction in general is proportional to the density of atoms, monomers etc. within ΔV, and thus our formalism applies to for instance neutron scattering. Using the form factor we can rewrite $P_i(\theta)$ as

$$P_i(\theta) = \frac{1}{\langle N\rangle^2}\langle \sum_{i,j=1}^{N} f(\vec{q}) f(-\vec{q}) e^{i\vec{q}\cdot\vec{r}_{ij}}\rangle\,, \qquad (109)$$

where $\vec{r}_{ij} = \vec{r}_i - \vec{r}_j$. N is the number of filled volume elements (let's say monomers) in the system. It is a convenient approximation to set the form factor equal to one, i.e. $f(\vec{q}) \to f(0) = 1$. This is reasonable because we shall be interested in the scattering from at least an entire polymer coil, which has a much larger linear dimension than the entities producing the form factor. Due to the reciprocal relation between linear dimension in real space vs. q-space $f(\vec{q})$ varies little in the q-range we are interested in. Thus our final formula for $P_i(\theta)$ becomes

$$P_i(\theta) = \frac{1}{\langle N\rangle^2}\langle \sum_{i,j=1}^{N} e^{i\vec{q}\cdot\vec{r}_{ij}}\rangle\,. \qquad (110)$$

However, there are situations when instead of summing over the positions of monomers we prefer an integration in the continuum. For this purpose we can represent the monomer number density via

$$\rho(\vec{r}) = \sum_{i=1}^{N} \delta(\vec{r} - \vec{r}_i)\,. \qquad (111)$$

Note that $\int_V d^3r...$ yields the same results, i.e. N, on the two sides of this equation. Hence we obtain the following continuum form of Eq. (110):

$$P_i(\theta) = \frac{1}{\langle N\rangle^2}\int_V d^3r d^3r' e^{i\vec{q}\cdot(\vec{r}-\vec{r}')}\langle\rho(\vec{r})\rho(\vec{r}')\rangle\,. \qquad (112)$$

In what follows we shall first employ the discrete summation, i.e. (110), to obtain the angular dependence of the scattering intensity collected from polymer coils, before returning to the continuum formula.

Let's suppose that we momentarily study a closed system in which the number of monomers is constant, i.e. $N = \langle N\rangle$. The meaning of $\langle\sum_{i,j=1}^{N}\ldots\rangle$ in this case is twofold. Suppose someone rotates our sample. Will this change $P_i(\theta)$? No - because we look at many polymers at the same time and our overall system is isotropic. Thus, one piece of $\langle\sum_{i,j=1}^{N}\ldots\rangle$ is an orientation average, keeping the relative positions (and therefore $r_{ij} = |\vec{r}_{ij}|$) of the scattering centers fixed, i.e.

$$\langle e^{i\vec{q}\cdot\vec{r}_{ij}}\rangle_{orient} = \frac{1}{4\pi}\int_0^{2\pi} d\varphi \int_0^{\pi} d\vartheta \sin\vartheta\, e^{iqr_{ij}\cos\vartheta} = \frac{\sin(qr_{ij})}{qr_{ij}}\,. \qquad (113)$$

Here we have used the direction of $\vec{q}$ as our z-direction.

Now suppose we scatter from a single chain for a long time or our scattering intensity is independently contributed from many identical chains. Is r_{ij}, where i and j denote monomers either in the single chain or the i^{th} and j^{th} monomers in each of the many chains, a constant? No, it changes due to conformation changes and our scattering intensity is an average over all possible values of r_{ij} for all pairs ij. Hence

$$\langle e^{i\vec{q}\cdot\vec{r}_{ij}}\rangle = \langle\frac{\sin(qr_{ij})}{qr_{ij}}\rangle_{conf} = \int d^3r_{ij} p(r_{ij})\frac{\sin(qr_{ij})}{qr_{ij}}\,, \qquad (114)$$

where $p(r_{ij})$ is the normalized probability density that the distance between i and j is r_{ij}. So, how do we find $p(r_{ij})$?

Scattering from Ideal Chains:

The answer depends on the level of approximation we chose. Eq. (81) gives $p(r_{ij})$ when i and j are the monomers at the chain's ends. But if i and j are inside the chain we can still use Eq. (81). Instead of the end-to-end distance R we now substitute the i-to-j distance r_{ij} and n becomes $|i-j|$, i.e.

$$p(r_{ij}) = \left(\frac{3}{2\pi|i-j|b^2}\right)^{3/2}\exp\left[-\frac{3}{2}\frac{r_{ij}^2}{|i-j|b^2}\right]\,. \qquad (115)$$

Inserting (115) into (114) yields

$$\langle e^{i\vec{q}\cdot\vec{r}_{ij}}\rangle = \exp[-|i-j|b^2q^2/6]\,. \tag{116}$$

Hence

$$\begin{aligned} P_i(\theta) &= \frac{1}{N^2}\sum_{i,j=1}^{N} e^{-|i-j|b^2q^2/6} \\ &\stackrel{*}{=} \frac{1}{N^2}\frac{\left(N(e^{2a}-1)+2e^a(e^{-aN}-1)\right)}{(e^a-1)^2}\,, \end{aligned} \tag{117}$$

where $a = b^2q^2/6$ (*: here I use Mathematica to do the summation). Note that the summation is analogous to the one in Eq. (44). If $a \ll 1$ we can use $e^a \approx 1+a$ and keeping the leading order only we obtain

$$P_i(\theta) \approx \frac{2(e^{-x}+x-1)}{x^2} \to \begin{cases} \frac{2}{x} & (x \gg 1) \\ 1-\frac{1}{3}x & (x \ll 1) \end{cases}\,. \tag{118}$$

Here $x = aN = q^2\langle R_g^2\rangle$. This formula was first derived by P. Debye in 1947. Note that $x \gg 1$ is sensible, despite our previous assumption $a \ll 1$, when N is sufficiently large. The limit for $x \ll 1$ is known as **Guinier's law**. Debye's formula and its two limits are depicted in Fig. 28. Note that at $x \sim 1$ the intensity shows the strongest change as we had stated above. We may say that Debye's formula, or Guinier's law for that matter, is the form factor of a polymer based on (81). In the limit $x \ll 1$ or $q^2\langle R_g^2\rangle \ll 1$ we look at the whole polymer, whereas in the limit $x \gg 1$ or $q^2\langle R_g^2\rangle \gg 1$ we look at the Gaussian structure inside.

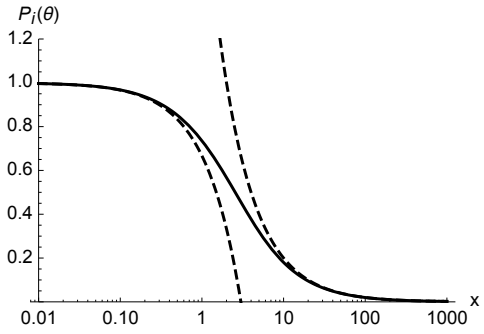

Fig. 28 $P_i(\theta)$) vs. x according to Eq. (118). The dashed lines show the two limiting forms.

But let us now return to our original motivation, the experimental confirmation of our calculation for C_N. We introduce the characteristic ratio $C_N \approx C_\infty$ into (118) realising that b^2N is just $\langle R_N^2\rangle$ and using its generalization (26) (with $\nu = 1/2$) we now consider b a bond length and x becomes $x = q^2C_\infty N/6$, where, in addition, we also use b as the unit of length, i.e. q is now in units of $1/b$. Consequently, a plot of $q^2NP_i(\theta)$ should yield a plateau of the data, i.e. $q^2NP_i(\theta) \to 12/C_\infty$ for large q (note: 'large q', as we shall see shortly, really means 'intermediate q' for real chains). Such experimental results are shown in Fig. 29. Here the reduced intensity is multiplied by q^2 in order to bring out the 'Gaussian plateau', which is called **Kratky plot**. Note that Eq. (118) is a good approximation to the experimental data and $C_\infty \approx 7$ is in good accord with our result obtain from the RIS/TM method for this temperature.

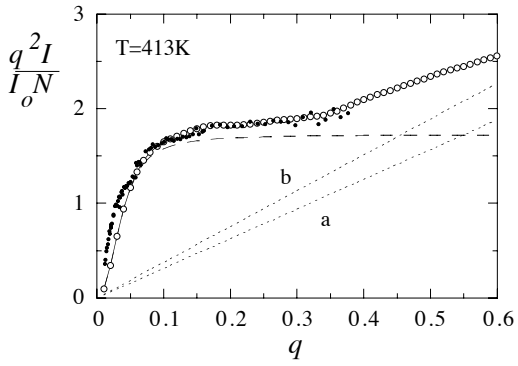

Fig. 29 Kratky plot of the reduced scattering intensity obtained from polyethylene in the melt by small-angle neutron scattering (G. Lieser, E. W. Fischer, K. Ibel J. Polym. Sci., Polym. Lett. *13*, 39 (1975)). Here $I/(I_oN) = NP_i(\theta)$ and $q = q_{exp}b$ with $b = 1.53$ Å. The data are the solid dots. The long-dashed line shows Eq. (118) using $C_\infty \approx 7$. The open symbols were obtained using the RIS/TM method to build chains as explained in the text. The two straight dotted lines labeled a and b correspond to straight rows of C-atoms spaced 1 unit (a) or $\cos 34°$ units (b) apart.

Fig. 29 contains also open circles, which appear to be close to the actual data - closer than (118). Where do the open symbols come from? The answer brings us back to Eq. (114) and to the average over chain conformations. Suppose we generate many independent conformations of 'united atom' PE chains by some method - we explain the method below. We then compile a histogram of distances r_{ij} between pairs of united-atom carbon atoms (scattering centers) within each chains and average all the histograms. The result is $n(r,\Delta r)$ shown in Fig. 30. Here Δr is the bin width and r is the distance between pairs corresponding to this bin. Note the numerous 'spikes' at small r. There must be, for instance, a pronounced spike at $r = 1$, because there are $N-1$ pairs separated by exactly one bond distance. At small C-C separations the PE chain is not really a random walk and these separations are not yet 'fuzzy' as they are when the separations between C-atoms become large.
Using $n(r,\Delta r)$ the scattering intensity becomes

$$P_i(\theta) \approx \frac{1}{N^2}\sum_k n(\Delta rk,\delta r)\frac{\sin(q\Delta rk)}{q\Delta rk}\,. \tag{119}$$

Here the k-summation is over all bins and $r = \Delta rk$. We also omit a term $\propto N$.

In order to better understand what is happening for $q > 0.35$, we must look at the next figure, Fig. 31, which shows Kratky plots for PE chains of very different length. All curves apparently converge when q becomes large. This is because at large q we

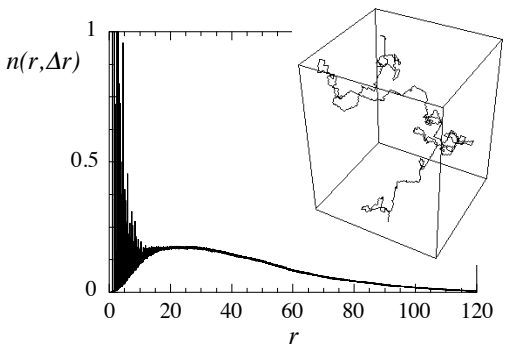

Fig. 30 Distance distribution $n(r,\Delta r)$ (shown here truncated at 1) compiled from hundred PE chain conformations at $T = 413$ K using $\Delta r = 0.01$ (in units of the C-C bond length) and $N = 1000$. The inset depicts a selected conformation.

are probing short distances in real space and on short distances a short chain differs little from a long chain. When q is decreased, however, we begin to probe larger and larger distances in real space and a $N = 20$-chain then differs greatly from a $N = 1000$-chain. For PE to be well represented by a Gaussian random walk, i.e. by (115), we need chains containing at least several hundred effective C-atoms. By the way, the two straight dotted lines labeled a and b in Fig. 29 represent Kratky plots of straight rows of C-atoms spaced 1 (a) unit or $\cos 34°$ (b) units apart.

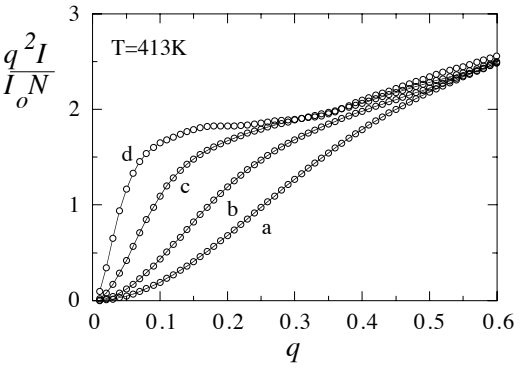

Fig. 31 Kratky plot of the reduced scattering intensities (note: $I/(I_o N) = NP_i(\theta)$) for numerically generated chains of different length: $N = 20$ (a), $N = 50$ (b), $N = 200$ (c), and $N = 1000$ (d).

What is the construction method for the chain conformations used to generate the open symbols-results in Figs. 29 and 31? Since we want to generate PE chains we use $\phi = 112\pi/180$. The torsion angles are $\vartheta_{g-}, \vartheta_t$ and ϑ_{g+}, which we had used when we discussed the transfer matrix-method. We also use the potential energy functions (36) and (60). The bond length is the unit of length. Finally, $P(l \mid k) \equiv P(lk)/P(k)$ is the conditional probability that torsion angle l follows after torsion angle k.

For any number of torsion angles the algorithm is the following:

1. Generate a uniform random number z in the interval $[0,1]$.
2. Continue an existing chain, whose last torsion angle is $\vartheta^{(k)}$, with the new torsion angle

$$\begin{array}{lll} \vartheta^{(1)} & \text{if} & z \le P(1 \mid k) \\ \vartheta^{(2)} & \text{"} & P(1 \mid k) < z \le P(1 \mid k) + P(2 \mid k) \\ \vartheta^{(3)} & \text{"} & P(1 \mid k) + P(2 \mid k) < z \le P(1 \mid k) + P(2 \mid k) + P(3 \mid k) \\ \vdots & \vdots & \vdots \\ \vartheta^{(m)} & \text{if} & P(1 \mid k) + \ldots + P(m-1 \mid k) < z\,. \end{array}$$

   The new bond vector $\vec{b}_{i+1}$ is then generated via $\vec{e}_{i+1} = -\vec{e}_i \cos\phi + \vec{e}_i \times \vec{e}_{i-1} \sin\vartheta^{(l)} - (\vec{e}_i \times \vec{e}_{i-1}) \times \vec{e}_i \cos\vartheta^{(l)}$, based on its predecessors. The $\vec{e}$ are unit vectors along the bonds indicated by the subscripts. [Start the chain from two arbitrary but not parallel vectors, e.g. $\vec{e}_{-1} = (1,0,0)$ und $\vec{e}_0 = (0,1,0)$].
3. Continue with step 1 while $i+1$ is less than the desired chain length.

In the present case we can use the probabilities according to Eq. (59) instead of the full conditional probabilities.

Perhaps you are puzzled by the following question regarding the actual experiment. If the sample is a dense melt, how can we be sure that the two scattering centers i and j do belong to the same chain? The answer is that the experimentalists use a mixture of protonated and deuterated polymers. A small amount of chains in which deuterium replaces the ordinary hydrogen is mixed into a much larger amount of ordinary chains. The diluted and thus isolated deuterated polymers provide a much stronger contrast and 'outshine' the protonated polymers. This does not work with X-rays (or visible light) since the latter interact with the electron shells.

Static Light Scattering Revisited:

This is a good point to return to our discussion of light scattering in chapter 2 and in particular to Eq. (18). Eq. (18) can be combined with Eq. (118) plus a third piece into a new equation which is used to obtain the weight average molar polymer mass, the radius of gyration and the second osmotic virial coefficient in a widely used standard procedure called the **Zimm plot** (B.H. Zimm *Apparatus and methods for measurement and interpretation of the angular variation of light scattering; preliminary results on polystyrene solutions*, J. Chem. Phys. *16*, 1099 (1948)). We first write down this equation, then provide a justification for it and finally discuss its use. The equation is

$$\frac{K\langle c_w\rangle}{R_\theta} = \left(1 + \frac{1}{3}q^2\langle R_g^2\rangle\right)\left(\frac{1}{\bar{M}_w} + 2A_2\langle c_w\rangle\right)\,. \qquad (120)$$

The first term in brackets on the right hand side results if we approximate $P_i(\theta)$ by Guinier's law from Eq. (118). The sign is different because we use $(1-z)^{-1} \approx 1+z$ for small z. The second factor, i.e. $(1/\bar{M}_w + 2A_2\langle c_w\rangle)$, requires additional work however.

In order to find this factor we must look at $P_i(\theta)$ in its form in Eq. (112), i.e.

$$P_i(\theta) = \frac{1}{\langle \nu_1 \rangle^2} \frac{1}{V^2} \int_V d^3r d^3r' e^{i\vec{q}\cdot(\vec{r}-\vec{r}')} \langle \nu_1(\vec{r}) \nu_1(\vec{r}') \rangle \,, \qquad (121)$$

where we use $N = m_1 \nu_1$. m_1 is the number of monomers within a polymer and ν_1 is the number of polymers. You may object to this because we just stated 'The first term in brackets on the right hand side results if we approximate $P_i(\theta)$ by Guinier's law from Eq. (118)', which would mean that we have taken care of $P_i(\theta)$ already. This is not quite right though. What we have done thus far means that we have included the scattering from single chains. However, if we look at our system on a much larger scale we begin to include more and more polymers. The situation is comparable to what we did when we discussed the form factor of a monomer. Guinier's law here essentially is the form factor of a polymer. Now we are interested in the contribution to the scattering intensity on this much larger scale - in fact we are looking at an infinite volume in which the polymer mass density nevertheless is $\langle c_w \rangle$ on average. This means we want to compute $P_i(\theta)$ in the limit $\vec{q} \to 0$. In this limit (121) becomes

$$P_{i,f}(0) = \frac{1}{\langle \nu_1 \rangle^2} \frac{1}{V^2} \int_V d^3r d^3r' \langle \nu_1(\vec{r}) \nu_1(\vec{r}') \rangle \,. \qquad (122)$$

Note in particular that we are dealing with an open system in which the number of polymers ν_1 fluctuates. ν_1 is given by

$$\nu_1 = \frac{1}{V} \int_V d^3r \, \nu_1(\vec{r}) \,. \qquad (123)$$

Hence

$$P_{i,f}(0) = \frac{\langle \nu_1^2 \rangle}{\langle \nu_1 \rangle^2} \,. \qquad (124)$$

In standard textbooks on Statistical Mechanics or Statistical Thermodynamics (e.g. R. Hentschke *Thermodynamics* (2nd ed.), section 5.3.2) the quantity $\langle \nu_1^2 \rangle$ is discussed in the context of the grand canonical ensemble applied to a one-component system in which the particle number can fluctuate. Here our system is a solute in a solvent but the general computation remains the same - except that the chemical potential becomes the chemical potential of the solute and the pressure becomes the osmotic pressure, i.e.

$$\langle \nu_1^2 \rangle = \frac{\partial \langle \nu_1 \rangle}{\partial(\beta\mu_1)}\Big|_{\beta,V} = \frac{1}{-\beta \frac{V^2}{\langle \nu_1 \rangle^2} \frac{\partial \Pi_1}{\partial V}\big|_{\beta,\langle \nu_i \rangle}} \,, \qquad (125)$$

where μ_1 is the polymer chemical potential and $\beta = (k_B T)^{-1}$. In section 4.4 we shall discuss the osmotic pressure of polymers in solution. We shall see that

$$\Pi_1 = \frac{1}{\beta} \left[\frac{\langle \nu_1 \rangle}{V} + B_2 \left(\frac{\langle \nu_1 \rangle}{V} \right)^2 + \mathcal{O}\left(\left(\frac{\langle \nu_1 \rangle}{V} \right)^3 \right) \right] \qquad (126)$$

in the limit of small polymer concentration and therefore

$$\langle \nu_1^2 \rangle = (1 + 2B_2 \langle c_w \rangle / \bar{M}_w)^{-1} \langle \nu_1 \rangle \,. \qquad (127)$$

Hence

$$P_{i,f}(0) = (1 + 2B_2 \langle c_w \rangle / \bar{M}_w)^{-1} \langle \nu_1 \rangle^{-1} \qquad (128)$$

(note: $A_2 = B_2/(\bar{M}_w)^2$). The final step consist in the approximation

$$P_i(\theta) \approx P_{i,G}(\theta) P_{i,f}(0) \,, \qquad (129)$$

which means that we approximate the total $P_i(\theta)$ by the product of the Guinier law, $P_{i,G}(\theta)$, with $P_{i,f}(0)$ due to the number fluctuations of the number of polymers in the volume. In other words, we assume that the shape of the scattering intensity is well described by Guinier's law and the leading q-independent correction is contributed by the polymer-polymer interaction expressed in terms of the second osmotic virial coefficient. Fig. 32 shows light scattering intensity obtained form a linear polymer in solution at variable concentrations including 0.033, 0.052, 0.097, 0.142, 0.194, 0.288, 0.391, and 0.530 g/dL from bottom to top. Note that the mass average molecular weight of the polymer is $7.47 \cdot 10^6$ g/mol. The data are reasonably linear - and therefore in line with our 'ad hoc approximation (129) - only for the lowest polymer concentrations.

Let's discuss how to use Eq. (120). We could for instance try to make a plot of $\frac{K\langle c_w \rangle}{R_\theta}$ vs. $\langle c_w \rangle$ at $q = 0$. From the intercept of a line through the data with the y-axis we would find $1/\bar{M}_w$ and the slope would be $2A_2$. However, data at $q = 0$ are not available, since this means looking directly into the incoming beam. Likewise we cannot plot $\frac{K\langle c_w \rangle}{R_\theta}$ vs. q^2 at $\langle c_w \rangle = 0$ to obtain $1/\bar{M}_w$ from the intercept and $\langle R_g^2 \rangle/(3\bar{M}_w)$ from the slope. Without polymer we cannot make this measurement. Instead, measurements are carried out which yield $\frac{K\langle c_w \rangle}{R_\theta}$ for a series of non-zero concentrations and non-zero scattering angles as shown in the Zimm plot of Fig. 33. The trick is that on the x-axis it is not just q^2 but $q^2 + c_o \langle c_w \rangle$ which is plotted, where c_o is an arbitrary constant. This shift of q^2 will not change the slope or intercept of the $c_w = 0$-line, which we construct by drawing a line parallel to the thin blue lines through the data for $\langle c_{w,1} \rangle$, $\langle c_{w,2} \rangle$ and $\langle c_{w,3} \rangle$. However, this line is subject to a constraint. The constraint is that the line, the thick red line in Fig. 33, must, on the y-axis, intersect with another line, the thick blue line, drawn parallel to the red lines through the data for q_1, q_2 and q_3. This is because for $\langle c_w \rangle = q = 0$ we must have $\frac{K\langle c_w \rangle}{R_\theta} = 1/\bar{M}_w$ (independent of c_o!). Hence the Zimm plot yields the desired information, i.e. $\bar{M}_w$, $\langle R_g^2 \rangle$ and B_2. Remark 1: The procedure also works if fitting the data requires slightly bent lines! Remark 2: An expression for B_2 in Eq. (120) is given in Eq. (179) in the context of osmotic pressure in a dilute polymer in a solvent computed using a mean field lattice model.

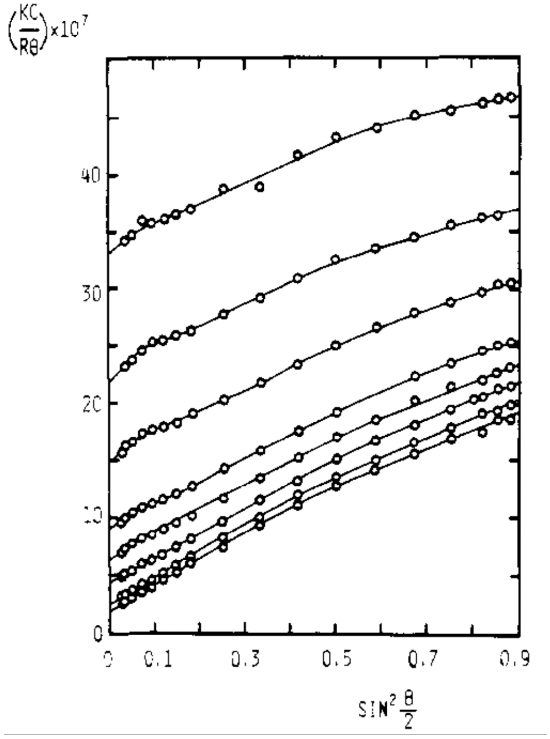

Fig. 32 Light scattering intensity from from poly(α-methylstyrene) in toluene at 25° C. (copied from Fig. 1 in I. Noda et al. *Thermodynamic Properties of Moderately Concentrated Solutions of Linear Polymers* Macromolecules *16*, 668 (1981)).

Scattering from Non-ideal Chains:

Thus far we have sidestepped the exponent ν. What is the effect of $\nu \neq 1/2$ on the scattering intensity? Or in other words, how can we determine ν from scattering experiments?

Equation (95) tells us essentially what $p(R)$ is, i.e. the $p(r)$ which for intersecting random walks or ideal chains is given by (81). Note that (95) is a configuration free energy equal to $-TS_{conf} = -Tk_B \ln p(R) + const$. This immediately tells us

$$p(R) \propto \exp[-k_\nu (R/bN^\nu)^{1/(1-\nu)}] \,, \tag{130}$$

where k_ν is a factor which equals 3/2 if $\nu = 1/2$. We can try and use this $p(R)$ to express $p(r_{ij})$ in Eq. (114) and then proceed as before with the calculation of the scattering intensity. However this is quite tedious and another approach is better and provides more physical insight.

Before we start, let us briefly look at the effect of ν on $\langle R_g^2 \rangle$. We make a short calculation, i.e.

$$\sum_{i>j}^{N} |i-j|^{2\nu} = (N-1)1^{2\nu} + (N-2)2^{2\nu} + \ldots$$

$$\approx \int_1^N dx (N-x) x^{2\nu} \approx \frac{N^{2\nu}}{(2\nu+1)(2\nu+2)}$$

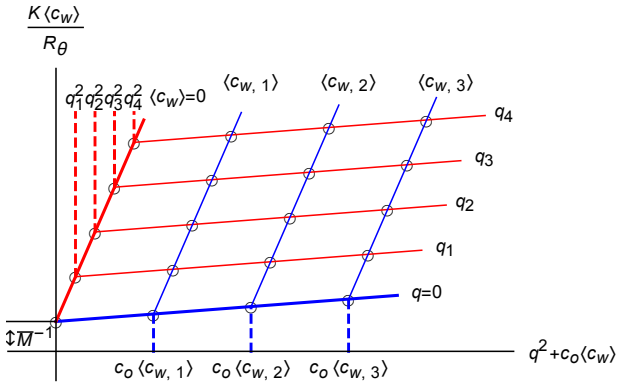

Fig. 33 Illustration of a Zimm plot.

for large N. Hence, in this limit, we have

$$\langle R_g^2 \rangle \propto N^{2\nu} \,. \tag{131}$$

In other words, it does not really matter here whether we look at a linear polymer or maybe a polymer with a more complex architecture.

What we have is the general relation

$$n \sim r^{1/\nu} \,. \tag{132}$$

The quantity n is the number of monomers or Kuhn segments we expect to find inside a circle with radius r. Ordinarily we expect the number of things to increase with the d^{th} power in a d-dimensional uniform system. In a poor solvent in three dimensions, for instance, in which the polymer collapses into essentially a dense drop, we have $1/\nu = 3$ (cf. Tab. 5). Here, however, we usually look at systems possessing regions, which come in all sizes, devoid of monomers or Kuhn segments. We can tell because generally $1/\nu < d$. We are looking therefore at **fractals** and

$$d_f \equiv 1/\nu \tag{133}$$

is their **(mass) fractal dimension**.

So, how do we calculate the scattering intensity of a fractal structure based on (132)? We can use Eq. (119). Remember that $n(\Delta rk, \Delta r)$ is the number of scatterers in a shell of thickness Δr and radius r. Based on (132) this means that

$$n(r, dr) \sim r^{d_f - 1} \,, \tag{134}$$

where we have made the transition to the infinitesimal form, $\Delta r \to dr$ and $\Delta rk \to r$. Consequently the summation of k is replaced by an integration over r, i.e. $\sum_k \to \int dr$. Hence

$$I(q) \sim \int_0^\infty dr\, r^{d_f - 1} e^{-r/\xi} \frac{\sin(qr)}{qr} \,. \tag{135}$$

The exponential is a convenient cutoff, accounting for the finite-

ness of the fractal. Using $x = qr$ this becomes

$$I(q) \sim \frac{1}{q^{d_f}} \int_0^\infty dx x^{d_f-1} e^{-x/(q\xi)} \frac{\sin x}{x} \sim q^{-d_f} \text{ if } q \gg \xi^{-1} . \quad (136)$$

The integral is a slowly varying function of $q\xi$ if this quantity is significantly larger than unity, i.e. this condition means that we are looking inside the fractal objects. Clearly, there is another limit if q becomes 'too large'. 'Too large' here means that we begin to see the details within the fractal which themselves possess a different structure. But in the intermediate regime $I \sim q^{-d_f}$ or in the case of polymers

$$I(q) \sim q^{-1/\nu} \quad (137)$$

holds.

If we apply this formula to the ideal chain or $\nu = 1/2$ we find $q^2 I(q) \sim const$, which is the plateau of the dashed line in Fig. 29. Real chains in three dimensions would yield $q^2 I(q) \sim q^{1/3}$ instead. Note that the experimental data in this figure indeed exhibit a slow increase. But this increase is also obtained with the transfer matrix model, which produces again ideal chains. Thus, in this case, the slow increase in the 'plateau regime' is likely due to the steeper increase at still larger q, where the observed objects do not posses the expected fractal structure. In addition, other experiments have confirmed that chains in melts are indeed ideal chains (e.g. D. Ballard et al. Eur. Polymer J. *9*, 965 (1973), J. P. Cotton et al. Macromolecules *7*, 863 (1974), R. Kirste et al. Polymer *16*, 120 (1975)). The general idea is to carry out experiments in a sufficiently wide q-range, either on melts or polymer solutions, and then plot $\ln I(q)$ vs. $\ln q$. This should yield a straight line with slope $-1/\nu$ in the proper q-range. Also possible are plots where the inverse intensity is plotted vs. $q^{5/3}$ as in Fig. 34. This is an example of a study where the authors look at the cross-over between $\nu = 1/2$ vs. $\nu = 3/5$ in solutions at variable polymer concentration.

Overlap Concentration:

A concentration of particular importance is the **overlap concentration** ρ^* at which the individual volumes of isolated polymers begin to overlap. Intuitively this should happen when the overall monomer concentration is the same as the monomer concentration within the volume occupied by the isolated polymer, i.e.

$$\rho^* = \frac{N}{R_g^d} \sim \frac{N}{N^{d\nu}} = N^{1-d\nu} . \quad (138)$$

Here $R_g \equiv= \sqrt{\langle \vec{R}_g^2 \rangle}$. For $d = 3$ this means $\rho^* \sim N^{-1/2}$ when the chains are ideal and $\rho^* \sim N^{-4/5}$ when they are not. Note that ρ^* is very small when the chains are long. Another important quantity by which the solvent quality itself can be controlled is temperature.

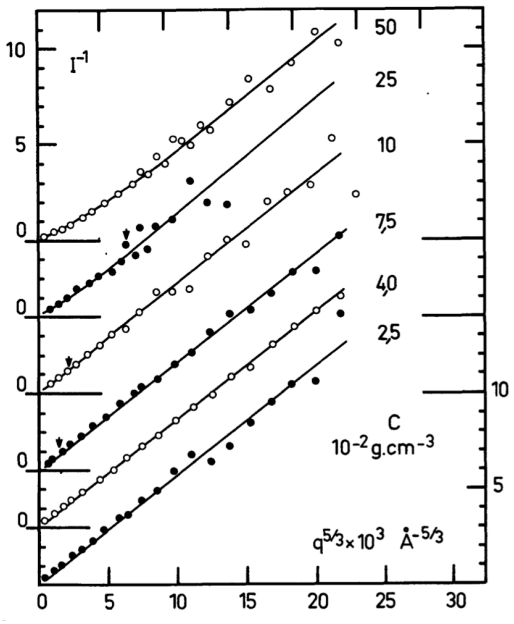

Fig. 34 Inverse scattering intensity vs. momentum transfer raised to the power 5/3 from Fig. 2 in B. Farnoux, F. Boue, J. P. Cotton, M. Daoud, G. Jannink, M. Nierlich, P. G. De Gennes *Cross-over in polymer solutions.* Journal de Physique *39*, 77 (1978). The polymer is polystyrene dissolved in carbon disulfide. The data sets are results for a fixed concentration of deuterated PS (0.005 g cm^{-3} within an overall variable amount of protonated PS.

Question: What is ρ^* in the system for which light scattering data are shown in Fig. 32? Assume 'good solvent'. You should find that ρ^* is less or at best about equal to the lowest of the concentrations in that figure.

However, we want to move on and not get overwhelmed by what can be done and a multitude of power laws. Additional information on the topic of scattering from polymers can be found in a book edited by O. Glatter and O. Kratky (Small Angle X-ray Scattering, Academic Press, 1982) - in particular in the article by R.G. Kirste and R.C. Oberthur (Synthetic Polymers in Solution) or in G. Strobl *The Physics of Polymers*, Springer.

4 Thermodynamics of Blends, Solutions, and Networks

What follows, at first glance, may appear unrelated to our exposition of single chain statistical thermodynamics. This is because the focus is no longer on conformations of single chains or quantities like the end-to-end distance or the radius of gyration but rather on the 'combinatorial' or 'packing' entropy of many chains in a certain volume as well as on their free enthalpy. In the following we develop a simple mean field theory on the lattice, which nevertheless can be applied to blends, solutions, and networks. There are cases when our results will not be correct and will have to be revised. However, the lattice approach is certainly worthwhile since it provides an overview without immediately blinding us with complexity.

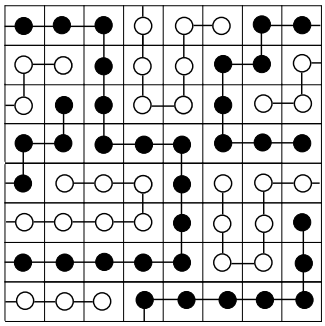

Fig. 35 Binary mixture of linear polymers represented by paths on a lattice.

4.1 A Lattice Model for Polymer Mixtures and Solutions

In the following we study binary mixtures assuming that the two components are linear polymers. We know already that a simple but instructive approximation of a linear polymer is a path on a lattice as depicted in Fig. 35. Note that this figure is quite similar to Fig. 22, except that here we do not focus on the end-to-end distance. The lattice is a square lattice and every lattice cell contains one straight polymer segment or Kuhn segment. Kuhn segments belonging to the same polymer are connected by a solid line. The solid and hollow circles indicate two chemically different types of Kuhn segments. In the following we consider ν_i polymers of type i with length (or 'mass') m_i ($i = 1,2$) Kuhn segments. This means that all polymers of type i posses the same length, i.e. they are monodisperse. In reality (technical) polymers are polydisperse, i.e. they do have a distribution of lengths. Here we avoid this complication. There are $N = N_1 + N_2$ Kuhn segments total ($N_i = m_i \nu_i$) and N is equal to the number of lattice cells (Here and in the following we use N or N_i to count Kuhn segments, because n or n_i is reserved for the number of moles of a species). This means that the lattice is fully occupied.

Having specified our model we want to estimate the number of distinct polymer configurations on the lattice:

(i) We proceed by severing all bonds connecting the Kuhn segments in each polymer chain. The individual Kuhn segments, which we consider distinguishable at this point, are then placed on an empty but otherwise identical lattice. There are $N!$ ways to accomplish this.

(ii) Now we ask: What is the probability that in one such configuration all Kuhn segments do have the same neighbors which they had before?

We first approximate the probability that a particular Kuhn segment is placed in a cell next to its polymer-neighbor Kuhn segment via

$$\left(\frac{q-1}{N}\right)^{m_1-1} \qquad \text{or} \qquad \left(\frac{q-1}{N}\right)^{m_2-1} .$$

Here q is the coordination number of the lattice. This is the number of neighbors each cell has. On a square lattice $q = 4$; on a simple cubic lattice $q = 6$. This means that if we have a polymer partially laid out on the lattice and we put the next Kuhn segment, of which we know that it is the neighbor in the polymer, down on the lattice blindfolded, then there are $q-1$ "good" cells compared to N cells total. Of course we neglect occupancy of the cells by previous Kuhn segments - a truly crude approximation. Nevertheless we approximate the above probability as

$$\left(\frac{q-1}{N}\right)^{(m_1-1)\nu_1} \left(\frac{q-1}{N}\right)^{(m_2-1)\nu_2} .$$

(iii) This number we multiply with $N!$, the total number of configurations. But we also must divide by the product $\nu_1!\nu_2!$, because two polymers of the same type are indistinguishable. All in all we find that the number of distinguishable ways to accommodate the polymers on the lattice, Ω, may be approximated via

$$\Omega \approx \frac{N!}{\nu_1!\nu_2!} \left(\frac{q-1}{N}\right)^{(m_1-1)\nu_1} \left(\frac{q-1}{N}\right)^{(m_2-1)\nu_2} . \tag{139}$$

We can now work out the entropy, which is the configuration entropy, via

$$S = k_B \ln \Omega . \tag{140}$$

Using the Stirling formula, i.e.

$$\ln N! \approx N\ln N - N + \ln\sqrt{2\pi N} \approx N\ln N - N \quad \text{(if } N \text{ is large)} , \tag{141}$$

we obtain

$$\begin{aligned} \frac{S}{Nk_B} &= -\frac{\phi_1}{m_1}\ln\frac{\phi_1}{m_1} - \frac{\phi_2}{m_2}\ln\frac{\phi_2}{m_2} \\ &\quad + \left[(1-\frac{1}{m_1})\phi_1 + (1-\frac{1}{m_2})\phi_2\right]\ln\frac{q-1}{e} , \end{aligned} \tag{142}$$

where $\phi_i = N_i/N$.

Before we discuss this, we compute the entropy of mixing given by

$$\frac{\Delta S}{k_B} = -\nu_1 \ln\phi_1 - \nu_2 \ln\phi_2 . \tag{143}$$

This is the entropy change if we combine two lattices of size N_1 and N_2, each filled with the respective polymers of type 1 and 2, into one lattice of size $N = N_1 + N_2$, i.e.

$$\Delta S = S - S_1 - S_2 , \tag{144}$$

where $S_i = k_B \ln \Omega_i$ and

$$\Omega_i \approx \frac{N_i!}{\nu_i!} \left(\frac{q-1}{N_i}\right)^{(m_i-1)\nu_i} . \tag{145}$$

Using again $\nu_i = N_i/m_i$ and $\phi_i = N_i/N$ Eq. (143) becomes

$$\frac{\Delta S}{Nk_B} = -\frac{\phi_1}{m_1}\ln\phi_1 - \frac{\phi_2}{m_2}\ln\phi_2 \,. \tag{146}$$

Interaction on the Lattice:

Thus far we have only expressions for the configuration entropy and the attendant configuration entropy of mixing. We still need to construct an expression for the interaction free enthalpy in a binary system.

The likelihood for a lattice site to be occupied by a 1- or a 2-polymer is ϕ_1 or ϕ_2, respectively. For a 2-polymer it is ϕ_2. The number of $1-2$-contacts (neighboring segments) is given by

$$\approx \phi_1\phi_2 Nq \,.$$

Analogously we obtain for the average number of $1-1$- and $2-2$-contacts

$$\approx \frac{1}{2}\phi_1\phi_1 Nq$$

and

$$\approx \frac{1}{2}\phi_2\phi_2 Nq \,,$$

respectively. The factor $1/2$ prevents overcounting of contacts. Finally we assign each type of contact an interaction free enthalpy g_{12}, g_{11} and g_{22}. Hence the total interaction free enthalpy becomes

$$G_i = \left(g_{12}\phi_1\phi_2 + \frac{1}{2}g_{11}\phi_1^2 + \frac{1}{2}g_{22}\phi_2^2\right)Nq \,. \tag{147}$$

This is not yet the final expression since it is common to use the following definitions:

$$\chi \equiv -\frac{q}{2k_BT}\left(g_{11} + g_{22} - 2g_{12}\right) \tag{148}$$

$$\chi_1 \equiv -\frac{q}{2k_BT}g_{11} \tag{149}$$

$$\chi_2 \equiv -\frac{q}{2k_BT}g_{22} \,. \tag{150}$$

This means that Eq. (147) becomes

$$\frac{G_i}{Nk_BT} = \chi\phi_1\phi_2 - \left(\chi_1\phi_1 + \chi_2\phi_2\right)\phi \,. \tag{151}$$

The the first term is the interaction free enthalpy of mixing

$$\frac{\Delta G_i}{Nk_BT} = \chi\phi_1\phi_2 \,. \tag{152}$$

This agrees with our intuition, because $-g_{11} - g_{22} + 2g_{12}$ means that the formation of two $1-2$-contacts comes at the expense of one $1-1$- and one $2-2$-contact.

The combination of Eqs. (146) and (152) yields

$$\Delta g \equiv \frac{\Delta G}{Nk_BT} = \frac{\Delta G_i}{Nk_BT} - \frac{\Delta S}{Nk_B} \tag{153}$$

and thus the important equation

$$\Delta g = \frac{\phi_1}{m_1}\ln\phi_1 + \frac{\phi_2}{m_2}\ln\phi_2 + \chi\phi_1\phi_2 \,. \tag{154}$$

This is the **Flory-Huggins equation** for a binary polymer mixture or for a polymer in solution. The quantity χ is the **Flory-Huggins parameter**.

Remark: You may wonder why we do not call the g_{ij} simply interaction 'energy' or interaction 'enthalpy'. The point is that we add these expressions to $(-T\times)$ the configuration entropy or the configuration entropy of mixing to obtain the full enthalpy or enthalpy of mixing. However, $S = -dG/dT|_{P,n_i}$ and since the g_{ij} themselves may at some point depend on T (if the fit of the theory to the data requires it) this would mean that the g_{ij} themselves contribute to the entropy.

The lattice approach outlined here was pioneered independently by Staverman and van Santen (A. J. Stavermann, J. H. van Santen, Rec. Trav. Chim. *60*, 76 (1941)), Huggins (M. L. Huggins, J. Chem. Phys. *9*, 440 (1941); Ann. NY Acad. Sci. *43*, 1 (1942)) and Flory (P. J. Flory, J. Chem. Phys. *9*, 660 (1941); *10*, 51 (1942)) (cf. R. Koningsveld, L. A. Kleintjens *Fluid phase equilibria in macromolecular systems.* Acta Polymerica *39*, 341 (1988)).

4.2 Phase Separation in Polymer Mixtures

Before we come to the subject proper, we want to look at two special types of phase separation.

A Digression - One-component Gas-Liquid Phase Behavior:

Eqs. (142) and (146) can be applied to a number of interesting situations. We introduce the replacements $\phi_1 = \phi$, $m_1 = m$, and $\phi_2 = 1-\phi$. In addition we assume $m_2 = 1$. This corresponds to polymers in a solvent, where the index 2 indicates the solvent. The resulting configuration entropy is

$$\frac{S_{conf}}{nR} = -\frac{\phi}{m}\ln\frac{\phi}{m} - (1-\phi)\ln(1-\phi) + \phi\left(1-\frac{1}{m}\right)\ln\frac{q-1}{e} \,. \tag{155}$$

If we replace the solvent cells by empty cells, we describe the same type of physical situation described by the van der Waals equation. Here the total volume is $V = bN$, where b, the cell size, also is the monomer size. We may obtain the attendant configurational pressure via

$$P_{conf} = -\frac{\partial}{\partial V}(-TS_{conf})\Big|_T = \frac{RT}{N_A b}\left[-\phi\left(1-\frac{1}{m}\right) - \ln(1-\phi)\right] \,. \tag{156}$$

Analogous to the van der Waals approach we must add a term accounting for attractive interaction between the monomers. Our choice, in analogy to the van der Waals equation of state, is

$$\frac{N_A bP}{RT} = \frac{N_A bP_{conf}}{RT} - \frac{1}{2}\frac{N_A \varepsilon_o}{RT}\phi^2 \,. \qquad (157)$$

Here $\varepsilon_o > 0$ is a parameter.

The closeness of this and the van der Waals equation of state becomes even more clear if we compute the gas-liquid critical parameters via $\frac{\partial P}{\partial V}\,|_T = \frac{\partial^2 P}{\partial V^2}\,|_T = 0$. We find

$$T_c = \frac{N_A \varepsilon_o}{R}\frac{m}{(\sqrt{m}+1)^2} \qquad (158)$$

$$\phi_c = \frac{1}{\sqrt{m}+1} \qquad (159)$$

$$\frac{bP_c}{\varepsilon_o} = \frac{\frac{1}{2} - \sqrt{m}\left(1+\sqrt{m}\ln\left(\frac{\sqrt{m}}{\sqrt{m}+1}\right)\right)}{(\sqrt{m}+1)^2} \,. \qquad (160)$$

In the limit $m = 1$ we therefore have

$$\frac{RT_c}{N_A\varepsilon_o} = \frac{1}{4} \qquad \phi_c = \frac{1}{2} \qquad \frac{bP_c}{\varepsilon_o} = \frac{2\ln 2 - 1}{8} \,. \qquad (161)$$

We may work out the relation between critical and Boyle temperature, i.e.

$$T_{Boyle} = 4T_c \,, \qquad (162)$$

or the critical compressibility factor

$$\frac{N_A P_c}{RT_c\rho_c} = 2\ln 2 - 1 \approx 0.39 \,. \qquad (163)$$

Both values are very close to the same quantities in the van der Waals theory.

But we are not interested in a competition with the van der Waals equation. We therefore look at the opposite limit, i.e. very long polymer chains, which is not described by the van der Waals equation. In the limit $m \to \infty$ we have to leading order

$$\frac{RT_c}{N_A\varepsilon_o} \approx 1 \qquad \phi_c \approx \frac{1}{m^{1/2}} \qquad \frac{bP_c}{\varepsilon_o} \approx \frac{1}{3m^{3/2}} \,. \qquad (164)$$

The corresponding leading behavior of the critical compressibility factor is

$$\frac{N_A P_c}{RT_c\rho_c} \approx \frac{1}{3m} \,. \qquad (165)$$

Here ρ_c is the number density of the monomer units - not the polymers! Notice that the critical compressibility factor is not a constant independent of the type of molecule as before. Fig. 36 shows the critical compressibility factor for n-alkanes ($1 \le n \le 18$). The symbols are data from E. D. Nikitin *The critical properties of thermally unstable substances: measurement methods, some results and correlations.* High Temperature *36*, 305 (1998). The mass density was converted to the monomer number density using CH_2 as the monomer unit. This also implies $m = n$. The lines are fits to the data using the full expressions, i.e. Eqs. (158) to (160), (solid line) and the limiting law, Eq. (165), (dashed line). The only fit parameter is a multiplicative constant, i.e. instead of $1/(3m)$ we use $0.24/m$ to match the data for large m.

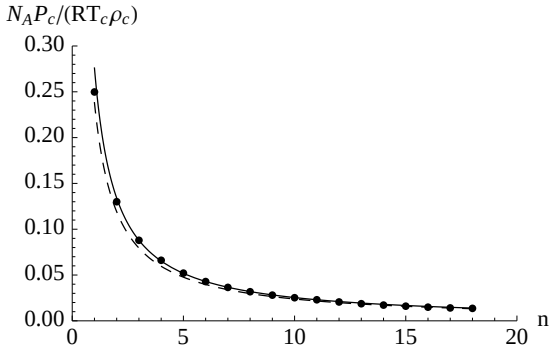

Fig. 36 Critical compressibility factor for n-alkanes.

Notice also that expressing pressure, temperature, and volume or density in terms of their critical values eliminates the material parameters b and ε_o, but it does not eliminate m. This means that the resulting equation of state is not universal in the sense that it is different for molecules with different length, i.e. different m. Therefore the law of corresponding states is not obeyed by molecules with different m.

Another Digression - a Model for Liquid-Liquid Coexistence:

Another type of phase separation is observed in binary low molecular weight mixtures. Depending on thermodynamic conditions the components may be miscible or not. A simple model describing this is based on the following molar free enthalpy approximation

$$g = x_A^{(l)} g_A + x_B^{(l)} g_B + x_A^{(l)} \ln x_A^{(l)} + x_B^{(l)} \ln x_B^{(l)} + \chi x_A^{(l)} x_B^{(l)} \,. \qquad (166)$$

Here g_A and g_B are the (reduced) molar free enthalpies of two pure liquid components A and B. Mixing A and B gives rise to the mixing free enthalpy described by the ln-terms. Note that the mole fractions are $x_A^{(l)}$ and $x_B^{(l)} = 1 - x_A^{(l)}$. We immediately see that this is identical to the lattice model which we have developed since $\phi_1 = N_1/(N_1+N_2) = x_1 \equiv x_A^{(l)}$ and $\phi_2 = N_2/(N_1+N_2) = x_2 \equiv x_B^{(l)}$.

Fig. 37 shows g for different values of the χ-parameter. If χ is less than a critical value then g is a convex function of $x_A^{(l)}$ (or $x_B^{(l)}$). This situation is analogous to the free energy in the van der Waals theory for temperatures above the critical temperature. If $\chi = \chi_c$ then the curvature of g at $x_A^{(l)} = 1/2$ becomes zero. For still larger values of χ a 'bump' develops - again analogous to the free energy in the van der Waals theory for temperatures less than the critical temperature. Driven by the second law the system now lowers its free enthalpy by separating into two types of regions, which over time will coagulate into two large domains, one depleted of A and one enriched with A. The resulting phase diagram is shown

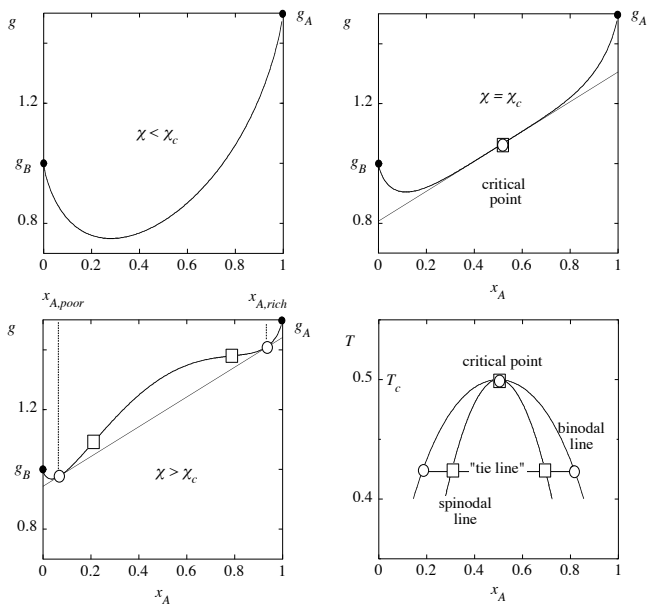

Fig. 37 Schematic of the x_A-dependence of g for different χ-values. The curves shown here are for $\chi = 1$ (upper left), $\chi = 2$ (upper right), and $\chi = 3$ (lower left) using $g_A = 1.5$ and $g_B = 1.0$. Lower right: T-x_A-phase diagram of our model of a binary mixture, where we assume that $T = 1/\chi$.

in the lower right panel in Fig. 37. The binodal line is obtained via a common tangent construction applied to the free enthalpy (cf. the lower left panel). Note

$$\left.\frac{\partial g}{\partial x_A}\right|_{T,P} = \frac{1}{k_B T}\left.\frac{\partial G}{\partial N_A}\right|_{T,P} = \frac{\mu_A}{k_B T} \,. \tag{167}$$

This means that the chemical potential of A is the same along the tangent. The common tangent is the lowest possible free enthalpy inbetween $x_{A,poor}$ and $x_{A,rich}$. For a given x_A in this range the quantity $(x_A - x_{A,poor})/(x_{A,rich} - x_{A,poor})$ is the fraction of A in the $A,rich$-phase relative to the total amount of A in the system. The second special line is the spinodal line. It marks the stability limit

$$\left.\frac{\partial^2 g}{\partial x_A^2}\right|_{T,P} = 0 \,. \tag{168}$$

Both lines meet at the critical point where

$$\left.\frac{\partial^3 g}{\partial x_A^3}\right|_{T,P} = 0 \,, \tag{169}$$

because at the critical point the curvature obviously changes sign.

Note that temperature here enters via the assumed proportionality $\chi \propto 1/T$. This assumption accounts for the observation that phase separation usually occurs upon lowering temperature. Nevertheless this is purely empirical and more complex descriptions of χ can be found.

Fig. 38 shows experimental liquid-liquid equilibria data for the binary mixtures water/phenol (solid squares) and methanol/hexane (solid circles) (data from the CRC Handbook of Thermophysical and Thermochemical Data, D. R. Lide and H. V. Kehiaian (Eds.) CRC Press: Boca Raton (1994)). Here x_A is the mole fraction of water and methanol, respectively. Notice that while both systems show the basic behavior predicted by our theory, only the second system also exhibits the symmetry around $x_A = 0.5$. Nevertheless, the solid lines are 'theoretical' results, which where obtained using

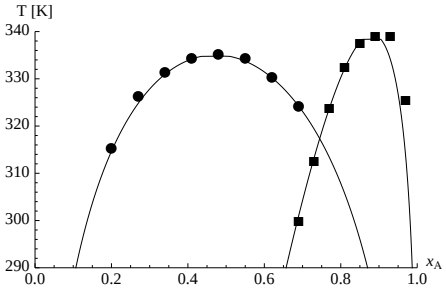

Fig. 38 Liquid-liquid equilibria data for the binary mixtures water/phenol (solid squares) and methanol/hexane (solid circles).

$$\chi = \frac{c_0 + c_1 x_A}{T} + c_2 \,. \tag{170}$$

Here c_0, c_1, and c_2 are constants, which are adjusted so that the theory matches the data points. In particular the c_1-term breaks the symmetry around $x_A = 0.5$. While it is quite common to introduce such expressions for χ, it is not easy to provide reasonable physical explanations of the individual terms. In addition, the 'best fit' usually does not correspond to a unique set of values for c_0, c_1, and c_2.

However, let us return to polymer mixtures. Fig. 39 shows analogous binodal data points for a macromolecular fluid mixture determined by observation of the cloud points. The term 'cloud point' refers to the turbidity observed upon passing from the homogeneous mixture into the coexistence region, where droplet formation increases the scattering of light. In our theoretical description we assume a fully occupied lattice.

Figure 39 shows polystyrene-polybutadiene mixture cloud point data taken from Fig. 3 in R.-J. Roe, W.-C. Zin *Determination of the polymer-polymer interaction parameter for the Polystyrene-Polybutadiene pair.* Macromolecules *13*, 1221 (1980); PS2-PBD2 (solid circles); PS3-PBD2 (open squares), and PS5-PBD26 (open triangles); $m_{PS2} = 2220$, $m_{PS3} = 3500$, $m_{PS5} = 5200$, $m_{PBD2} = 2350$, $m_{PBD26} = 25000$. Note that ϕ_1 refers to PS. The solid lines are the results of a calculation analogous to the one which produced the solid lines in Fig. 38, i.e. we determine the binodal line by the common tangent construction applied to the mixing free enthalpy (It does not matter whether we apply the common tangent construction to the mixing free enthalpy or to the full free enthalpy.)

$$\frac{\Delta G}{N k_B T} = \frac{\phi_1}{m_1}\ln\phi_1 + \frac{1-\phi_1}{m_2}\ln(1-\phi_1) + \chi\phi_1(1-\phi_1) \,. \tag{171}$$

Again we use Eq. (170) to describe χ. Notice that the χ-term in

the literature sometime is denoted as an enthalpic contribution. This is not necessarily true, as we have already pointed out, because $\partial G/\partial T|_P = -S$, and if χ depends on temperature, as it usually does, then the χ-term contributes to the entropy as well. Here significant insight is needed into the microscopic interaction of polymer systems. A good starting point for the interested reader is R. Koningsveld, L. A. Kleintjens *Fluid phase equilibria in macromolecular systems.* Acta Polymerica *39*, 341 (1988).

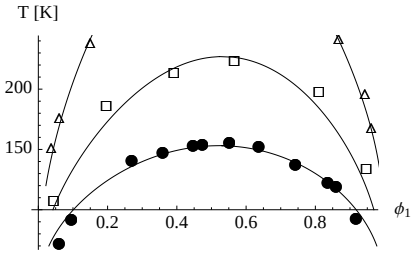

Fig. 39 Binodal data points and theoretical fits for three binary polymer mixtures.

4.3 Polymers in Solution

We briefly want to discuss Eq. (171) when $m_2 = 1$, i.e.

$$\frac{\Delta G}{nRT} = \frac{\phi}{m}\ln\phi + (1-\phi)\ln(1-\phi) + \chi\phi(1-\phi)\,, \tag{172}$$

where $\phi_1 = \phi$. This situation describes a polymer-solvent-system. The phase behavior of this system is in principle described by Fig. 37 (bottom-right panel), except of course without the symmetry around $x_A = 0.5$, i.e. $\phi_1 = 0.5$, unless $m_1 = 1$. Setting the coefficient $c_1 = 0$ in Eq. (170) we easily work out the critical temperature and the critical packing fraction, i.e.

$$\frac{c_0}{T_c} = \frac{1}{2} - c_2 + \frac{1}{\sqrt{m}} + \frac{1}{2m} \qquad \text{and} \qquad \phi_c = \frac{1}{\sqrt{m}+1}\,, \tag{173}$$

according to Shultz and Flory (A. R. Shultz, P. J. Flory *Phase equilibria in polymer-solvent systems.* J. Am. Chem. Soc. *74*, 4760 (1952)) (Notice that T_c and ρ_c do agree with the same critical parameters in the case of the previously discussed gas-liquid critical point, cf. Eqs. (158) and (159), if $c_o = N_A\varepsilon_o/(2R)$ and $c_2 = 0$). These critical parameters follow via simultaneous solution of

$$\frac{\partial^2}{\partial\phi^2}\Delta G = 0 \qquad \text{and} \qquad \frac{\partial^3}{\partial\phi^3}\Delta G = 0 \tag{174}$$

(cf. Eqs. (168) and (169)). The critical solution temperature, T_c, measured for different m may be fitted via (173), i.e. T_c^{-1} vs. $m^{-1/2} + (2m)^{-1}$, to determine c_0 and c_2 experimentally (for this particular mixture).

4.4 Osmotic Pressure in Polymer Solutions

Eq. (172) may be used to calculate the osmotic pressure Π of polymers in solution. However, here we want to use Eq. (171) instead where m_2 is not yet equal to one. Again we employ the Gibbs-Duhem equation at constant temperature (see for instance R. Hentschke *Thermodynamics* (2nd ed.) p. 78):

$$\begin{aligned} V\Pi_1 &= \int_0^{\nu_1} d\mu_1(\nu_1')\frac{\nu_1'}{N_A} \qquad (175)\\ &= \int_0^{\nu_1} d\nu_1'\,\frac{\nu_1'}{N_A}\frac{\partial^2\Delta G}{\partial\nu_1^2}\Big|_{\nu_1=\nu_1'} = -\frac{1}{N_A}\frac{\partial\Delta G/\nu_1}{\partial(1/\nu_1)}\,. \end{aligned}$$

Notice that $d\mu_1(\nu_1)$ is due to altering the relative polymer content of the solution, which solely affects the mixing contribution of the free enthalpy. After some work, using $n = N/N_A$, $N = m_1\nu_1 + m_2\nu_2$, and $\phi_i/m_i = \nu_i/(nN_A)$, we find

$$\Pi_1 = \frac{RT}{V}n_2\left(-\phi_1\left[1-\frac{m_2}{m_1}\right] - \ln(1-\phi_1) - m_2\chi\phi_1^2\right)\,, \tag{176}$$

where $n_i = \nu_i/N_A$ $(i = 1,2)$. It is instructive to expand the right side for small n_1, i.e.

$$\Pi_1 = \frac{RT}{V}\left(n_1 + \left[\frac{1}{2m_2} - \chi'\right]\frac{m_1^2n_1^2}{m_2n_2} + \mathscr{O}(n_1^3)\right)\,, \tag{177}$$

where $\chi' = \chi + 1/m_1$. Or if we express the expansion in terms of ϕ_1

$$\Pi_1 = \frac{k_BT}{b^3}\left(\frac{\phi_1}{m_1} + \left[\frac{1}{2m_2} - \chi'\right]\phi_1^2 + \mathscr{O}(\phi_1^3)\right)\,. \tag{178}$$

The quantity b^3 is the cell volume, i.e. $V = b^3N$. In the case of polymers in solution we set $m_2 = 1$ (solvent) whereas m_1 is large.

We do not want to discuss Eqs. (176) and (177) in much detail. A few remarks must suffice here.

Remark 1: Note that the first term in (177) is proportional to the number concentration polymer, whereas the second term is proportional the square of the weight concentration. That this is indeed the case can be seen in Fig. 6.

Remark 2: From Eq. (177) we also conclude that the quantity B_2 in Eq. (120), used to produce the Zimm-plot, is given by

$$B_2 = \left[\frac{1}{2} - \chi\right]\frac{m_1\upsilon_s}{m_b}\,, \tag{179}$$

where υ_s is the volume of a solvent molecule and m_b is the mass of a monomer or segment corresponding to one lattice cell.

Remark 3: The term in square brackets in the Eqs. (177) and (178) is proportional to the second virial coefficient of type-1-molecules in type-2-molecules. Suppose that the type-

2-molecules are also chains. In fact they are the same type of polymer as type 1 - maybe just somewhat shorter to make them a little different. In this case we expect that χ (cf. (148)) is very small -as is χ'. Since $1/(2m_2)$ is also small if the type-2-molecules are chains, we conclude that the entire second virial coefficient is small. Essentially we are looking at a situation which is very similar to our discussion of the θ-solvent in the context of Eq. (88). This equation led us to conclude that the exponent ν, in a situation when the second viral coefficient vanishes, assumes its ideal chain-value. Following this line of reasoning we can see why polymer chains in a melt of identical chains should be ideal.

An insightful discussion of osmotic pressure in polymer solutions, including the present result, can be found in P.-G. de Gennes *Scaling Concepts in Polymer Physics.* Cornell University Press (1988).

4.5 Swelling of Polymer Networks

Eq. (172) describes the mixing free enthalpy of a polymer-solvent system on a lattice, where ϕ is the volume fraction polymer. If we express the solvent volume fraction $1-\phi$ via $1-\phi = N_s/N$, where N_s is the number of solvent cells and N is the total number of cells, the result is

$$\frac{\Delta G}{k_B T} = \nu \ln\phi + N_s \ln(1-\phi) + \chi\phi N_s \,. \tag{180}$$

The quantity ν is the number of polymer chains (do not confuse with the exponent ν!). How can we adopt this equation to the swelling of a polymer network?

What we mean by 'network' is depicted in Fig. 40. Panel (a) shows a cartoon of several polymer chains or segments joined with other chains at their ends. These junction points are cross-links. Typically four chain segments are joined together in one cross-link. This happens for instance due to a covalent bridge between two linear chains. Aside from chemical cross-links two polymer chains may be entangled when one is making a hairpin-type bend around the other. In the following we are not interested in the true nature of the cross-link. We merely assume that the polymer network is a network of ν cross-linked chain segments containing n Kuhn-lengths each. In addition, if a macroscopic volume element inside the network, possessing the edge lengths L_x, L_y, and L_z, it is deformed during swelling, then its new edge lengths are $L'_x = \lambda_x L_x$, $L'_y = \lambda_y L_y$, and $L'_z = \lambda_z L_z$. We also assume that the segment end-to-end vectors contained in this volume element will change their components analogously. Hence

$$\frac{L_\alpha}{R_{i,\alpha}} = \frac{L'_\alpha}{R'_{i,\alpha}} \,, \tag{181}$$

which is an affine deformation (cf. Fig. 40 (b)).

Here we want to study uniform swelling, i.e. $\lambda_x = \lambda_y = \lambda_z \equiv \lambda > 1$. But there is another important case, which we shall discuss as well. Elastomers are a certain class of polymers which are used to make rubber. Rubber possess a very small compressibility, i.e. $V' = L'_x L'_y L'_z \approx L_x L_y L_z = V$. If we stretch a rubber band by a factor $\lambda_z \equiv \lambda$ in z-direction, i.e. $L'_z = \lambda L_z$, volume conservation, i.e. $\lambda_x \lambda_y \lambda_z = 1$, implies $\lambda_x = \lambda_y = \lambda^{-1/2}$.

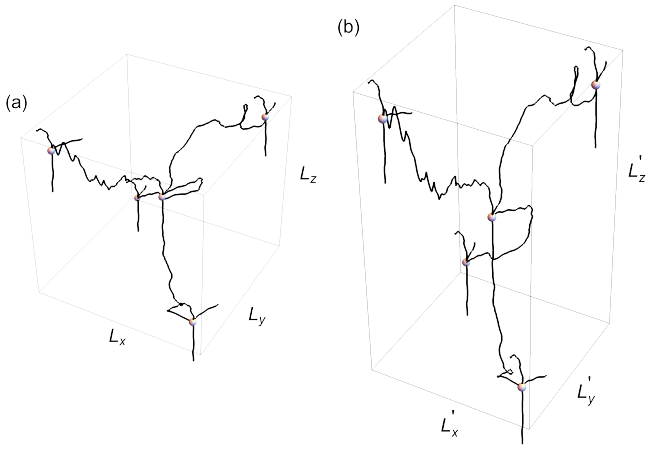

Fig. 40 A polymer network volume element containing cross-linked chain segments in the undeformed (a) and in the deformed (b) state. Cross-links are indicated by the dots.

Let us come back to our original question - how must we modify Eq. (180) in order to describe the free enthalpy change during swelling of a polymer network in contact with a solvent? In a simple approximate theory of polymer network swelling due to P. J. Flory and J. Rehner (J. Chem. Phys. *11* 521 (1943)) the translational entropy term $\nu \ln\phi$ is replaced by an elastic entropy contribution $\frac{3\nu}{2}(\lambda^2 - 1 - \ln\lambda)$ when the network undergoes uniform swelling, i.e. $\lambda_x = \lambda_y = \lambda_z \equiv \lambda$. Note that the cross-links provide a framework which fixes the positions of the chain segments in space, i.e. the 'translational entropy' does not change for these segments. However, their end-to-end distance changes during swelling (or, more generally, during the deformation) of the network. Thus we may remove the term which arises from the number of ways in which we may put the polymer chains on the lattice and replace this term by the entropy change (times $-T$) due to the changes of the chain's end-to-end distances.

Why this entropy change has the above form, we shall discuss in detail below. Momentarily we just assume that this is indeed the correct form and proceed. Minimizing the new ΔG with respect to N_s, i.e. $0 = \partial(\Delta G/(k_B T))/\partial N_s$, which means equating the solvent chemical potentials inside and outside the network, yields the **Flory-Rehner equation** in its standard form:

$$\rho_P \frac{v_s}{m_P} = -\frac{\ln(1-\phi) + \phi + \chi\phi^2}{\phi^{1/3} - \phi/2} \,. \tag{182}$$

The quantity ρ_P is the mass density of the (dry) polymer, v_s is the molecular volume of the solvent, and m_P is the (average) mass of a network segment. Note that $\lambda^3 = V_{swollen}/V_P = 1/\phi = (V_P + N_s v_s)/V_P$, where $V_{swollen}$ is the equilibrium volume of the swollen network (or gel) and V_P is the dry polymer volume. Note also that $\partial\phi/\partial N_s = -\phi^2 v_s/V_p$

(caveat: It is incorrect to use the above formula $\phi = 1 - N_s/N$, assuming $N = const$, for the derivative of ϕ with respect to N_s. This means that the volume is kept constant - which is not the case.), $\partial\lambda/\partial N_s = \upsilon_s/(3V_P\lambda^2)$, as well as $\rho_P \frac{\upsilon_s}{m_P} = \frac{\upsilon_s}{V_P}\nu$. In the original paper, cf. Eq. (11) in J. Chem. Phys. *11*, 521 (1943), the $-\phi/2$-term in the denominator of Eq. (182), which results from the $-\ln\lambda$-term in the elastic entropy, is not included. This persisted for some time (e.g. Eq. (5.9) in L. R. G. Treloar, Reports on Progress in Physics *The elasticity and related properties of rubbers. 36*, 755 (1973)), but finally 'converged' to the above form. However, the significance of the $-\phi/2$-term is somewhat questionable. The factor $1/2$ resulted from a rather approximate entropy contribution of the network nodes and, in addition, is based on the assumption of a regular 4-fold coordinated network. In addition, in many cases of practical importance $\phi^{1/3}$ dominates over $\phi/2$ and the latter can be neglected. Nevertheless, Eq. (182) ties the quantity ν to the swollen volume of a polymer network. Therefore it provides another means for the determination of the cross-link density (see also the footnote in the context of Eq. (218)).

• Derivation of the elastic entropy contribution $\frac{3\nu}{2}(\lambda^2 - 1 - \ln\lambda)$:

The entropy change ΔS^{el} due to the deformation of the network has two contributions, i.e.

$$\Delta S^{el} = \Delta S^{el,f} + \Delta S^{el,\nu} \,. \tag{183}$$

$\Delta S^{el,f}$ is the change in entropy without considering cross-links explicitly relative to the undeformed state. $\Delta S^{el,\nu}$ is a correction due to the explicit presence of cross-links.

We start with $\Delta S^{el,f}$, which is given by

$$\Delta S^{el,f} = k_B \ln\left[\frac{\Omega'}{\Omega}\right] \,. \tag{184}$$

The quantity Ω is the number of different ways by which N polymer segments can be accommodated inside the undeformed volume V. Here and in the following primes indicate corresponding quantities in the deformed state. Note that we group the segments according to their end-to-end vectors $\vec{R}_i$. Hence

$$\Omega \propto \frac{N!}{\prod_i N_i!} \prod_i p_i^{N_i} \,. \tag{185}$$

Here $p_i^{N_i}$ is the probability for finding N_i polymer segments with end-to-end distance in the same volume element at $\vec{R}_i$ (all segments start at the same origin) - with p_i being this probability for a single segment. The factor $N!(\prod_i N_i!)^{-1}$ accounts for the distinguishable permutations of segments provided that their distinguishing feature is their end-to-end vector (i.e. the volume element it points to). The deformation redistributes the segments, i.e. $N_i \to N_i'$. Hence

$$\Omega' \propto \frac{N!}{\prod_i N_i'!} \prod_i p_i^{N_i'} \,.$$

Note that p_i does not change! p_i is the probability density $p(R_i)$ in Eq. (81) multiplied by the volume element at $\vec{R}_i$. Therefore p_i is the ratio of the number of conformations which let a single polymer segment end up in the volume element at $\vec{R}_i$ divided by the number of all its possible conformations. This ratio, which is based on the intrinsic polymer properties, is not altered by volume deformation provided that we keep looking at the same volume element regardless of the deformation state. What changes though is the number of segment endpoints N_i in this volume element. Swelling for instance will dilute these points and reduce their number to $N_i' < N_i$.

Now we apply Stirling's approximations to $N_i!$ and $N_i'!$, i.e. $\ln N_i! \approx N_i \ln N_i - N_i$ and $\ln N_i'! \approx N_i' \ln N_i' - N_i'$. In addition we use $p_i = N_i/N$, $p_i' = N_i'/N$ and $\sum_i N_i = \sum_i N_i' = N$. The result is

$$\ln\left[\frac{\Omega'}{\Omega}\right] = N \sum_i p_i' \ln\left[\frac{p_i}{p_i'}\right] \,. \tag{186}$$

Let's briefly discuss $p_i = N_i/N$ and $p_i' = N_i'/N$. The first equation applies in the undeformed state and is (hopefully) evident. As a difinition of p_i' the second equation is evident also. But what maybe confusing is the difference between p_i' and p_i. As we have already mentioned p_i is the probability density $p(R_i)$ in Eq. (81) multiplied by the volume element at $\vec{R}_i$, i.e.

$$p_i = \Delta R_{i,x}\Delta R_{i,y}\Delta R_{i,z} \frac{c^3}{\pi^{3/2}} \exp\left[-c^2\left(R_{i,x}^2 + R_{i,y}^2 + R_{i,z}^2\right)\right] \,, \tag{187}$$

where $c^2 \equiv (2\langle\vec{R}^2\rangle/3)^{-1}$. Network deformation means that the old and the new coordinates are related via

$$R_{i,\alpha} = \frac{1}{\lambda_\alpha} R_{i,\alpha}' \quad (\alpha = x,y,z) \,. \tag{188}$$

Inserting this into (187) yields

$$\begin{aligned} p_i' \;\; = \;\; & \Delta R_{i,x}'\Delta R_{i,y}'\Delta R_{i,z}' \frac{c^3}{\pi^{3/2}\lambda_x\lambda_y\lambda_z} \\ & \times \exp\left[-c^2\left((R_{i,x}'/\lambda_x)^2 + (R_{i,y}'/\lambda_y)^2 + (R_{i,z}'/\lambda_z)^2\right)\right] \end{aligned} \tag{189}$$

and Eq(186) becomes

$$\begin{aligned}\ln\left[\frac{\Omega'}{\Omega}\right] &= N\ln\left[\lambda_x\lambda_y\lambda_z\right] - N\sum_i c^2 p_i'\left[{R'_{i,x}}^2\left(1-\frac{1}{\lambda_x^2}\right)+\dots\right]\\ &= N\ln\left[\lambda_x\lambda_y\lambda_z\right]\\ &\quad -N\int dR'_x dR'_y dR'_z \frac{c^3\exp\left[-c^2\left((R'_x/\lambda_x)^2+\dots\right)\right]}{\pi^{3/2}\lambda_x\lambda_y\lambda_z}\\ &\quad \times\left[c^2{R'_x}^2\left(1-\frac{1}{\lambda_x^2}\right)+\dots\right]\\ &= N\ln\left[\lambda_x\lambda_y\lambda_z\right]-\frac{N}{2}\left(\lambda_x^2+\lambda_y^2+\lambda_z^2-3\right)\end{aligned}$$

or

$$\Delta S^{el,f} = Nk_B\ln\left[\lambda_x\lambda_y\lambda_z\right]-\frac{Nk_B}{2}\left(\lambda_x^2+\lambda_y^2+\lambda_z^2-3\right)\,. \qquad (190)$$

Hence, for a uniform volume change $V'=\lambda^3 V$ we find

$$\Delta S^{el,f}_{iso} = 3Nk_B\ln\lambda-\frac{3Nk_B}{2}\left(\lambda^2-1\right)\,, \qquad (191)$$

whereas for a volume conserving uniaxial stretch ($\lambda_z=\lambda$, $\lambda_x=\lambda_y=\lambda^{-1/2}$)

$$\Delta S^{el,f}_{stretch} = -\frac{Nk_B}{2}\left(\lambda^2+\frac{2}{\lambda}-3\right)\,. \qquad (192)$$

Figure 41 shows $\Delta S^{el,f}_{iso}/(Nk_B)$ and $\Delta S^{el,f}_{stretch}/(Nk_B)$ vs. λ. Any deviation from the undeformed state $\lambda=1$ results in a negative entropy contribution. When $\lambda>1$ the chain segments are stretched in both situations and the number of possible chain conformations are reduced. When $\lambda<1$ it is the 'ideal gas volume term' $\ln\lambda^3$, which causes the entropy change to become negative in the case of $\Delta S^{el,f}_{iso}/(Nk_B)$. In the volume conserving case of $\Delta S^{el,f}_{stretch}/(Nk_B)$ a reduction of λ below one again means chain stretching albeit in the xy-plane.

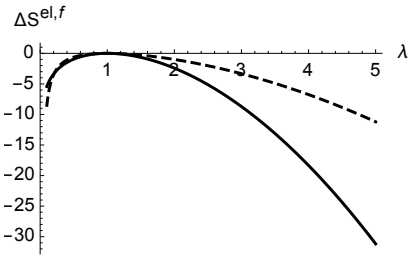

Fig. 41 $\Delta S^{el,f}_{iso}/(Nk_B)$ (solid line) and $\Delta S^{el,f}_{stretch}/(Nk_B)$ (dashed line) vs. λ

Next we focus on $\Delta S^{el,v}$, the correction to ΔS^{el} due to the the cross-links. Let's assume a network consisting of N segments. In the most common situation we have four segments 'emanating' from one cross-link. Since only half of each segment belongs to this cross-link (the other half belongs to the next cross-link), there are two full segments per cross-link or $N/2$ cross-links total.

Flory has argued that there is an entropy change, i.e. $\Delta S^{el,v}$, originating from the confinement of each cross-link to essentially a small volume δV due to the network structure. We estimate this entropy change via

$$\Delta S^{el,v} = k_B\ln\frac{(\delta V/V')^{N/2}}{(\delta V/V)^{N/2}} = -\frac{Nk_B}{2}\ln\left[\lambda_x\lambda_y\lambda_z\right]\,. \qquad (193)$$

Note that $\delta V/V$ and $\delta V/V'$ is the probability for finding a cross-link in the small volume δV in the undeformed and in the deformed state, respectively. Assuming that the $N/2$ cross-links are independent, which is rather crude, we obtain the first equation in (193). Note that this contribution to the entropy does not enter if the volume is conserved, i.e. $\Delta S^{el,f}_{stretch}$ is the total $\Delta S^{el}_{stretch}$. In other words,

$$\Delta S^{el}_{iso} = 3Nk_B\left(\ln\lambda-\lambda^2+1\right) \qquad (194)$$

and

$$\Delta S^{el}_{stretch} = -\frac{Nk_B}{2}\left(\lambda^2+\frac{2}{\lambda}-3\right)\,. \qquad (195)$$

In general the total ΔS^{el} becomes

$$\Delta S^{el} = \frac{Nk_B}{2}\left(\ln\left[\lambda_x\lambda_y\lambda_z\right]-\lambda_x^2-\lambda_y^2-\lambda_z^2+3\right)\,. \qquad (196)$$

With an extra factor $-T$, $\lambda=\lambda_x=\lambda_y=\lambda_z$, and N replaced by ν this is exactly the term which replaces $T\nu\log\phi$ in Eq. (180).

Before moving on we want to address the important case of ΔS^{el} due to uniform shear depicted in Fig. 42. Again $V=const$. Instead of (188) we now have

$$\begin{aligned}R_{i,x} &= R'_{i,x}-\gamma_{xz}R'_{i,z}\quad(\gamma_{xz}\equiv\frac{L_x}{L_z}\varepsilon)\\ R_{i,y} &= R'_{i,y}\\ R_{i,z} &= R'_{i,z}\,,\end{aligned} \qquad (197)$$

which, after insertion into the expression for $\ln[\Omega'/\Omega]$, yields

$$\Delta S^{el} = \Delta S^{el,f}_{shear} = -\frac{Nk_B}{2}\gamma_{xz}^2\,. \qquad (198)$$

5 Polymer Dynamics

5.1 Linear Deformation Mechanics

This subsection applies mainly to polymer networks and gels. Experiments studying the time-dependent behavior of these systems often involve the mechanical deformation of a bulk sample. Even though this is a somewhat narrow scope, there are a number of concepts and quantities with broader importance addressed here, e.g. storage and loss modulus, complex modulus,

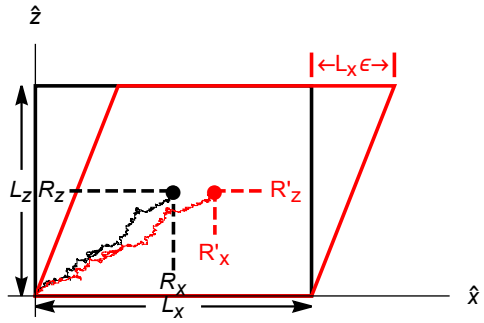

Fig. 42 Uniform shear of a block of material.

compliance, etc. It is this which justifies the somewhat cursory discussion of linear deformation mechanics at this point. On a first reading the 'boxes' *Equations and Concepts from Isotropic Elasticity* (cf. L. D. Landau, E. M. Lifshitz *Theory of Elasticity*) and *Equations and Concepts from Fluid Mechanics* (cf. L. D. Landau, E. M. Lifshitz *Fluid Mechanics*) may be skipped over. However, both boxes contain essential physics underlying what is called 'viscoelasticity', the main feature of polymers in motion, which means that they should not be neglected entirely.

Equations and Concepts from Isotropic Elasticity:

Deformation of an elastic body will displace the interior point $\vec{r}$ by $\vec{u}(\vec{r})$. This means that the new position $\vec{r}\,'$ is

$$\vec{r}\,' = \vec{r} + \vec{u}(\vec{r}) \,. \tag{199}$$

If two points are infinitesimally close, the vector from one to the other, $d\vec{r}$, transforms according to

$$d\vec{r}\,' = d\vec{r} + d\vec{u}(\vec{r}) = d\vec{r} + d\vec{r}\cdot\vec{\nabla}\vec{u}(\vec{r}) \,. \tag{200}$$

The square of $d\vec{r}\,'$ is therefore

$$dr'^2 = (dx_i + dx_j\partial_j u_i)^2 \approx dx_i^2 + 2\,dx_i dx_j \partial_j u_i \,. \tag{201}$$

Here we use the summation convention and we assume that $\vec{u}(\vec{r})$) varies slowly in space. The last term can be written as

$$2\,dx_i dx_j \partial_j u_i = 2\,dx_i dx_j \frac{1}{2}(\partial_j u_i + \partial_i u_j) \equiv 2\,dx_i dx_j\, u_{ij} \,. \tag{202}$$

This defines the components of the **strain tensor**, i.e.

$$u_{ij} = \frac{1}{2}\left(\frac{\partial u_i}{\partial x_j} + \frac{\partial u_j}{\partial x_i}\right) \,. \tag{203}$$

Note that the strain tensor is the central quantity here, which contains all the local information regarding the deformation.

Since the strain tensor is symmetric, i.e. $u_{ij} = u_{ji}$ it may be diagonalized at every point, i.e.

$$\begin{aligned} dr'^2 &= \left(\delta_{ij} + 2u_{ij}\right) dx_i dx_j \\ &= \left(1 + 2u^{(1)}\right) dx^2 + \left(1 + 2u^{(2)}\right) dy^2 + \left(1 + 2u^{(3)}\right) dz^2 \,. \end{aligned}$$

The quantities $u^{(i)}$ are the attendant principal values or eigenvalues of the strain tensor. Therefore

$$dx_i' = \sqrt{\left(1 + 2u^{(i)}\right)}\, dx_i \,. \tag{204}$$

If $dV' = dx'dy'dz'$ is the volume element in the deformed state and $dV = dxdydz$ is the volume element in the undeformed state, we can use Eq. (204) to obtain

$$\begin{aligned} dV' &= \sqrt{1 + 2u^{(1)}}\sqrt{1 + 2u^{(2)}}\sqrt{1 + 2u^{(3)}}\, dx_1 dx_2 dx_3 \\ &\approx \left(1 + u^{(1)}\right)\left(1 + u^{(2)}\right)\left(1 + u^{(3)}\right) dV \\ &\approx \left(1 + u^{(1)} + u^{(2)} + u^{(3)}\right) dV \,. \end{aligned} \tag{205}$$

The quantity $u^{(1)} + u^{(2)} + u^{(3)}$ is the trace of the strain tensor. Because the trace is independent of the coordinate system this yields

$$dV' = (1 + u_{ll})\, dV \,. \tag{206}$$

Note that zero trace of the strain tensor implies local volume conservation.

Every deformation in the type of system we are interested in, i.e. an isotropic system, can be thought of as the being composed of a pure shear plus a pure dilation. Therefore it is usefully to rewrite u_{ij} as

$$u_{ij} = \frac{1}{3}\delta_{ij} u_{ll} + \left(u_{ij} - \frac{1}{3}\delta_{ij} u_{ll}\right) \,. \tag{207}$$

Note that the trace of the term in brackets on the right side of this equation is zero ($\delta_{ll} = 3$). This term therefore describes a volume conserving shear deformation as depicted in Fig. 42. The other term describes a pure dilatation.

It is reasonable to assume that we can link u_{ij}, or more specifically these two terms individually, to a corresponding **elastic stress tensor** σ_{ij} via the linear equation

$$\sigma_{ij} = K\,\delta_{ij} u_{ll} + 2G\left(u_{ij} - \frac{1}{3}\delta_{ij} u_{ll}\right) \,, \tag{208}$$

where K and G are constants. In order to find out whether this guess is sensible we study three special cases.

First we apply formula (208) to a gas and calculate the trace on both sides. We find

$$3\sigma = 3K u_{ll} \overset{(206)}{=} 3K\frac{\delta V}{V} \,. \tag{209}$$

Due to the nature of the system $\sigma \equiv \sigma_{xx} = \sigma_{yy} = \sigma_{zz}$. Comparing this to the formula for the isothermal compressibility, $\kappa_T = -V^{-1}\delta V/\delta P|_T$, we conclude $\sigma = -\delta P$ and $K = 1/\kappa$. Therefore σ_{ij} has units of force per area. In addition, K is the **compression modulus**.

Next we apply (208) to Fig. 42, which yields

$$\sigma_{xz} = 2G u_{xz} = G\frac{\partial u_x}{\partial z} = G\frac{L_x \varepsilon}{L_z} \tag{210}$$

or

$$\sigma_{xz} = G\gamma_{xz} \,. \tag{211}$$

Hence, σ_{xz} is a force per area in x-direction applied to the face of the sample defined by its normal in z-direction and G is the **shear modulus**. If we assume that G is entirely due to the entropy elasticity of the chains in the sample, we can use our previous result (198) to obtain G via

$$\sigma_{xz} = \frac{1}{V}\frac{\partial(-T\Delta S^{(el)})}{\partial\gamma_{xz}} = \frac{N}{V}k_B T\gamma_{xz} \tag{212}$$

(Note that σ_{xz} is a local quantity referring to a certain volume element. Here all volume elements are identical and we divide simply by the total sample volume V.) or

$$G = \frac{N}{V}k_B T \,, \tag{213}$$

i.e. G is the chain density in the sample times $k_B T$.

The third case is uniaxial stretching or compression of the sample. Here it is useful to invert Eq. (208). We can do this by computing the trace which yields $\sigma_{ll} = 3Ku_{ll}$. Inserting $u_{ll} = \sigma_{ll}/(3K)$ back into Eq. (208) gives

$$u_{ij} = \frac{1}{9K}\delta_{ij}\sigma_{ll} + \frac{1}{2G}\left(\sigma_{ij} - \frac{1}{3}\delta_{ij}\sigma_{ll}\right) \,. \tag{214}$$

We apply this equation to a stretched column as depicted in Fig. 43. The forces stretching the column are distributed uniformly across the top and bottom faces of the column. No forces are applied to the other faces. This implies that the only component of the stress tensor which is not zero is σ_{zz}. Eq. (214) tells us therefore that $u_{ij} = 0$ if $i \neq j$. For the diagonal elements of the strain tensor we obtain

$$\sigma_{zz} = E\,u_{zz} \quad \text{and} \quad u_{xx} = u_{yy} = -\nu u_{zz} \,, \tag{215}$$

where

$$E = \frac{9KG}{3K+G} \quad \text{and} \quad \nu = \frac{1}{2}\frac{3K-2G}{3K+G} \,. \tag{216}$$

The quantity E is the **elastic modulus** or **Young's modulus**, whereas ν is **Poisson's ratio** (Again - do not confuse Poissons's ratio with the exponent ν we had introduced in Eq. (26).). In the limit that the volume does not change during the deformation, which means the the compression modulus is very large - essentially infinite, this becomes

Table 7 Elastic modulus, shear modulus and Poisson's ratio for selected materials.

material	E [GPa]	G [GPa]	ν
iron	210	82	0.28
aluminum	71	26	0.34
polystyrene	3.2	1.2	0.35
rubber, unfilled	$\approx 1\cdot10^{-3}$ to $5\cdot10^{-3}$	E/3	≈ 0.5
rubber, filled	$\approx 1\cdot10^{-2}$ to $5\cdot10^{-2}$	E/3	≈ 0.5

$$E = 3G \quad \text{and} \quad \nu = \frac{1}{2} \,. \tag{217}$$

We can compare this to our previous result (195). This equation describes the entropy change in a sample containing N polymer chains when the sample is uniaxially stretched without volume change. Analogous to Eq. (212) we write

$$\begin{aligned}\sigma_{zz} &= \frac{1}{V}\frac{\partial(-T\Delta S^{el}_{stretch})}{\partial\lambda} \\ &= \frac{N}{V}k_B T\left(\lambda - \frac{1}{\lambda^2}\right) \overset{(\lambda\approx 1)}{\approx} 3\frac{N}{V}k_B T(\lambda - 1)\end{aligned} \tag{218}$$

or

$$E = 3\frac{N}{V}k_B T \overset{(213)}{=} 3G \tag{219}$$

*. This is a reassuring result in the sense that there appears to be consistency between the formalism for continuous isotropic elastic media in this subsection and our previous picture of elasticity based on conformation entropy of polymer chains.

Nevertheless, we should not be overly confident. The applicability of, for instance, Eq. (218) is limited as demonstrated by an example in Fig. 44. The description of entropy elasticity underlying Eq. (218) does not include the finite extensibility of real polymer chains. The latter gives rise to the marked increase of the stress. Even though this is the most obvious deviation, the rather insufficient inclusion of the network structure into the derivation

* Note that Eq. (218) as well as the Flory-Rehner equation (182), describing the equilibrium swelling of a polymer network, can be used to in principle measure the density of cross-links in the network (for a comparative overview of these and other methods see Anke Blume, Jens Kiesewetter *Determination of the Crosslink Density of Tire Tread Compounds by Different Analytical Methods* Kautschuk Gummi Kunststoffe *9*, 33 (2019)). Both equations contain the number of polymer chains segments, defined as the (average) length of chain between two successive cross-links as one moves along the polymer chain from one cross-link to the next. In praxis, however, Eq. (218), whose accuracy is quite limited, is replaced by a related one - the **Mooney-Rivlin equation** discussed in the section on aspects of the mechanics of polymers.

that lead to (218) limits this equation to strains λ less than 1.5 to 2.

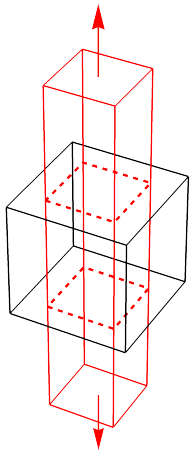

Fig. 43 Stretching of a rectangular sample in z-direction.

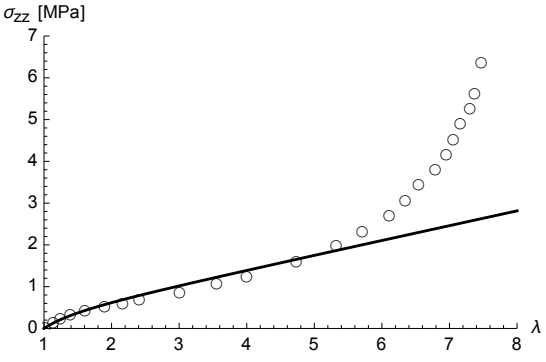

Fig. 44 Stress-strain curve of a highly vulcanized (8% S) NR at 20°C. The data are from Fig. 3 (graph (a)) in L. R. G. Treloar *Stress-strain data for vulcanised natural rubber under various types of deformation.* Trans. Faraday Soc. 40, 59-70 (1944). The solid line is $\sigma_{zz} = G(\lambda - \lambda^{-2})$ according to Eq. (218) fitted to the first four data points with $G \approx 0.35$ MPa.

Finally, it is worth highlighting the following difference between Eq. (212) and Eq. (218). σ_{xz} depends linearly on γ_{xz}, independent of the magnitude of the shear strain. The same is not true for the λ-dependence of σ_{zz} during stretching of the sample, which is non-linear except in the limit $\lambda - 1 \ll 1$.

Remark 1: Figure 45 shows a measurement of stress versus temperature at constant strain for different strains using an elastomer sample. The results obtained for the larger strains meet our expectation, since the straight lines fitting the data exhibit positive slopes in accord with Eq. (218). At small strain, i.e. the lowest three of the curves, the slope is noticeably negative. This apparently disagrees with Eq. (218). How do we explain this?

The elastomer sample possess a positive thermal expansion coefficient. Thermal expansion, however, is due to a part in the elastomer's free energy, which is not part of the conformation entropy that is underlying Eq. (218). In the experiment both effects, the thermal expansion (causing expansion of the sample when it is heated) and entropy elasticity (causing contraction of the sample when it is heated), are present. At small strains the former dominates, whereas at large strains the latter dominates. The cross-over from one dominating to the other dominating is called **thermoelastic inversion**.

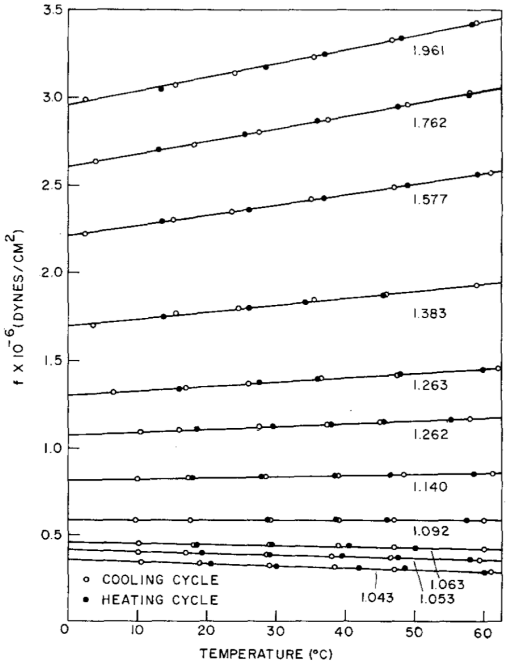

Fig. 45 Thermoelastic data of natural rubber. Numbers on the right-hand side of the graph indicate λ-values. This figure is from M. C. Shen, D. A. McQuarrie, J. L. Jackson *Thermoelastic Behavior of Natural Rubber* J. Appl. Phys. *38*, 791 (1967); note: 1 dyne = 10^{-5} N.

Remark 2 - finite chain extension: Figures 46 and 47 illustrate finite chain extensibility by stretching a bead-spring model chain containing N beads in a Langevin Dynamics computer simulation. Neighbor beads along the chain are linked via Morse potential functions $u_{morse}(r) = D(1 - \exp[-a(r - r_o)])^2$ (here: $D = a = r_o = 1$). Note that the Morse function has a finite depth and therefore the Morse bonds can break. There is no other interaction between the beads. When the simulation box is stretched in z-direction so is the chain, which eventually ruptures. Initially the stress is governed by entropy elasticity. But as the elongation of the chain increases this contribution is reduced in comparison to the effect due to the strain on the individual bonds. Note that $L_{z,o}\lambda/N = 1$ corresponds to a value of λ at which the chain is fully stretched if the bond lengths are at their equilibrium value of r_o. Details of this calculation can be found in R. Hentschke *Including temperature effects in the theory and simulation of problems in rubber reinforcement.* (to appear 2024 in *Advances in understanding*

thermal effects in rubber (G. Heinrich et al. (eds.), Springer Nature:Heidelberg). It is also important to mention that the force required to stretch an isolated polymer chain can be measured in real experiments (see C. Ortiz, G. Hadziioannou *Entropic Elasticity of Single Polymer Chains of Poly(methacrylic acid) Measured by Atomic Force Microscopy.* Macromolecules *32*, 780 (1999)).

It is prudent to note that this is not the standard approach to finite extensibility (cf. section 7.2.3 in Rubinstein and Colby), where it is assumed that increasing strain leads to increasing orientation of bonds in the direction of applied load. In a simple model description each bond is linked to an energy $fb\cos\alpha$, where α is the angle between the bond and the direction of the force f. Assuming in addition that the bonds are independent, it is easy to calculate the thermal average $\langle\cos\alpha\rangle$ (this calculation, even though in a different context, is carried out at the beginning of section 6.3), i.e. $\langle\cos\alpha\rangle = \mathscr{L}(\beta fb)$, where $\mathscr{L}(x) = \coth(x) - 1/x$ is the Langevin function and $\beta = 1/(k_B T)$. Since $\langle\cos\alpha\rangle = R/Nb$, where R is the end-to-end distance of an already stretched chain consisting of N bonds of length b, we obtain $f(R)$ from the inverse Langevin function via

$$f(R) = (\beta b)^{-1}\mathscr{L}^{-1}(R/(Nb)) \,. \tag{220}$$

This is a simple analytic expression relating the stretching force to the chain length in the regime of high elongation, whereas our result in Fig. 47 is a numerical one. However, the latter provides useful information regarding the breaking of the chain and its dependence on temperature and bond potential parameters.

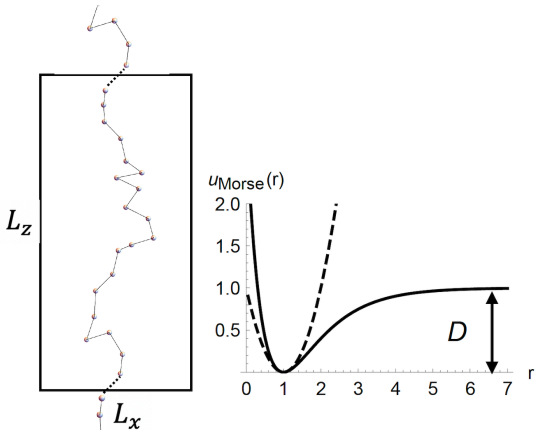

Fig. 46 Beads linked by Morse potentials (right) form a chain (left) which is periodically extended in z-direction. The dashed line is a harmonic approximation at the minimum of the Morse potential function.

Equations and Concepts from Fluid Mechanics:

The mass of fluid, whose uniform mass density is ρ, flowing out of a volume V per unit time is given by

$$\oint_V \rho\vec{v}\cdot d\vec{f} = \int_V \vec{\nabla}\cdot(\rho\vec{v})\,dV \,. \tag{221}$$

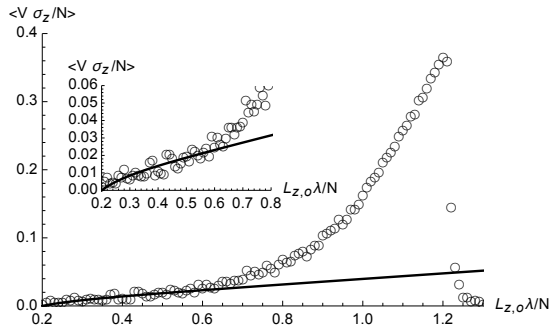

Fig. 47 Reduced stress vs. reduced stretch for a Morse chain simulated using the Langevin Dynamics simulation technique. Data are obtained at a single run without extensive averaging. The z-dimension of the simulation box is $L_{z,o}\lambda$. Lines represent a fit to the data at low strain using (218). Here $N = 50$ and $L_{z,o} = 10\,r_o$.

Here $\vec{v}$ is the fluid velocity within a volume element at position $\vec{r}$. Hence, the **mass continuity equation** becomes

$$\frac{\partial\rho}{\partial t} + \vec{\nabla}\cdot(\rho\vec{v}) = 0 \,. \tag{222}$$

The total force acting on the volume is

$$-\oint_V P\,d\vec{f} = -\int_V \vec{\nabla}P\,dV \,, \tag{223}$$

where P is the pressure. Hence, the equation of motion of a liquid volume element is

$$\rho\frac{d\vec{v}}{dt} = -\vec{\nabla}P \,. \tag{224}$$

The same equation with $d/dt = \partial/\partial t + \vec{v}\cdot\vec{\nabla}$, i.e.

$$\frac{\partial\vec{v}}{\partial t} + (\vec{v}\cdot\vec{\nabla})\,\vec{v} = -\frac{1}{\rho}\vec{\nabla}P \tag{225}$$

is called **Euler's equation**.

The momentum carried by the moving fluid per unit volume is $\rho\,\vec{v}$ and the attendant i-component of the momentum flux is

$$\frac{\partial}{\partial t}\rho\,v_i = \frac{\partial\rho}{\partial t}v_i + \rho\frac{\partial v_i}{\partial t} \,. \tag{226}$$

Using the continuity equation to replace $\partial\rho/\partial t$ and Euler's equation to replace $\partial v_i/\partial t$ we arrive at

$$\frac{\partial}{\partial t}\rho\,v_i = -\frac{\partial\Pi_{ik}}{\partial x_k} \,, \tag{227}$$

where

$$\Pi_{ik} = P\,\delta_{ik} + \rho v_i v_k \,. \tag{228}$$

In a **viscous fluid** we must add an extra contribution $-\tau'_{ik}$ to Π_{ik}, i.e.

$$\Pi_{ik} = P\,\delta_{ik} + \rho v_i v_k - \tau'_{ik}\,, \tag{229}$$

which describes the irreversible 'viscous' transfer of momentum in the fluid. In particular,

$$\tau_{ik} = -P\,\delta_{ik} + \tau'_{ik} \tag{230}$$

defines the **stress tensor** in this context.

We can deduce τ'_{ik} as follows: (i) Internal friction in the liquid implies that there must be velocity gradients $\partial v_i/\partial x_k$, and we assume that τ'_{ik} depends linearly on these gradients. (ii) If the liquid undergoes a uniform rotation we expect no friction, i.e. $\tau'_{ik} = 0$. The velocity due to this rotation is $\vec{v} = \vec{\omega} \times \vec{r}$, or in terms of its components $v_\alpha = \varepsilon_{\alpha\beta\delta}\omega_\beta x_\delta$ where $\vec{\omega}$ is the angular velocity of the rotation and $\varepsilon_{\alpha\beta\delta}$ are the components of the ε-tensor. Using the properties of the ε-tensor we can quickly show that $\partial v_i/\partial x_k + \partial v_k/\partial x_i$ as well as $\partial v_l/\partial x_l \equiv \vec{\nabla}\cdot\vec{v}$ (summation convention!) are zero when rotated. Therefore we express τ'_{ik} as a linear combination of these two terms:

$$\tau'_{ik} = \eta\left(\frac{\partial v_i}{\partial x_k} + \frac{\partial v_k}{\partial x_i} - \frac{2}{3}\delta_{ik}\frac{\partial v_l}{\partial x_l}\right) + \eta'\delta_{ik}\frac{\partial v_l}{\partial x_l}\,. \tag{231}$$

Note that we chose this combination so that the trace of the first term, multiplied by the **(shear) viscosity coefficient** η (cf. the selected examples in Tab. 8), is zero. The coefficient η' is the **second viscosity**.

Here we concentrate on incompressible liquids, which according to the continuity equation implies

$$\vec{\nabla}\cdot\vec{v} = 0 \tag{232}$$

and thus

$$\tau_{ik} = -P\delta_{ik} + \eta\left(\frac{\partial v_i}{\partial x_k} + \frac{\partial v_k}{\partial x_i}\right)\,. \tag{233}$$

Notice that the combination of Eqs. (227), (229), (230), and (233) yields

$$\frac{\partial\vec{v}}{\partial t} + (\vec{v}\cdot\vec{\nabla})\vec{v} = -\frac{1}{\rho}\vec{\nabla}P + \frac{\eta}{\rho}\Delta\vec{v}\,, \tag{234}$$

where $\Delta = \vec{\nabla}^2$. This is the **Navier-Stokes equation** for an incompressible fluid. It will become important when we need to consider hydrodynamic interactions in polymer systems. We shall assume steady flow, i.e. $\partial\vec{v}/\partial t = 0$, and that the **Reynolds number** R, i.e.

$$R = \frac{\rho}{\eta}ul\,, \tag{235}$$

where l is a typical linear dimension of the body in the flow of the viscous liquid and u is the liquid's velocity far from the body, is small. Note that the quantity η/ρ is called **kinematic viscosity**.

Small R implies that the term $(\vec{v}\cdot\vec{\nabla})\vec{v}$ can be neglected compared to $(\eta/\rho)\Delta\vec{v}$. This follows since the first term is on the order of u^2/l whereas the second one is on the order of $(\eta/\rho)u/l^2 = (1/R)u^2/l$. Therefore (234) reduces to

$$\eta\Delta\vec{v} = \vec{\nabla}P\,. \tag{236}$$

If there is an additional external force density $\vec{\varphi}(\vec{r})$ present this equation becomes

$$\eta\Delta\vec{v}(\vec{r}) - \vec{\nabla}P(\vec{r}) + \vec{\varphi}(\vec{r}) = 0\,. \tag{237}$$

Let us briefly digress and solve this equation so that we do not have to do this later when we need the solution. We replace the components of $\vec{v}(\vec{r})$ and $\vec{\varphi}(\vec{r})$ as well as $P(\vec{r})$ by their Fourier transforms, i.e.

$$f(\vec{r}) = (2\pi)^{-3/2}\int d^3k f_k \exp[-i\vec{k}\cdot\vec{r}]\,. \tag{238}$$

The result is

$$-\eta k^2\vec{v}_k + i\vec{k}P_k + \vec{\varphi}_k = 0\,. \tag{239}$$

Scalar multiplication of this equation by $\vec{k}$ and using (232), i.e. $\vec{k}\cdot\vec{v}_k = 0$ yields

$$P_k = i\frac{\vec{k}\cdot\vec{\varphi}_k}{k^2}\,. \tag{240}$$

Inserting this into (239) we obtain for the flow field in $\vec{k}$-space

$$\vec{v}_k = \frac{1}{\eta k^2}\left(\vec{\varphi}_k - \frac{\vec{k}(\vec{k}\cdot\vec{\varphi}_k)}{k^2}\right) \tag{241}$$

or in component form

$$v_{k,\alpha} = \frac{1}{\eta k^2}\left(\delta_{\alpha\beta} - e_{k,\alpha}e_{k,\beta}\right)\varphi_{k,\beta}\,, \tag{242}$$

where $\vec{e}_k = \vec{k}/k$. We find the flow field in $\vec{r}$-space using the convolution theorem, i.e.

$$v_\alpha(\vec{r}) = (2\pi)^{-3/2}\int d^3k\frac{1}{\eta k^2}\left(\delta_{\alpha\beta} - e_{k,\alpha}e_{k,\beta}\right)\varphi_{k,\beta}\exp[i\vec{k}\cdot\vec{r}]$$

or

$$v_\alpha(\vec{r}) = \int d^3r' H_{\alpha\beta}(\vec{r}-\vec{r}')\varphi_\beta(\vec{r}')\,, \tag{243}$$

where

$$H_{\alpha\beta}(\vec{x}) = (2\pi)^{-3}\int d^3k\frac{1}{\eta k^2}\left(\delta_{\alpha\beta} - e_{k,\alpha}e_{k,\beta}\right)\exp[i\vec{k}\cdot\vec{x}]\,. \tag{244}$$

The last step in our solution therefore is the calculation of the integral in Eq. (244), which is given by †

$$H_{\alpha\beta}(\vec{x}) = \frac{1}{8\pi\eta x}\left(\delta_{\alpha\beta} + e_{x,\alpha}e_{x,\beta}\right) \tag{245}$$

($\vec{e}_x = \vec{x}/x$). The quantities $H_{\alpha\beta}$ are the components of the **Oseen tensor**.

Now let's return to Eq. (233), which is of more immediate importance. Figure 48 depicts a fluid between two plates. The bottom plate is at rest while the upper plate moves in x-direction, causing a uniform velocity gradient in the fluid. The stationary profile is maintained by the force F_{xz} on the upper plate, i.e.

$$\tau_{xz} \propto \frac{\delta v_x}{\delta z} = \frac{L_x \varepsilon}{\Delta t\, L_z} = \dot{\gamma}_{xz}\,, \tag{246}$$

where we use the same notation as in Fig. 42. Hence

$$\tau_{xz} = \eta\, \dot{\gamma}_{xz}\,. \tag{247}$$

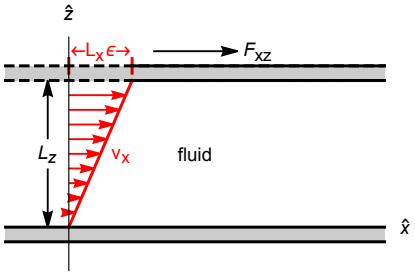

Fig. 48 Laminar flow profile between two plates.

Table 8 Shear viscosity of selected substances

substance	η [Pa s]
air	$17.2\cdot10^{-6}$
water	$1.002\cdot10^{-3}$
olive oil	$80.8\cdot10^{-3}$
S-SBR M_w=276 [kg/mol]	ca. $1\cdot10^{11}$

A Phenomenological Model for Linear Viscoelasticity:

Equation (211) together with Eq. (247) furnish the basic elements in the phenomenological description of **linear viscoelasticity**. In the following we represent (211) in simplified form via

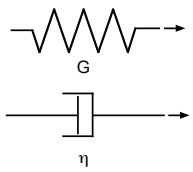

Fig. 49 Symbolic elements representing elastic and viscous contributions. The spring symbol stands for (211), whereas the dashpot symbol represents (247).

$$\sigma_G = G\,\gamma_G \tag{248}$$

and analogously (247) via

$$\sigma_\eta = \eta\,\dot{\gamma}_\eta\,. \tag{249}$$

A pictorial representation of the two equations is shown in Fig. 49. These basic elements can be combined into simple models describing linear viscoelastic material behavior. Three such models are depicted in Fig. 50. Here we consider model (a) only, the so-called Kelvin-Voigt (KV) model, mainly because it is well known to physicists.

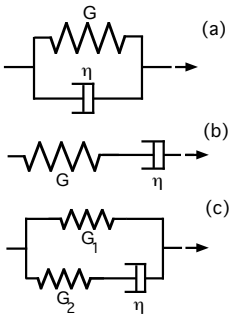

Fig. 50 (a) Kelvin-Voigt model; (b) Maxwell model; (c) Zener model

The mathematical form of the KV-model is

$$\sigma = \sigma_G + \sigma_\eta \qquad \gamma = \gamma_G = \gamma_\eta\,. \tag{250}$$

The quantity σ is the total stress and γ is the total strain. Notice that due to the parallel arrangement of the two basic elements in the KV-model, σ is the sum of the stresses σ_G and σ_η contributed by the respective branches. The total strain γ, on the other hand, is identical to the strain, γ_G and γ_η, in each individual branch. Using (248) and (249) we obtain for the KV-model

$$\sigma(t) = G\,\gamma(t) + \eta\,\dot{\gamma}(t)\,. \tag{251}$$

Let's pause for a moment and compare this equation to the equation of motion of the one-dimensional damped harmonic os-

† Note first that the change of variables $\vec{k}' = x\vec{k}$ immediately yields $H_{\alpha\beta}(\vec{x}) \propto x^{-1}$. The standard solution (cf. Doi&Edwards or Grossberg&Khokhlov) assumes the general form $H_{\alpha\beta}(\vec{x}) = A(x)\delta_{\alpha\beta} + B(x)e_{x,\alpha}e_{x,\beta}$. Taking the trace yields $H_{\alpha\alpha}(\vec{x}) = 3A(x) + B(x)$ or, from (244) $H_{\alpha\alpha}(\vec{x}) = (2\pi)^{-3}\int d^3k \frac{2}{\eta k^2}\exp[i\vec{k}\cdot\vec{x}] = (2\pi\eta x)^{-1}$. We also have $e_{x,\alpha}H_{\alpha\beta}(\vec{x})e_{x,\beta} = A(x) + B(x)$ and, again from (244), $e_{x,\alpha}H_{\alpha\beta}(\vec{x})e_{x,\beta} = (2\pi)^{-3}\int d^3k \frac{1}{\eta k^2}\left(1 - (\vec{e}_x\cdot\vec{e}_k)^2\right)\exp[i\vec{k}\cdot\vec{x}] = (4\pi\eta x)^{-1}$. Combination of the two equations for A and B yields $A = B = (8\pi\eta x)^{-1}$. Note also that the $\vec{k}$-integrals in $H_{\alpha\alpha}$ and $e_{x,\alpha}H_{\alpha\beta}e_{x,\beta}$ are easier compared to the one in (244). This is because $H_{\alpha\alpha}$ and $e_{x,\alpha}H_{\alpha\beta}e_{x,\beta}$ are invariant under rotations. Hence we can chose $\vec{x}$ as our z-axis, something we cannot do in (244), and use for instance polar coordinates.

cillator driven by a time-dependent external force $f(t)$, i.e.

$$f(t) = k\,x(t) + \zeta\,\dot{x}(t) + m\,\ddot{x}(t)\;. \tag{252}$$

Here $x(t)$ is the position of the oscillator relative to its position at rest, k is the spring constant, ζ is a friction constant, and m is the mass of the oscillator. The only difference between Eqs. (251) and (252) is the absence of the acceleration term in Eq. (251). This means that the acceleration of the mass of a volume element within the sheared viscoelastic sample is not important. Instead the volume element moves according to the equilibrium of the forces acting on it.

We remember that the long-time solution of the oscillator subject to an oscillatory force possess the same form as the force except for a phase shift. Here we try an analogous ansatz in the case of (251), i.e.

$$\sigma(t) = \sigma_o \sin(\omega t + \delta) \quad \text{and} \quad \gamma(t) = \gamma_o \sin(\omega t)\;. \tag{253}$$

We may be surprised that the stress ansatz includes the phase shift δ and not the strain. Fig. 51 depicts the type of rheometer frequently used in shear experiments. The specimen, a disc-shaped piece of rubber in this case, is clamped between two dies. One of the dies imposes a rotary oscillation upon the specimen. The corresponding angle at time t is $\varphi(t)$. The other die keeps the opposite side of the sample stationary during the oscillation, which shears the sample. Keeping the opposite side of the sample fixed requires the torque $N_\varphi(t)$. An interesting feature of this design is the biconical shape of the die assembly (the sample is thick at its rim but is thin at the center), which ensures that the strain inside the sample is uniform. The protrusions on the sample surface are necessary for a tight grip of the die on the sample. Note that $\gamma(t)$ and $\sigma(t)$ are related to $\varphi(t)$ and $N_\varphi(t)$ via

$$\gamma(t) = \frac{\varphi(t)}{\phi} \quad \text{and} \quad \sigma(t) = \frac{3N_\varphi(t)}{2\pi R^3}\;. \tag{254}$$

A typical value of ϕ is 7°. This means that a rotation φ of 1° corresponds to a strain of $\varphi/\phi \approx 14\%$.

Inserting the ansatz (253) into (251) and using the identity

$$\sin(\omega t + \delta) = \cos(\delta)\sin(\omega t) + \sin(\delta)\cos(\omega t) \tag{255}$$

yields

$$G' \equiv \frac{\sigma_o}{\gamma_o}\cos\delta = G \tag{256}$$

$$G'' \equiv \frac{\sigma_o}{\gamma_o}\sin\delta = \eta\,\omega \tag{257}$$

$$\tan\delta = \frac{G''}{G'} = \tau_{KV}\,\omega \quad (\tau_{KV} = \eta/G)\;. \tag{258}$$

Here G' is the **storage modulus**, G'' is the **loss modulus**, and their ratio, $\tan\delta$, is the **loss tangent**. The quantity τ_{KV} is a relaxation time. We see this if we set the stress in Eq. (251) equal to zero. Separation of variables then leads to

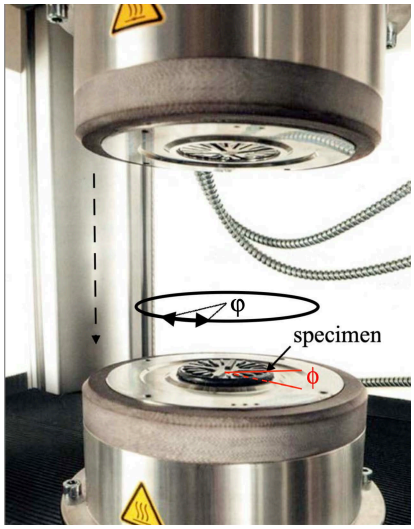

Fig. 51 A MonTech® Moving Die Rheometer with biconical die assembly. The biconical rubber sample, whose radius is R, is thin at its center and gets wider with increasing radial distance from the center. The corresponding angle is ϕ.

$$\gamma(t) = \gamma(0)\exp[-t/\tau_{KV}]\;, \tag{259}$$

which describes the strain relaxation after the stress is 'turned off'.

However, let's discuss G' and G'' in more detail. First of, why are they important? Their measurement yields information on the dependence of the dynamic mechanical properties of a viscoelastic material on frequency, temperature and composition. From this information a material developer of tire tread rubber can estimate a new tire's performance during breaking or what its rolling resistance will be compared to some other tire. G' and G'' are also important in the food industry, just to give you an impression of the range of their application, since they affect the processing and even determine how food feels when you eat it.

G' and G'' are difficult quantities - both theoretically and experimentally. Our results in Eq. (256), i.e. $G' = G$ and $G'' = \eta\,\omega$, are specific to the KV-model. Had we used the Maxwell model in Fig. 50 the result would have been different. The Zener model, we would find, is a combination of both the KV- and the Maxwell model. The problem with these phenomenological models is that they do not connect well to the molecular scale. This means that we have to do the measurement first and decide only afterwards which phenomenological model yields the best qualitative description of the experimental data. Nevertheless, phenomenological models of viscoelasticity furnish a rough understanding of the interplay between elasticity and viscosity - and they are simple, which makes them sufficiently useful.

If $G' = G$ and $G'' = \eta\,\omega$ is a result specific to the KV-model, how general are the definitions $G' \equiv \frac{\sigma_o}{\gamma_o}\cos\delta$ and $G'' \equiv \frac{\sigma_o}{\gamma_o}\sin\delta$? These definitions are general as long as the ansatz (253) works, i.e. equations into which we insert the ansatz must be linear in

$\gamma(t)$ and $\sigma(t)$. Rheometer like the one depicted in Fig. 51 are sold with software which analyses **stress-strain curves**. For a linear viscoelastic sample, i.e. the ansatz works, the experimental result will look like the elliptical closed curve shown in Fig. 52. Each closed curve corresponds to a complete cycle of $\gamma(t)$. The enclosed area is the dissipated energy during the cycle. Let's calculate this energy:

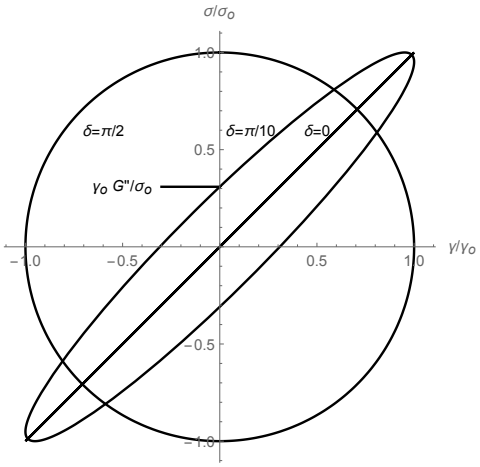

Fig. 52 Stress-strain cycles for three different phase shifts.

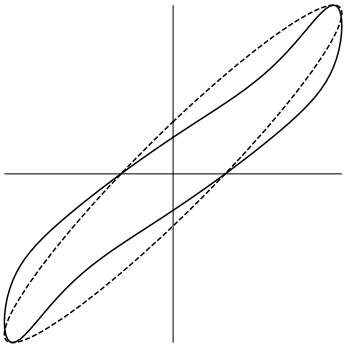

Fig. 53 Schematic of a distorted stress-strain cycle compared to its elliptical approximation.

$$w = \oint \sigma \, d\gamma = \int_0^{2\pi/\omega} \sigma \, \dot{\gamma} \, dt \; . \tag{260}$$

Inserting (253) yields

$$w = \pi \, \gamma_o \sigma_o \sin\delta = \pi G'' \gamma_o^2 \; , \tag{261}$$

i.e. only G'' does contribute to w. Note that w is the dissipated energy per unit volume. The three stress-strain curves in Fig. 52 therefore describe no loss $w(\delta = 0) = 0$, intermediate loss $w(\delta = \pi/10$, maximum loss $w(\delta = \pi/2)$. In other words, the rheometer's software will try and fit the recorded stress-strain data with (253), which yields δ and σ_o and, using the definitions $G' \equiv \frac{\sigma_o}{\gamma_o}\cos\delta$ and $G'' \equiv \frac{\sigma_o}{\gamma_o}\sin\delta$, G' and G''. However, the experimental stress-strain curves may be distorted (e.g. when the shear modulus depends on the strain amplitude for various reasons). A schematic example of a distorted stress-strain/torque-rotation angle-cycle is depicted in Fig. 53. Despite this the software still attempts to find the best fit based on the linear theory. In fact, many experimental results for G' and G'' in the literature have been obtained in this fashion (which, if one is aware of this procedure, still yields useful information ‡). Note that Eq. (260) is completely general and independent of whether the viscoelastic behavior is linear or not. Eq. (261) therefore could be used as an independent definition of G'', i.e. G'' would solely result from the enclosed area of the stress-strain curve.

The real ansatz (253) can be replaced by its complex version:

$$\tilde{\sigma} = \sigma_o e^{i(\omega t + \delta)} \qquad \tilde{\gamma} = \gamma_o e^{i\omega t} \; . \tag{262}$$

It is common practice to define the **complex modulus** $G^* = \tilde{\sigma}/\tilde{u}$. Insertion of (262) into Eq. (251) yields

$$G^* = G' + iG'' \; , \tag{263}$$

i.e. G' and G'' are the real and imaginary parts of the complex modulus. The inverse of the complex modulus G^* is called **compliance** J^*, i.e.

$$J^* = \frac{1}{G^*} \; . \tag{264}$$

The compliance is a measure for how easy it is to deform the sample. Note

$$J' = \frac{G'}{|G^*|^2} \quad \text{and} \quad J'' = \frac{G''}{|G^*|^2} \; , \tag{265}$$

where $|G^*|^2 = G'^2 + G''^2$.

Finally, let us look at some experimental results. The solid symbols in Fig. 54 depict the shear storage modulus of S-SBR and the open symbols show the corresponding shear loss modulus. Both quantities are plotted versus frequency f. You may wonder how a machine like the one shown in Fig. 51 is capable of up to 10^8 Hz. Well, it is not. The rheometer acquires data at much lower frequencies in a comparatively narrow frequency range - perhaps 0.01 Hz to 1 Hz. Using what is called **time-temperature superposition**, which we discuss below, a **master curve** is constructed - like the one shown in Fig. 54. The meaning of the master curve is that if we had an instrument capable of covering the indicated frequency range, then it would yield this result at 23°C.

Let's concentrate on panel (b) first. Below 1 Hz we obtain the result predicted by the KV-model in Eqs. (256) and (257). The storage modulus is constant and the loss modulus decreases with

‡ This is under the assumption that the structure of the material is responsible for the distortion and not, for instance, slippage in the interface between die and sample, which may occur at large strain amplitudes.

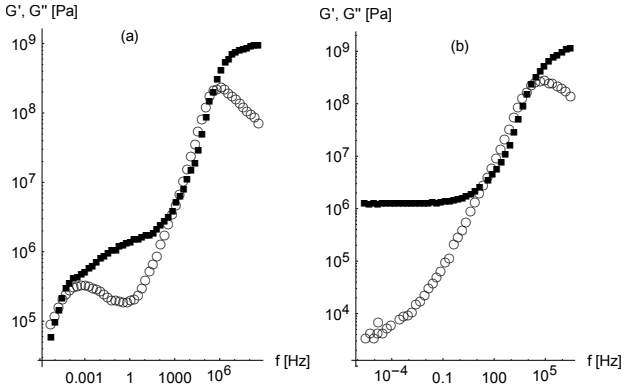

Fig. 54 Comparison of the master curves for non-cross-linked (a) and cross-linked (b) S-SBR. Solid symbols: G'; open symbols: G''.The reference temperature is 23°C. The 0 or 4 phr (parts per hundred rubber by weight) is the amount of sulfur added in order to create cross-links during vulcanization. The data in this figure are form Fig. 2.99 in C. Wrana *Introduction to Polymer Physics*.

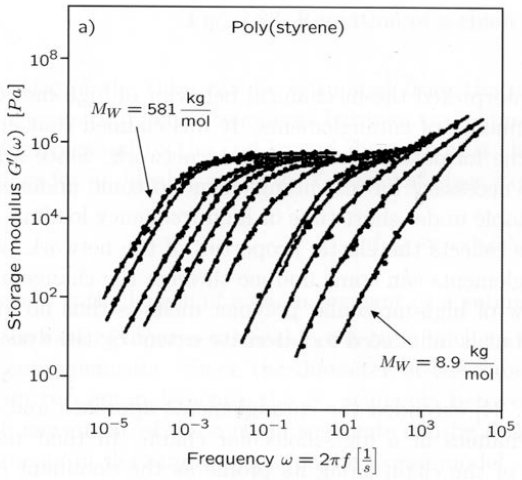

Fig. 55 Frequency dependence of the storage modulus of polystyrene in the molten state as function of molecular weight. This figure is copied from C. Wrana *Introduction to Polymer Physics* (Fig. 2.82). Original source: S. Onogi, T. Masuda, K. Kitagawa *Rheological Properties of Anionic Polystyrenes. I. Dynamic Viscoelasticity of Narrow-Distribution Polystyrenes.* Macromolecules *3*, 109 (1970).

decreasing frequency, albeit with a power less than one. Above 1 Hz, however, G' rises and appears to level off eventually. G'' on the other hand exhibits a maximum. In panel (a) the behavior of G' and G'' above 1 Hz is pretty much unaltered in comparison to panel (b). But below 1 Hz the storage modulus decreases with variable degree of steepness and G'' exhibits another maximum. The main difference between the two panels is the amount of cross-linking. The results in panel (a) are for a polymer, which is not chemically cross-linked. Hence, when the shear frequency is low, the polymer chains possess much more mobility as compared to panel (b). Finally, Fig. 55 shows that a constant storage modulus is not just due to chemical cross-linking. In this case the so-called **plateau modulus** develops by increasing the molecular weight. As the polymer chains get longer we expect more entanglement - again an obstacle to the mobility of certain modes of motion the chains do otherwise possess.

Overall, this should be obvious at this point, our understanding of G' and G'' as functions of frequency is insufficient and we must aim for a better and more comprehensive understanding - preferably on the molecular level.

Time-Temperature Superposition:

Figure 56 shows measurements of both the storage and the loss modulus of a SBR sample. On the left hand side of this figure the original data are depicted. These consist of measurements at different temperatures over a frequency range from roughly 0.01 Hz to 1 Hz. The arrows indicate the next step. The red data points obtained at T_r =20°C - the arbitrarily chosen reference temperature - are left untouched. All other data sets, obtained at temperatures T_i, are shifted horizontally along the frequency axis. This shift is towards the right, i.e. towards higher frequencies, when $T_i < T_r$. Otherwise, $T_i > T_r$, it is towards the left, i.e. towards lower frequencies. The amount of shifting is controlled by the condition that the shifted data sets form a smooth continuous curve. The claim is that this final curve is the G' or the G'' at T_r, which one obtains with an instrument capable of scanning the entire frequency range from 10^{-3} Hz to 10^{11} Hz in Fig. 56. The final result looks good, but is there a justification for this procedure?

Looking at our only expressions for G' and G'' thus far, i.e. Eqs. (256) and (257), we notice that $\omega = 2\pi f$ appears multiplied with the viscosity η, which is strongly dependent on temperature T. In other words, if frequency enters into a dynamical expression g via the product $\eta(T)\omega \equiv y$, i.e. $g = g(y)$, we can obtain the value $g(y)$ using either the product of $\eta(T')$ with ω' or η with ω as long as $y = \eta(T')\omega' = \eta(T)\omega$. Hence, if a particular dynamical feature (a particular measured value for G' or G'' in the original data sets depicted in Fig. 56) appears at the frequency ω' at the temperature T', then the very same feature will appear at the frequency ω when the temperature is T. Hence,

$$\omega = \frac{\eta(T')}{\eta(T)}\omega' \tag{266}$$

converts the original frequencies into the shifted ones. Let's find out what the η-ratio is in terms of explicit temperature.

The temperature dependence of η is empirically described by the **Dolittle relation**

$$\eta(T) \propto \exp[A/v_f(T)]\,. \tag{267}$$

The quantity A is a constant and $v_f(T)$ is the **free volume**. The free volume is illustrated in Fig. 57 for a spherical particle which can move freely within a larger likewise spherical cavity. The volume indicated by the dashed circle in the figure is the volume accessible to the center of mass of the particle, which is its free volume in this example. Mathematically the free volume of a

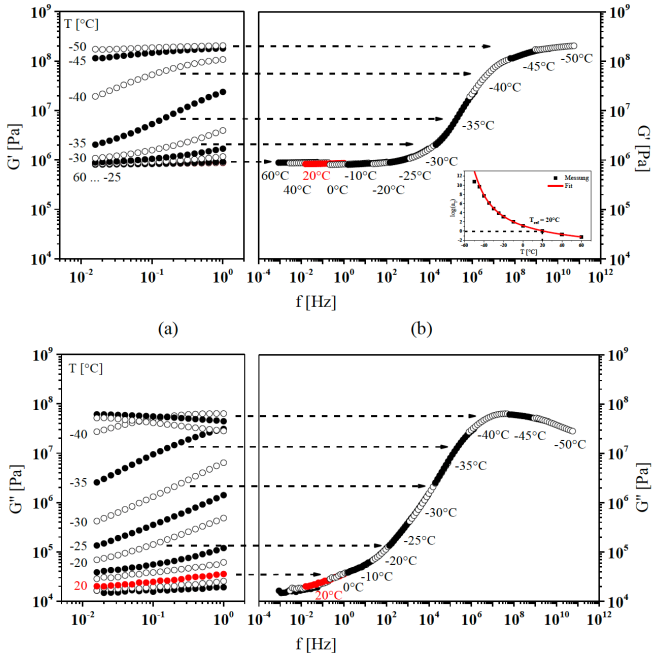

Fig. 56 Illustration of time-temperature superposition (Fig. 37 from A. Lang, PhD thesis, University of Hannover (2018)).

particle within a potential $u(\vec{r})$ is given by

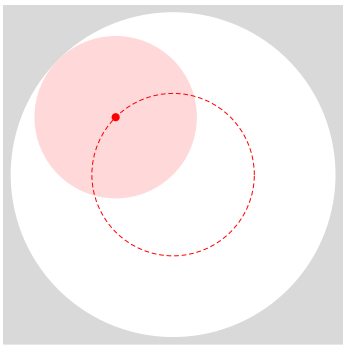

Fig. 57 Free volume illustration. The particle is shown in light red.

$$v_f = \int_V d^3r \exp[-\beta(u(\vec{r}) - u(0))] \,, \tag{268}$$

where $\beta = (k_B T)^{-1}$ and $u(0)$ is the potential minimum within the cavity. Clearly, as the shape of the particle as well as the shape of the cavity become more complicated so does v_f. Nevertheless to leading order we may express the temperature dependence of v_f via the linear equation

$$v_f(T) = v_f(T_r) + \alpha(T - T_r) \,. \tag{269}$$

Here α is a constant and T_r an arbitrary reference temperature.

Inserting (269) into (267) we obtain for the ratio $\eta(T)/\eta(T_r)$

$$a_T \equiv \frac{\eta(T)}{\eta(T_r)} = \exp\left[-\frac{A}{v_f(T_r)}\frac{T - T_r}{v_f(T_r)/\alpha + T - T_r}\right] \,. \tag{270}$$

This is the **WLF equation**, named after Williams, Landel and Ferry, who first applied it to polymer melts (J. D. Ferry *Viscoelastic Properties of Polymers* John Wiley & Sons:New York (1961); M. L. Williams, J. D. Ferry *Second approximation calculations of mechanical and electrical relaxation and retardation distributions* J. Polymer Science *11*, 169 (1953); M. L. Williams, R. F. Landel, J. D. Ferry *The Temperature Dependence of Relaxation Mechanisms in Amorphous Polymers and Other Glass-forming Liquids* J. American Chemical Society *77*, 3701 (1955)). The quantity a_T is also called the **shift factor**. Hence, the shifted frequencies in Fig. 56 are obtained from their reference or original values ω_r via

$$\omega = \frac{1}{a_T}\omega_r \,. \tag{271}$$

The shift factor belonging to the master curves in Fig. 56 is depicted in this figure as an inset and enlarged as a separate graph in Fig. 58. a_T contains the two parameters $A/v_f(T_r)$ and $v_f(T_r)/\alpha$, which are adjusted until the result is a smooth master curve as described above.

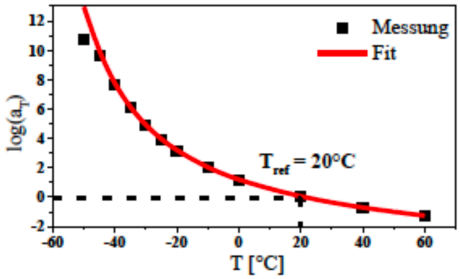

Fig. 58 Shift factor enlarged from Fig. 56. Each solid square corresponds to a series of data points obtained in the original frequency intervall (here 0.01 Hz to 1 Hz) at the respective temperature.

Equation (270) is based on qualitative arguments and rough approximations. Despite this, in pure polymer systems time-temperature superposition works extremely well and is frequently used. In fact, 'mastering' is not restricted to G' and G'', but is applied to other frequency/temperature-dependent quantities as well. Before we leave this section, let us briefly study an important example in the context of rubber sliding friction.

In school or in undergraduate physics courses the coefficient of sliding friction μ is a material or interface dependent number. The top panel in Fig. 59 depicts μ for various rubbers sliding on glass over a wide range of sliding velocities v. This master curve for μ is obtained using the same procedure used to obtain the master curves for the dynamic moduli. Measurements of $\mu(v)$ in a comparatively narrow velocity interval are carried out at different temperatures. Subsequently the individual measurements are combined into a smooth master curve via horizontal shifting.

The first aspect we notice is that μ is not a constant at all. It starts low when the sliding velocity is small and it ends low when the sliding velocity is large. Inbetween it exhibits a pronounced

maximum. The bottom panel in Fig. 59 shows the corresponding loss moduli versus frequency f. Apparently there is a close correspondence between the maximum of μ and the maximum of G'' (Note that similar, but on the high frequency side truncated, maxima can be seen in Figs. (54) and (56) as well.). Can we understand why there should be this connection between μ and G''?

The sketch in Fig. 60 depicts the rubber sample sliding on a surface. The surface's roughness leads to the deformation of the rubber, which in turn leads to a viscoelastic response indicated by the two pictures of the KV model. Assuming linearity, the energy (per volume rubber) dissipated during sliding is given by Eq. (261). We can also express the dissipated energy as the product of the friction force, which itself is proportional to μ, times a certain sliding distance s. Combination of the two observations suggests

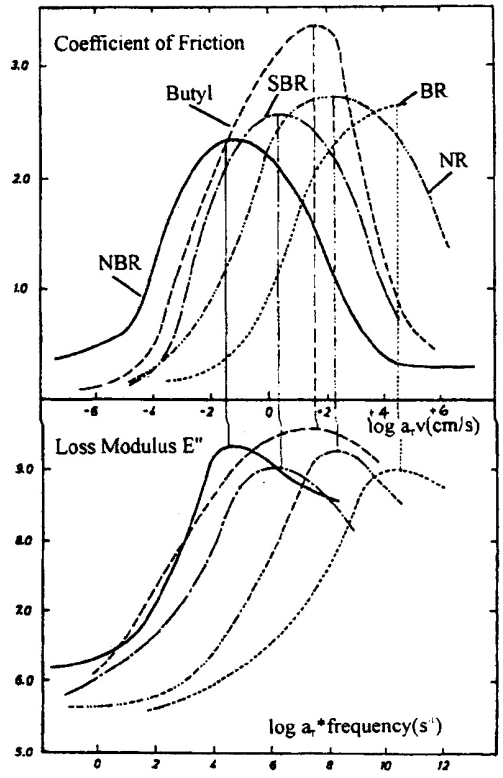

Fig. 59 Comparison between the friction master curves and the loss module master curves of five not chemically cross-linked rubbers on dry glass. The reference temperature is 20°C, i.e. the shift factor $a_T = 1$ at this temperature. For other temperatures we would have to know the corresponding a_T-value in order to calculate the attendant frequency. This figure is Fig. 7 copied from K. A. Grosch *The rolling resistance, wear and traction properties of tread compounds.* Rubber Chemistry and Technology *69*, 495 (1996).

$$\mu(v) \propto G''(f)\,, \tag{272}$$

where $f = f(v)$. If we simply assume that s is the distance between two (identical) protrusions deforming the rubber then $v = sf$, which explains why we find velocity on the x-axis of the

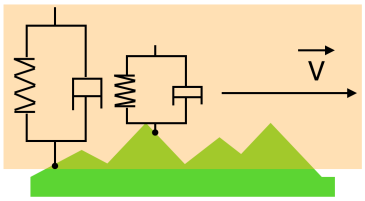

Fig. 60 Cartoon of a piece of rubber sliding on a rough surface with the velocity $\vec{v}$.

μ-master curve and frequency on the x-axis of the G''-master curve. However, it is important to note that we assume that the only contribution to friction is **hysteresis friction**. This is never quite the case, since we always have to include **adhesion** and **mechanical interdigitation** as well. In addition, the complex morphology of the interface between rubber and the solid must be taken into account. Hence, it is not surprising that friction of polymer materials is the subject of active research (e.g. B. Lorenz, Y. R. Oh, S. K. Nam, S. H. Jeon, B. N. J. Persson *Rubber friction on road surfaces: Experiment and theory for low sliding speeds* J. Chemical Physics *142*, 194701 (2015)).

The Shear Relaxation Modulus:

Our discussion of linear viscoelasticity thus far is based on the ad hoc combination of σ_G and σ_η, i.e. the combination of Eq. (248) and Eq. (249). The specific time or frequency dependence of the measurable quantities, e.g. the storage modulus G' or the loss modulus G'', varies depending on the kind of combination of σ_G and σ_η we choose to study. In addition, we only know how the calculate G' and G'' based on phenomenological models like the ones depicted in Fig. 50. All in all this is not a satisfactory situation.

In the next section we study the dynamics of polymer chain models. Since these models possess clear physical meaning compared to the phenomenological models, we want to be able to calculate their G' and G''. But how do we calculate the dynamic moduli when we do not have an equation like (251) for the KV-model?

The equation

$$\sigma(t) = \int_{-\infty}^{t} G(t-t')\,d\gamma(t') \tag{273}$$

is a generalization of (251) and others like it. G is called the **shear relaxation modulus**. The equation means that the shear stress at time t is accumulated from many small shear amplitude steps at previous times t'. In essence, the contribution of a small amplitude to the final stress depends on on the time interval $t-t'$. $G(t-t')$ is a modulus, but it is not G from Eq. (248). It combines the viscoelastic nature of the (polymer) material in one quantity. But even if we have this $G(t-t')$ for a specific chain model, how do we then calculate G' and G''?

Note first that $d\gamma(t) = \dot{\gamma}(t)dt$ and thus (273) becomes

$$\sigma(t) = \int_{-\infty}^{t} G(t-t')\,\dot\gamma(t')dt' \,. \tag{274}$$

If for instance the strain increases instantaneously from zero to its maximum value at $t = 0$, i.e.

$$\gamma(t) = \begin{cases} 0 & t<0 \\ \gamma_o & t>0 \end{cases} \,, \tag{275}$$

then Eq. (274) yields

$$\sigma(t) = G(t)\gamma_o \,. \tag{276}$$

Here we have used $\dot\gamma(t) = \gamma_o\delta(t)$. This means that if we can realize (275) experimentally, then we can obtain $G(t)$ by observing the decay of the shear stress.

Of particular interest is a sinusoidal shear strain, i.e.

$$\gamma(t) = \gamma_o \sin(\omega t) = \gamma_o \,\mathrm{Im}(e^{i\omega t}) \tag{277}$$

(cf. (253)), since we already have discussed this type of shear. Using (253) in conjunction with (255) and $G' = \frac{\sigma_o}{\gamma_o}\cos\delta$ as well as $G'' = \frac{\sigma_o}{\gamma_o}\sin\delta$ (cf. (256) and (257)) we obtain

$$\sigma(t) = G'(\omega)\gamma_o\sin(\omega t) + G''(\omega)\gamma_o\cos(\omega t) = \gamma_o\,\mathrm{Im}\left(G^*(\omega)e^{i\omega t}\right) \tag{278}$$

We can now show the validity of

$$G^*(\omega) = i\omega\int_0^\infty dt\, G(t)\, e^{-i\omega t} \tag{279}$$

by inserting (279) into (278) [§]. From Eq. (279) we immediatly find the desired equations for storage and loss modulus in terms of $G(t)$, i.e.

$$G'(\omega) = \omega\int_0^\infty dt\, G(t)\,\sin(\omega t) \tag{281}$$

and

$$G''(\omega) = \omega\int_0^\infty dt\, G(t)\,\cos(\omega t)\,. \tag{282}$$

Application examples of these two useful formulas will be discussed in the next section.

§

$$\sigma(t) = \gamma_o\,\mathrm{Im}\left(i\omega\int_0^\infty dt'\,G(t')\,e^{i\omega(t-t')}\right) \overset{t-t'=t''}{=} \gamma_o\int_{-\infty}^{t} dt''G(t-t'')\,\mathrm{Im}\left(i\omega e^{i\omega t''}\right) \tag{280}$$

Working out Im(...) we find that the result is again Eq. (274).

5.2 Single Chain Dynamics

In this section we discuss polymer dynamics based on a single chain model and its refinements.

Preliminaries:

Imagine a sphere of mass m and radius R moving in a liquid of small molecules possessing the mass density ρ and the viscosity η. The equation of motion of (the center of mass of) this sphere is

$$m\ddot{\vec r} = -\zeta\dot{\vec r}\,. \tag{283}$$

The right hand side is **Stoke's friction** force, i.e. $\zeta = 6\pi\eta R$. This may be expressed as

$$\dot{\vec v} = -\frac{1}{\tau}\vec v\,, \tag{284}$$

where $\vec v = \dot{\vec r}$ and

$$\tau = \frac{m}{\zeta} = \frac{2}{9}\frac{\rho R^2}{\eta}\,. \tag{285}$$

Equations (284) tells us that the initial velocity of the sphere decays exponentially with a relaxation time τ, i.e.

$$\vec v(t) = \vec v(0)\exp[-t/\tau]\,. \tag{286}$$

Assuming the liquid is water and using $R = 10$ nm we find $\tau \approx 2\cdot 10^{-11}s$. This is short compared to (most) relaxation times in polymer dynamics.

It is possible and useful to tie the friction coefficient ζ to the diffusion coefficient D in the Einstein law of diffusion (24). Our starting point is

$$6Dt = \langle\Delta\vec r^2\rangle = \int_o^t dt'\int_o^t dt''\langle\vec v(t')\cdot\vec v(t'')\rangle \tag{287}$$

or

$$\begin{aligned} 6D &= \frac{d}{dt}\langle\Delta\vec r^2\rangle = 2\langle\vec v(t)\cdot[\vec r(t)-\vec r(0)]\rangle \\ &= 2\langle\vec v(0)\cdot[\vec r(0)-\vec r(-t)]\rangle \\ &= 2\int_{-t}^{0} dt'\langle\vec v(0)\cdot\vec v(t')\rangle \\ &= 2\int_0^t dt'\langle\vec v(0)\cdot\vec v(t')\rangle \\ &= 2\langle\vec v(0)^2\rangle\int_0^t dt'\exp[-t'/\tau] \\ &= 2\langle\vec v(0)^2\rangle\tau(1-\exp[-t/\tau])\,. \end{aligned} \tag{288}$$

If we now use $\langle \vec{v}(0)^2 \rangle = 3k_BT/m$ (note that $m\langle \vec{v}(0)^2 \rangle/2$ is the average kinetic energy of the sphere) and assume $t \gg \tau$ we obtain

$$D = \frac{k_BT}{\zeta} \, . \tag{289}$$

Next we want to study the sustained **Brownian motion** of our sphere. We do this by adding a random force $\vec{Z}$ with $\langle \vec{Z} \rangle = 0$ to Eq. (283), i.e.

$$\dot{\vec{v}} = -\frac{1}{\tau}\vec{v} + \frac{1}{m}\vec{Z} \, . \tag{290}$$

The solution of this equation is

$$\vec{v}(t) = \vec{v}(0)e^{-t/\tau} + \frac{1}{m}e^{-t/\tau}\int_0^t dt' \vec{Z}(t')e^{t'/\tau} \, . \tag{291}$$

This can be checked by inserting (291) into (290). Here we are interested in the auto-correlation function $\langle Z(t')Z(t'') \rangle$, since we shall need it when we discuss the dynamics of the models of Rouse and Zimm. We find this auto-correlation function by working out the quantity $\langle \vec{v}(t)^2 \rangle$ using Eq. (291). As before $\langle \vec{v}(t)^2 \rangle = 3k_BT/m$ and thus

$$\frac{3k_BT}{m} = \langle \vec{v}(t)^2 \rangle = \frac{1}{m^2}e^{-2t/\tau}\int_0^t dt' \int_0^t dt'' \langle \vec{Z}(t') \cdot \vec{Z}(t'') \rangle e^{(t'+t'')/\tau} \tag{292}$$

On the right hand side we have used $t \gg \tau$ and $\langle \vec{Z} \cdot \vec{v} \rangle = 0$. A guess which solves Eq. (292), as we show via straightforward insertion, is

$$\langle \vec{Z}(t') \cdot \vec{Z}(t'') \rangle = 6\zeta k_BT\delta(t'-t'') \, . \tag{293}$$

If we extend Eq. (290) by a force derived from a potential U, i.e. $-\vec{\nabla}U$, we obtain the **Langevin equation** of motion

$$m\dot{\vec{v}} = -\zeta\vec{v} - \vec{\nabla}U + \vec{Z} \, . \tag{294}$$

We conclude our preliminary considerations with a specific example - the Brownian motion of a one-dimensional harmonic oscillator, i.e.

$$U(x) = \frac{1}{2}kx^2 \, , \tag{295}$$

where k is the force constant. If we are interested in times significantly greater than τ we expect that the inertia term in the Langevin equation is not important (cf. our numerical example in the context of Eq. (286)). Hence it is sufficient to study the balance of forces on the right hand side of Eq. (294), i.e. in one dimension

$$\frac{d}{dt}x(t) = -\frac{k}{\zeta}x(t) + \frac{1}{\zeta}Z_x(t) \, . \tag{296}$$

Here

$$\tau' = \frac{\zeta}{k} \tag{297}$$

is another relaxation time different form τ! The solution, as we can easily check, is

$$x(t) = \frac{1}{\zeta}\int_{-\infty}^t dt' e^{-(t-t')/\tau'} Z_x(t') \, . \tag{298}$$

From this we obtain the position auto-correlation function

$$\langle x(0)x(t) \rangle = \frac{1}{\zeta^2}\int_{-\infty}^t dt' \int_{-\infty}^0 dt'' e^{-(t-t'-t'')/\tau'} \langle Z_x(t')Z_x(t'') \rangle \, . \tag{299}$$

Assuming that the auto-correlation function $\langle \vec{Z}(t') \cdot \vec{Z}(t'') \rangle$ is not affected by U we can insert it from Eq. (293). Hence

$$\langle x(0)x(t) \rangle = \frac{k_BT}{k}\exp[-t/\tau'] \, . \tag{300}$$

This is a result we shall return to when we study the Rouse chain. Another function we shall need is the root-mean-square displacement $\langle (x(t)-x(0))^2 \rangle$ of the oscillator, i.e.

$$\begin{aligned} \langle (x(t)-x(0))^2 \rangle &= \langle x(t)^2 \rangle + \langle x(0)^2 \rangle - 2\langle x(0)x(t) \rangle \\ &= 2\Big(\langle x(0)^2 \rangle - \langle x(0)x(t) \rangle \Big) \\ &= 2\frac{k_BT}{k}\Big(1 - e^{-t/\tau'}\Big) \\ &\approx \begin{cases} 2Dt & t \ll \tau' \\ 2\frac{k_BT}{k} & t \gg \tau' \end{cases} \, . \end{aligned} \tag{301}$$

This means that at short times the root-mean-square displacement of the oscillator is diffusion controlled whereas for times significantly longer than τ' it is potential controlled. Note that the limit $t \ll \tau'$ really means $\tau \ll t \ll \tau'$.

The Models of Rouse and Zimm:

Figure 61 illustrates the **Rouse model**. Its construction begins with a freely jointed chain of Kuhn segments $\vec{b}_i$. The Kuhn segments are replaced with harmonic springs and the junctions of adjacent Kuhn segments become beads possessing masses m_i. The force constants of the springs are

$$k = \frac{3k_BT}{b^2} \, . \tag{302}$$

This assumes that the springs themselves are entropy elastic (cf. Eq. (82)).

The equation of motion for bead i in the chain, analogous to Eq. (296) for the one-dimensional oscillator, is given by

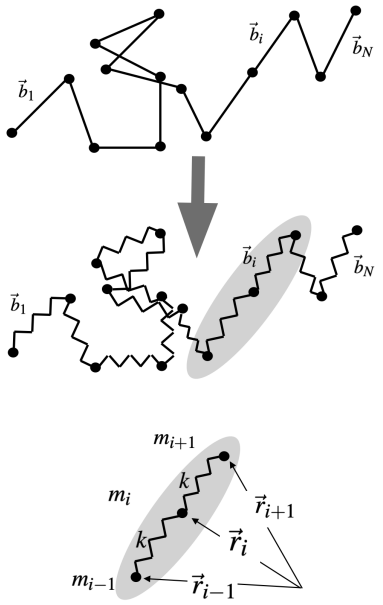

Fig. 61 Illustration of the Rouse model.

$$\frac{d}{dt}\vec{r}(i,t) = \frac{k}{\zeta}\frac{d^2\vec{r}(i,t)}{di^2} + \frac{1}{\zeta}\vec{Z}(i,t)\,. \tag{303}$$

But how do we explain the replacement of $-x(t)$ by $d^2\vec{r}(i,t)/di^2$? Note that for any bead i possessing a left and a right neighbor

$$-\vec{\nabla}_i U = -\left[k(\vec{r}_i - \vec{r}_{i+1}) - k(\vec{r}_{i-1} - \vec{r}_i)\right] \approx k\frac{d^2\vec{r}(i,t)}{di^2}\,. \tag{304}$$

We can also use this equation for the first bead $i = 0$ and the last bead $i = N$, when we provide them with 'artifical' neighbors located at $\vec{r}_{-1} = \vec{r}_0$ and $\vec{r}_{N+1} = \vec{r}_N$, respectively. This implies the boundary conditions

$$\frac{d\vec{r}(i,t)}{di} = 0 \quad \text{for} \quad i = 0, N\,. \tag{305}$$

Next we want to express the $\vec{r}(i,t)$ in terms of new coordinates $\hat{\vec{r}}(p,t)$ so that in these coordinates Eq. (303) assumes the form

$$\frac{d}{dt}\hat{\vec{r}}(p,t) = -\frac{k_p}{\zeta_p}\hat{\vec{r}}(p,t) + \frac{1}{\zeta_p}\hat{\vec{Z}}(p,t)\,. \tag{306}$$

This equation is the three-dimensional version of Eq. (296), which we found when we studied the dynamics of a one-dimension oscillator. If we succeed, it means that we have found normal mode coordinates for the Rouse chain, i.e. we can study its dynamics in terms of independent harmonic oscillators for each mode.

Following Doi & Edwards we consider the linear transformation

$$\hat{\vec{r}}(p,t) = \int_0^N di\,\phi(p,i)\,\vec{r}(i,t)\,. \tag{307}$$

Hence

$$\frac{d}{dt}\hat{\vec{r}}(p,t) = \int_0^N di\,\phi(p,i)\left(\frac{k}{\zeta}\frac{d^2\vec{r}(i,t)}{di^2} + \frac{1}{\zeta}\vec{Z}(i,t)\right)\,. \tag{308}$$

Using repeated partial integration we can manipulate the term containing the double derivative d^2/di^2, which yields

$$\int_0^N di\,\phi(p,i)\frac{d^2\vec{r}(i,t)}{di^2} = \int_0^N di\,\frac{d^2\phi(p,i)}{di^2}\vec{r}(i,t) - \Big|_0^N \frac{d\phi(p,i)}{di}\vec{r}(i,t)\,. \tag{309}$$

Here we have used the boundary condition (305) upon the first partial integration. Substituting (309) into (308) we see that we indeed obtain (306) if the following conditions are satisfied:

$$\frac{d^2}{di^2}\phi(p,i) = -\frac{\zeta/k}{\zeta_p/k_p}\phi(p,i) \tag{310}$$

$$\frac{d}{di}\phi(p,i) = 0 \qquad (i = 0, N) \tag{311}$$

$$\hat{\vec{Z}}(p,t) = \frac{\zeta_p}{\zeta}\int_0^N di\,\phi(p,i)\,\vec{Z}(i,t)\,. \tag{312}$$

A solution satisfying both (310) and (311) is

$$\phi(p,i) = \frac{1}{N}\cos\left(\frac{p\pi i}{N}\right) \quad \text{, where} \quad \frac{p^2\pi^2}{N^2} = \frac{\zeta/k}{\zeta_p/k_p} \tag{313}$$

¶.

Finally we shall need $\langle\hat{\vec{Z}}(p,t')\cdot\hat{\vec{Z}}(q,t'')\rangle$ when we study the dynamics of the Rouse chain. Using (312) we have

$$\langle\hat{\vec{Z}}(p,t')\cdot\hat{\vec{Z}}(q,t'')\rangle = \frac{\zeta_p^2}{\zeta^2 N^2}\int_0^N di\int_0^N dj\langle\vec{Z}(i,t')\cdot\vec{Z}(j,t'')\rangle \times\cos\left(\frac{p\pi i}{N}\right)\cos\left(\frac{q\pi j}{N}\right)\,. \tag{316}$$

Inserting

$$\langle\vec{Z}(i,t')\cdot\vec{Z}(j,t'')\rangle = 6\zeta k_B T\,\delta(t'-t'')\delta_{i,j} \tag{317}$$

(cf. (293)) the integration yields

¶ The inverse transform of (307) with $\phi(p,i)$ given by (313) is

$$\vec{r}(i,t) = \hat{\vec{r}}(0,t) + 2\sum_{q=1}^{N}\hat{\vec{r}}(q,t)\cos\left(\frac{q\pi i}{N}\right)\,. \tag{314}$$

We can check this by inserting $\hat{\vec{r}}(q,t)$ given by (307) into this equation and using

$$\int_0^N di\cos\left(\frac{q\pi i}{N}\right)\cos\left(\frac{p\pi i}{N}\right) = \frac{N}{2}\delta_{q,p}(1+\delta_{q,0})\,. \tag{315}$$

$$\langle \hat{\vec{Z}}(p,t')\cdot\hat{\vec{Z}}(q,t'')\rangle = 6\frac{\zeta_p^2}{\zeta N^2}N\delta(t'-t'')\delta_{p,q}\left(\frac{1}{2}+\frac{1}{2}\delta_{0,q}\right) . \quad (318)$$

We do have some freedom of choice in the case of ζ_p and use it to require that the right hand sides in (317) and (318) have the same form (with ζ in (317) becoming ζ_p in (318)). This in turn implies

$$\zeta_0 = \zeta N \quad \text{and} \quad \zeta_p = 2\zeta N \quad (p>0) , \quad (319)$$

i.e.

$$k_p = \frac{6\pi^2 k_B T}{b^2 N}p^2 \quad (p>0) . \quad (320)$$

Finally we adopt the two results (300) and (301) from the one-dimensional oscillator example to the Rouse chain, i.e.

$$\langle \hat{r}_\alpha(p,0)\hat{r}_\beta(q,t)\rangle = \delta_{p,q}\delta_{\alpha,\beta}\frac{k_B T}{k_p}\exp[-t/\tau_p'] \quad (p=1,2,\dots) , \quad (321)$$

where

$$\tau_p' \equiv \frac{\zeta_p}{k_p} \quad (322)$$

and

$$\langle(\hat{r}_\alpha(0,t)-\hat{r}_\alpha(0,0))(\hat{r}_\beta(0,t)-\hat{r}_\beta(0,0))\rangle = 2\delta_{\alpha,\beta}\frac{k_B T}{\zeta_0}t . \quad (323)$$

Now we can discuss predictions of the Rouse model:

• *Center of mass diffusion of the Rouse chain:*

Equation (307) immediately tells us that $\hat{\vec{r}}(0,t)$ is the center of mass of the chain. Hence Eq. (323) tells us what the mean square displacement of the center of mass is and, in particular, its diffusion coefficient:

$$D_{cm} = \frac{k_B T}{\zeta_0} = \frac{k_B T}{\zeta N} . \quad (324)$$

• *Rotational relaxation of the Rouse chain:*

We use the relaxation time τ_r of the auto-correlation function of the end-to-end vector, $\langle\vec{R}(0)\cdot\vec{R}(t)\rangle \sim \exp[-t/\tau_r]$, as a measure for rotational relaxation of the chain. Since

$$\vec{R}(t) = \vec{r}(N,t)-\vec{r}(0,t) \overset{(314)}{=} -4\sum_{p=1\,(p\text{ odd})}^{N}\hat{\vec{r}}(p,t) , \quad (325)$$

we find via (321)

$$\langle\vec{R}(0)\cdot\vec{R}(t)\rangle = 16\sum_{p=1\,(p\text{ odd})}^{N}\frac{3k_B T}{k_p}\exp[-t/\tau_p'] . \quad (326)$$

Obviously this is a sum over many exponentials. But of all the relaxation times

$$\tau_p' = \frac{\zeta_p}{k_p} = \frac{\zeta b^2 N^2}{3\pi^2 p^2 k_B T} \quad (327)$$

τ_1' is the longest. This one we identify with τ_r:

$$\tau_r \approx \frac{\zeta_1}{k_1} = \frac{\zeta b^2 N^2}{3\pi^2 k_B T} . \quad (328)$$

• *Storage and loss modulus in the Rouse model:*

In Eq. (273) we had introduced the shear relaxation modulus $G(t)$ from which we can calculate $G'(\omega)$ and $G''(\omega)$ using Eqs. (281) and (282). But how do we find $G(t)$? A formal derivation starting from the microscopic stress tensor can be found in Doi & Edwards (chapter 4). Here we want to merely venture a guess at a plausible form of $G(t)$.

Note that the unit of G is energy per volume. In the limit $t\to 0$ all modes contribute, since none has relaxed yet. The relevant energy is $k_B T\sum_p$ times the number of chains inside the volume, i.e.

$$G(0) = \rho k_B T\sum_p 1 . \quad (329)$$

Here ρ is the number of chains per volume. If we now consider the time behavior of $G(t)$, we may be tempted to simply assume that it follows the same autocorrelation function as the normal mode coordinates in Eq. (321). However, as was pointed out above, the unit of stress is energy per volume and, if we think back to the one-dimensional oscillator example, the energy is build from squares of the coordinates. Hence, rather than using $\langle x(0)x(t)\rangle$, referring to the one-dimensional oscillator, we need to base our guess of the stress module's relaxation on $\langle x^2(0)x^2(t)\rangle$ ||.

|| The calculation of $\langle x^2(0)x^2(t)\rangle$ is analogous to that of $\langle x(0)x(t)\rangle$ (cf. Eq. (300)). The main exception is that we need to deal with the 4-point function $\langle Z_x(t_1)Z_x(t_2)Z_x(t_3)Z_x(t_4)\rangle$, which can be expressed as a sum over products of 2-point functions:

$$\langle Z_x(t_1)Z_x(t_2)Z_x(t_3)Z_x(t_4)\rangle = \langle Z_x(t_1)Z_x(t_2)\rangle\langle Z_x(t_3)Z_x(t_4)\rangle \quad (330)$$
$$+\langle Z_x(t_1)Z_x(t_3)\rangle\langle Z_x(t_2)Z_x(t_4)\rangle + \langle Z_x(t_1)Z_x(t_4)\rangle\langle Z_x(t_2)Z_x(t_3)\rangle .$$

(cf. R. Hentschke *Statistische Mechanik* p. 192). With this we obtain

$$\langle x^2(0)x^2(t)\rangle - \langle x^2\rangle^2 = \frac{2k_B^2T^2}{k^2}\exp[-2t/\tau'] . \quad (331)$$

Note that $\langle x^2\rangle^2$ (aside from a factor) is the square of the thermal energy of the oscillator which we subtract.

Hence

$$G(t) = \rho k_B T \sum_p \exp[-2t/\tau_p'] \,. \tag{332}$$

Inserting this into Eqs. (281) and (282) and integrating term by term yields

$$G'(\omega) = \rho k_B T \sum_p \frac{(\omega\,\tau_p'')^2}{(\omega\,\tau_p'')^2+1} \tag{333}$$

and

$$G''(\omega) = \rho k_B T \sum_p \frac{\omega\,\tau_p''}{(\omega\,\tau_p'')^2+1} \tag{334}$$

($\tau_p'' = \tau_p'/2$).

Let us consider this result in its two limits, i.e. $\omega\tau_1'' \ll 1$ and $\omega\tau_1'' \gg 1$ (Note that we use the longest relaxation time!). In the case $\omega\tau_1'' \ll 1$

$$\sum_p \frac{(\omega\,\tau_p'')^2}{(\omega\,\tau_p'')^2+1} \approx \omega^2\,\tau_1''^2 \underbrace{\sum_{p=1}^{\infty} p^{-4}}_{=\pi^4/90\approx 1.1} \tag{335}$$

and

$$\sum_p \frac{(\omega\,\tau_p'')}{(\omega\,\tau_p'')^2+1} \approx \omega\,\tau_1'' \underbrace{\sum_{p=1}^{\infty} p^{-2}}_{=\pi^2/6\approx 1.6} \,. \tag{336}$$

In the opposite limit, i.e. $\omega\tau_1'' \gg 1$ we can replace the summation by and integration. Hence

$$\sum_p \frac{(\omega\,\tau_p'')^2}{(\omega\,\tau_p'')^2+1} \approx \int_0^\infty dp \frac{(\omega\,\tau_1'')^2}{(\omega\,\tau_1'')^2+p^4} = \frac{\pi}{2\sqrt{2}}(\omega\,\tau_1'')^{1/2} \tag{337}$$

and

$$\sum_p \frac{(\omega\,\tau_p'')}{(\omega\,\tau_p'')^2+1} \approx \int_0^\infty dp \frac{\omega\,\tau_1''\,p^2}{(\omega\,\tau_1'')^2+p^4} = \frac{\pi}{2\sqrt{2}}(\omega\,\tau_1'')^{1/2} \,. \tag{338}$$

The ω dependence of $G'(\omega)$ and $G''(\omega)$ is compiled in Table 9:

Table 9

	$\omega\tau_1'' \ll 1$	$\omega\tau_1'' \gg 1$
$G'(\omega)$	$\sim \omega^2$	$\sim \omega^{1/2}$
$G''(\omega)$	$\sim \omega$	$\sim \omega^{1/2}$

Finally, note that every term under the summation in Eqs. (333) and (334) corresponds to a Maxwell Model, one of the phenomenological models discussed in appendix A - in principle a justification, albeit with limitations, for using this phenomenological model.

Figures 62 and 63 show examples comparing experimental data for the dynamic moduli. The experimental data points in Fig. 62 are taken from Fig. 4 in D. F. Hodgson, E. J. Amis *Dynamic viscoelasticity of dilute polyelectrolyte solutions.* J. Chem. Phys. *94*, 4581 (1991). The authors present their results for the dynamic viscoelasticity of dilute polyelectrolyte solutions, where the polymer is poly(2-vinylpyridine). The solid lines are $G'/(\rho k_B T)$ and $G''/(\rho k_B T)$ from Eqs. (333) and (334) using $\tau_p'' = K/p^2$ and $K = 0.7$, i.e. K is the only adjustable parameter. The overall agreement between the experiment and the Rouse prediction is quite reasonable. However, there are many points here which we do not address. For a detailed discussion the reader is referred to the original publication. The additional dashed lines correspond to Zimm's modification of the Rouse model, which we discuss in the following. The experimental data points in Fig. 63 are taken from Fig. 5 in R. Johnson, J. Schrag, J. Ferry *Infinite-Dilution Viscoelastic Properties of Polystyrene in θ-Solvents and Good Solvents*. Polymer Japanese *1*, 742 (1970) for the case of two different good solvents ($\nu = 3/5$). As in the previous comparison, the solid lines are $gG'/(\rho k_B T)$ and $gG''/(\rho k_B T)$ from Eqs. (333) and (334) $\tau_p'' = K/p^2$, and $K = 0.008$. Here an additional factor $g = 110$ was used to shift the curves. The dashed lines again correspond to Zimm's modification of the Rouse model.

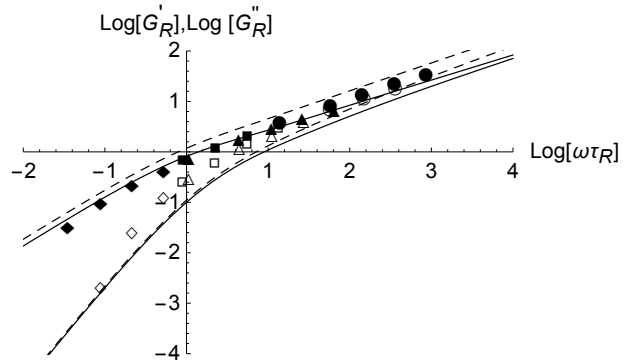

Fig. 62 Reduced storage modulus (open symbols) and reduced loss modulus (closed symbols) vs ω times a reduced relaxation time. Data from Fig. 4 in D. F. Hodgson, E. J. Amis *Dynamic viscoelasticity of dilute polyelectrolyte solutions.* J. Chem. Phys. *94*, 4581 (1991).The different symbols indicate molecular weights ranging from $3\cdot10^4$ to $1\cdot10^6$ MW in 0.0023 M HCl/ethylene glycol at a concentration of 2.0 mg mL^{-1}. The solid lines are $G'/(\rho k_B T)$ and $G''/(\rho k_B T)$ from Eqs. (333) and (334) using $\tau_p'' = K/p^2$ and $K = 0.7$. Dashed lines are $G'/(\rho k_B T)$ and $G''/(\rho k_B T)$ obtained with the Zimm model. In this case $\tau_p'' = K/p^{3\nu}$ ($K = 0.7$ and $\nu = 3/5$).

The Rouse model describes G' and G'' of polymers in dilute solution and, as we shall see, of 'short' polymers in the melt reasonably well ('reasonably well' may not always apply. Nevertheless, in a rough sense the statement is a fair assessment.). However, both the center of mass diffusion as well as the rotational diffusion, specifically their dependence on N, are generally incorrect. But why? Even though the beads in the Rouse chain are mechanically coupled, every bead interacts independently with

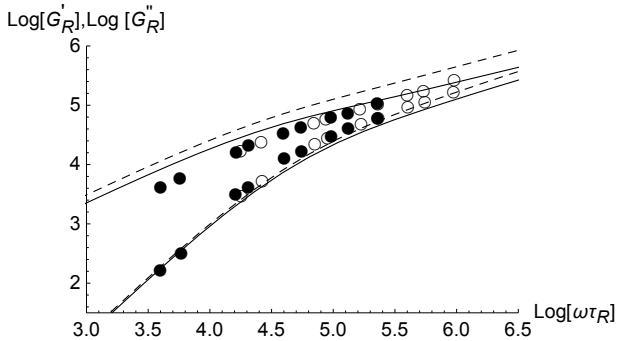

Fig. 63 Reduced storage modulus (bottom symbols) and reduced loss modulus (top symbols) vs ω times a reduced relaxation time. Data from Fig. 5 in R. Johnson, J. Schrag, J. Ferry *Infinite-Dilution Viscoelastic Properties of Polystyrene in θ-Solvents and Good Solvents*. Polymer Japanese *1*,742 (1970). The solid lines are $gG'/(\rho k_B T)$ and $gG''/(\rho k_B T)$ from Eqs. (333) and (334) using $g = 110$, $\tau_p'' = K/p^2$, and $K = 0.008$. Dashed lines are $G'/(\rho k_B T)$ and $G''/(\rho k_B T)$ obtained with the Zimm model. In this case $\tau_p'' = K/p^{3\nu}$ ($K = 0.008$ and $\nu = 3/5$).

the surrounding solvent. The drag force on the Rouse chain is therefore the sum over the drag forces on individual beads. Consequently the overall drag coefficient scales according to N. The Rouse model neglects the hydrodynamical coupling of the beads. In the following we shall fix this problem and we shall see that the main difference is that the chain in a solvent diffuses and rotates as one 'object' possessing linear dimension proportional to N^ν.

We began our discussion of chain dynamics by looking at a sphere moving within a liquid while experiencing Stoke's friction proportional to its velocity. Each bead in the Rouse model is such a sphere, which up to now we have treated as hydrodynamically independent. This is not correct. Instead we express the force a bead i exerts on its surroundings due to hydrodynamic interaction as

$$\vec{F}_i = 6\pi\eta R[\vec{v}_i - \vec{v}(\vec{r}_i)] \equiv \zeta\,[\vec{v}_i - \vec{v}(\vec{r}_i)]\ . \tag{339}$$

Here $\vec{v}_i$ is the velocity of bead i in the 'laboratory' frame and $\vec{v}(\vec{r})$ is the flow field in the laboratory frame created by the sum of the corresponding forces $\vec{\varphi}(\vec{r})$ of all other beads, i.e.

$$\vec{\varphi}(\vec{r}) = \sum_{j(\neq i)} \delta(\vec{r} - \vec{r}_j)\vec{F}_j(\vec{r}_j)\ . \tag{340}$$

The equation linking $\vec{v}_i$ to $\vec{\varphi}(\vec{r})$ is Eq. (243). Hence,

$$\begin{aligned} \vec{v}_i &= \frac{\vec{F}_i}{\zeta} + \vec{v}(\vec{r}_i) \qquad (341)\\ &= \frac{\vec{F}_i}{\zeta} + \int d^3r' \mathbf{H}(\vec{r} - \vec{r}')\vec{\varphi}(\vec{r}') \\ &= \frac{\vec{F}_i(\vec{r}_i)}{\zeta} + \sum_{j(\neq i)} \mathbf{H}(\vec{r}_i - \vec{r}_j)\vec{F}_j(\vec{r}_j) \end{aligned}$$

or

$$\vec{v}_i = \sum_j \mathbf{T}(i,j)\vec{F}_j\ , \tag{342}$$

where

$$\mathbf{T}(i,j) = \begin{cases} \frac{\mathbf{I}}{\zeta} & (i=j) \\ \mathbf{H}(\vec{r}_i - \vec{r}_j) & (i \neq j) \end{cases} \tag{343}$$

is the **mobility matrix** (**I** is the unit matrix.).

Applying (342) to the Rouse equation (303) we see that in order to integrate hydrodynamic interactions we must modify (303) to

$$\frac{d}{dt}\vec{r}(i,t) = \sum_j \mathbf{T}(i,j)\left(k\frac{d^2\vec{r}(j,t)}{dj^2} + \vec{Z}(j,t)\right)\ , \tag{344}$$

where

$$\langle Z_{i,\alpha} Z_{j,\beta}\rangle = 2(\mathbf{T})^{-1}_{\alpha\beta}(i,j)k_B T\delta(t-t')\ . \tag{345}$$

Note that $\mathbf{T}(i,j)$ does depend on $\vec{r}_j$, which means that (344) is a nonlinear equation. Zimm avoided this difficulty by replacing $\mathbf{T}(i,j)$ with its equilibrium average $\langle\mathbf{T}(i,j)\rangle$, i.e.

$$\langle\mathbf{T}(i,j)\rangle = \int d^3r_{ij}p(r_{ij})\mathbf{T}(i,j)\ , \tag{346}$$

where $p(r_{ij})$ is, for instance, the ideal chain distribution (81). This step, called **pre-averaging** in the literature, yields the **Zimm model**, i.e.

$$\frac{d}{dt}\vec{r}(i,t) = \int_0^N dj\langle\mathbf{T}(i,j)\rangle\left(k\frac{d^2\vec{r}(j,t)}{dj^2} + \vec{Z}(j,t)\right)\ , \tag{347}$$

where additionally the sum over j is replaced by an integration.

Instead of Eq. (81), the formula for $p(r_{ij})$ for the ideal chain, we are going to use Eq. (130) to evaluate $\langle\mathbf{T}(i,j)\rangle$. Remember that we found Eq. (130) by using scaling ideas and that this distribution function applies to ideal as well as real chains. Hence,

$$\langle T_{\alpha\beta}(i,j)\rangle = \frac{\int d^3r \exp[-k_\nu\left(\frac{r}{b|i-j|^\nu}\right)^{\frac{1}{1-\nu}}]\frac{\delta_{\alpha\beta}+e_{r,\alpha}e_{r,\beta}}{8\pi\eta r}}{\int d^3r \exp[-k_\nu\left(\frac{r}{b|i-j|^\nu}\right)^{\frac{1}{1-\nu}}]} \tag{348}$$

**. Note that

** k_ν can be determined via $\langle r^2\rangle = b^2N^{2\nu}$, which yields

$$k_\nu = \left(\frac{\Gamma[5(1-\nu)]}{\Gamma[3(1-\nu)]}\right)^{\frac{1}{2(1-\nu)}} = \begin{cases} 3/2 & (\nu = 1/2) \\ \approx 1.11 & (\nu = 3/5) \end{cases} \tag{349}$$

$$\langle e_{r,\alpha} e_{r,\beta} \rangle = \frac{1}{3}\delta_{\alpha\beta} \,. \tag{350}$$

The r-integrations can be done with the help of, for instance, Mathematica. The final result is

$$\langle \mathbf{T}(i,j) \rangle = t(i-j)\mathbf{I} \tag{351}$$

with

$$t(i-j) = \frac{1}{6\pi\eta}\frac{\Gamma[2(1-\nu)]}{\Gamma[3(1-\nu)]}\frac{k_\nu^{1-\nu}}{b|i-j|^\nu} \,. \tag{352}$$

In the case of an ideal chain ($\nu = 1/2$ and $k_\nu = 3/2$) $t(i-j)$ becomes

$$t(i-j) \stackrel{id.ch.}{=} \frac{1}{\eta(6\pi^3 b^2|i-j|)^{1/2}} \,. \tag{353}$$

The equivalent to the Rouse equation in normal mode coordinates, i.e. Eq. (306), is here

$$\frac{d}{dt}\hat{\vec{r}}(p,t) = \sum_q \hat{t}_{pq}\left(-k_q\hat{\vec{r}}(q,t) + \hat{\vec{Z}}(q,t)\right) \,, \tag{354}$$

where k_q is given in Eq. (313) and

$$\hat{t}_{pq} = \frac{1}{N^2}\int_0^N di \int_0^N dj \cos\left(\frac{p\pi i}{N}\right)\cos\left(\frac{q\pi j}{N}\right) t(i-j) \,. \tag{355}$$

In the case $p = 0$ or $q = 0$ the result is

$$\hat{t}_{0q} = \hat{t}\,\delta_{0,q} \quad \text{or} \quad \hat{t}_{p0} = \hat{t}\,\delta_{p,0} \,. \tag{356}$$

with

$$\hat{t} = \frac{1}{3\pi\eta}\frac{k_\nu^{1-\nu}\Gamma[2(1-\nu)]}{(1-\nu)(2-\nu)\Gamma[3(1-\nu)]}\frac{1}{bN^\nu} \,. \tag{357}$$

In the case $p,q > 0$ we resort to an approximate solution. Using the substitution $j - i = l$ we have

$$\begin{aligned}
&\frac{1}{N^2}\int_0^N di \int_{-i}^{N-i} dl \cos\left(\frac{p\pi i}{N}\right)\cos\left(\frac{q\pi(l+i)}{N}\right)|l|^{-\nu} \\
&\approx \frac{1}{N^2}\underbrace{\int_0^N di \cos\left(\frac{p\pi i}{N}\right)\cos\left(\frac{q\pi i}{N}\right)}_{=(N/2)\delta_{p,q}}\underbrace{\int_{-\infty}^{\infty} dl \cos\left(\frac{q\pi l}{N}\right)|l|^{-\nu}}_{=2(N/(\pi q))^{1-\nu}\Gamma[1-\nu]\sin(\pi\nu/2)} \\
&\quad -\frac{1}{N^2}\int_0^N di \cos\left(\frac{p\pi i}{N}\right)\sin\left(\frac{q\pi i}{N}\right)\underbrace{\int_{-\infty}^{\infty} dl \sin\left(\frac{q\pi l}{N}\right)|l|^{-\nu}}_{=0} \,.
\end{aligned}$$

Hence, for $p,q > 0$

$$\hat{t}_{pq} \approx \frac{1}{6\pi\eta}\frac{\Gamma[1-\nu]\Gamma[2(1-\nu)]}{\Gamma[3(1-\nu)]}\left(\frac{k_\nu}{\pi p}\right)^{1-\nu}\sin\left(\frac{\pi\nu}{2}\right)\frac{1}{bN^\nu}\delta_{p,q} \,. \tag{358}$$

Note that for $\nu = 1/2$

$$\hat{t}_{00} = \frac{8}{3(6\pi^3)^{1/2}\eta b\sqrt{N}} \tag{359}$$

and

$$\hat{t}_{11} \approx \frac{1}{\sqrt{2}(6\pi^3)^{1/2}\eta b\sqrt{N}} \,. \tag{360}$$

We observe that due to the δ_{pq} in the formulas (356) and (358), Eq. (354) truly assumes the form of its counterpart, Eq. (306), in the Rouse model, i.e.

$$\frac{d}{dt}\hat{\vec{r}}(p,t) = \hat{t}_{pp}\left(-k_p\hat{\vec{r}}(p,t) + \hat{\vec{Z}}(p,t)\right) \,. \tag{361}$$

Hence we directly obtain Zimm's version of our previous Rouse results:

• *Center of mass diffusion of the Zimm chain:*

Since $1/\zeta_o = \hat{t}_{00}$ we find for the case $\nu = 1/2$ using Eq. (359)

$$D_{cm} = k_B T\,\hat{t}_{00} = \frac{8k_B T}{3(6\pi^3)^{1/2}\eta b\sqrt{N}} \,. \tag{362}$$

In general, i.e. for general ν, we see from (357) that

$$D_{cm} \propto N^{-\nu} \,. \tag{363}$$

This makes good physical sense. Our starting point was Stoke's friction with a drag coefficient ζ proportional to the Radius R of the sphere. The linear dimension of a polymer chain is proportional to N^ν and thus the corresponding drag coefficient is expected to be proportional to N^ν. This type of reasoning of course depends on the range of the hydrodynamic interaction, which must be greater than the polymer dimension. However, the r^{-1}-dependence in the Oseen tensor means that the hydrodynamic interaction is virtually infinite.

• *Rotational relaxation of the Zimm chain:*

We seek the rotation relaxation time τ_r in the case of the Zimm model. According to Eq. (328)

$$\tau_r \approx \tau_1' = \frac{\zeta_1}{k_1} \,. \tag{364}$$

Here $\zeta_1 = 1/\hat{t}_{11}$. $\hat{t}_{11}$ is given in Eq. (360) for the ideal chain and in the general case we can use Eq. (358). But what about k_1? Does Eq. (320), derived in the context of the Rouse model, still apply

when $\nu = 1/2$ and what is k_1 when the chain is a real chain, i.e. $\nu = 3/5$? One answer is that Eq. (320) still applies when $\nu = 1/2$. In order to verify this statement and, in addition, find the answer to the second question we need to calculate k_p explicitly via the formula

$$\langle \hat{\vec{r}}(p)^2 \rangle = \frac{3k_BT}{k_p} \,. \tag{365}$$

Note that k_p is the force constant of an individual uncoupled oscillator. The above formula gives the position fluctuations of this oscillator (mode) for a particular temperature. For example, let us consider the one-dimensional oscillator with the potential energy (295). In this case

$$\langle x^2 \rangle = \frac{\int_{-\infty}^{\infty} dx x^2 \exp[-\beta k x^2/2]}{\int_{-\infty}^{\infty} dx \exp[-\beta k x^2/2]} = \frac{1}{\beta k} \,, \tag{366}$$

where $\beta = (k_BT)^{-1}$. The factor 3 in Eq. (366) results since the oscillator is three-dimensional.

For a reason not immediately obvious we do not use

$$\hat{\vec{r}}(p,t) = \frac{1}{N} \int_0^N di \cos\left(\frac{p\pi i}{N}\right) \vec{r}(i,t) \tag{367}$$

directly but

$$\hat{\vec{r}}(p,t) = -\frac{1}{p\pi} \int_0^N di \sin\left(\frac{p\pi i}{N}\right) \frac{d\vec{r}(i,t)}{di} \tag{368}$$

instead, which follows from (367) via partial integration. Hence

$$\langle \hat{\vec{r}}(p)^2 \rangle = \frac{1}{p^2\pi^2} \int_0^N di \int_0^N dj \sin\left(\frac{p\pi i}{N}\right) \times \sin\left(\frac{p\pi j}{N}\right) \langle \frac{d\vec{r}(i,t)}{di} \cdot \frac{d\vec{r}(j,t)}{dj} \rangle \,. \tag{369}$$

Now we use

$$\frac{d\vec{r}(i,t)}{di} \cdot \frac{d\vec{r}(j,t)}{dj} = -\frac{1}{2} \frac{d^2}{didj} (\vec{r}(i,t) - \vec{r}(j,t))^2 \tag{370}$$

in conjunction with

$$\langle (\vec{r}(i,t) - \vec{r}(j,t))^2 \rangle = b^2 |i-j|^{2\nu} \,. \tag{371}$$

Hence

$$\langle \frac{d\vec{r}(i,t)}{di} \cdot \frac{d\vec{r}(j,t)}{dj} \rangle = (2\nu - 1)\nu b^2 |i-j|^{2(\nu-1)} \,. \tag{372}$$

Substituting this back into Eq. (369), we are left with an integration just like the one in the case of $\hat{t}_{pq}$. Using as before the substitution $j - i = l$ and the subsequent extension of the l-integration limits to $\pm\infty$ we obtain (approximately)

$$\langle \hat{\vec{r}}(p)^2 \rangle = \frac{\nu\Gamma[2\nu]}{\pi^{2\nu+1}} \sin(\pi(1-\nu)) \frac{b^2 N^{2\nu}}{p^{2\nu+1}} (1 - \delta_{0p}) \,. \tag{373}$$

Inserting $\nu = 1/2$ into this formula and using (366) yields, as previously formulated as a question, Eq. (320) for k_p. More generally we obtain,

$$k_p \sim \frac{k_BT\, p^{2\nu+1}}{b^2 N^{2\nu}} \,. \tag{374}$$

Hence, for $\nu = 1/2$

$$\tau_r = \tau_1' = \frac{\zeta_1}{k_p} = \frac{\eta (bN^{1/2})^3}{\sqrt{3\pi} k_BT} \approx 0.33 \frac{\eta (bN^{1/2})^3}{k_BT} \tag{375}$$

and for $\nu = 3/5$

$$\tau_r = \tau_1' \approx 0.18 \frac{\eta (bN^{3/5})^3}{k_BT} \,, \tag{376}$$

and generally

$$\tau_p' \sim \frac{\eta (bN^\nu/p^\nu)^3}{k_BT} \,. \tag{377}$$

If we compare this result of the Zimm model with τ_p' in the Rouse model (Eq. (328)), we find

$$\frac{\tau_p'(\text{Rouse})}{\tau_p'(\text{Zimm})} \sim \left(\frac{N}{p}\right)^{2-3\nu} \,, \tag{378}$$

where $2 - 3\nu$ is equal to 1/2 (1/5) for $\nu = 1/2$ (3/5). This means that long wavelength modes in particular (small p) have significantly longer relaxation times in the Rouse model compared to the Zimm model.

• *Storage and loss modulus in the Zimm model:*

The functional form of the moduli in the Eqs. (335) and (336) remains the same. What is different is τ_p' and therefore $\tau_p'' = \tau_p'/2$. This means that the two limits, i.e. $\omega\tau_1'' \ll 1$ and $\omega\tau_1'' \gg 1$, and thus Eqs. (335) through (9) need modification:

In the case $\omega\tau_1'' \ll 1$

$$\sum_p \frac{(\omega\tau_p'')^2}{(\omega\tau_p'')^2 + 1} \approx \omega^2 \tau_1''^2 \underbrace{\sum_{p=1}^{\infty} p^{-(6\nu)}}_{=\zeta(6\nu)=\begin{cases} \approx 1.2 & \nu = 1/2 \\ \approx 1.1 & \nu = 3/5 \end{cases}} \tag{379}$$

and

$$\sum_p \frac{(\omega\tau_p'')}{(\omega\tau_p'')^2+1} \approx \omega\tau_1'' \underbrace{\sum_{p=1}^{\infty} p^{-(3\nu)}}_{=\zeta(3\nu)=\begin{cases} \approx 2.6 & \nu=1/2 \\ \approx 1.9 & \nu=3/5 \end{cases}} . \tag{380}$$

In the opposite limit, i.e. $\omega\tau_1'' \gg 1$,

$$\sum_p \frac{(\omega\tau_p'')^2}{(\omega\tau_p'')^2+1} \approx \int_0^\infty dp \frac{(\omega\tau_1'')^2}{(\omega\tau_1'')^2+p^{6\nu}} = \tag{381}$$

$$\underbrace{\frac{\pi}{6\nu}\csc(\frac{\pi}{6\nu})}_{=\begin{cases} \approx 1.2 & \nu=1/2 \\ \approx 1.1 & \nu=3/5 \end{cases}} (\omega\tau_1'')^{1/(3\nu)}$$

and

$$\sum_p \frac{\omega\tau_p''}{(\omega\tau_p'')^2+1} \approx \int_0^\infty dp \frac{\omega\tau_1'' p^{3\nu}}{(\omega\tau_1'')^2+p^{6\nu}} = \tag{382}$$

$$\underbrace{\frac{\pi}{6\nu}\sec(\frac{\pi}{6\nu})}_{=\begin{cases} \approx 2.1 & \nu=1/2 \\ \approx 1.4 & \nu=3/5 \end{cases}} (\omega\tau_1'')^{1/(3\nu)} .$$

The ω dependence of $G'(\omega)$ and $G''(\omega)$ in the Zimm model is compiled in Table 10:

Table 10

	$\omega\tau_1'' \ll 1$	$\omega\tau_1'' \gg 1$
$G'(\omega)$	$\sim \omega^2$	$\sim \omega^{1/(3\nu)}$
$G''(\omega)$	$\sim \omega$	$\sim \omega^{1/(3\nu)}$

Note that small differences in the factors aside, the ω-dependence in the low frequency limit is the same as in the Rouse case. In the high frequency limit the power of $\omega\tau_1''$ is different and in the Zimm model depends on ν. However, as the comparisons in the Figs. 62 and 63 show, the difference between the dynamic moduli computed with the Zimm model for $\nu = 3/5$ are not so very different from the corresponding Rouse results. Note however that no particular effort is made to 'tweak' the parameter K, which is different in the two models but here is assumed to be the same to keep things simple. Note also in this context that the dependence of τ_1'' on N in the two models is different, i.e.

$$\tau_1'' \sim \begin{cases} N^2 & \text{Rouse} \\ N^{3\nu} & \text{Zimm} \end{cases} . \tag{383}$$

5.3 Entanglement

Figure 64 is a copy of Fig. 55 in which the red lines possess slopes predicted by the Zimm model for the storage modulus G' at low and high frequencies, respectively. Note that the experimental system is a melt and thus $\nu = 1/2$. The frequency dependence of G' observed previously for polymers in dilute solution, i.e. in Figs. 62 and 63, here is only seen when the chains are short. The limiting molecular masses in Fig. 64 correspond to about $0.9 \cdot 10^2$ and roughly $6 \cdot 10^3$ monomers per polymer chain, respectively. It appears that when the chains exceed a certain length, somewhere above 10^2 monomers, the two limits become separated by a third frequency range in which the storage modulus is constant and independent of molecular weight (or chain length). How do we explain the occurrence of this so-called **plateau modulus**?

From the point of view of the individual chain its environment is an 'entangled mess' of other chains. How does this chain move? Fig. 65 is a cartoon of an idea which has proven useful with regard to this question. The central part of the cartoon depicts a polymer chain consisting of N monomers (or perhaps Kuhn segments). Again there are statistical 'blobs' containing on average N_e monomers along this chain stuck inside a 'tube'. The diameter of the tube corresponds to the linear dimension of the blobs. But what defines the length N_e and thus the linear dimension of the blobs? It is assumed that this dimension is determined by 'entanglements', i.e. interlaced 'hairpins' formed by the polymer with its neighbors (or even with itself). Hence the polymer contour length between hairpins is N_e, the **entanglement length**. When the polymer moves, 'trying' to free itself from the entanglements, its motion is akin to a snake moving forward via a looping motion of its body. Hence the term **'reptation'** was coined in this context by de Gennes. Note that the lower left corner of Fig. 65) is a closeup view of a section of the aforementioned tube. The entire tube contains and is made up by the entire polymer chain. This tube itself is a random walk with a characteristic end-to-end distance or linear dimension R_{tube}. In the following we exploit this picture using the scaling concept previously developed.

The entanglements divide the entire polymer chain into N/N_e 'pieces'. To the N_e effective monomers or Kuhn segments between two entanglements we apply the formulas (92) and (101) (polymer inside a tube), where $N_\xi = N_e$ and $\xi = D_e$. Here D_e, given by

$$D_e \sim N_e^\nu , \tag{384}$$

is the diameter of a tube along which the polymer chain reptates. The tube's contour length, i.e. the length of tube containing the polymer, is

$$L = \frac{N}{N_e} D_e . \tag{385}$$

The time τ_{rep} it takes for the polymer to reptate this length we describe in terms of Einsteinian diffusion, i.e.

$$\tau_{rep} \sim \frac{L^2}{D} , \tag{386}$$

where D is the diffusion constant of the chain given by

$$D \sim \frac{k_B T}{N} . \tag{387}$$

You may wonder why here we use $D \sim N^{-1}$ instead of $D \sim N^{-\nu}$ as in (363)? This is because the polymer does not move as a 'blob' of effective diameter N^{ν}! Instead of N^{ν} we decide that N is the better scaling variable. Putting the last four equations together we find

$$\tau_{rep} \sim \frac{N^3}{k_B T N_e} , \tag{388}$$

where we have used $\nu = 1/2$.

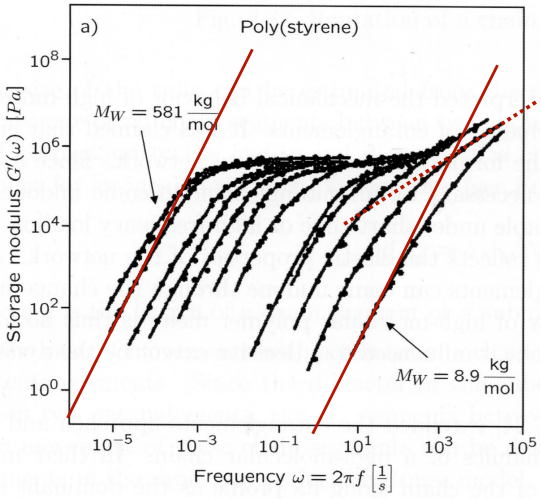

Fig. 64 Frequency dependence of the storage modulus of polystyrene in the molten state as function of molecular weight. This figure is identical to Fig. 55 except for the red lines. The solid lines possess the slope 2, whereas the dotted line has slope $2/3$. These are the limiting slopes expected for $\log G'$ vs. $\log \omega$ according to the Zimm model (cf. Tab. 10.)

We understand the significance of this formula if we apply it to Fig. 64. Note that the horizontal separation of the red solid lines is about six orders of magnitude on the frequency axis. The ratio of the largest molecular weight to the smallest, which is reasonably close to the molecular weight at which the G'-curves begin to show the bend which develops into the plateau, is roughly 10^2. This means that the attendant ratio of the τ_{rep}s for the two molecular weights is (again roughly) 10^6 - which are just the above six decades. What Eq. (388) is telling us is that for times longer than τ_{rep} the chain does not 'remember' its original tube and effectively acts like the Rouse chain in the low frequency limit!

There is another quantity which we can compute to support this notion - the plateau modulus G_o, i.e. the value of G' on the plateau. We use Eq. (213), i.e.

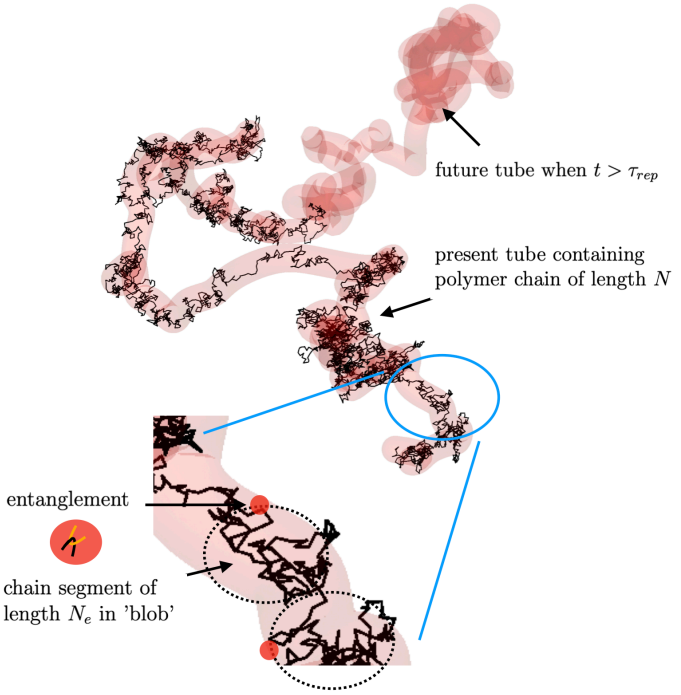

Fig. 65 Cartoon of a chain reptating on a path determined by entanglements with other chains or other sections of itself.

$$G_o = \frac{c}{M_e} k_B T , \tag{389}$$

(Note that N in (213) is the number of chains - in the present case the number chain sections of length N_e between entanglements (or physical cross-links)!). The quantity c is the polymer mass density and $M_e \propto N_e$ is the mass of the segment of length N_e. Again we use the mass of the shortest chain in the figure, i.e. 8.9 kg mol^{-1} (The mass of the segment between two entanglements is about twice this value. But we have used the curve obtained for this mass in our above estimate and thus we stick to it here as well. After all - this is a rough calculation!). For the density we use $c = 10^3$ kg m^{-3}. The result is $G_o \approx 4 \cdot 10^5$ Pa. This is not too bad!

Remark: If we compare the storage modulus in the two panels of Fig. 54, we notice that the one in panel (a) behaves just as if it was one of the curves somewhere in the middle of Fig. 55. However, the storage modulus in panel (b) shows a plateau which apparently persists at even the smallest frequencies. In this case the chemical cross-links prevent the diffusion of the chain segments and, effectively, $\tau_{rep} = \infty$.

An even better quantity to support reptation is the translational diffusion of the chains. Here we mean spatial center of mass diffusion and not the diffusion along the tube's contour as described by Eq. (386). According to our above picture the tube's contour is a random path and its linear dimension R_{tube} should scale as

$$R_{tube} \sim N^{1/2} . \tag{390}$$

This implies for the translational center of diffusion coefficient D_{cm}

$$D_{cm} \sim \frac{R^2_{tube}}{\tau_{rep}} \sim \frac{1}{N^2} \,. \tag{391}$$

The above result of the reptation model is quite distinct from our previous results for D_{cm} based on the Rouse or the Zimm model (cf. Eqs. (324) and (363)).

The current experimental status is that neither $\tau_{rep} \sim N^3$ nor $D_{cm} \sim N^{-2}$ are quite correct. Perhaps this is not too surprising. Scaling, as elegant as it may be, relies on physical intuition, which may not capture the phenomenon in its entirety. Experiments appear to support exponent values which are roughly 10% larger, i.e. 3.4 instead of 3 and 2.3 instead of 2. Fig. 66 shows a figure copied from the article T. P. Lodge *Reconciliation of the Molecular Weight Dependence of Diffusion and Viscosity in Entangled Polymers.* Phys. Rev. Lett. *83*, 3218 (1999).

Detailed discussions/calculations related to entanglement can be found in the books written by those who invented these ideas, i.e the books by Doi and Edwards and de Gennes.

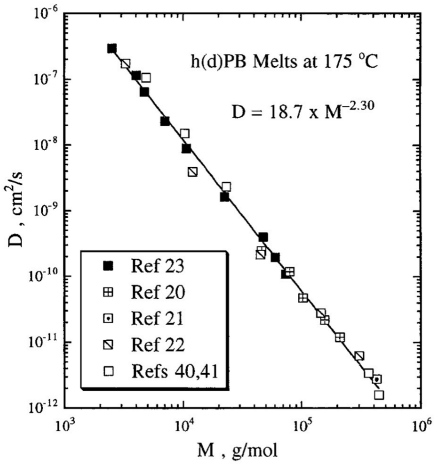

Fig. 66 Self-diffusion in the melt obtained from hydrogenated or deuterated polybutadiene samples adjusted to 175°C, as a function of molecular weight. Copy of Fig. 1 in T. P. Lodge *Reconciliation of the Molecular Weight Dependence of Diffusion and Viscosity in Entangled Polymers.* Phys. Rev. Lett. *83*, 3218 (1999).

5.4 The Glass Process

In this section we discuss what is commonly called the **glass transition**. We start with a number of observation which can be made in this context. Subsequently we shall focus on one particular theoretical concept, the so called **mode coupling theory**. Even though mode coupling theory does not appear to be the ultimate answer to all the observations, it yields partial answers and interesting insights despite a strongly simplified presentation.

Looking at Figs. 54 or 56 we notice that the storage modulus rises by about three orders of magnitude beyond its plateau value when the frequency becomes very high. The loss modulus on the other hand exhibits a pronounced maximum in the limit of high frequencies. Instead of changing frequency at constant temperature, we can hold the frequency constant and change the temperature. An example where this is done is shown in Fig. 67.

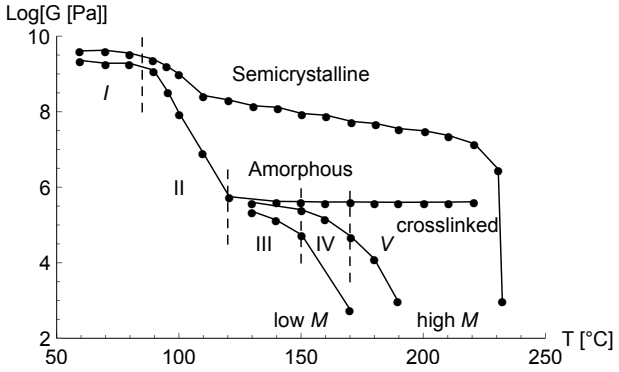

Fig. 67 Logarithm of the relaxation modulus (10 s) versus temperature. The polymer is isotactic (semicrystalline) and atactic (amorphous) polystyrene. Low M and High M stand for low and high molecular weight, respectively. This figure is adopted from Fig. 1.15 in U. W. Gedde *Polymer Physics* Chapman & Hall: London (1995).

This figure shows the logarithm of the relaxation modulus for different types of polystyrene versus temperature. An atactic polymer has a very irregular structure along its contour length. The structure of bulk samples of such polymers is therefore amorphous. In the case of atactic polystyrene, as we start from high temperatures, we make the same observations which we already discussed in the context of Figs. 55 and 64. Depending on molecular weight, we observe a plateau of a certain 'width'. If the polymer is chemically cross-linked the plateau extends to the highest temperature (cf. Fig. 54 (b)). Below around 120°C the relaxation modulus rises and finally levels off about three orders of magnitude above the plateau. So, what is happening here? We have already discussed the regions labeled V, IV, and III in the case of amorphous polymers. But what is going on in the regions II and I?

A simple low-molecular liquid will undergo a phase transition into a crystalline phase if the temperature is continuously decreased. Can we expect something of this nature in the case of polymers? Not really. The attendant ordering necessary to align and pack the polymer chains is entropically very unfavourable. If the polymer's architecture is very regular, e.g. it is isotactic, then ordering, at least in small spatial regions ($\sim$ 10 nm), can be favourable. In this case the bulk polymer matrix may be composed of crystallites surrounded by amorphous polymer.

Remark 1: If we are willing to invest work, e.g. by straining the polymer sample, this situation may be attained at temperatures when ordinarily the polymer is amorphous throughout. This is called **strain crystallization** (cf. section 6.1). The most prominent polymer in this context is 1,4-cis-isoprene in natural rubber.

Remark 2: The degree of crystallinity can be as high as 90% for certain low molar mass polyethylenes and as low as 5% for polyvinylchloride.

The crystallite's effect on the modulus is similar to the effect of cross-links, i.e. they increase the modulus. In Fig. 67 this explains the curve labeled 'Semicrystalline'. The increase in region II upon lowering the temperature is much less pronounced since the amorphous volume fraction in the sample is smaller compared to the crystalline volume fraction, which does nothing special at this point.

All in all, regions I and II appear to be distinguished by a hard, i.e. very immobile, but still amorphous polymer matrix or a certain amorphous volume fraction thereof. In region I the amorphous polymer is in a glassy state and the transition to this state in region II is called the **glass transition**. The glass transition is associated with the **glass transition temperature** T_g - in general the temperature beyond which the storage modulus has levelled out. However, this is essentially a mere definition, since the glass process extends over a finite temperature range and other features, e.g. inflection points, may be used to define T_g. In addition T_g may be measured with different experimental methods producing somewhat different results.

The glass process, and therefore any value of T_g, is rate dependent. This is illustrated in the following figures. Figure 68 shows the specific volume versus temperature at different heating rates. Figure 69 shows the same for the heat capacity. Finally, Fig. 70 shows the dynamic moduli at different frequencies as the temperature passes through T_g. Especially, the last figure, if we compare it to Fig. 67, tells us that we are looking at regions II and I in the Fig. 67. Figure 70 does not surprise us, as we do expect this behavior based on our discussion of time-temperature superposition in amorphous polymer systems. Increasing the rate or frequency shifts 'everything' towards higher temperatures. However, Fig. 71, which is an expanded version of Fig. 70, shows something new. There is another maximum of the loss modulus at a temperatures below what we just defined as T_g. This is another relaxation process.

Why can we tell that this is a relaxation process? Remember our calculation of Eqs. (333) and (334) based on the relaxation modulus (332). If we consider a single τ_p' only, we obtain (333) and (334) without the summation - corresponding to a single step and a single maximum. In other words, different slopes of the relaxation modulus along the time axis, signalling different processes, translate into corresponding features in the G' and G''.

In particular, the two maxima of the loss modulus exhibit different shifts when different frequencies are compared. Fig. 72 shows this explicitly. The first maximum, i.e. the maximum at or close to T_g, follows the curve labeled 'β-process' and the second maximum, the one occurring at a lower temperature, follows the curve labeled 'γ-process'. Based on our previous discussion of time-temperature superposition our expectation would have been that there is only one curve.

A Remark on notation: It is customary to assign greek letters, α, β, γ, δ,... to relaxation processes in their order of appearance as temperature decreases. The α process is customary the glass transition. Here the sequence starts with β, however.

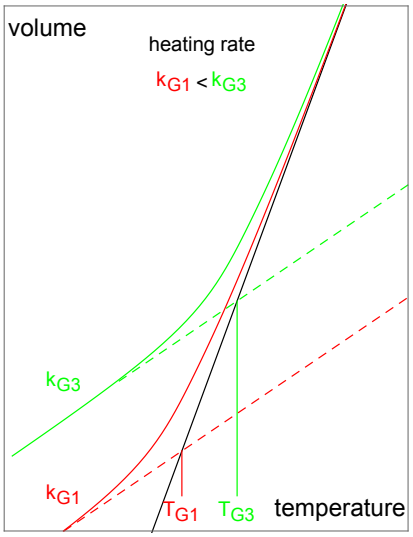

Fig. 68 Schematic dependence of the specific polymer volume on temperature at different heating rates.

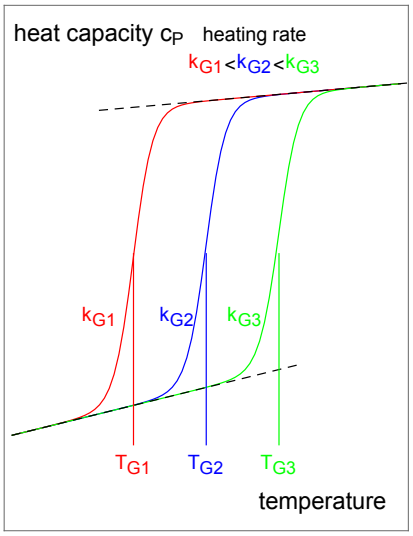

Fig. 69 Schematic dependence of the isobaric polymer heat capacity on temperature at different heating rates.

The curve labeled 'β-process' in Fig. 72 can be described quite well using Eq. (271), where a_T is given by Eq. (270) and the reference temperature is taken to be T_g for a particular ω_g, i.e.

$$\ln \omega = \ln \omega_g + c_1 \frac{T - T_g}{c_2 + T - T_g} , \tag{392}$$

where

$$c_1 = A/v_f(T_g) \quad \text{and} \quad c_2 = v_f(T_g)/\alpha . \tag{393}$$

Note that in the literature Eq. (392) can be found with log instead of ln. In this case c_1 differs from c_1 in Eq. (392) by a factor

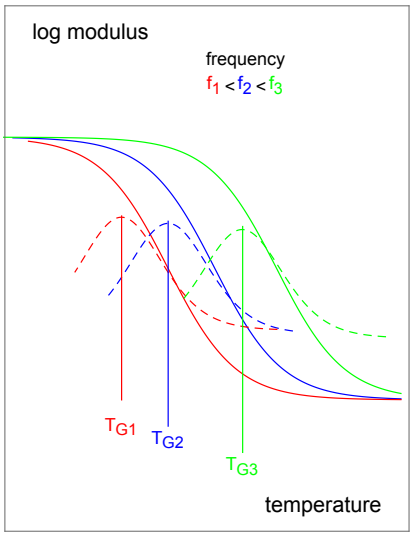

Fig. 70 Schematic dependence of the dynamic moduli (solid lines: G'; dashed lines G'') on temperature at different frequencies.

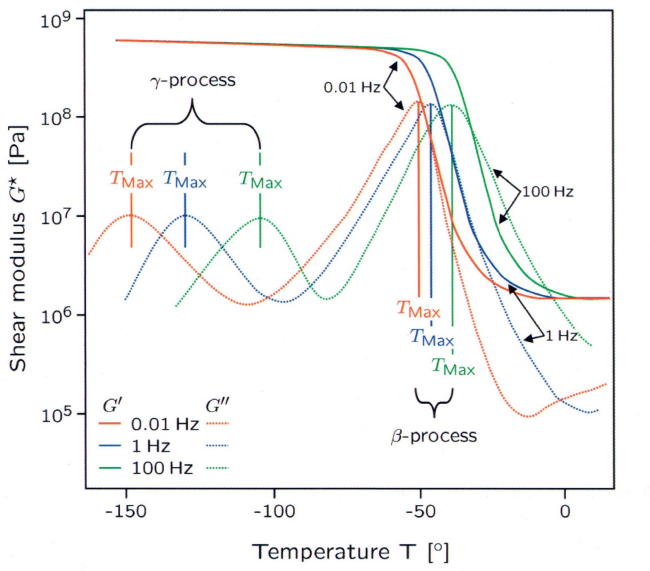

Fig. 71 Essentially an extended version of Fig. 70 revealing two different relaxation processes. The specific polymer here is a solution styrene-butadiene rubber (SSBR). This is an excerpt from Fig. 2.47 in Wrana's book.

$\log e \approx 0.43$.

Before we discuss the application of this fit function to data in Fig. 72, we want to mention an equivalent (empirical) form of the Dolittle relation (267) (after it is combined with Eq. (269)), which is meant to specifically describe the viscosity at or near T_g, i.e.

$$\eta(T) = B \exp\left[T_a/(T - T_{VF})\right] . \tag{394}$$

Equation (394) is called the **Vogel-Fulcher law** and T_{VF} is the Vogel or **Vogel-Fulcher temperature**. The temperature T_a is an activation temperature, whereas B is a constant independent of temperature. T_{VF} and T_a are connected to c_1 and c_2 in Eq. (392) via

$$T_{VF} = T_g - v_f(T_g)/\alpha \equiv T_g - c_2 \tag{395}$$

and

$$T_a = A/\alpha \equiv c_1 c_2 . \tag{396}$$

(check this!). Multiplied with the gas constant R this activation temperature yields an activation energy $E_a = RT_a$. Why there should be an activated process involved here becomes plausible if we look at the curve labeled 'γ-process' in Fig. 72. This curve, apparently a straight line, appears to coincides with the curved line based on (392) if the temperature is sufficiently high.

The fact that the maxima of the 'γ-process' appear to fall onto a straight line suggests that this process can be described by an *Arrhenius Equation*:

$$\ln k = \ln A_a - \frac{E_a/R}{T} . \tag{397}$$

Here A_a is a factor and E_a is the **activation energy** in mole for the process. The rate constant k gives the frequency of the process. If we expand Eq. (392) in the limit $T \gg T_g$, we find

$$\ln \omega = \ln \omega_g + \frac{A}{v_f(T_g)} - \frac{A/\alpha}{T} \tag{398}$$

to leading order in T^{-1}. Since, as already mentioned, the data points for both processes seem to come together at high temperatures, we may concluded that T_a from Eq. (396) is indeed the same as E_a/R in Eq. (397). This means that both processes should be closely related, if not identical, in this temperature limit.

Figure 73 shows the data points labeled β-process in Fig. 72 fitted using Eq. (392). First we select a point along the curve mapped out by the data in Fig. 72 which defines the reference $\omega_g = 2\pi f_g$ and reference T_g in Eq. (392). For this pair (ω_g, T_g) we attempt the best fit through the data points in Fig. 72 by adjusting c_1 and c_2. Here this is done for three pairs (ω_g, T_g) indicated by the red circles. The resulting values of c_1 and c_2 are compiled in Table. 11. What the tables also shows is that no matter which pair (ω_g, T_g) we use in Eq. (392), we always get the same T_{VF} and E_a. The Vogel-Fulcher temperature T_{VF} is T in the limit $\omega \to 0$ in Eq. (392), i.e. T_{VF} is the limiting T_g for an infinitely slow process [††]. The value for E_a is what one expects for interactions between neighboring polymer chain segments containing only a few car-

[††] For those of you who compare and check values: The data in this example are taken from Fig. 2.47 in Wrana's book. The polymer is an SSBR. In table 2.2 in the same reference T_{VG} for SSBR is -60 °C, i.e. 30°C higher in comparison to the value in Table 11. However, T_{VF} depends critically on the styrene to vinyl ratio, which in the case of T_{VG} =-60 °C is 25% styrene to 50% vinyl. In other words, it appears that the styrene content in the SSBR in Fig. 2.47 is lower.

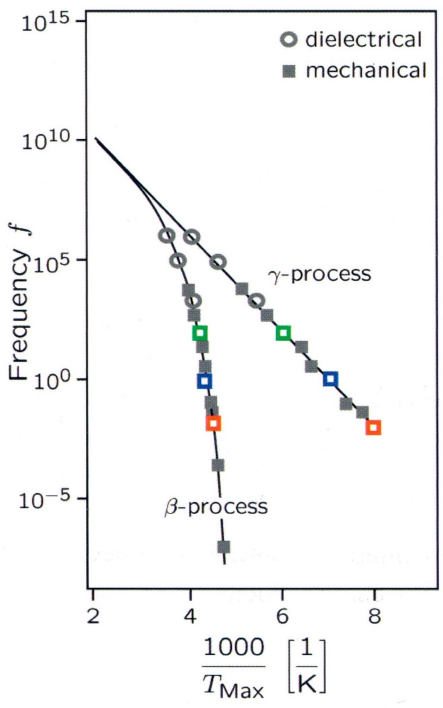

Fig. 72 Frequency vs. inverse temperature for the processes denoted β- and γ-processes in Fig. 71. This is another excerpt from Fig. 2.47 in Wrana's book.

bon atoms. Hence, while T_g depends on frequency or the rate of the process, it is possible to obtain a meaningful limiting T_g via T_{VF}. In addition, we obtain E_a, providing additional information about molecular processes at play. When we talk about polymers containing fillers, we shall return to E_a and learn that the observed E_a can be due to processes which have nothing to do with the polymer itself (cf. J. Fritzsche, M. Klüppel *Structural dynamics and interfacial properties of filler-reinforced elastomers.* Journal of Physics: Condensed Matter *23*, 035104 (2011).

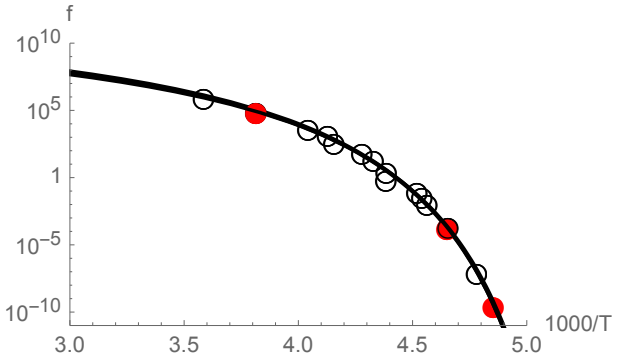

Fig. 73 The data points labeled β-process in Fig. 72 fitted with (392) using three distinct pairs (ω_g, T_g) (red circles) along the curve mapped out by the data points.

Our phenomenological description of the glass process thus far has heavily relied on free volume as a central ingredient. It turns out that free volume is also useful when we want to understand how T_g is affected by molecular weight or molecular architecture

Table 11 Application of Eq. (392).

f_g [Hz]	T_g [K]	c_1	c_2 [K]	$T_{VF} = T_g - c_2$ [K]	$E_a = Rc_1c_2$ [kJ/mol]
$10^{-9.5}$	206	47	23	183	9.0
$10^{-3.7}$	215	34	32	183	9.0
$8.4 \cdot 10^{4}$	262	13.3	79	183	8.7

in general. Here we avoid a general discussion though. Instead we focus on the molecular weight dependence of T_g for linear polymers.

We consider a constant volume V containing N polymers containing M monomers each. Equation (269) ties the free volume $v_f(T)$ in this system at temperature T to the glass transition temperature T_g if it is our T_r. Hence can rewrite Eq. (269) as

$$v_f(T) = v_f(T_{g,\infty}) + \delta v_f(M) + \alpha(T - T_g)\,. \tag{399}$$

This means that $v_f(T_g)$ is split into the free volume at $T_{g,\infty}$ when M is infinite, i.e. there are no free ends inside V, plus a piece $\delta v_f(M)$, which accounts for the extra free volume due to the presence of the free ends when M is finite. Setting $T = T_{g,\infty}$ in (399) yields

$$T_g = T_{g,\infty} - \frac{\delta v_f(M)}{\alpha}\,. \tag{400}$$

We also assume $\delta v_f(M) \propto 2N$, where $2N$ is the number of polymer ends. Since $NM/V = \rho$, where ρ is the constant number density of monomers, we obtain

$$T_g = T_{g,\infty} - \frac{c}{M}\,, \tag{401}$$

where c is a quantity independent of M. In other words, according to this line of argument, decreasing M should decrease the glass transition temperature. This relation between the glass transition temperature and polymer molecular weight was first discussed by Fox and Flory in T. G. Fox, P. J. Flory *Second-Order Transition Temperatures and Related Properties of Polystyrene. I. Influence of Molecular Weight.* J. Appl. Phys. *21*, 581 (1950) (Fig. 3 in this paper shows a nice example confirming (401)).

There is another observation to be made. This one concerns the relaxation modulus $G(t)$ near T_g. The exponential form

$$G(t) \sim \exp[-t/\tau] \tag{402}$$

yields

$$G''(\omega) \sim \frac{\omega\tau}{(\omega\tau)^2 + 1} \tag{403}$$

as we had found during our discussion of the Rouse and the Zimm model. The solid line in Fig. 74 is a fit based on this form to data (open circles) obtained for the loss modulus of a sample of

highly cross-linked polyisoprene. We notice that the experimental peak, corresponding to what we called the β-process, in this log-log plot is quite asymmetric, whereas the exponential $G(t)$ in (402) produces a symmetric peak. Also included in the figure is a dashed line, which is a much better fit capturing the aforementioned asymmetry. The dashed line is calculated with a **Kohlrausch-Williams-Watts** or **stretched exponential** form for the relaxation modulus, i.e.

$$G(t) \sim \exp[-(t/\tau)^{\beta}] \,, \tag{404}$$

where β is an exponent - usually between 0.3 and 0.5 (here $\beta = 0.5$). Since the attendant $G''(\omega)$ can only be presented as an unwieldy expression involving special functions, we do not give it here.

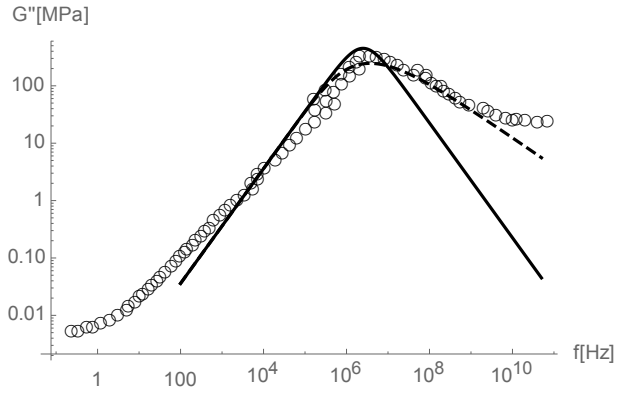

Fig. 74 Experimental loss modulus of highly cross-linked polyisoprene compared to $G''(\omega)$ ($\omega = 2\pi f$) calculated from the exponetial (solid line) and a stretched exponential form (dashed line) of the relaxation modulus. (data reproduced with the permission of Continental Reifen Deutschland).

Remark: If $G(t)$ has a power-law form, i.e.

$$G(t) \sim t^{-\beta} \,, \tag{405}$$

then

$$G'(\omega), G''(\omega) \sim \omega^{\beta} \,, \tag{406}$$

respectively.

Nevertheless, despite all of this, the inescapable conclusion thus far is the following: Close to T_g and below we find relaxation processes of different nature for which, at this point, we have no microscopic theory in accord with even most of the aforementioned observations. Since free volume has been a key ingredient to our discussion of the observations in conjunction with the glass process (remember in particular our prediction of how T_g depends on molecular weight), one might try to base a theory of the glass transition on free volume (the free volume based description of dense gases and liquids dates back to the 1930s (see J. O. Hirschfelder, C. F. Curtiss, R. B. Bird *Molecular Theory of Gases and Liquids.* John Wiley & Sons:New York (1954))). However, there are many theoretical models, including free volume theories, attempting to describe the glass transition and here we cannot do justice to even the more important ones. Instead we want to discuss the so called **mode coupling theory** theory (MCT) - albeit in a very much abbreviated and idealized form.

MCT is not a polymer theory per se. Much rather it is a theory for the glass process in general, i.e. the reversible process during which liquid-like amorphous order is replaced by solid-like amorphous order and vice-versa, which occurs in low molecular weight systems as well. Neither does MCT describes all our observations. But MCT features a number of interesting and thought-provoking ingredients and results, which a student of polymer physics might want to now about. Most of the following is borrowed from an article by L. M. C. Janssen (*Mode-Coupling Theory of the Glass Transition: A Primer*, Frontiers in Physics (2018)). A discussion of the glas transition in polymer systems, including a number of theoretical approaches, can be found for instance in I. M. Kalogeras *Glass-Transition Phenomena in Polymer Blends.* Encyclopedia of Polymer Blends: Volume 3: Structure, First Edition. Edited by Avraam I. Isayev, Wiley-VCH Verlag (2016).

Standard MCT seeks to predict the dynamics of the function $F(q,t)$, a time-dependent structure factor, given by

$$F(q,t) = \frac{1}{N}\langle \hat{\rho}(-\vec{q},0)\hat{\rho}(\vec{q},t)\rangle \tag{407}$$

where

$$\hat{\rho}(\vec{q},t) = \int d^3 r e^{i\vec{q}\cdot\vec{r}}\rho(\vec{r},t) \tag{408}$$

and

$$\rho(\vec{r},t) = \sum_{i=1}^{N} \delta(\vec{r} - \vec{r}_i(t)) \,. \tag{409}$$

Note that $\rho(\vec{r},t)$ is the same as in Eq. (111), except that this is not specifically a monomer number density but a general particle density. Hence $F(q,t)$ is very much like $P_i(\theta)$, except that now the time dependence is included.

We shall not derive the equation governing the dynamic evolution of $F(q,t)$. This calculation can be found in the references in the aforementioned article by Janssen. Instead we want to study this equation in an idealized approximation, i.e.

$$\ddot{x}(t) + \omega^2 x(t) + a\int_0^t x^2(t-t')\dot{x}(t')dt' = 0 \,. \tag{410}$$

Here $x(t)$ stands for $F(q,t)/F(q,0)$ and in particular $x(t=0) = 1$. In Eq. (410) the q-dependence is ignored and, in addition, ω (> 0) and a (> 0) are functions which here are treated as constants. Despite this, Eq. (410) captures most of the essence of the full MCT equation for $F(q,t)$.

Note that Eq. (410) becomes the equation of motion of a one-

dimensional damped harmonic oscillator if we replace $x^2(t-t')$ with $\delta(t-t')$, i.e. $\ddot{x}(t)+\omega^2 x(t)+a\dot{x}(t)=0$. We can solve Eq. (410) numerically using a Verlet algorithm. First we expand $x(t)$, i.e.

$$x(t\pm\delta t)=x(t)\pm\dot{x}(t)\delta t+\frac{1}{2}\ddot{x}(t)\delta t^2+\dots\,. \tag{411}$$

Subsequently we add the two equations ($\pm$!) and insert $\ddot{x}(t)$ from Eq. (410), i.e.

$$x_{n+1}\approx 2x_n-x_{n-1}-\left[\omega^2 x_n+a\sum_{i=0}^{n-1}{x_{n-i}}^2\left(x_{i+1}-x_i\right)\right]\delta t^2\,. \tag{412}$$

Note $x(t=n\delta t)\equiv x_n$. In addition we approximate the integral by a summation. Our starting x-values are $x_0=1$ and $x_1\approx 1-(\omega^2/2)\delta t+(a\omega^2/6)\delta t^3$. The latter we obtain by inserting a power series expansion of $x(t)$ into the above damped harmonic oscillator-approximation of (410). Straightforward iteration of (412) yields the graphs depicted in Fig. 75. Compared to the simple damped harmonic oscillator the solutions of the idealized MCT, i.e. Eq. (410), exhibit an increasing slowdown of the decay of $x(t)$ as a is increased. The slowdown of the decay of $x(t)$ is the result of the non-linearity of Eq. (410). Careful analysis reveals that the slowdown becomes infinite for $a\geq 4$. With regard to $F(q,t)$ this means that the system becomes non-ergodic for $a\geq 4$.

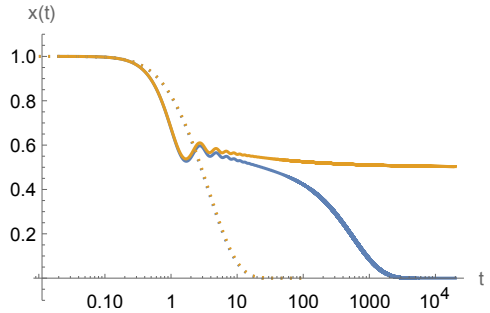

Fig. 75 Numerical solutions of Eq. (410) for $\omega^2=1$ and for $a=3.9$ (blue) in comparison to $a=4.0$ (golden). The dotted curves are the corresponding solutions of the damped harmonic oscillator, i.e. $\ddot{x}(t)+\omega^2 x(t)+a\dot{x}(t)=0$.

In order to better understand what is going on, we digress from the glass process and briefly turn to chemical reactions - or more precisely to rate equations. Eq. (413) describes how the mole fraction of the chemical component X changes with time during a reaction. Specifically this is a non-linear autocatalytic reaction due to the term proportional to ${n_X}^2$ on the right side of the equation. $n_Y(0)$ is the mole fraction of chemical Y, which is constant and the various ks are rate constants. Eq. (413) is one equation within a larger reaction schema discussed in section 7.3.1 of R. Hentschke *Thermodynamics* (Springer:Heidelberg (2022)).

$$\frac{d}{dt}n_X=(k_1 n_Y(0)-k_3)n_X-k_{-1}{n_X}^2 \tag{413}$$

Integration of this equation yields the solution

$$n_X(t)=\frac{(k_1 n_Y(0)-k_3)n_X(0)}{k_{-1}n_X(0)-[k_{-1}n_X(0)-k_1 n_Y(0)+k_3]\exp[(-k_1 n_Y(0)+k_3)t]}$$

Depending on whether $n_Y(0)<n_{Y,crit}$ or $n_Y(0)>n_{Y,crit}$, where $n_{Y,crit}=k_3/k_1$, there are two steady state solutions $n_X(\infty)=0$ or $n_X(\infty)=(k_1 n_Y(0)-k_3)/k_{-1}$ if $n_X(0)>0$. The system's choice which of the two solutions it prefers, i.e. the stable solution, depends on the parameter $n_Y(0)/n_{Y,crit}$. Fig. 76 illustrates this showing the stable solutions for $n_Y(0)$ slightly below in comparison to $n_Y(0)$ slightly above $n_{Y,crit}$. Autocatalytic reactions are interesting because of the possible bifurcation of the long time concentration of chemical components, depending on the value of a control parameter. This mechanism is believed to be important during chemical evolution, i.e. without violation of the second law nature can produced increasingly complex systems .

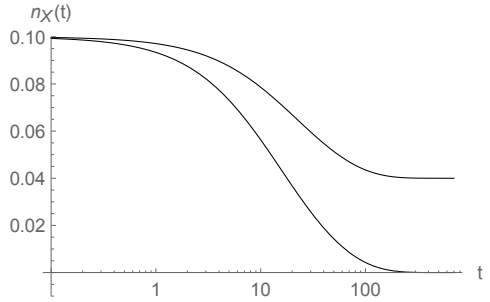

Fig. 76 Stable solutions of Eq. (413) for $n_Y(0)$ slightly below $n_{Y,crit}$ in comparison to $n_Y(0)$ slightly above $n_{Y,crit}$. Here $n_{Y,crit}=0.5$. $n_Y(0)=0.49$ (lower curve) and $n_Y(0)=0.51$ (upper curve); $k_{-1}=0.5$, $n_X(0)=0.1$, $k_3=1$, and $k_1=2$.

Comparing (410) with (413) we note that a/a_c ($a_c=4$) in the former equation is akin to $n_Y(0)/n_{Y,crit}$ in the latter equation. The difference, however, is that $x(t)$ exhibits a delayed decay. This has to do with the memory kernel in the integral, which links t to all previous times.

Figure 77 is a schematic summary of the full MCT result (note that $S(q)=F(q,0)$) obtained for particle systems. The central element is a cage around each particle. For very short times the particle moves more or less without noticing the other particles forming the cage. This is the ballistic regime. In our idealized MCT this time regime is dominated by the harmonic potential. In an intermediate time regime (here the β-relaxation), which grows as T approaches T_c (in the idealized MCT this means a approaches $a_c=4$; in the full MCT the factor corresponding to a is a function linearly dependent on temperature.), the cage restrains the particle's motion. Both limits of this regime are characterized by power law behavior. Finally, when $T<T_c$, the particle escapes the cage (here α-relaxation). This ultimate decay of $F(q,t)/F(q,0)$, characterized by the relaxation time τ, follows a stretched exponential.

But how does this relate to our observations during the glass process? Within MCT T_c is the glass transition temperature and one finds that $\tau\sim(T-T_c)^{-\gamma}$ ($\gamma>0$). With $\tau\propto\eta$, this power law of course is different from the exponential forms of the Vogel-Fulcher law (394) or the Dolittle relation (267) in conjunction

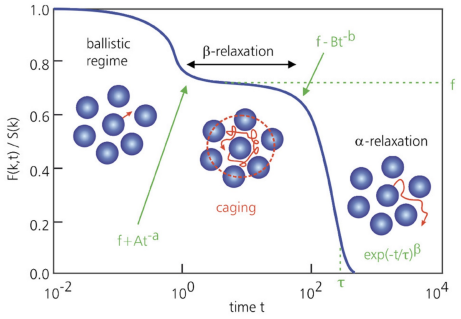

Fig. 77 Schematic summary of the full MCT result . This is Fig. 7 from L. M. C. Janssen (*Mode-Coupling Theory of the Glass Transition: A Primer*, Frontiers in Physics (2018)).

with the linear temperature dependence of the free volume (269). On the other hand, MCT predicts that $F(q,t) = \tilde{F}(q,t/\tau(T))$, where $\tilde{F}(q,t/\tau(T))$ is a master function. This corresponds to time-temperature superposition! And of course there is the streched exponential decay, during the α-relaxation in MCT. There are a number of other predictions of MCT which have been confirmed, but since these do not pertain to our above observation we shall not discuss them here.

6 Selected Topics

The following collection of 'selected topics' offers a mere glims of what the respective heading announces. This is because each topic by itself may fill an entire book or even several books. In turn this means that what you find under each heading is biased by this author's personal experience with the subject and therefore may neglect material considered essential by others. For this I apologize. However, I have included references which most likely cover the omitted material.

6.1 Aspects of the Mechanics of Polymers

• *Basic Stress-Strain Curves*

The measurement of (tensile) stress-strain curves ranks among the most common mechanical tests on polymer samples. However, note that there are different types of stress. **True stress**, for instance, is the applied load divided by the actual sample cross-sectional area. **Engineering stress** or **nominal stress**, on the other hand, is the applied load divided by the original cross-sectional area of the sample.

Figure 78 shows schematic stress-strain curves for different types of polymers. Polymer single crystal fibers show the steepest increase of stress with increasing strain. This is because the covalent bonds of the polymer backbone usually are highly aligned with the drawing direction. How this is done we shall briefly discuss in the section on liquid crystalline polymers. Since covalent bonds are very strong, the stress at break of these polymers is quite high (in the GPa range). On the other hand, the strain at break is only a few %.

Figure 79 shows an example of the fracture strength of polymer single crystal fibers as a function of their diameter. The solid line fitting the data quite well is simply based on $\sigma_T \propto D^{-1}$, where σ_T is the **tensile strength** and D is the fiber diameter. This proportionality is motivated by the idea that the initial 'damage' or cause leading to the failure of the fiber originates at its surface. The observation that 'thinner is stronger' actually is quite general in the context of technical as well as natural polymer fibers. Another quantity important for the tensile strength of fibers is the molecular weight of the polymers. Higher molecular weight generally means higher tensile strength (P. J. Flory *Tensile Strength in Relation to Molecular Weight of High Polymers* J. Am. Chem. Soc. *67*, 2048 (1945)).

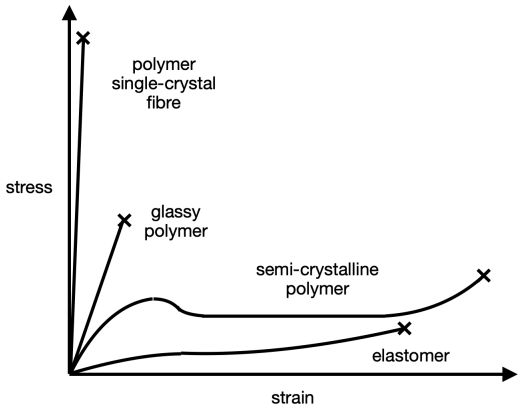

Fig. 78 Schematic stress-strain curves of the indicated polymer types. Crosses indicate the end of the respective curve due to sample failure.

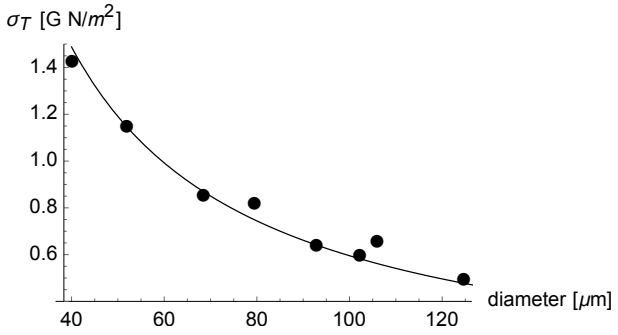

Fig. 79 Tensile strength of polydiacetylene single crystal fibres as function of their diameter. The data points are from Fig. 5.64 in R. J. Young, P. A. Lovell *Introduction to Polymers* (1991). The solid line is a fit using $\sigma_T \propto (\text{diameter})^{-1}$.

The interesting shape of the stress-strain curve of semi-crystalline polymers is due to the complex structure consisting of amorphous and crystalline regions. On the molecular level the crystalline regions restructure by various mechanisms (slip, twinning, ...) in the different strain regions. The stress-strain curve of elastomers is discussed in various places and in some detail in these notes.

Sample failure, indicated by the crosses, is a difficult topic. This is because failure and where is happens along the stress-strain curve, is influenced by diverse structural and dynamic effect. We do not want to discuss this topic and refer the reader

to the literature dedicated to it (e.g. H.H. Kausch *Polymer Fracture* Springer:Heidelberg (2012); A. J. Kinloch, R. J. Young *Fracture Behaviour of Polymers* Springer Science+Business Media: Dordrecht (1995))

• *Mooney-Rivlin Theory*

In section 4.5 we derived the elastic free energy contribution due to the macroscopic deformation of a polymer bulk sample expressed in terms of the quantities λ_x, λ_y, and λ_z. Each of these quantities is a factor by which the attendant edge of a rectangular volume is compressed or stretched during a deformation of the original rectangular volume.

Mooney and Rivlin had the idea to derive a free energy of deformation expressed in terms and valid for arbitrary λ_α based on symmetry arguments (M. Mooney *The Thermodynamics of a Strained Elastomer. I. General Analysis.* J. Appl. Phys. *19*, 434 (1948); R. S. Rivlin *Large Elastic Deformations of Isotropic Materials. IV. Further Developments of the General Theory.* Philosophical Transactions of the Royal Society of London. Series A, Mathematical and Physical Sciences *241*, 379 (1948)). The upshot is that the following expressions, quadratic in the λs and valid for any type of deformation, do not change if we exchange our coordinate system with another:

$$I_1 \equiv {\lambda_x}^2 + {\lambda_y}^2 + {\lambda_z}^2 \tag{414}$$

$$I_2 \equiv {\lambda_x}^2{\lambda_y}^2 + {\lambda_y}^2{\lambda_z}^2 + {\lambda_y}^2{\lambda_z}^2 \tag{415}$$

$$I_3 \equiv {\lambda_x}^2{\lambda_y}^2{\lambda_z}^2 \tag{416}$$

These invariants appear most clearly in Rivlins article (cf. his equation 3.4). Essentially he uses the fact that the strain tensor can be diagonalized at every point in the elastic body. The λ_α are the stretch factors associated with the orthogonal axes (principal axes of strain) in the coordinate system in which the strain tensor is diagonal (Remark 1: The λ_α are the same as the factors $(1+u^{(1)})$ in Eq. (205); Remark 2: In the case of uniform stretch of a square column the principal axes and the identification of the λs is rather obvious. In the case of shear this is much less so!). Note that I_1 as well as (in principle) I_3 appear in the elastic entropy (190). I_2 is new and if we include it we may construct an elastic free energy of the following form:

$$\Delta F^{el} = C_1(I_1-3) + C_2(I_2-3) + C_3(I_3-3)\,. \tag{417}$$

Here C_1, C_2, and C_3 are as yet unknown constants. Note also that $\Delta F^{el} = 0$ if there is no deformation.

In the case of uniaxial stretch at constant volume, i.e. $I_3 = 0$, (cf. Eqs. (195) and (218)) ΔF^{el} becomes

$$\Delta F^{el} = C_1\left(\lambda^2 + \frac{2}{\lambda} - 3\right) + C_2\left(2\lambda + \frac{1}{\lambda^2} - 3\right)\,. \tag{418}$$

Hence, using the same notation as in Eq. (218)),

$$\sigma_{zz} = \frac{1}{V}\frac{\partial \Delta F^{el}}{\partial \lambda} = 2\left(C_1 + \frac{C_2}{\lambda}\right)\left(\lambda - \frac{1}{\lambda^2}\right)\,. \tag{419}$$

It is customary to define a reduced stress via

$$\sigma_{zz,red} \equiv \frac{\sigma_{zz}}{\lambda - \frac{1}{\lambda^2}} = 2\left(C_1 + \frac{C_2}{\lambda}\right)\,. \tag{420}$$

Figure 80 shows stress-strain measurements in standard form (a) and as **Mooney-Rivlin plot** (b) compared to Eq. (419) (a) and Eq. (420) (b), respectively. The Mooney-Rivlin plot exhibits a nice straight portion over a significant range of values $1/\lambda$, which can be fitted with (420). The coefficient $2C_1$, which is the intercept with the reduced stress axis, is equated with Nk_BT and therefore yields the cross-link density. Here N is the number of chain segments joining (on average) two successive cross-links along a polymer chain. The number of cross-links is $N/2$ (think about a justification for this!).

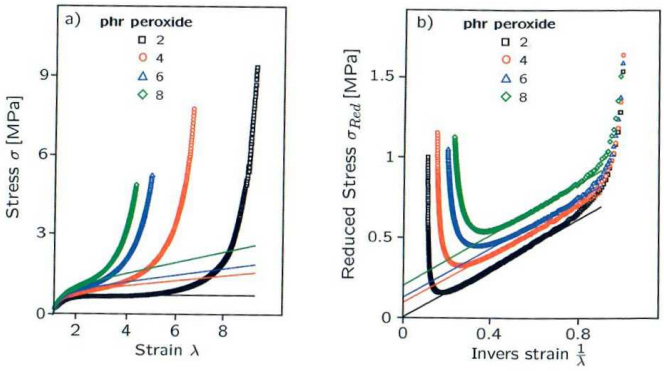

Fig. 80 Stress-strain measurements in standard form (a) and as Mooney-Rivlin plot (b). The material is a rubber (HNBR with 34% ACN) with variable concentration of a chemical cross-linking agent. The lines are fits using to Eq. (419) (a) and Eq. (420) (b), respectively. This figure is Fig. 3.11 from Wrana's book.

The reasoning why $2C_1$ should be equal to Nk_BT is based on the comparison between our previous expression for the elastic entropy (192) and (418). Since (192) contains the factor $\lambda^2 + 2/\lambda - 3$ we take its coefficient (multiplied with $-T$) and equate it with the coefficient of the same λ-term in (418). This is hardly a 'clean' procedure however. For instance, note that the two expressions for the elastic free energy are different in the limit $\lambda \to 1$ (unless we ignore C_2 again) and neither expression is valid when λ becomes large. In other words, there is no easily identifiable limit in which $2C_1 = Nk_BT$ holds. Nevertheless, this is a commonly applied procedure.

Remark: The apparent deviation between the data and Eq. (420) in the limit $\lambda \to 1$ can be fixed by addition of an adjustable 'offset' $\sigma_{zz,o}$ to the right hand side of Eq. (419) (check this!).

• *Mullins Effect*

If a 'sufficiently elastic' polymer material is subjected to consecutive loadings, the stress, measured for a strain that was already reached in a previous loading, is found to be reduced. The cartoon in Fig. 81 illustrates this. The sample is strained and the stress follows path 1. Upon reaching the end of path 1, i.e. the largest strain during the initial loading, the sample is relaxed. During a second loading the stress does not increase along path 1, as before, but follows path 2 and then continues along path 3. When the end of path 3 is reached, the sample again is relaxed. During the third loading the stress increases along path 4 and then continues along path 5, etc. The curve corresponding to the combined paths 1, 3, 5, .. is sometimes called the virgin curve. It is important to note that the strains used here are quite large (cf. the next figure). It is also important to note that this effect, called the **Mullins softening effect**, is most apparent in well vulcanized and/or filled samples (we discuss fillers in the next section). The next figure, Fig. 82, shows the result of an actual experiment. Here the sample experiences repeated stretching at constant strain amplitude before the latter is increased. Note that most of the softening is observed during the first deformation cycle. After a few additional cycles the rubber approaches a steady state or limiting cycle whose hystersis is much reduced.

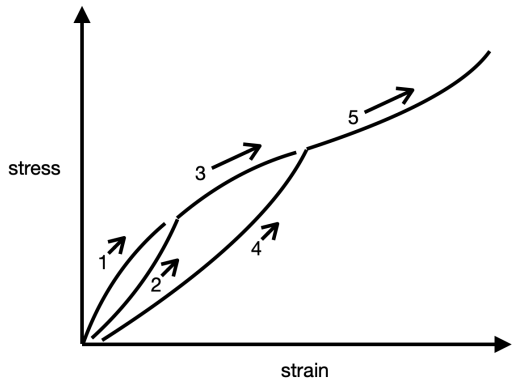

Fig. 81 Schematic illustration of the Mullins effect.

We do not want to discuss the Mullins effect in detail - except for a few comments: (i) the Mullins effect should not be confused with the so-called **Payne effect** occurring at much lower strain (cf. the next section); (ii) the generally accepted explanation for the Mullins effect is that high strain causes 'partially irreversible' (i.e. structural effects with very long relaxation times) movements of entanglements, network junctions or slippage of chain segments attached on filler particle surfaces as well as restructuring of filler particle networks and chain rupture; (iii) for more information the interested reader is referred to the aforementioned PhD Thesis by Plagge and to T. A. Vilgis, G. Heinrich, M. Klüppel *Reinforcement of Polymer Nano-Composites.* Cambridge University Press: Cambridge (2009). I also recommend the much older but very insightful article *Network Theories of Reinforcement.* by F. Bueche in *Reinforcement of Elastomers.* (G. Kraus, Editor) J. Wiley & Sons: New York (1965).

Remark: You may wonder why the stress-strain curves depicted

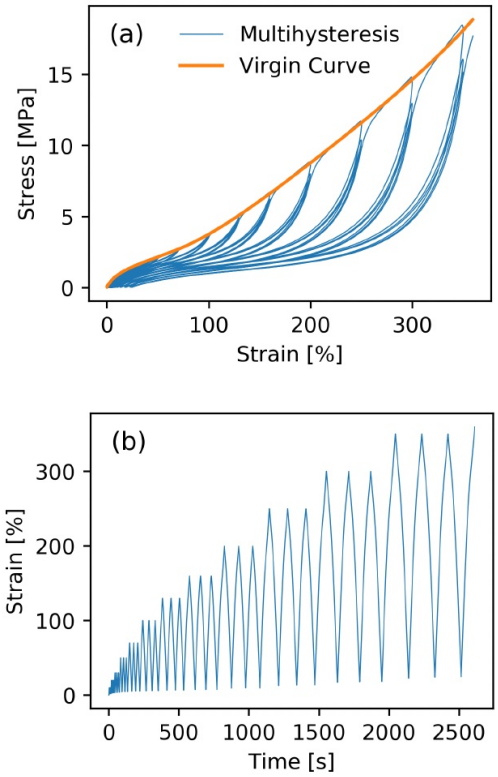

Fig. 82 (a) Example of a material experiencing Mullins effect: 40 phr carbon black (N339) filled, sulfur cured EPDM. Continuous stretching (virgin curve) and multihysteresis experiment, consisting of repeated loading of increasing strain levels. (b) Corresponding strain protocol. Copy of Fig. 1.4 from J. Plagge *On the Reinforcement of Rubber by Fillers and Strain-Induced Crystallization.* PhD Thesis, Universität Hannover (2018).

in Fig. 52 look so different from the ones depicted in Fig. 82. Figure 52 corresponds to an ideal linear model subject to a sinusoidal excitation. Figure 82 corresponds to a real material which is non-linear and the excitation has a saw-tooth shape rather than being sinusoidal. In addition, the hysteresis observed in stress-strain experiments has numerous contributions beyond the viscoelasticity of the neat polymer matrix. The material in Fig. 82 contains filler. We have already learned that filler networks can break and restructure when a load is applied. Moreover, load (and rate) dependent processes at the filler-polymer interface, e.g. chain slippage, contribute to hysteresis. When strain crystallization occurrs, as we explain next, it also contributes to the observed hysteresis.

• *Strain-Induced Crystallization*

Strain-induced crystallization (SIC) is a process during which crystallites form within an originally amorphous polymer matrix in response to (usually large) strain (cf. the cartoon in Fig. 83). SIC occurs in natural rubber (NR), as well as other elastomers and polymers - even though much of the interest in SIC is due to the importance of NR in technical applications (perhaps foremost among these are tires in particular for trucks).

Figure 84 shows stress-strain curves of NR together with the

observed crystallinity during loading and unloading. To the superficial observer the curve in panel (a) looks somewhat similar to the stress-strain curves we have already discussed in the context of the Mullins effect. However, the curve depicted in Fig. 84 was obtained after a certain number of previous cycles and the central portion of in particular the unloading part of the cycle is quite flat. It looks very much like a phase transformation from one phase to another (e.g., gas-liquid or liquid-solid coexistence in the *P-V* plane). X-ray scattering in fact reveals the presence of crystallites (their size is roughly 10 nm) formed beyond a certain strain threshold. Comparing panels (a) and (b) it appears that the stress is lower if the crystallinity is higher at any fixed strain.

Is there a theoretical argument why this should be the case? Yes - and, as one might expect, it was suggested by P. Flory (*Thermodynamics of Crystallization in High Polymers. I. Crystallization Induced by Stretching* J. Chem. Phys. *15*, 397 (1947).).

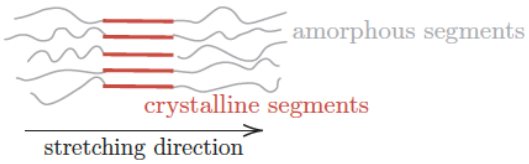

Fig. 83 Cartoon of a crystallite within an amorphous network. From L. Tarrach, PhD thesis, University of Wuppertal (2024).

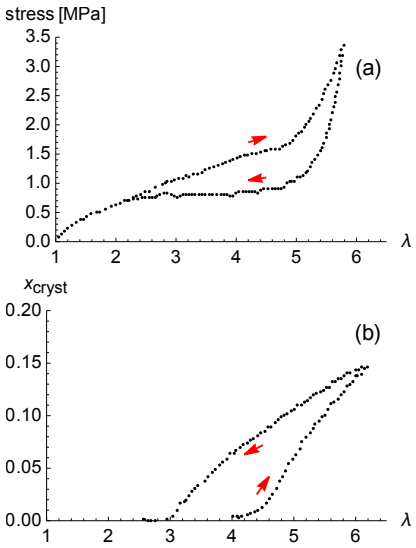

Fig. 84 (a) Stress-strain (λ) curves of natural rubber. The curves were obtained after the fourth mechanical cycle at a strain rate of 1 mm/min. (b) Crystallinity measured during the cycle in panel (a) at room temperature. Arrows distinguish the loading from the unloading part of the strain cycle. The data are taken from Fig. 2 in S. Trabelsi, P.-A. Albouy, J. Rault, Macromolecules *36*, 7624 (2003).

However, before going into the details, it is useful to discuss the example in Fig. 85. The cartoon shows two ideal polymer chains containing an identical number of Kuhn segments n attached to opposite walls. The length of the Kuhn segments is b and the separation of the walls is R. It is assumed that $nb \gg R$. The entropic force on the anchoring points of the chain on the left is

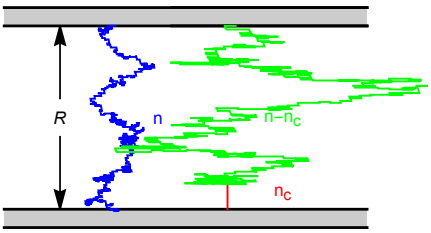

Fig. 85 Illustration of chain conformations without (blue) and with (green) strain crystallization (red).

$$f = -T\frac{dS(R)}{dR} \propto \frac{R}{n}\,, \tag{421}$$

where $S(R)$ is given in Eq. (82). The chain on the right, even though it possess the same number of Kuhn segments, differs from the first. It contains n_c consecuetive Kuhn segments which are fully aligned and perpendicular to the walls. The rest of the chain, however, is a regular (amorphous) chain of the remaining $n-n_c$ Kuhn segments. At this point we are not interested in what causes the first n_c Kuhn segments to be special. Instead we want to know how these n_c Kuhn segments affect the force on the anchoring points of the chain.

Due to the constraint, the force f_c on the ends of the right chain is

$$f_c \propto \frac{R-n_c b}{n-n_c}\,. \tag{422}$$

Since the proportionality constants in (421) and (422) are the same, we must compare R/n to $(R-n_c b)/(n-n_c)$ to decide which force is larger. For simplicity we assume $b=1$ and use the numerical example $R=10$, $n=100$ and $n_c=4$. This yields

$$\frac{R}{n} = 0.1 \quad \text{and} \quad \frac{R-n_c b}{n-n_c} \approx 0.06\,, \tag{423}$$

Hence $|f_c| < |f|$. Now let's increase R from 10 to 12. If we want f_c to be constant, what does this imply for n_c? In order for f_c to remain constant, we must increase n_c from 4 to approximately 6. And this is essentially what we see in Fig. 84.

In other words, the formation of the crystallites, containing aligned polymer segments oriented predominantly in the direction of the applied strain/stress, 'buys' the remaining amorphous Kuhn segments conformational freedom, which they otherwise would not possess. This in turn reduces the force on the anchoring points of the chains in their network. SIC therefore is a means by which an elastomer material can reduce the stress acting on it. The crystallites can 'pop up' (on a time scale of ms) where needed and thus create a flexible response to large local strain. When the strain is reduced the crystallites melt. SIC therefore has important effects on strength and fatigue properties of the strain crystallizing material.

However, let's return to the aforementioned work of Flory. His

is a single-chain theory described by a two-term free energy

$$\Delta F/T = -\Delta S^{el} + n(1-x)\theta \; . \tag{424}$$

The first term is an elastic entropy given by

$$\Delta S^{el}/k_B = -\frac{1}{2}\left\{\left(\lambda^2+\frac{2}{\lambda}\right)\frac{1}{x} - 3 - 2\lambda\frac{1-x}{x}\sqrt{3n}\,p + \frac{(1-x)^2}{x}3n\right\} \; . \tag{425}$$

Here the quantity x is defined via $n_c = n(1-x)$. n_c is the number of straightened Kuhn segments in a chain composed of n Kuhn segments (cf. the above example). Note that for $n_c = 0$, i.e. $x = 1$, $\Delta S_{\rm el}$ agrees with $\Delta S^{el}_{stretch}/N$ in Eq. (195). In Flory's paper $p = \sqrt{2/\pi}$. however, here we use a slightly adjusted value in order to achive $n_c = 0$ for $\lambda = 1$ (see below).

But what is the meaning of the second term - in particular the quantity θ? It is due to straightening of $n_c = n(1-x)$ consecutive Kuhn segments within a chain. If we force a 'crystallite' to exist above the melting temperature we must pay a positive 'penalty' in the form of work, i.e. by deforming the sample. The equilibrium x-value, i.e. x_o, follows via $\partial\Delta F/\partial x|_\lambda = 0$:

$$x_o^2 = \frac{\left(\frac{\lambda^2}{2}+\frac{1}{\lambda}\right)\frac{1}{n}+\frac{3}{2}-\lambda\sqrt{\frac{3}{n}}\,p}{\frac{3}{2}-\theta} \; . \tag{426}$$

If we require that $n_c = 0$, i.e. $x_o = 1$, for $\lambda = 1$ then

$$\sqrt{\frac{3}{n}}\,p = \theta + \frac{3}{2n} \; . \tag{427}$$

Finally, we find the average force f on a chain's ends via

$$f/T = -\frac{d\Delta F/T}{d\lambda} = -\frac{\partial\Delta F/T}{\partial\lambda}\Big|_x - \underbrace{\frac{\partial\Delta F/T}{\partial x}\Big|_\lambda}_{=0}\frac{dx}{d\lambda} \tag{428}$$

$$= \left(\lambda - \frac{1}{\lambda^2}\right)\frac{1}{x_o} - \sqrt{3n}\,p\left(\frac{1-x_o}{x_o}\right) \; .$$

Figure 86 shows an example where $n = 36$ and $\theta = 0.19$. Thus, from Eq. (427) it follows that $p \approx 0.803$ (very close to the aforementioned Flory value of 0.798). Like in the previous example, we find that the force at constant strain in a chain with SIC is less than that in a chain without SIC.

However, Fig. 86 is far from being a complete theory for experiments like the one illustrated in Fig. 84. Aside from the fact that the force curve in Fig. 86 does not show the pronounced upturn at high λ due to the absence of finite chain extensibility, there are other significant shortcomings. First, there is only a single curve and no hysteresis. This is because this is an equilibrium single-chain theory. Second, crystallization in this theory begins immediately. The experiments, on the other hand, find rather distinct and quite elevated strain values upon loading and unloading where crystallites are formed or disappear. This is because the

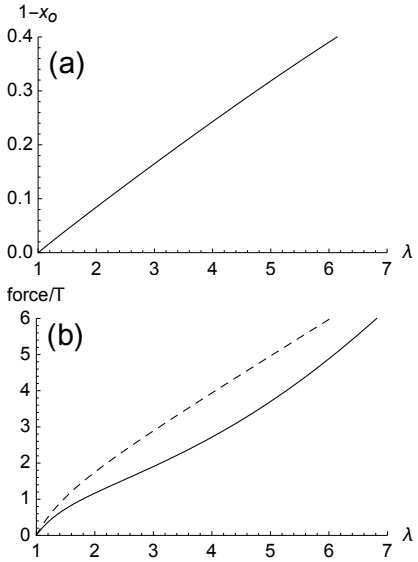

Fig. 86 (a) Crystallization $1-x_o$, vs. strain, λ. (b) Force, f, divided by temperature T, on a segment vs. λ. Solid line: Eq. (428); dashed line: $\lambda - 1/\lambda^2$. Parameter values: $n = 36$, $\theta = 0.19$ and p according to (427). This is figure 3 in R. Hentschke, J. Plagge *Strain-induced self-assembly of crystallites in elastomers.* Phys. Rev. E *104*, 014502 (2021).

time-dependent formation and cooperative behavior of crystallites is not addressed in Flory's theory. A suggestion for the rather distinct onset of crystallite formation is made in R. Hentschke, J. Plagge *Strain-induced self-assembly of crystallites in elastomers.* Phys. Rev. E *104*, 014502 (2021). The authors propose that $1-x_o$, shown in Fig. 86 (a), is the sum of two contributions, i.e. $1-x_o = x_1 + x_{agg}$. Here x_{agg} is due to the crystallites observed via scattering experiments. x_1, on the other hand, corresponds to straightened chain segments in a largely amorphous environment, which are not yet part of a crystallite. Both x_1 and x_{agg} are described analogous to free and bound monomers in the context of reversibly assembly of labile polymeric aggregates - which in these lecture notes are discussed in section 6.3. The theory of reversible assembly of molecular aggregates implies a critical concentration required for aggregates, or crystallites in the case at hand, to form. And this threshold concentration might just explain why there is such a distinct onset of strain induced crystallisation.

Subsequent to Flory's seminal work, numerous other researchers have made contributions to SIC. However, this is not the place for a comprehensive overview. Instead the interested reader may want to consult the following references as well as the references therein: J. Plagge and M. Klüppel *A Theory Relating Crystal Size, Mechanical Response, and Degree of Crystallization in Strained Natural Rubber.* Macromolecules *51*, 3711 (2018); P.-A. Albouy and P. Sotta *Draw Ratio at the Onset of Strain-Induced Crystallization in Cross-Linked Natural Rubber.* Macromolecules *53*, 992 (2020); J. Plagge, R. Hentschke *Microphase Separation in Strain-Crystallizing Rubber.* Macromolecules *54*, 5629 (2021).

- *Loss Tangent*

We had introduced the loss tangent or $\tan\delta$ in the context of Eq. (258), where it is defined as the ratio of the loss modulus to the storage modulus. Aside from the dynamic moduli themselves, the loss tangent is one of the quantities most likely measured during mechanical testing of a polymer sample. Since it is an important laboratory indicator for rubber performance in the tire industry, we want to briefly discuss it here. The importance of $\tan\delta$ as a tire rubber performance indicator is illustrated in Fig. 87.

The figure shows two experimental loss tangent curves plotted versus temperature. For the designer of tire tread materials the comparison between two such curves provides information about the relative performance of the materials in terms of rolling resistance, i.e. fuel efficiency, and/or breaking under wet and/or icy conditions. Just like the storage modulus and the loss modulus individually, the loss tangent is affected by almost all changes made to a rubber's recipe and processing. Being the ratio of two moduli, $\tan\delta$ is a dimensionless quantity. When filler, which we discuss in the next section, is added, the peak (usually) does not shift but the height of the peak is reduced (e.g. Figs. 2.63 and 2.64 in C. Wrana's *Introduction to Polymer Physics*). More or less the same happens when the filler amount does not change but the filler particle size is reduced (e.g. C. G. Robertson et al. Macromolecules *41*, 2727 (2008)).

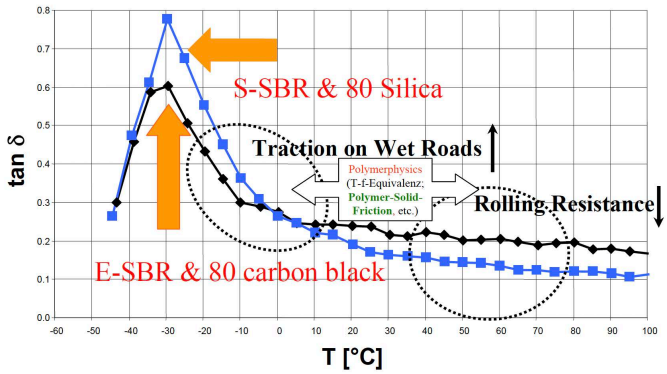

Fig. 87 Loss tangent versus temperature for SBR filled with carbon black and silica nanoparticles. The strain amplitude is 10% and the frequency is 10 Hz. The figure is taken from a talk given by G. Heinrich.

Figure 88 shows a picture of two rubber balls. If you hold them in your hands, you cannot really distinguish one from the other. Their weight and hardness appears to be the same. But dropping them onto a hard surface reveals a pronounced difference. One of the balls bounces, whereas the other one just hits the surface and does not bounce back into the air. I have been told, that candidates for a position in a well known tire company are regularly asked to explain this table top experiment during their job interviews. What is your explanation based on what you have learned in these notes thus far?

Fig. 88 A bouncy and a not so bouncy rubber ball.

6.2 Filler Effects

Modern polymer based materials contain numerous components which are not polymers. Prominent among these components are particulate fillers. In the following discussion of why fillers are added and how they affect the behavior of the polymer matrix, we shall concentrate on elastomer materials used in the tire industry (M.-J. Wang, M. Morris *Rubber Reinforcement with Particulate Fillers*. Hanser:Munich (2021)). However, much of what is said applies to other polymer materials as well.

Figure 89 depicts a typical filler used in tire rubbers - carbon black. The upmost panel in the figure shows transmission electron micrographs or TEM images. Each TEM is based on a thin slice -usually 60 to 100 nm thick on average - cut from a material sample. What we see are aggregates of carbon black nanoparticles embedded in a polymer matrix. The aggregates vary in darkness because in certain places there are particles stacked along the line of sight. But what is a particle? Usually the smallest distinguishable 'spheres' are the so-called primary particles. However, primary particles do not occur isolated from one another. Instead they are fused into small aggregates - let's call the minimum aggregates. These minimum aggregates usually do not break during the mixing process when the filler is introduced into the polymer matrix. The size of the minimum aggregates and the size of the primary particles appear to be correlated, i.e. their linear dimensions differ by roughly a factor of three (W. M. Hess, G. C. McDonald *Improved particle size measurements on pigments for rubber*. Rubber Chem. Technol. *56*, 892 (1983)). Driven by the interface free energy, fillers show the tendency to form larger aggregates over time in a process called **flocculation**. Attractive dispersion forces between the filler particles let them form larger aggregates and structures beyond. The larger size and the weaker bonding means that the aggregates formed during flocculation can be broken when the material is mechanically deformed.

Filler come in certain grades. In the case of carbon black different grades are distinguished by a code starting with the letters N

or S followed by a number (see American Society for Testing and Materials ASTM D1765-21). The letters give indication of the influence of the carbon black on the rate of cure (vulcanization speed) of a typical rubber compound . The first digit is indicative of the (primary) particle size (or actually its surface area). Following digits contain additional information regarding the particle morphology. When the concentration of filler is increased it will form a spanning network in the polymer matrix as shown in the middle panel of Fig. 89. Note that the polymer matrix itself usually is not conductive but carbon black is. The measurement of the filled polymer's resistivity versus carbon black concentration reveals a distinct step or filler **percolation threshold**. An example measurement is shown in the bottom panel of Fig. 89. The unit of concentration here is phr (parts per hundred) (in weight) rubber. The filler concentration in commercial elastomer materials varies but usually exceeds the percolation threshold.

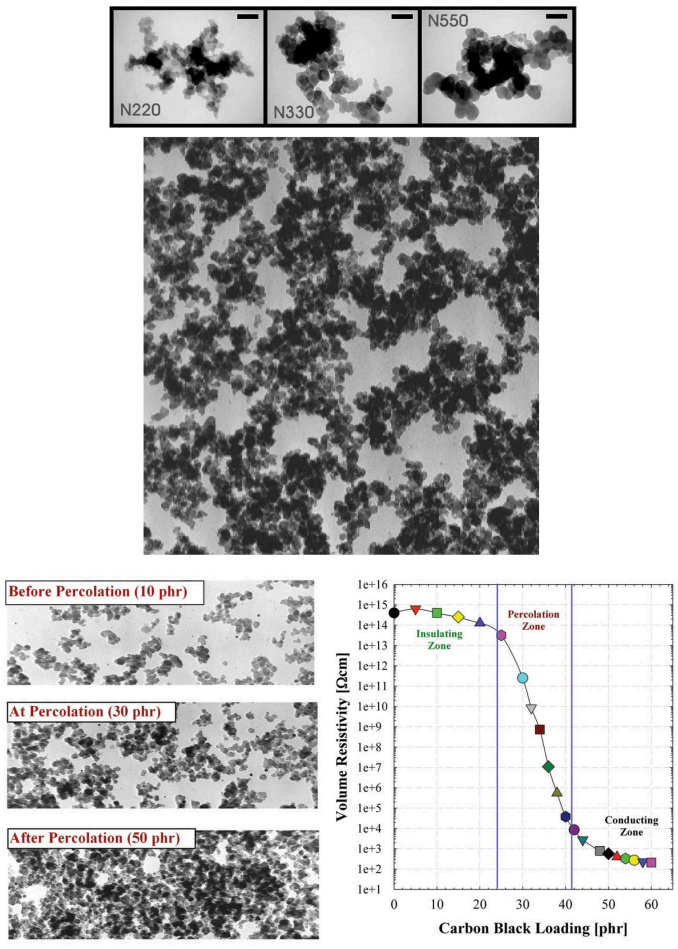

Fig. 89 Top: Transmission electron micrographs (TEM) of three different grades of carbon blacks - N220, N330, and N550. (bar length: 100 nm). This is Fig. 17 from M. Klüppel *The Role of Disorder in Filler Reinforcement of Elastomers on Various Length Scales* Adv. Polym. Sci. *164*, 1 (2003). Middle: TEM-micrograph of a carbon black (N330) network obtained from an ultra-thin cut of a filled rubber sample. This is Fig. 25 in the aforementioned reference. Bottom: The volume resistivity of carbon black filled solution SBR including TEM images of carbon black in-rubber network at 10, 30 and 50 phr loading. This figure is Fig. 7 from L Nikiel, W. Wampler, J. Neilsen, N. Hershberger *How carbon black affects electrical properties.* Rubber & Plastics News, March 23 (2009).

In the following we shall use the volume fraction ϕ to measure the fractional amount of volume occupied by filler. Hence, we shall need to convert between phr and ϕ. As we have already stated, phr is the abbreviation of *part per one hundred base polymer*, i.e. the unit phr means proportion by weight, with respect to 100 parts of the crude rubber used. Carbon black has a density of around 1.8 to 2.1 g cm^{-3} and silica, another prominent filler (cf. below), has a density of around 2.2 to 2.3 g cm^{-3}, whereas rubber densities are close to 1 g cm^{-3}. The conversion from phr to filler volume fraction, ϕ, is

$$\phi = \frac{\frac{phr}{c_{filler}}}{\frac{phr}{c_{filler}} + \frac{100}{c_{rubber}}} \tag{429}$$

(neglecting additional components). Here c_{filler} and c_{rubber} denote the filler and the rubber density, respectively. The formula is shown in Fig. 90 for $c_{filler} = 2.7$ g cm^{-3} (dotted line), $c_{filler} = 2.3$ g cm^{-3} (solid line), and $c_{filler} = 1.8$ g cm^{-3} (dashed line) using $c_{rubber} = 1$ g cm^{-3}.

Carbon black nanoparticles are not the only filler used. The second prominent filler system is the silica-silane system. Silica particles consist of amorphous SiO_2. The surface of silica nanoparticles is covered with silanol groups, i.e. various types of OH-groups. In order to improve the dispersion of silica in most polymers, the surface of the silica particles is compatibilized using silanes. The silane molecules are chemically bonded to the silica surface and usually also to the polymer matrix. Hence the silica-silane system is quite versatile and can be modified to optimize material performance. Aside from carbon black and silica there are numerous other fillers including nanotubes, organic particles, etc..

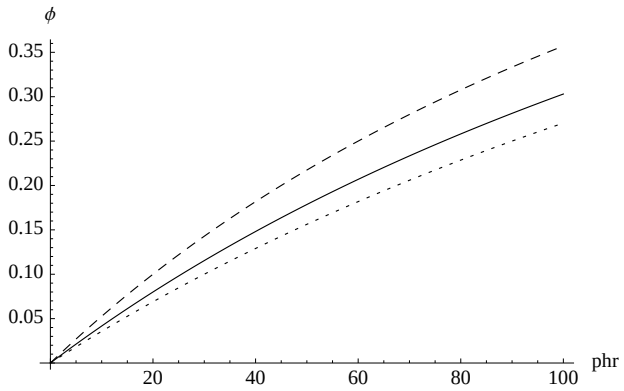

Fig. 90 Filler content: conversion between phr and volume fraction ϕ. Dashed line: carbon black; solid line: silica; dotted line aluminum ($c_{Al} = 2.7$ g cm^{-3}).

Figure 91 compiles the effect of variable filler concentration on a number of mechanical quantities. It is the goal of the theory of course to provide explanations for these observations.

Suppose we use the rheometer depicted in Fig. 51 to carry out a shear experiment on one of the polymers whose storage modulus master curve is depicted in Figs. 54 and 55. Let's assume the shear frequency is 1 Hz, which means we are on the plateau in Fig. 54 (b) or, if the molecular weight is sufficiently large, in Fig.

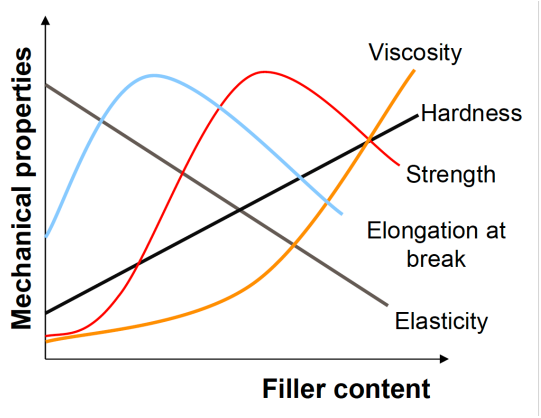

Fig. 91 Overview how filler affects mechanical properties of elastomers. Taken from M. Warskulat, A. Wehmeier Verstärkung · Reinforcement, Carbon Black & Silica/Silane, Educational symposium presentation at DKT/IRC 2021, Nürnberg, Germany (2022).

55 as well. In the following G_o is this plateau value of the storage modulus. If the polymer matrix also contains filler G_o is replaced by G.

What happens if we keep the shear frequency constant at 1 Hz but change the shear amplitude? The qualitative answer is depicted in the top panel of Fig. 92. Without filler essentially nothing happens. In the case of a linearly elastic network the storage modulus does not depend on the amplitude of deformation. However, with the addition of filler this changes. An increase of the storage modulus is observed, which has several contributions. First there is a **hydrodynamic effect**. Then there is a **in-rubber-structure effect**. These two effects depend weakly on the deformation amplitude. However, the third contribution, denoted here as 'filler-filler interaction', strongly depends on deformation amplitude. In the limit of small deformations and for filler concentrations near or above the percolation threshold it is by far the largest of all four of the shown contributions.

The reason behind the strongly non-linear behavior of the storage modulus is explained in the bottom panel of Fig. 92. The explanation starts with the spanning filler network still intact at small strain (roughly $< 1\%$ strain). Somewhere between 1% and 10% strain the network is broken up into smaller pieces. But why should the network begin to break up already at 1% strain - and sometimes even at strains as low as 0.1%?

Before we address the question directly, let's construct a (local) theoretical picture of the filler network. The left panel in Fig. 93 depicts filler aggregates (shown as disks) forming network braches. The branches are embedded in tightly bound polymer sheaths. Filler branches plus their polymer sheaths together constitute filler network strands. The polymer beyond is bulk-like. A central element is the contact, depicted in the middle, consisting of adjacent filler particles plus surrounding amorphous 'sheath polymer'. When the contact is stretched, voids between the aggregates will occur at some point.

Note that the close proximity of neighboring filler particles causes pronounced **strain enhancement** as illustrated in the cartoon depicted in Fig. 94. The green circles are two neighboring

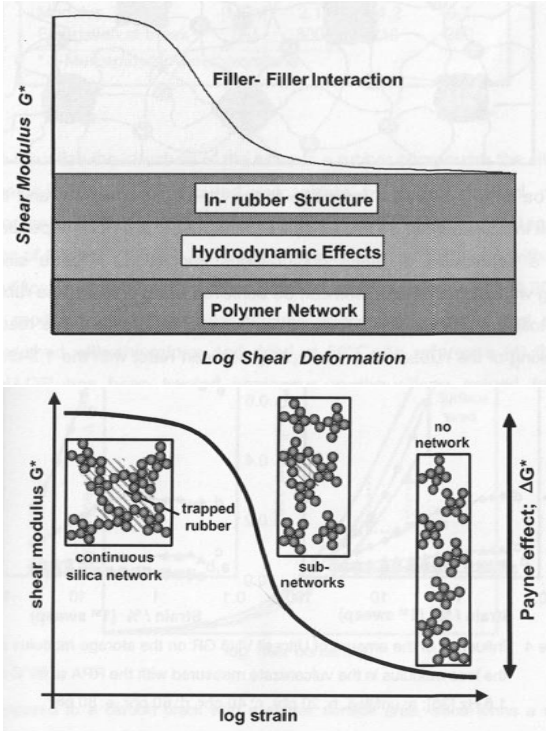

Fig. 92 Top: Contributions to the complex modulus (for the purpose of the present discussion we can replace the complex modulus with the storage modulus). Both figures are taken from H.-D. Luginsland *A Review on the Chemistry and the Reinforcement of the Silica-Silane Filler System for Rubber Applications.* Shaker Verlag:Aachen (2002). Bottom: Breakdown of the filler network with increasing strain.

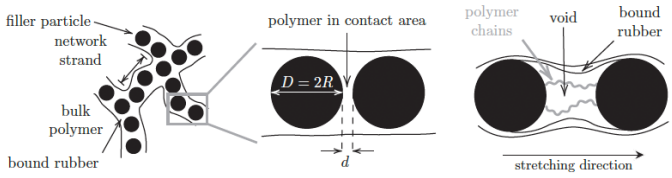

Fig. 93 Left: Filler strands within bulk-like polymer; middle: a filler-filler contact; right: Voids between aggregates due to caused by straining the network strands. From L. Tarrach, PhD thesis, University of Wuppertal (2024).

filler particles, whose diameter is D, in the unstrained sample. The resistivity experiments suggest that the gaps d between many of the filler particles must indeed be very small (<1 nm), i.e. $d \ll D$. Since the filler particles are not deformed when the sample experiences an external force, it must be the gap that widens from d to d'. Therefore the strain γ on a (one-dimensional) volume element containing the filler particles is related to the strain inside the gap γ_{gap} via

$$\gamma = \frac{d' + D - (d + D)}{d + D} \approx \frac{d' - d}{D} = \frac{d}{D}\gamma_{gap} \,. \tag{430}$$

Hence, $\gamma_{gap} \gg \gamma$. This calculation pertains to the cartoon. Nevertheless, the general idea applies also in a real network.

In the aforementioned strain range, the storage modulus undergoes a marked reduction commonly denoted as **Payne effect**.

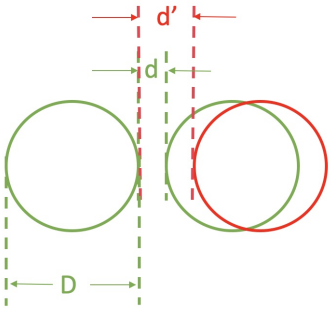

Fig. 94 Cartoon illustrating strain enhancement in filler-filler contacts.

Somewhere between 10% and 100% strain the storage modulus levels off. The filler-filler interaction and the in rubber structure are mostly gone. Nevertheless, it is important to note that whatever is left still is significant, because the tensile strength of a filled polymer network considerably exceeds the tensile strength of the pure network (cf. Fig. 91) (see for instance R. Hentschke *Tensile strength of rubber described via the formation and rupture of load-bearing polymer chains* Phys. Rev. E *106*, 014505 (2022)). The amorphous polymer sheath in Fig. 93 is replaced by a multitude of taut polymer chains anchored in part on the filler particle surfaces (depicted in Fig. 95).

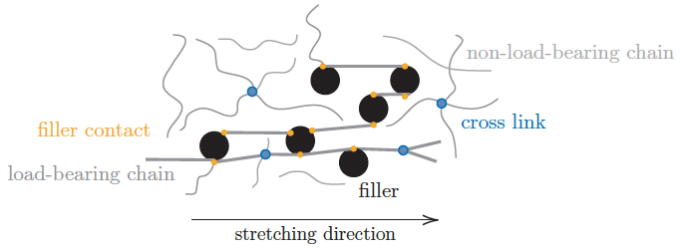

Fig. 95 Cartoon of load bearing polymer chains occurring at large strains. From L. Tarrach, PhD thesis, University of Wuppertal (2024) (with permission).

In the following we want to discuss selected theoretical concepts, which will help us to better understand (some of) the mechanical behavior of filled polymer matrices. We shall talk about 'particles' a lot - meaning minimum aggregates.

The 'hydrodynamic effect' primarily refers to the continuum approach initially introduced by Einstein in a different but related context (A. Einstein, Ann. d. Physik *19*, 289 (1906); *34*, 591 (1911)). Einstein devised a method for determining molecular dimension via the viscosity increase when 'large particles' are added to a fluid of 'small particles'. Subsequently Smallwood (H. M. Smallwood *Limiting Law of the Reinforcement of Rubber.* J. Appl. Phys. *15*, 758 (1944)) published a formally identical equation:

$$G = G_o\left(1+\frac{2}{5}\phi\right) . \tag{431}$$

Here ϕ is the filler volume fraction (The factor 2/5 is missing in Einstein's original calculation. But this he later notices and corrects the mistake.). This result is valid in the limit of small ϕ, assuming that the filler particles are hard spheres, and assuming 'no-slip' boundaries on their surface. It is obtained by solving the elastic equilibrium condition of the rubber treated as isotropic elastic material with filler particle inclusions. Generalizations of this equation to a power law series in terms of ϕ are discussed by Guth (E. Guth *Theory of Filler Reinforcement.* J. Appl. Phys. *16*, 20 (1945)); in particular we mention the expression due to Guth and Gold (E. Guth, O. Gold Phys. Rev. *53*, 322 (1938)):

$$G = G_o\left(1+\frac{2}{5}\phi+14.1\phi^2\right) . \tag{432}$$

While $G = G_o(1+(5/2)\phi$ is an exact result in the above limit, which is an appealing feature, it has major shortcomings. Perhaps most seriously, Eqs. (431) and (432) predict that the compound modulus is independent of the size of the filler particles. This is incorrect for modern sub-micron fillers. In the following we shall discuss the filler induced increase of the shear modulus from another angle.

In contrast to the no-slip boundary conditions underlying the Smallwood equation, we assume that the adhesion of the matrix material on the filler surface can be thought of as being due to surface bonds contributing strength analogous to the elastomer's bulk cross-links. But what do we mean by **'bonds'**? An example is a polymer segment physisorbed on the surface of a filler particle. The same polymer may possess another segment on a neighboring particle and thus connect the two particles. Or the polymer may be cross-linked to another polymer connected to the neighboring particle, etc. Another example is the covalent bonding between a particle's surface and the polymer matrix via a silane molecule. Yet another example is a hydrogen bond formed between the silanol groups of two neighboring silica particles. Hence there are many types of such molecular bonds. Of course, there are also dispersion forces between neighboring particles involving all atoms in the two particles (cf. for instance J. Israelachvili *Intermolecular & Surface Forces.* Academic Press (1991)). However, in most cases the latter interactions are not the dominant interactions affecting the mechanical properties of the material. It is important to note that the molecular bonds have their own temperature dependence (see for instance R. Hentschke *The Payne effect revisited* eXPRESS Polymer Letters *11*, 278 (2017)). This means that a (highly) filled polymer matrix follows time-temperature superposition to a lesser extend than an unfilled one.

Let's model the filler as composed of isolated monodisperse spherical particles with radius R. Under these conditions the modulus increase, in the limit of small shear amplitude, due to the particle-matrix interface should scale as ϕR^{-1}, i.e.

$$G - G_o \sim \frac{\phi}{R} . \tag{433}$$

Again we find a proportionality to ϕ. But we find also that a small particle size increases G. The derivation is as follows: N_P is the number of particles with volume v_P and surface area, a_P. Thus

we have $N_P v_P = \phi$. Likewise we have for the total surface area A of the particles $N_P a_P = A$. With $v_P \propto R^3$ and $a_P \propto R^2$ one finds

$$A \propto \frac{\phi}{R} \,. \tag{434}$$

Because the increase of G_o should be due to the surface bonds, we arrive at the above conclusion. Fig. 96 shows the storage modulus of carbon black filled polybutadiene in the limit of small strain plotted versus the inverse diameter of the minimum aggregates. These data follow the predicted $1/R$-dependence quite nicely. However, the volume fraction filler in this experiment is 0.18. This is close to the percolation threshold and the assumption of isolated aggregates is not valid. Unfortunately, this author was not able to find data for G' vs. $1/R$ at filler volume fractions significantly below the percolation threshold.

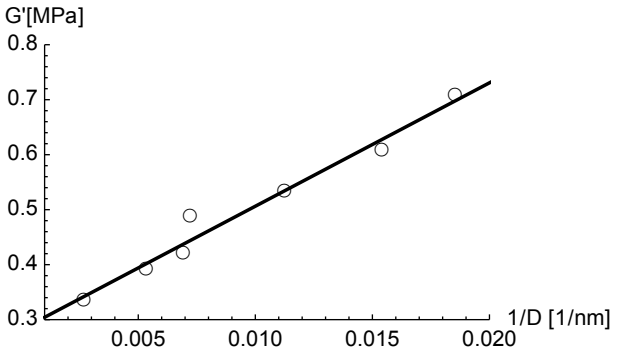

Fig. 96 G' at small strain amplitude vs. the inverse diameter $1/D$ of the minimum aggregates according to Fig. 8 and Tab. 1 in C. G. Robertson, C. J. Lin, M. Rackaitis, C. M. Roland *Influence of Particle Size and Polymer-Filler Coupling on Viscoelastic Glass Transition of Particle-Reinforced Polymers* Macromolecules *41*, 2727 (2008). Shown here is G' for polybutadiene at a constant volume fraction of 0.18. Measurements were made at $T = -70^o$C and $\omega = 31.4$ rad/s.

However, there is more information which can be gained by our simple reasoning. We can argue that there is an upper limit beyond which particle size has an adverse effect on hardness. This is because the volume of a large particle can displace more bulk cross-links in the elastomer compared to the increase of the number of surface bonds. This is illustrated by the sketch in Fig. 97. Note that the number of bulk cross-links is proportional to R^3, whereas the number of surface bonds is proportional to R^2. We may estimate the cross-over radius, R_c, based on rough estimates of both the surface bond density, n_s, and the bulk cross-link density, expressed in cross-links per rubber monomer, ν. With $1/50$ Å$^{-2} < n_s < 1/20$ Å^{-2} (in the case of silica) and $1/500 < \nu < 1/200$ we find $0.1\mu m < R_c < 1\mu m$, which is in accord with experimental observation (F. Schön *Elastomer / Schichtsilikat Komposite: Einfluss der Füllstoffstruktur auf mechanische, dynamische und Gasbarriere-Eigenschaften.* PhD thesis, Universität Freiburg (2004); page 11). Small filler particles far below this limit are called **active**.

Next we want to study the effect of the filler structure near the percolation threshold. Generally, it is observed that the shear modulus in the limit of small strain does not increase linearly with

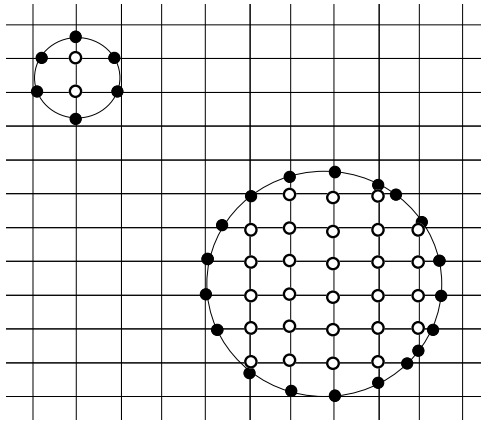

Fig. 97 Open circles: bulk cross-links; solid circles: surface bonds.

ϕ but with some power y instead, i.e.

$$G - G_o \sim \phi^y \,, \tag{435}$$

where y can be significantly larger than unity. Let us construct an explanation for (435) and find y.

We consider N filler particles in a volume $V = L^3$. The filler volume fraction, ϕ, therefore is given via

$$\phi \propto \frac{N}{L^3} \,. \tag{436}$$

In a uniform system we expect in addition $N \propto L^3$, i.e. the filler volume fraction does not depend on L. This means that ϕ is an intensive quantity. However, if we assume instead

$$N \sim L^{d_f} \tag{437}$$

with $d_f < 3$, then the situation is different, because the system now contains 'filler voids' on all length scales. Such cluster structures are called **fractal** structures and d_f is their mass **fractal dimension**. By combination of (436) with (437) we find

$$\phi \sim L^{-(3-d_f)} \to 0 \quad \text{for} \quad L \to \infty \,. \tag{438}$$

This means that a fractal filler distribution on all length scales throughout the rubber is not realistic!

Mechanical mixing results in a uniform system on a macroscopic scale, i.e. the mixing process does not allow a fractal filler network beyond a certain linear dimension. In this case ϕ is finite of course. Because this is an important aspect let us be more specific and call this length ξ, i.e. our material is a filled polymer matrix containing fractals of size ξ, which in turn contain N_ξ filler particles. Hence

$$\frac{N}{N_\xi} \propto \frac{L^3}{\xi^3} \tag{439}$$

and therefore

$$\phi \propto \frac{N_\xi}{\xi^3} \, . \tag{440}$$

Consequently we arrive at

$$\frac{1}{A_\xi} \sim \phi^{\frac{2}{3-d_f}} \, , \tag{441}$$

where $A_\xi = \xi^2$.

What is the significance of the expression (441)? The quantity A_ξ is the cross-sectional area of a fractal cluster containing N_ξ particles. Thus we may consider $1/A_\xi$ as a measure of the density of filler-filler contacts in a (shear) plane cross-section through a fractal patch. Because there are on average L^2/A_ξ fractal patches in the entire sample cross-section, we may consider the product of L^2/A_ξ with $1/A_\xi$ as a measure for the shear strength of the entire sample cross-section. In order to obtain the modulus we divide by L^2, which yields

$$G - G_o \sim \frac{1}{A_\xi} \frac{L^2}{A_\xi} \frac{1}{L^2} \sim \phi^{\frac{4}{3-d_f}} \, . \tag{442}$$

Of course, this should hold only if ϕ is large enough for the spanning filler network to form.

Meakin et al. (P. Meakin, B. Donn, G. W. Mulholland *Collisions between Point Masses and Fractal Aggregates.* Langmuir *5*, 510 (1989)) have studied the collisions between point masses and fractal aggregates via computer simulation of different models. They obtain d_f-values ranging from 1.8 to 2.1 depending on the model (i.e. $3.3 < y = 4/(3-d_f) < 4.5$). The resulting structures all look very similar to experimental filler structures obtained from transmission electron micrographs. Thus, a certain variation of the exponent y appears permissible. Fig. 98 shows an experimental confirmation, where $y \approx 3.5$, of the picture developed here.

The fractal concept we have just outlined is not new. Significant insight was originally provided via computer simulation. For instance the cluster-cluster aggregation model introduced by Meakin (P. Meakin, Phys. Rev. Lett. *51*, 1119 (1983)) and Kolb (M. Kolb, R. Botet, R. Julien, Phys. Rev. Lett. *51*, 1123 (1983)) initiated an upsurge of interest in the properties of aggregated colloids. Subsequent simulation studies suggested that colloidal aggregates behave as stochastic mass-fractals on a scale large compared with the primary particle size. Experimental studies did confirm this and provided values for the fractal dimension d_f in good agreement with those obtained from Simulation (D. A. Weitz, M. Oliveria, Phys. Rev. Lett. *52*, 1433 (1984); M. Matsushita, K. Sumida, Y. Sawada, J. Phys. SOC. Jpn. *54*, 2786 (1985); W. D. Brown, R. C. Ball *Computer simulation of chemically limited aggregation.* J. Phys. A: Math. Gen. *18*, L517 (1985); P. N. Pusey, J. N. Rarity, paper presented at Royal Society of Chemistry Symposium on Fractals in Physics and Chemistry, Salford, 1986)).

Our final expression (442) is close to one proposed by Brown (W. D. Brown, PhD Thesis, Department of Physics, University of Cambridge, 1987), i.e. $y = (3 + d_{chem})/(3 - d_f)$, where d_{chem} is the so-called chemical length exponent. An in depth discussion of the development and application of fractal networks in the context of colloidal systems can be found in A.G. Marangoni, L.H. Wesdorp *Structure and Properties of Fat Crystal Networks.* Second Edition, CRC Press (2012). Full appreciation of these ideas in the context of filled rubbers came with the works of Heinrich, Klüppel, and Vilgis (M. Klüppel, G. Heinrich *Fractal structures in carbon black reinforced rubbers* Rubber Chemistry and Technology, *68*, 623 (1995); G. Huber, T.A. Vilgis *Universal properties of filled: Mechanisms for reinforcement on different length scales.* Kautschuk Gummi Kunststoffe *52*, 102 (1999)) (as well as references therein).

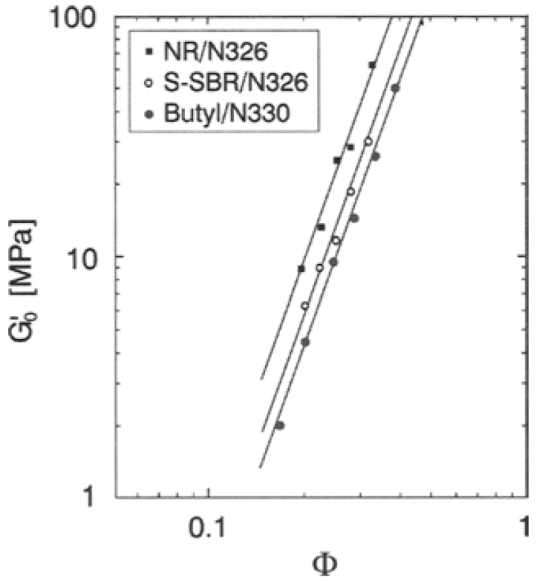

Fig. 98 Small strain storage modulus vs filler volume fraction for a variety of carbon black filled composites. The solid lines posses slope 3.5. This figure is a copy of Fig. 39 from M. Klüppel *The Role of Disorder in Filler Reinforcement of Elastomers on Various Length Scales* Adv. Polym. Sci. *164*, 1 (2003).

Strictly speaking the above applies close to the percolation threshold only. At filler volume fractions far above the percolation threshold we must expect a different and likely less fractal structure. What would the result be if the filler was forming completely random connections? We consider N filler particles distributed over L^3 cells in a cubic grid. The probability that a particular particle finds a particle in a neighboring cell is (neglecting correlations) qN/L^3, where q is the coordination number of the lattice. The number of pairs formed in this fashion therefore is proportional to N^2/L^3. The density of pairs is proportional to $N^2/L^6 = \phi^2$. Thus we expect

$$G - G_o \sim \phi^2 \tag{443}$$

in the case of random filler distribution. Indeed, many measurements of $G - G_o$ vs. ϕ yield y-values close to 2.

Let us return to the dependence on particle size in the context of a dense filler network. Let's assume we compare systems composed of spherical particles whose radii are R and $2R$, respec-

tively. In both systems the filler network structure is the same and the filler volume fraction is also the same. This means that we can transform the system containing the smaller particles into the system containing the larger particles by scaling its axes by a factor of 2. Within a fixed area in the shear plane, i.e. this area is not scaled, this reduces the number of particle-particle contacts by a factor 4. Our premise is that $G - G_o$ is proportional to the number of particle-particle contacts in a shear plane and thus $G - G_o \propto R^{-2}$. However, the interaction between particles in a contact also depends on R. This is illustrated in the sketch shown in Fig. 99. If the forces bonding the spheres only act near the surface (e.g. short chain segment physisorption or hydrogen bonds), we assume a certain range between d and $d + 2h$, then the interacting surface area S is given by

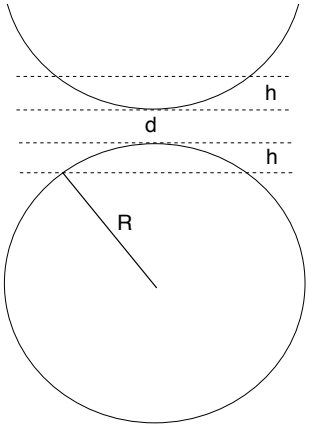

Fig. 99 Primary filler particles pictured as spheres at close proximity.

$$S = 2\pi R h \,. \tag{444}$$

But even if we consider the interaction to be contributed from atomic pair-interactions throughout the spheres the resulting interaction still scales proportional to R (J. Israelachvili *Intermolecular & Surface Forces.* Academic Press (1991)) (the force between two spheres of equal radius R should be $-\frac{A}{12}\frac{R}{d^2}$, where A is the Hamaker constant and d ($d \ll R$) is a small surface-to-surface separation between the spheres). Therefore all in all the two contributions yield a resulting R^{-1}-dependence, i.e.

$$G - G_o \sim \frac{\phi^y}{R} \,. \tag{445}$$

This R dependence is the same which we had found previously in the limit of isolated particles - and this time Fig. 96 can be viewed as a confirmation.

The position of the percolation threshold along the volume fraction axis, ϕ_c, does depend on the particle grade / size. An example is shown in Fig. 100. How can we understand this dependence? In Eq. (441) the length ξ is expressed in units of particle size R, i.e.

$$\frac{R^2}{(\xi R)^2} \sim \phi^{\frac{2}{3-d_f}} \,. \tag{446}$$

We have stated that the length scale over which fractal filler structure can exist is determined by ξ or rather by ξR in absolute units. It is plausible to assume that this length scale is similar for different R, i.e. $\xi R \approx const$. Hence, we find

$$\phi_c \sim R^{3-d_f} \,. \tag{447}$$

This means that the percolation threshold shifts to larger filler volume fractions when the filler particles are larger - in agreement with the experimental observation in Fig. 100. The bottom panel in Fig. 100 is a test of this relation. The slope of the linear fit to the data is about 0.6 and thus $d_f \approx 2.4$. This is larger than what we have discussed before and larger than the d_f-value needed to obtain $y \approx 3.5$. However, $y \approx 3.5$ is far from universal and larger values are found as well (cf. Fig. 8 in He Xi, R. Hentschke *The influence of structure on mechanical properties of filler networks via coarse-grained modeling.* Macromolecular Theory and Simulation (2014)). In addition, the conversion from phr to volume fraction is approximate and so are the particle sizes, which contributes considerable sources of error to this comparison.

Before leaving this section we want to mention the effect of fillers on time-temperature superposition. Fig. 101 shows master curves of the storage modulus G' of an unfilled S-SBR sample and the same samples filled with 60 and 80 phr of silica created with (horizontal) shift factors from the unfilled sample. While Eqs. (271) and (270) work very well for unfilled samples, as we have seen numerous times before, they do not work equally well when there is filler in the polymer. Why is this? The temperature dependence of our shift factor a_T rests on the assumed linear temperature dependence of the free volume. By adding filler we introduce interfaces into the system. These are interfaces between filler and polymer and between filler particles contain bonds (cf. above). In the case of silica, for instance, we find hydrogen bridge bonds. These hydrogen bridge bonds may connect adjacent particle surfaces or they may connect an OH-group on a silica surface to a water molecule above the surface (in the case of silica, a certain amount of water, perhaps a couple of % by filler weight, is always present). In any case, the number of such bonds depends on temperature akin to the equilibrium constant in a chemical reaction (cf. R. Hentschke *The Payne effect revisited* eXPRESS Polymer Letters *11*, 278 (2017)). Since the number of (reversible) bonds does affect the coupling of the filler particles among themselves as well as their coupling to the polymer matrix, it may not be surprising that this new temperature dependence, which is different from the temperature dependence of a_T in a pure polymer system, does interfere with time-temperature superposition as we had discussed it. Improved master curves in filled systems can be obtained if the horizontal shift factor a_T is supplemented by a second vertical shift factor (see J. Fritzsche, M. Klüppel *Structural dynamics and interfacial properties of filler-reinforced elastomers.* Journal of Physics: Condensed Matter *23*, 035104 (2011)).

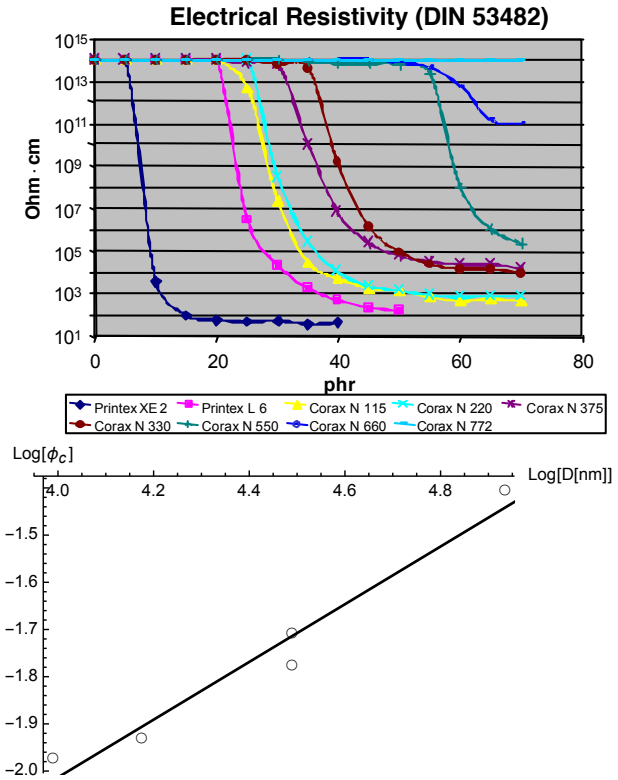

Fig. 100 Top: Resistivity data across the percolation threshold for different grades of carbon black from Carbon Blacks for Electrically Conductive Rubber Products, Technical Report 812, Degussa AG, Advanced Fillers and Pigments Division, Applied Technology Advanced Fillers (Remark: the company is now Evonik and the (nice) technical reports are difficult to obtain, unfortunately.). Bottom: determination of the exponent $3-d_f$ from a plot of $\log\phi_c$, where ϕ_c is the filler volume fraction at the inflection point of the resistivity data, versus $\log D$, where D is the corresponding aggregate size taken again from Tab. 1 in C. G. Robertson, C. J. Lin, M. Rackaitis, C. M. Roland *Influence of Particle Size and Polymer-Filler Coupling on Viscoelastic Glass Transition of Particle-Reinforced Polymers* Macromolecules *41*, 2727 (2008). The data points are for N115, N220, N375, N330, N550, and N660. The polymer is SBR 1500.

Finally, we have not yet and will not discuss filler particles possessing anisotropic shape, e.g. carbon nanotubes (CNT). Particularly CNTs have been the focus of intensive research for some time. Even in small amounts (a few % by weight) they reinforce an elastomer matrix considerably. However, fillers possessing high shape anisotropy can be difficult to disperse properly. They tend to align and aggregate (we shall learn something about the underlying physical principles in the section on liquid crystallinity), which may not always be desired. In addition, the interface between the CNTs and polymer matrices poses additional new challenges. The interested reader may look up the following reference: M. Loos *Carbon Nanotube Reinforced Composites*. CNR Polymer Science and Technology, Elsevier Inc. (2015).

Even though this discussion of filler effects is rather limited, it highlights that fillers do have a very significant influence on the properties of a polymer material. It should also be clear that reliable or quantitative (and sometimes even qualitative) theories for the prediction of filler effects do not exist at this time.

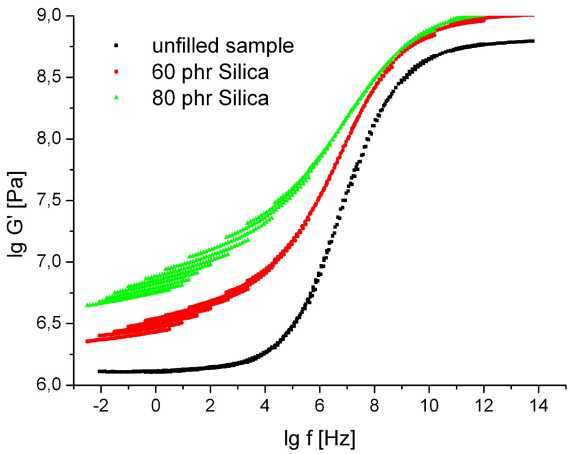

Fig. 101 Master curves of the storage modulus G' of an unfilled S-SBR sample and the same samples filled with 60 and 80 phr of silica created with (horizontal) shift factors from the unfilled sample. This is Fig. 4(a) taken from J. Fritzsche, M. Klüppel *Structural dynamics and interfacial properties of filler-reinforced elastomers*. Journal of Physics: Condensed Matter *23*, 035104 (2011).

6.3 Stable and Labile Liquid Crystalline Polymers

Stable Liquid Crystalline Polymers:

A summary of what we want to talk about in this section is depicted in Fig. 102. The cartoon at the top shows randomly oriented, bend-elastic rod-like polymers in solution at low concentration. Remember that in section 3.1 we had mentioned polymers which can be described as homogeneously bend-elastic. One example, PBLG, is shown in Fig. 14. The quantity characterizing their flexibility is the persistence length P defined in Eq. (40). Upon increasing the concentration, the polymers are forced to align along a spontaneously chosen direction called the **director**. Here we consider polymers with fairly short-ranged interactions, which to good approximation can be described as hard but flexible cylindrical rods. What forces them to align is their excluded volume. Specifically, it is the competition of orientation entropy versus packing entropy. The alignment is measured using the orientation distribution function $f(\theta)$, where θ is the angle relative to the director. If the orientation is isotropic, then $f(\theta)$ is constant. Otherwise it exhibits maxima at $\theta = 0, \pi$. The two types of ordering correspond to two phases, the **isotropic phase** and the **nematic phase**. How to describe the transition from one phase into the other is our main objective here. However, other so-called liquid crystalline phases can occur as well. Two examples are shown at the bottom of Fig. 102. In a **hexagonal columnar phase** the centers of mass of the rods tend to form a hexagonal lattice if we look along the rods' axes. If we look at the rods from the side, their centers of mass appear distributed randomly. In this sense a columnar phase can be described as a combination of a two-dimensional solid with one-dimensional liquid. A second example of a liquid crystalline phase is a **smectic phase**. In a smectic phase the molecules form layers. Hence a smectic phase may be described as the combination of a two-dimensional liquid parallel to the layer boundaries with a one-dimensional crystal in

the perpendicular direction. If concentration (via excluded volume) is the main driving variable taking the system from one phase to another we call this type of liquid crystalline behavior **lyotropic**. If temperature is the main driving variable we call that type of liquid crystalline behavior **thermotropic**. However, this distinction is not absolute and lyotropic liquid crystals do posses temperate dependence as well - either via the temperature dependence of their bending rigidity or via 'soft' interactions. Since the persistence length P is important for the relative stability of the liquid crystalline phases formed by rod-like polymers, we briefly digress and discuss the temperature dependence of P.

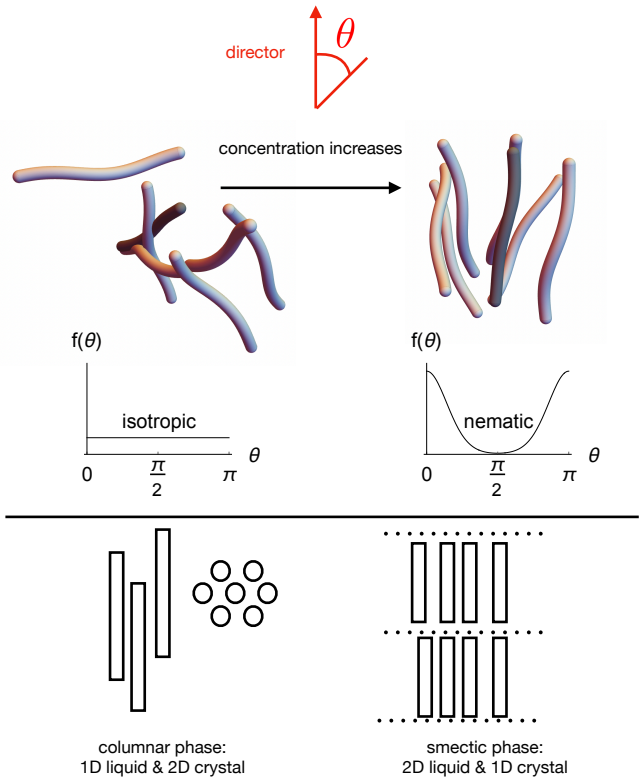

Fig. 102 Top: Randomly oriented rod-like polymers in solution at low concentration on the left vs. the same polymers at a higher concentration when their interaction forces them to preferentially align. Middle: Sketches of the orientation distribution function $f(\theta)$ in the two cases or, as we shall find out, phases called the isotropic phase and the nematic phase. Bottom: Cartoons depicting two other possible liquid crystalline phases, i.e. a hexagonal columnar and a smectic phase.

We may express the partition function of a persistent flexible polymer via

$$Q = \int \left(\frac{d\Omega}{4\pi}\right)^N \exp[-\beta H] \,, \tag{448}$$

where

$$H = -J\sum_i \vec{t}_i \cdot \vec{t}_{i+1} \quad (J>0) \,. \tag{449}$$

Let's momentarily assume that J is a constant. Hence

$$Q = \Pi_{i=1}^N \int_0^\pi \frac{d\theta \sin\theta}{2} \exp[J\cos\theta] = \left(\frac{\sinh\beta J}{\beta J}\right)^N \,. \tag{450}$$

Here the quantity θ is the angle between neighboring tangent vectors along the contour. From (450) we find $\langle\cos\theta\rangle$, i.e.

$$\langle\cos\theta\rangle = \frac{1}{N}\frac{\partial \ln Q}{\partial(-\beta J)} = \coth\beta J - \frac{1}{\beta J} \approx 1 - \frac{1}{\beta J} \quad (\beta J \gg 1) \,. \tag{451}$$

Note that $\beta J \gg 1$ is the proper limit, because we want $\langle\cos\theta\rangle \approx 1 - \langle\theta^2\rangle/2$ (cf. Eq. (42)). Using Eq. (43) we find

$$P = \frac{bJ}{k_B T} \,. \tag{452}$$

Thus, $P \sim T^{-1}$. Note however, that this is a model in which bJ is a constant. In a real persistent flexible molecule bJ itself usually depends on temperature, which modifies $P \sim T^{-1}$ of course.

Eq. (452) can be obtained quite differently using fluctuation theory. This approach is very insightful - as we shall see when we discuss the persistence length of polyelectrolytes. However, in order to avoid distraction from our current line of thought, the calculation of P from fluctuation theory is moved to appendix B.

The following consists of three parts. First we want to study the statistical mechanics of the isotropic to nematic transition of monodisperse rods depending on number concentration ρ, aspect ratio $x = L/D$, where L and D are the length and the diameter of the rod-like polymers respectively, and flexibility L/P. Subsequently we want to discuss, without explicit calculations, how to modify our theory in order to accommodate other phases exhibiting orientational and translational order. Finally, we need to discuss applications.

We begin by deriving the orientation entropy [‡‡], expressed in terms of $f(\theta)$, of what we had called a wormlike chain, i.e. a cylindrical object to which Eq. (40) applies. We use the self-consistent field method, where our starting point is Eq. (64):

$$\begin{aligned} Q_{n+1}(\vec{t}_1,\vec{t}_{n+1}) &= Q_n(\vec{t}_1,\vec{t}_{n+1}) \\ &+ \frac{1}{2}\int' \frac{d\Omega_n}{4\pi}\left(\vec{t}_n - \vec{t}_{n+1}\right)^2 \Delta_\Omega Q_n(\vec{t}_1,\vec{t})\big|_{\vec{t}_{n+1}} + \\ &- \beta u(\vec{t}_{n+1}) Q_n(\vec{t}_1,\vec{t}_{n+1}) \,. \end{aligned} \tag{453}$$

Here x_n is replaced by $\vec{t}_n$, which is the unit tangent vector of the worm's contour at the nth element of length b (cf. Fig. 14). The linear term in the expansion vanishes as before in Eq. (64). In addition, $\sum_{x_n}{}'$ is replaced with $\int' d\Omega_n/(4\pi)$. Note that the orientation of each tangent vector is defined by the angles φ and θ, i.e. $\vec{t} = \vec{t}(\varphi,\theta)$. θ_{n+1} is the angle between $\vec{t}_n$ and $\vec{t}_{n+1}$ and φ_{n+1} is the rotation angle of $\vec{t}_{n+1}$ around the direction defined by $\vec{t}_n$. Hence $d\Omega_n = \sin\theta_n d\theta_n d\varphi_n$. Finally, $\Delta_\Omega = (\sin\theta)^{-2}\partial_\varphi^2 +$

[‡‡] At this point 'conformation entropy' may be the better expression. What this has to do with orientation will become clear as we move along.

$(\sin\theta)^{-1}\partial_\theta(\sin\theta\,\partial_\theta)$ is the angular part of the Laplace operator. We evaluate the integration as follows:

$$\int' \frac{d\Omega_n}{4\pi}\left(\vec{t}_n-\vec{t}_{n+1}\right)^2 = \tag{454}$$

$$2\int' \frac{d\Omega_n}{4\pi}(1-\cos\theta_n) \approx \int' \frac{d\Omega_n}{4\pi}\theta_n^2 = \frac{1}{2}\langle\theta_n^2\rangle\,.$$

Here we have used that the local bending of the contour is small. And note that, as the prime on the integral indicates, there is only one general direction for $\vec{t}_n$, which is responsible for the factor $1/2$. Similarly we may expand the two sides in Eq. (40), which yields

$$\langle\theta_n^2\rangle \approx \frac{2b}{P}\,. \tag{455}$$

Putting (454) and (455) together and following the step from (65) to (66), Eq. (453) becomes

$$\frac{dQ_L(\vec{t}',\vec{t})}{dL} = \frac{1}{2P}\Delta_\Omega Q_L(\vec{t}',\vec{t}) - \beta\frac{u(\vec{t})}{b}Q_L(\vec{t}',\vec{t})\,, \tag{456}$$

where $L=nb$.

Since (456) is the equivalent of Eq. (66), we find

$$-\frac{\mu_o}{b}\psi_o(\vec{t}) = \frac{1}{2P}\Delta_\Omega\psi_o(\vec{t}) - \beta\frac{u(\vec{t})}{b}\psi_o(\vec{t}) \tag{457}$$

and

$$\frac{\Delta F_{orient}}{Lk_BT} \approx \frac{1}{b}\mu_o\,. \tag{458}$$

Hence the conformational entropy becomes

$$\frac{\Delta S_{orient}}{k_B} = \frac{\Delta E_{orient}}{k_BT} - \frac{\Delta F_{orient}}{k_BT} = \frac{L}{b}\int\frac{d\Omega}{4\pi}f(\vec{t})\beta u(\vec{t}) - \frac{L}{b}\mu_o\,. \tag{459}$$

Note that $f(\vec{t})$ is the orientation probability distribution of the $\vec{t}$. It plays the role of $c(x)$ in Eq. (71) and thus $f(\vec{t})=\psi_o^2(\vec{t})$. If we use this in conjunction with Eq. (457), the conformational entropy becomes

$$\frac{\Delta S_{orient}}{k_B} = \frac{L}{2P}\int\frac{d\Omega}{4\pi}\psi_o(\vec{t})\Delta_\Omega\psi_o(\vec{t})\,. \tag{460}$$

Our worms possess a cylindrical cross section and thus $f(\vec{t}) = f(\theta)$. Hence

$$\frac{\Delta S_{orient}}{k_B} = \frac{L}{2P}\int\frac{d\theta}{2}\psi_o(\theta)\partial_\theta\sin\theta\partial\theta\psi_o(\theta) \tag{461}$$

$$\stackrel{p.i.}{=} -\frac{L}{2P}\int\frac{d\Omega}{4\pi}\left(\partial_\theta\psi_o(\theta)\right)^2\,,$$

where p.i. stand for 'partial integration'. We obtain ΔS_{orient} in its final form by replacing $\psi(\theta)$ with $\sqrt{f(\theta)}$, i.e.

$$\frac{\Delta S_{orient}}{k_B} = -\frac{L}{8P}\int\frac{d\Omega}{4\pi}\left[\partial_\theta f(\theta)\right]\left[\partial_\theta\ln f(\theta)\right]\,. \tag{462}$$

There is another limit, which is of interest here. In this limit $P\gg L$, which means that the worms essentially are rigid cylinders. What is ΔS_{orient} in this limit? The classical partition function of an N-point particle gas contains a factor $N!^{-1}$, which accounts for the indistinguishability of the particles. If the particles come in groups i $(=1,2,\dots)$ and if only the N_i particles belonging to the same group are indistinguishable, then this factor becomes $\Pi_iN_i!^{-1}$ instead, where $\sum_iN_i=N$.

Here the particles in group i are the cylinders whose axes lie within the solid angle $d\Omega_i$ and $N_i/N=f(\theta_i)$. With this we find

$$\ln\Pi_iN_i!^{-1} = N\sum_i\left(-\frac{N_i}{N}\ln\frac{N_i}{N}+\frac{N_i}{N}\right) - N\ln N \tag{463}$$

$$= -N\int\frac{d\Omega}{4\pi}f(\theta)\ln f(\theta) - N\ln N + N\,.$$

Note that we have made use of Stirling's formula (141). Obviously, the integral accounts for the entropy tied to the orientation distribution of the particles, i.e. the cylinders. Specifically,

$$\frac{\Delta S_{orient}}{k_B} = -\int\frac{d\Omega}{4\pi}f(\theta)\ln f(\theta) \tag{464}$$

is the equivalent to (462) in this limit.

A formula for the orientation entropy joining the two limits (462) and (464) was derived by Khokhlov and Semenov (A. N. Semenov and A. R. Khokhlov *Statistical physics of liquid-crystalline polymers.* Sov. Phys. Usp. *31* 988 (1988)) based on work by I. M. Lifshitz (see also R. Hentschke *Equation of State for Persistent-Flexible Liquid-Crystal Polymers. Comparison with Poly(γ-benzyl-L-glutamate) in Dimethylformamide.* Macromolecules *23*, 1192 (1990)). For the purpose of this section, however, the limiting expressions (462) and (464) are sufficient.

In order to be able to find out whether there is a phase transition from an isotropic to a nematic phase, we need to derive the entire free energy for the system. In particular we need to include the interaction between the polymers. For this purpose we return to the first and prototypical calculation of this type carried out by Lars Onsager (*The Effects of Shape on the interaction of Colloidal Particles.*, Ann. N.Y. Acad. Sci. *51*, 988 (1949)). Onsager's free energy for hard rigid cylinders has the form

$$\frac{F}{Nk_BT} = \frac{\mu_o}{k_BT} + \sigma(f) + \ln\rho - 1 + x\phi\,g(f)\,. \tag{465}$$

The first term lumps together all contributions to the free energy which do not depend on the orientation and/or concentration of the rodlike particles. $\sigma(f)$ is simply $-\Delta S_{orient}/k_B$ in Eq. (464). In the next term, $\rho=N/V$ is the number density of cylinders. In the last term $x=L/D$, the length of the cylinder divided by its diameter, and $\phi=xb$, where b is the volume of a cylinder. This term, which corresponds to the second order in a virial expansion,

is the excluded volume between the cylinders. The function $g(f)$ is given by

$$g(f) = 64\pi \int\int \frac{d\Omega}{4\pi}\frac{d\Omega'}{4\pi} f(\theta) f(\theta') |\sin(\Omega - \Omega')| \,, \qquad (466)$$

where $\Omega - \Omega'$ denotes the angle between the axes of two interacting cylinders. Note that $DL^2|\sin(\Omega-\Omega')|$ is the volume which one cylinder excludes to the center of mass of the other (remember the geometrical meaning of the cross product between to vectors). Onsager did his calculation for spherocylinders, i.e. cylinders with hemispherical endcaps, in order to avoid the complexity of the 'naked' cylinder ends.

It is useful to describe $f(\theta)$ via a trial function, which is close to the expected shape of the true orientation distribution function. Onsager choses

$$f(\theta) = \frac{\alpha}{\sinh(\alpha)} \cosh(\alpha \cos\theta) \,. \qquad (467)$$

Note that this orientation distribution is equal to one if $\alpha = 0$, which is the isotropic situation. In the nematic case it exhibits two maxima at $\theta = 0$ and $\theta = \pi$, respectively. Using this trial function we obtain for $\sigma(f)$

$$\sigma(f) = \begin{cases} 0 & \alpha = 0 & \\ \ln\alpha - 1 & \alpha \to \infty & (P \gg L) \\ \frac{L}{4P}(\alpha - 1) & \alpha \to \infty & (P \ll L) \end{cases} \,. \qquad (468)$$

Note that we still concentrate on the limit $P \gg L$, even though here we have added $\sigma(f)$ in the opposite limit for later use! In addition, Onsager obtains an analytic solution of the interaction integral for which it is straightforward to also write down the limiting expressions:

$$g(f) = \frac{2I_2(2\alpha)}{\sinh^2\alpha} = \begin{cases} 1 & \alpha = 0 \\ 4(\pi\alpha)^{-1/2} & \alpha \to \infty \end{cases} \,. \qquad (469)$$

Here I_2 is a modified Bessel function (e.g. M. Abramowitz, I. A. Stegun *Handbook of Mathematical Functions.* Dover:New York (1972); section 9.6).

In a potential anisotropic phase (index a) the parameter α must satisfy $dF_a/d\alpha = 0$, which yields

$$\alpha_a = \frac{4}{\pi} x^2 \phi_a^2 \,. \qquad (470)$$

The coexisting volume fractions ϕ_i and ϕ_a along an isotropic to anisotropic (nematic) phase boundary follow from the conditions that the osmotic pressure

$$\Pi = -\frac{dF}{dV} = k_B T b^{-1} \phi \left(1 + x\phi g(f)\right) \qquad (471)$$

and the chemical potential

$$\mu = \frac{dF}{dN} = \mu_o + k_B T \left(\sigma(f) + \ln(\phi/b) + 2x\phi g(f)\right) \qquad (472)$$

of the rods are the same on the two sides of the transition. Setting $\Pi_i = \Pi_a$ and $\mu_i = \mu_a$ leads to

$$\phi_i'(1 + \phi_i') = 3\phi_a' \qquad (473)$$

$$\ln\phi_i' + 2\phi_i' = 3\ln\phi_a' + 3 + \ln(4/\pi) \,, \qquad (474)$$

where $\phi_i' = x\phi_i$ and $\phi_a' = x\phi_a$. These equations possess the stable solution

$$\phi_i \approx 3.45\frac{D}{L} \quad , \quad \phi_a \approx 5.12\frac{D}{L} \quad \text{, and} \quad \alpha_a \approx 33 \qquad (475)$$

(the exact numerical values of the numbers multiplying D/L are 3.29 and 4.19, respectively). Note that the large value of α_a justifies the assumption of large α in the anisotropic phase.

Ordinarily, the second virial approximation of the particle-particle interaction is not sufficient for this type of calculation. Here, however, we assume that x is so large that both ϕ_i and ϕ_a are sufficiently small to permit the use of the second virial approximation with reasonable accuracy. The experimental system which Onsager originally had in mind is tobacco mosaic virus (TMV). TMV is a highly elongated, stiff virus particle 300nm in length and 18 nm wide ($x \approx 17$) composed of over 2000 protein segments. Fig. 103 shows a electron micrograph image of TMV.

Perhaps it is worth noting that Onsager's inspiration most likely did not come from possible industrial applications of liquid crystalline polymers - this type of research gained traction later in the 1960s with the advent of liquid crystal display technology and high strength polymer fibers. He was interested in the physics of phase transitions in general.

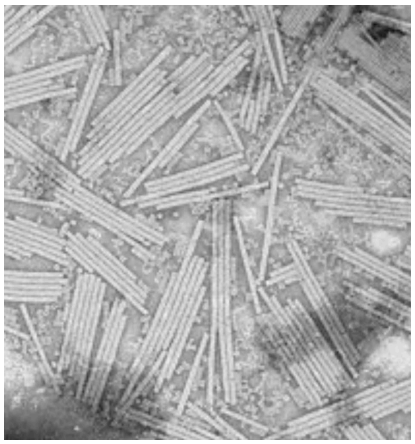

Fig. 103 Electron micrograph of TMV.

Let's look what happens if we consider the other limit, i.e. $L \gg P$. The free energy we use in his case is again (466) with $\sigma(f)$ now being the second expression in Eq. (468)

$$\frac{F}{Nk_BT} = \frac{\mu_o}{k_BT} + \frac{L}{P}\frac{\alpha-1}{4} + \ln(\rho_p/b_p) - 1 + \frac{L}{P} x\,\phi_p\, g(f)\,, \quad (476)$$

where $b_p = \frac{\pi}{4}D^2P$ and $\phi_p = b_p\rho$. We want to study the limit $L/P \to \infty$ and this form of the free energy highlights the dominant terms in this limit. In addition we assume that the excluded volume interaction remains what it was before. This is not really correct, but the approximation has proven to be useful. As before we minimize the free energy with respect to α and work out the osmotic pressure as well as the chemical potential. This yields

$$-\frac{1}{4} = \tilde{\phi}_a\, g'(\alpha_a) \quad (477)$$

$$\tilde{\phi}_i^2 = \tilde{\phi}_a^2\, g(\alpha_a) \quad (478)$$

$$\tilde{\phi}_i = \tilde{\phi}_a\, g(\alpha_a) + \frac{\alpha_a - 1}{8}\,, \quad (479)$$

with $\tilde{\phi} = \frac{P}{D}\phi$, $g(\alpha) = 4/\sqrt{\pi\alpha}$ and $g'(\alpha) = -2/\sqrt{\pi\alpha^3}$. This time the numerical solution is

$$\phi_i \approx 7.12\frac{D}{P} \quad , \quad \phi_a \approx 8.75\frac{D}{P} \quad \text{and} \quad \alpha_a \approx 11.6\,. \quad (480)$$

The value we find for α_a is not very large, which means that our solution is not accurate. We also need $D \ll P$ in order for the transition to occur at sufficiently small volume fractions. However, here we are interested in the qualitative picture only. Most importantly we learn that the coexistence is shifted to higher volume fractions with increasing flexibility, i.e. smaller persistence length.

Figure 104 is an application of what we have discussed thus far. The osmotic pressure data were obtained for PBLG in an organic solvent - dimethylformamide (DMF). The dashed line is Onsager's theory as we have discussed it except for one difference. Here the authors have not used the approximations for large α. Instead they compute the free energy, the osmotic pressure as well as the chemical potential numerically, but nevertheless based on the above trail function. The solid line, which is a much better fit to the data, includes the flexibility of PBLG. Again the authors do not use the limiting forms of $\sigma(f)$. Instead they use the aforementioned interpolation formula, which approximates $\sigma(f)$ for arbitrary L/P. Here the persistence length ($P \approx 200$ nm) is an adjustable parameter.

In addition to the isotropic-to-nematic transition, the figure also includes a third phase, i.e. a columnar phase. Avoiding all details, which can be found in R. Hentschke, J. Herzfeld *Isotropic, nematic, and columnar ordering in systems of persistent flexible hard rods*. Phys. Rev. A *44*, 1148 (1991), the underlying idea is quite straightforward. In a columnar phase, the part of the free energy modelling the excluded volume interaction is assumed to be the sum of two terms, i.e.

$$F_{ex.vol.}(\Delta) = F^{1D}_{fluid}(\Delta) + F^{2D}_{crystal}(\Delta)\,. \quad (481)$$

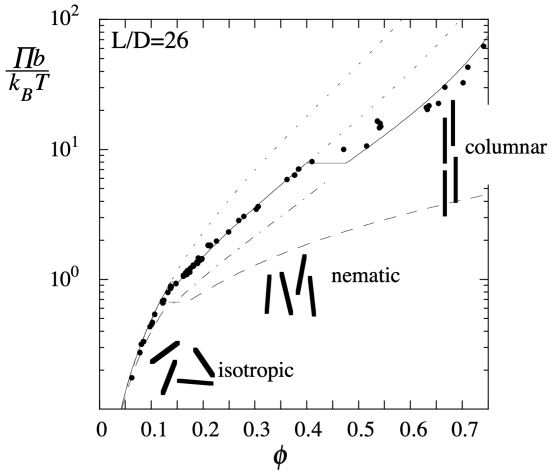

Fig. 104 Experimental and theoretical reduced osmotic pressure of PBLG in DMF vs. solute volume fraction. This is Fig. 3 from R. Hentschke, B. Fodi *Theory of the Supramolecular Liquid Crystal* (Chapter 2 in *Supramolecular Polymers* (Marcel Dekker:New York) edited by A. Ciferri (2000)). Here b is the molecular volume. Solid line: Theory based on the Khokhlov-Semenov approach to flexibility in combination with the decoupling approximation and the dimensional separation approach based on Eq. (8) in R. Hentschke, J. Herzfeld. Phys. Rev. A *44*, 1148 (1991). Upper dotted line: Extension of the isotropic branch. Lower dotted line: Extension of the nematic branch. Dashed-dotted line: Result for completely rigid molecules. Dashed line: Onsager's 2nd virial coefficient-approximation for rigid rods.

$F^{1D}_{fluid}(\Delta)$ is the excluded volume part of the free energy of a one-dimensional hard body fluid. $F^{2D}_{crystal}(\Delta)$ is the analogous part of the free energy of a two-dimensional system of hard disks exhibiting hexagonal ordering. Here $F^{1D}_{fluid}(\Delta)$ is realized via the so-called *scaled particle theory* (see for instance R. Hentschke *Thermodynamics* (2nd ed.)), whereas $F^{2D}_{crystal}(\Delta)$ is realized using a cell model (see for instance J. O. Hirschfelder, C. F. Curtiss, R. B. Bird *Molecular Theory of Gases and Liquids*. John Wiley & Sons:New York (1954)). What combines these two expressions into the three-dimensional $F_{ex.vol.}(\Delta)$ is the quantity Δ. This quantity is depicted in Fig. 105. It is the width of a tube to which the polymer is confined. Viewed along the direction of the polymer backbone, it is the width of the aforementioned 2D cell (a hexagon in this particular case). Note that the 3D polymer volume fraction ϕ therefore is a unique function of Δ as well. Note also that Δ in conjunction ϕ determines the 1D polymer volume fraction in $F^{1D}_{fluid}(\Delta)$, i.e. this is why F^{1D}_{fluid} also depends on Δ. For any fixed value of ϕ the most stable free energy is found via minimization of the 3D free energy with respect to Δ.

If the polymer is flexible, then there also exists a relation between Δ and α. According to Fig. 105 the polymer contour winds its way along the tube and is defected by the tube's wall every so often. The mean distance between successive deflections is λ, which is called the **deflection length** (a term originally coined by T. Odijk). Based on this picture we construct a relation between Δ and λ via

$$\Delta - D \sim \int_0^{\lambda} \langle \theta(s)^2 \rangle^{1/2} ds \sim \frac{\lambda^{3/2}}{P^{1/2}} \,, \tag{482}$$

where we use $\langle \theta(s)^2 \rangle \sim s/P$ according to $\langle \vec{t}(0) \cdot \vec{t}(s) \rangle = \langle \cos \theta(s) \rangle \approx 1 + \frac{1}{2} \langle \theta(s)^2 \rangle \approx 1 + s/P$. Similarly we make use of $\langle \theta^2(\lambda) \rangle \sim \lambda/P$ and $\langle \theta^2(\lambda) \rangle \sim \alpha^{-1}$, i.e.

$$\lambda \sim \frac{P}{\alpha} \,. \tag{483}$$

Putting everything together we have

$$\alpha = \kappa [P/(\Delta - D]^{2/3} \,, \tag{484}$$

where $\kappa = O(1)$ is an undetermined (and thus adjustable) proportionality constant.

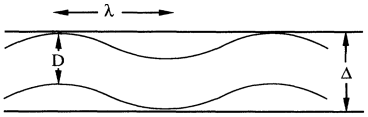

Fig. 105 Cartoon of a persistent flexible polymer inside a tube of diameter Δ. The quantity D is the diameter of the polymer and λ is the so-called deflection length explained in the text. This is Fig. 1 from R. Hentschke, J. Herzfeld. Phys. Rev. A *44*, 1148 (1991).

Figure 106 shows the phase behavior of persistent flexible polymer with hard-body excluded volume interactions as a result of this theory. Independent of the value of κ, the general phase behavior is the following. Stiff polymers undergo a transition from isotropic (I) to nematic (N) at a volume fraction determined by their aspect ratio, i.e. the larger L/D becomes the smaller ϕ_i and ϕ_a will be. At significantly higher volume fractions a transition into a columnar (C) phase occurs. With increasing flexibility the transition from I to N is postponed to larger ϕ until finally the nematic phase is squeezed out between the I and C phases.

It is important to note that this theoretical approach to translational ordering, intuitive though it is, has one significant drawback. Since the free energies of these orderings are constructed as separate branches, the resulting transition will always be a first order transition even if the true transition is not first order.

Thus far we have dealt with hard-body or athermal interactions between rod-like flexible polymers. A rich and different phase behavior is encountered for soft interactions. Fig. 107 shows an example taken from the book by Grossberg and Khokhlov. Here the interaction between the rod-like molecules, possessing a small aspect ratio, is attractive. The resulting phase diagram resembles the gas-liquid-solid phase diagram of a simple liquid, except that the narrow phase coexistence separates an isotropic fluid from a nematic liquid at fairly high volume fraction. When the aspect ratio is large, a similar phase diagram is obtained. In this case the narrow phase coexistence funnel appears at low volume fractions. In addition, the one phase region bracketed between the critical temperature T_{cr} and the triple point temperature T_t as well as between the funnel and the broad coexistence region is

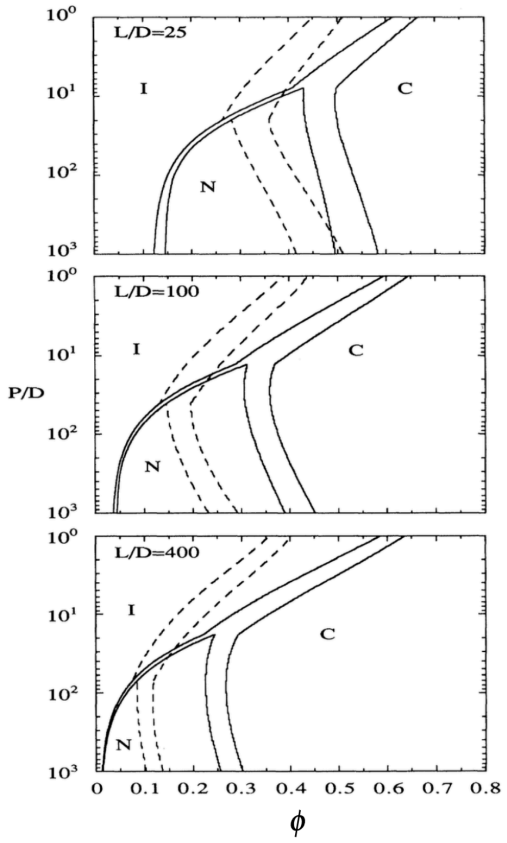

Fig. 106 Phase diagrams for persistent flexible polymers for three different axial ratios and continuously variable persistence length. Solid lines: $\kappa = 3.5$; dashed lines $\kappa = 2.5$. This is Fig. 2 from R. Hentschke, J. Herzfeld. Phys. Rev. A *44*, 1148 (1991).

not an isotropic fluid as before but a nematic - albeit less ordered than the nematic phase on the far side of the funnel. What is not shown here, but is discussed in the aforementioned book, is what happens to this phase diagram in the crossover region between small and large aspect ratios or what happens as function of the persistence length.

All in all the above is only a very small fraction of what has been studied. Important aspects include not only different types of interactions but also polydispersity, molecular shape, or, more generally, molecular architecture (e.g. instead of the macromolecular contour, on which we have concentrated here, much smaller side groups tethered to the backbone may be the actual mesogens causing liquid crystalline ordering). Since this is not the place for an in depth discussion, a few references must suffice. Early but nonetheless valuable references include T. Odijk *Theory of Lyotropic Polymer Liquid Crystals.* Macromolecules *19*, 2313 (1986), G. J. Vroege, H. N. W. Lekkerkerker *Phase transitions in lyotropic colloidal and polymer liquid crystals* Rep. Prog. Phys. *55*, 1241 (1992), and H. N. W. Lekkerkerker, G. J. Vroege. *Lyotropic Colloidal and Macromolecular Liquid Crystals.* Philosophical Transactions: Physical Sciences and Engineering *344*, 419 (1993). A comprehensive discussion of the subject can be found in A. M. Donald, A. H. Windle, S. Hanna *Liquid Crystalline Polymers* Cambridge University Press:Cambridge (2005). Quite recently there

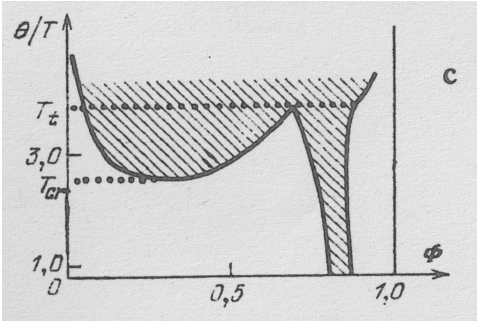

Fig. 107 Theoretical phase diagram, inverse reduced temperature vs. polymer volume fraction, of a liquid crystalline solution of rod-like polymers with a short aspect ratio. θ is the θ-temperature. The shaded region indicates phase coexistence. Excerpt from Fig. 5.4 in the book by Grossberg and Khokhlov.

is renewed interest from the computer simulation community in this subject. See for example K. Binder, S. A. Egorov, A. Milchev, A. Nikoubashman *Understanding the properties of liquid-crystalline polymers by computational modeling.* J. Phys. Mater. *3* 032008 (2020) and references therein.

We have not yet mentioned any applications of liquid crystalline polymers. Here are a few: ropes & cables, electronic support structures, recreation & leisure industry aerospace & military, new textiles, industrial applications. One material property of particular importance is tensile strength (which can easily surpass that of steel). Tensile strength is greatly enhanced if one succeeds in aligning the polymer backbones in the direction of the force (Kevlar perhaps is the best-known example). This is the principle underlying the high strength polymer fibers can exhibit. When such fibers are spun from the melt or a solution, the flow field in the nozzle already tends to promote alignment of the stiff backbones. Subsequently the fiber is stretched. Again, the crowding of the backbones enhances alignment. Since the molecules are highly stretched, the elongation of such a fiber at break is only a few percent. The amount of stretching is described by the so-called spin stretch factor. While these industrial manufacturing processes are complicated in detail, theoretical concepts like the ones just outlined help to understand and optimize them. It is worth noting that the resulting high strength fibers are highly anisotropic, which has an important consequence. While the tensile strength is greatly enhanced by molecular alignment, the compressive strength suffers significantly, i.e. the fiber's shear modulus is small. The tensile strength of a high strength fiber tied into a knot therefore is very much reduced. An informative reference in this context is I. M. Ward (Ed.) *Structure and Properties of Oriented Polymers.* Springer:Dordrecht (1997).

Reversibly Assembling Liquid Crystalline Polymers:

Thus far we have considered systems possessing a stable mesogenic unit, i.e. the mesogen itself does not change, e.g. as a function of concentration. This is quite different in so-called self-assembling systems, where the molecules form labile supramolecular structures above a critical concentration (the **critical micelle concentration** or CMC). Here, labile means that these structures are generally not held together by covalent bonds, but by much weaker van der Waals, hydrophobic, hydrogen bridge or electrostatic interactions, so that they can break down and rebuild. Such structures appear, for example, as spheres or cylinders (compact forms are usually referred to as micelles), as lamellar bilayers or as complex sponge-like structures (see for instance J. Israelachvili *Intermolecular and Surface Forces.* Academic: New York (1992); D. F. Evans, H. Wennerstrom *The Colloidal Domain.* VCH Publishers:Weinheim (1994)). Which structures are observed, or whether the existing supramolecular structure transforms into a different new supramolecular structure, depends in detail on many variables in addition to the concentration, such as the temperature, the composition (in multicomponent systems), the ionic strength, etc. In the following we shall focus on reversibly aggregating amphiphilic systems, forming simple compact shapes that can be described as flexible rods. Note that **amphiphiles** are bi-polar molecules, such as surfactants or lipids, which have a hydrophobic and a hydrophilic part, so that in aqueous solution there is a tendency for the hydrophobic parts to combine (as far as sterically possible) in order to reduce the unfavorable interaction with water as much as possible ('hydrophopic effect').

In the case of shape-anisotropic aggregates one can imagine that the excluded-volume interaction of the aggregates may lead to the formation of liquid crystalline mesophases. And indeed, many self-aggregating amphiphilic systems exhibit mesophases characterized by different, e.g. nematic, smectic, columnar, or crystalline, ordering of their aggregates (M. P. Taylor, J. Herzfeld, J. Phys.: Condens. Matter *5*, 2651 (1993)). However, since the underlying mesogen is no longer a stable unit, there is an interesting coupling tying the variability of the mesogen to the phase behavior. Before we progress further along this direction, it is useful to summarize the basic picture of micellar assembly.

Figure 108 is a sketch of amphiphilic molecules reversibly assembling into spherical micelles. Here the head groups, shown as filled black circles, preferentially mix with water, whereas the tails, depicted as zigzag-lines, do not like to mix with water. This leads to a clustering of the zigzag tails into droplets shielded on the outside by the head groups. Clearly, we are interested in aggregation leading to aggregates with a pronounced shape anisotropy, because we want to study the type of liquid crystalline ordering which we have discussed in the preceding section. Nevertheless, the following thermodynamic considerations apply independent of the aggregate shape.

The starting point is the reaction equilibrium

$$sA_1 \rightleftharpoons A_s \,. \tag{485}$$

A_s denotes a s-aggregate containing s monomers A_1. In terms of the chemical potential we have

$$s\mu_1 = \mu_s \,. \tag{486}$$

Assuming that the solute concentration is low, this can be ex-

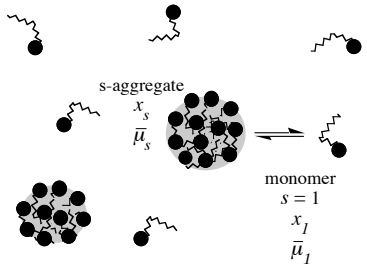

Fig. 108 Illustration of the reversible assembly of amphiphilic molecules. Here the aggregates are spherical micelles. This is Fig. 3.12 from R. Hentschke *Thermodynamics* (2nd ed.) Springer:Heidelberg (2022).

pressed as

$$s\bar{\mu}_1 + sRT\ln x_1 = \bar{\mu}_s + RT\ln(x_s/s)\,. \tag{487}$$

Note that the quantity x_s/s is the mole fraction s-aggregates and therefore x_s is the mole fraction of monomers in s-aggregates. Solving (487) for x_s yields

$$x_s = s\,(x_1 e^{\alpha})^s\,, \tag{488}$$

where

$$\alpha = \frac{1}{RT}\left(\bar{\mu}_1 - \frac{1}{s}\bar{\mu}_s\right)\,. \tag{489}$$

Eq. (488) has an interesting consequence. Note that the total monomer mole fraction is given by

$$x = x_1 + \sum_{s=m}^{\infty} x_s\,. \tag{490}$$

Here x_1 is the mole fraction of the free monomers, whereas the sum is equal to the mole fraction contributed by the monomers bound in aggregates. The quantity m is a minimum aggregate size. For spherical micelles it results form the requirement that a certain number of head groups are needed to form a closed surface. This number may be large - say $m \approx 50$ - depending of course on the type of monomer. But $m = 2$ is also possible, for instance in the case of stacking amphiphiles forming rod-like aggregates (see for example N. Boden in Micelles, Membranes, Microemulsions, and Monolayers (W. M. Gelbart, A. Ben-Shaul, D. Roux; Eds.) Springer-Verlag:Heidelberg (1994)). Since $x \leq 1$, the right side of Eq. (490) is bounded. This implies that $x_1 e^{\alpha} < 1$, because the sum $\sum_{s=m}^{\infty} sq^s$ diverges at $q = 1$ (geometric series!). Hence,

$$x_{CMC} = e^{-\alpha} \tag{491}$$

defines a threshold mole fraction, which the free monomers cannot exceed. Instead they condense into aggregates if the overall solute mole fraction increases beyond x_{CMC}. The corresponding concentration is called *critical micelle concentration* (CMC) or, more generally, *critical aggregate concentration*. The sharpness of this condensation transition is governed by the size of m, i.e. increasing m sharpens the onset of aggregate formation.

Let's conclude this discussion by studying the dependence of the size $\langle s\rangle$ of linear aggregates, i.e. $m = 2$, on the overall solute mole fraction x. This requires a model for $\bar{\mu}_s$. A simple one is

$$\bar{\mu}_s = s\bar{\mu}_1 - RT\alpha_o(s-1)\,. \tag{492}$$

The quantity $-RT\alpha_o$ is a contact free enthalpy for each of the $s-1$ contacts between neighboring monomers in s-aggregates. With this we have $\alpha = \alpha_o(s-1)/s$. It is straightforward to work out

$$\langle s\rangle = \frac{\sum_{s=1}^{\infty} sx_s}{\sum_{s=1}^{\infty} x_s} = \frac{1+q}{1-q} \quad \text{and} \quad x = \sum_{s=1}^{\infty} x_s = e^{-\alpha_o}\frac{q}{(1-q)^2}\,, \tag{493}$$

where $q = x_1 e^{\alpha_o}$. Solving the left equation for q and inserting the result into the right equation yields

$$\langle s\rangle = \sqrt{1+4e^{\alpha_o}x}\,. \tag{494}$$

This tells us that the mean aggregate size increases proportional to $\sqrt{x}$ for sufficiently large $\langle s\rangle$. This aggregate growth in the ideal system is enhanced when the aggregates interact (W. M. Gelbart and A. Ben-Shaul in Micelles, Membranes, Microemulsions, and Monolayers (W. M. Gelbart, A. Ben-Shaul, D. Roux; Eds.) Springer-Verlag:Heidelberg (1994)).

Theoretical studies of the statistical mechanics of reversibly aggregating systems can be divided roughly into three groups. The first mainly comprises the formation of the isolated micelles and their internal structure at low concentrations (just above the CMC), so that the interaction of the aggregates can be neglected. The second comprises the phase theory of more (than two) component systems (microemulsions) by means of mostly lattice or field theoretical models (see e.g. B. Widom, K. A. Dawson, M. D. Lipkin, In Statistical Physics: Invited lectures from STATPHYS 16; H. E. Stanley, Ed.; North-Holland: Amsterdam, (1986); p. 26.). The third group, which is the subject here, involves the study of the liquid crystalline behavior of the labile polydisperse aggregate population at higher solute concentrations by means of a synthesis of the excluded-volume models discussed above with phenomenological descriptions of the amphiphilic interactions (cf. M. P. Taylor, J. Herzfeld, J. Phys.: Condens. Matter *5*, 2651 (1993)).

In the following we consider the above case of linear rigid aggregates consisting of strung together monomers. A simple expression for the change in free energy during the transition from the isotropic to the nematic phase in such a system is given by

$$\frac{F}{Vk_BT} = \sum_{s=1}^{\infty}\int\frac{d\Omega}{4\pi}f(s,\theta)\ln f(s,\theta) + \frac{1}{2}\sum_{s,s'=1}^{\infty}\int\int\frac{d\Omega}{4\pi}\frac{d\Omega'}{4\pi}f(s,\theta)f(s',\theta')b^{ex}(s,s',\Omega-\Omega') + \tilde{f}^{trans/rot}+\tilde{f}^{aggregate}. \quad (495)$$

This is a generalization of Eq. (465). The generalization is that the population of rods or aggregates is variable polydisperse, i.e. $\rho f(\theta) \to \sum_{s=1}^{\infty} f(s,\theta)$. Here $f(s,\theta)$ is the number of aggregates consisting of s monomers with orientation θ in the volume V. ρ is the aggregate number density. The $g(f)$-term in Eq. (465) is replaced by the b^{ex}-term. As in the Onsager model, the aggregates are absolutely stiff, hard rods, whose interaction is again only taken into account up to and including the 2nd virial coefficient. $\tilde{f}^{trans/rot}$ stands for the translational free energy term, which in Eq. (465) merely is $\ln\rho - 1$, including the equivalent of $\mu_o/(k_BT)$ accounting for the vibrational and rotational degrees of freedom. These contributions appear because, unlike in the case of inert rods, the length distribution of the aggregates in the isotropic and in the nematic phase is different. Originally, these terms were considered important to prevent 'catastrophic' growth of the aggregates in the nematic phase. It is now known that this unphysical growth is prevented if the flexibility (T. Odijk J. Physique *48*, 125 (1987); R. Hentschke Liquid Crystals *10*, 691 (1991); P. van der Schoot, M. E. Cates Europhysics Letters *25*, 515 (1994)) or a short-range soft repulsion (R. Hentschke, J. Herzfeld J. Chem. Phys. *91*, 7308 (1989)) is taken into account in addition to the hard-body repulsion. The last term is an internal free energy of the aggregates, the simplest description of which is a negative temperature-dependent free energy per monomer-monomer contact $-k_BT\Phi(T)$, i.e.

$$\tilde{f}^{aggregate} = -\Phi(T)\sum_{n=1}^{\infty}\int\frac{d\Omega}{4\pi}f(s,\theta)(s-1) \quad (496)$$

(cf. Eq. 492). If one wishes to be more precise, or if one is dealing with more complicated aggregates, this expression must of course be modified accordingly, and $\Phi(T)$ is not only a function of T but also a function of, for example, the monomer position within the aggregate and/or the local curvature of the aggregate (or micelle) surface, as well as the surrounding solvent, etc. However, let's refrain from a more detailed discussion, because the exact treatment of these terms in this context is quite subtle.

Equation (495) is solved as soon as the distribution function $f(s,\theta)$ is known. Using the equilibrium condition $\mu_s = s\mu_1$, where $\mu_s = \partial(\Delta F/V)/\partial f(s,\theta)|_{V,T,f(s',\theta')}$ is the chemical potential of an aggregate of s monomers with orientation θ, it follows that

$$f(s,\theta) = \left(f(1,\theta)e^{\Phi-\chi(s)/s}\right)^n e^{-(\Phi-\chi(1))}. \quad (497)$$

The function $\chi(s) = 2\pi\sum_{s'=1}^{\infty}\int\frac{d\Omega'}{4\pi}f(s',\theta')b^{ex}(s,s',\Omega-\Omega') + \partial(\tilde{f}^{trans/rot}+\tilde{f}^{aggregate})/\partial f(s,\theta)|_{V,T,f(s',\theta')}$ is the contribution of the external interaction as well as the various degrees of freedom mentioned above. For general s, Eq. (497) must be solved numerically. However, if we first assume that $\chi(s)$ is negligible (for the external interaction this is the case for low amphiphile concentrations), then with the help of the additional condition $\phi = b_1\sum_{s=1}^{\infty}\int\frac{d\Omega}{4\pi}sf(s,\theta)$, where b_1 is the monomer volume, we can easily calculate the mean aggregation number $\langle s\rangle$ as a function of the amphiphile volume fraction ϕ, i.e.

$$\langle s\rangle \sim \left(\phi e^{\Phi}\right)^{1/2} \quad (498)$$

(cf. Eq. (494).

Analogous to the Onsager model, this model can also be extended to isotropic-nematic phase behavior of linear aggregates at higher concentrations, including flexibility of the aggregates as well as soft interactions. Likewise, possible translationally-ordered phases can be included as well. Since these calculations are more complicated than for inert particles, we shall not go into details. A comprehensive discussion of the different approaches and an overview of the literature can be found in M. P. Taylor, J. Herzfeld J. Phys.: Condens. Matter *5*, 2651 (1993). Here a single example must suffice.

Figure 109 illustrates the molecular effects of sickle cell anaemia. Pauling, Itan and Ingram have shown that in this disease a genetic defect leads to a faulty amino acid sequence of the haemoglobin molecule and thus to the formation of a hydrophobic 'pocket'. Under certain conditions (low oxygen partial pressure), this leads to reversible aggregation of the hemoglobin molecules in the erythrocytes of sickle cell patients. The aggregates formed are stiff rods of approximately 180-240 Å in diameter, whereby the globular monomer has a size of approx. 60 Å. The aggregation and the associated nematic orientation of the aggregates (see Fig. 109 (bottom)) leads to sickle-shaped deformation of the erythrocytes (see Fig. 109 (middle)), making them rigid and thus hindering or preventing their capillary flow, i.e. oxygen transport. In addition, the erythrocyte membrane is often damaged (see Fig. 109 (bottom)). The theoretical description of this phenomenon via the osmotic equation of state, in particular across the isotropic-nematic transition, within the framework of an excluded volume theory is shown in Fig. 110.

6.4 Polyelectrolytes

• *Preliminaries*

Polyelectrolytes are water soluble polymers bearing dissociable groups along their contour. An example is poly(sodium styrene sulfonate) (PSS) shown in Fig. 111. PSS is a synthetic polyelectrolyte. However, many biological molecules are also polyelectrolytes. A famous example is DNA shown in Fig. 112. Polyelectrolytes combine the properties of both electrolytes (salts) and polymers. The following brief discussion of concepts important for the understanding of polyelectrolytes is preceded by an even briefer compilation of important concepts and quantities in the context of electrolyte solutions.

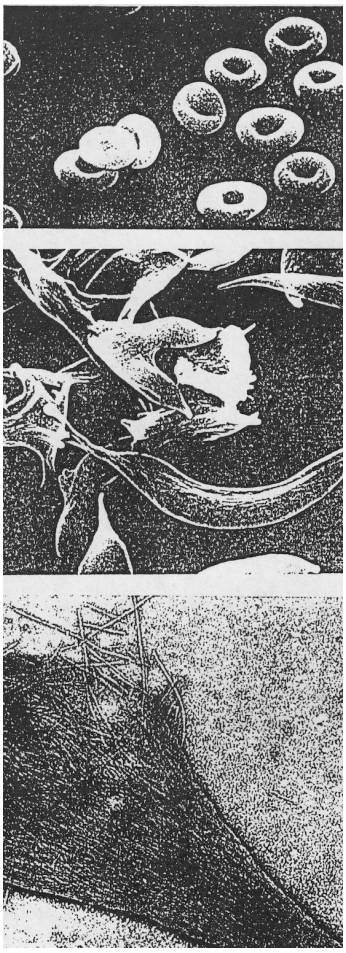

Fig. 109 Top: Image showing 'donut'-shaped normal red blood cells (size approximately 10 μm). Middle: Red blood cells of a sickle cell patient distorted by bundles of aggregated hemoglobin. Bottom: Close-up image of a burst red blood cell with protruding rod-like aggregates composed of globular HbS protein. Pictures reproduced from R. E. Dickerson, I. Geis *Hemoglobin* Bejamin (1983).

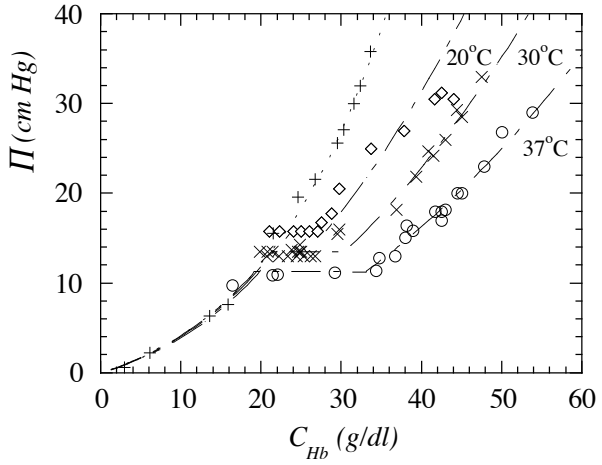

Fig. 110 Osmotic pressure vs. concentration for deoxygenated hemoglobin from R. Hentschke, J. Herzfeld Phys. Rev. A *43*, 7019 (1991). Symbols: experimental data for normal hemoglobin (plusses) and sickle hemoglobin (37°C (circles), 30°C (crosses), and 20°C (diamonds)). Dotted line: theoretical result for normal hemoglobin (T = 37°C). Dashed-dotted lines: theoretical fits for highly concentrated deoxygenated sickle cell hemoglobin.

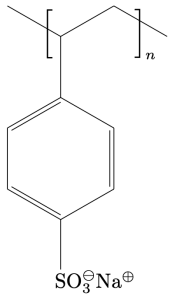

Fig. 111 Chemical structure of poly(sodium styrene sulfonate).

The standard theoretical starting point for the interaction of charges in an electrolyte solution is the **Debye-Hückel theory**. In this theory the potential of a charge q at point $\vec{r}$ from the charge is

$$\phi(\vec{r}) \approx \frac{q}{r}\exp[-r/\lambda_D]\,. \tag{499}$$

You can find the discussion of this formula, including the assumptions it involves, in every textbook on physical chemistry and statistical thermodynamics (e.g. R. Hentschke *Thermodynamics* (2nd ed.) Springer:Heidelberg (2022)). The spatial range of this interaction is determined by the Debye screening length

$$\lambda_D = \sqrt{\frac{k_B T}{8\pi e^2 I}}\,, \tag{500}$$

where e is the magnitude of the elementary charge and

$$I = \frac{1}{2}\sum_i c_i z_i\,. \tag{501}$$

is the **ionic strength**. The index i indicates the different types of charges present, c_i is the number concentration of these charges, and z_i is the charging of type i. For example, in the case of NaCl in aqueous solution we have Na^+ and Cl^- ions, i.e. $z_{Na} = +1$ and $z_{Cl} = -1$.

But how large is λ_D? First we note that the system of our current units requires the replacement of q and e by $e/\sqrt{4\pi\varepsilon_o\varepsilon_r}$ if we want to use SI-units. Here ε_r is the dielectric constant of the background medium containing the charges, e.g. ions in water (water: $\varepsilon_r = 78.3$ at $T = 298$ K and $P = 1$ bar). Thus we have

$$\lambda_D = 1.988\cdot 10^{-3}\sqrt{\frac{T\varepsilon_r}{I}}\ \text{nm} \quad \text{with } [T] = \text{K and } [c] = \text{mol/l}\,. \tag{502}$$

For example, in the case of a 0.1molar aqueous NaCl solution $\lambda_D = 0.96$ nm.

A related length is the **Bjerrum length** λ_B defined via

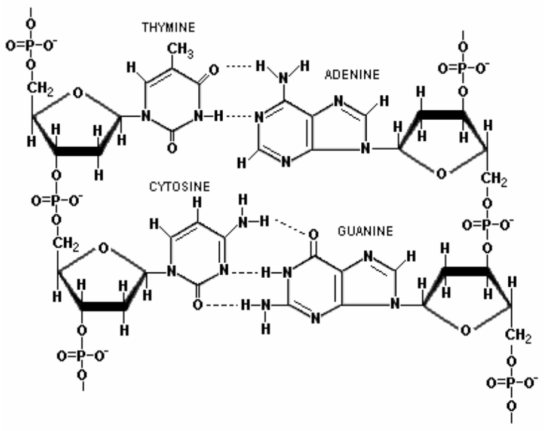

Fig. 112 Chemical structure of DNA. Note the proton dissociation in the phosphate groups.

$$\lambda_B = \frac{e^2}{k_B T} \,. \tag{503}$$

λ_B is the length at which the interaction of two charges of magnitude e is equal to the thermal energy $k_B T$. In water at $T = 298$ K we find $\lambda_B \approx 0.7$ nm.

A simple model picture of a polyelectrolyte, albeit without additional ions other than the counterions it supplies itself, is that of a (straight) line charge density of e per unit length l surrounded by counterions. The charge density is homogeneously distributed on a cylinder with radius r_0. The interaction of a counterion $-e$ at a distance r from the cylinder axis is $-e\Delta\phi_{cyl}(r) = 2e(e/l)\ln(r/r_o)$. Assuming that this is the only relevant interaction in the system and that the counterions are distributed between r_0 and a maximum distance r_1 from the central axis, we obtain the configuration free energy (without the $1/N!$-factor multiplying the partition function) per e and l in units of $k_B T$:

$$\begin{aligned} \beta F &= -\ln \int_{r_0}^{r_1} 2\pi r\, dr \exp[-2a\ln(r/r_o)] \qquad (504) \\ &= -\ln\left(\frac{\pi r_0^2 \left(1-(r_1/r_0)^{2-2a}\right)}{a-1} \right) \,, \end{aligned}$$

where $a \equiv \lambda_B/l$. Figure 113 depicts βF vs. a for $r_0 = 1$ and $r_1 = 10$ (dotted line), 10^3 (dashed line) and 10^5 (solid line). Obviously, if $a < 1$ or $\lambda_B < l$ the counterions and thereby the rod-like polyelectrolytes favour infinite dilution. For $a > 1$ or $\lambda_B > l$ this no longer is the case. This region is interpreted in terms of a **counterion condensation** occurring (also called **Manning condensation**). Even though this is a very much simplified picture it still provides interesting insight. Nevertheless, we do not want to dwell on this phenomenon. Instead the interested reader should consult the following publications: G. S. Manning *The critical onset of counterion condensation: A survey of its experimental and theoretical basis.* Ber. Bunsen. phys. Chem. *100*, 909 (1996); G. S. Manning *Counterion condensation theory of attraction between like charges in the absence of multivalent counterions.* Eur. Phys. J. E *34*, 132 (2011).

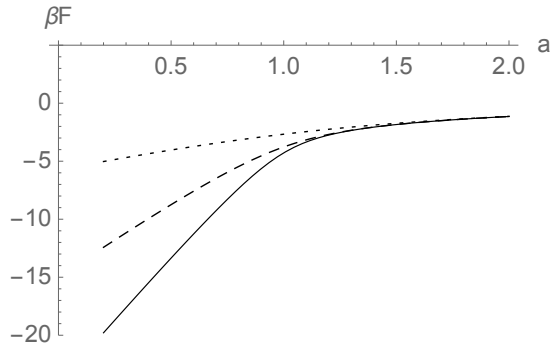

Fig. 113 βF vs. a for $r_0 = 1$ and $r_1 = 10$ (dotted line), 10^3 (dashed line) and 10^5 (solid line).

• *Electrostatic Persistence Length*

It appears natural that the 'stiffness' of a polyelectrolyte should depend on quantities like λ_D or λ_B. This question was addressed first by J. Skolnick, M. Fixman *Electrostatic Persistence Length of a Wormlike Polyelectrolyte.* Macromolecules *10*, 944 (1977) and T. Odijk *Polyelectrolytes near the Rod Limit* J. Poly. Sci.: Polymer Physics *15*, 477 (1977). Here we employ a simple two-dimensional model for stiff but nevertheless persistent flexible polyelectrolytes (e.g. DNA) to illustrate the main result. Figure 114 shows two charges q (in units of e) separated by a distance s along a circular contour. Their direct separation is x. Using $s = \varphi R$ and $(x/2)^2 + R^2\cos^2(\varphi/2) = R^2$ we obtain for small φ

$$s - x \approx \frac{R\varphi^3}{24} \,. \tag{505}$$

We want to compare the electrostatic interaction energy of the two charges in two cases: (i) $R = \infty$, i.e. the circular contour becomes a straight line and the distance between the charges is s; (ii) R is finite but still large, i.e the curvature is small so that (505) applies, and the distance between the charges is x. The result is

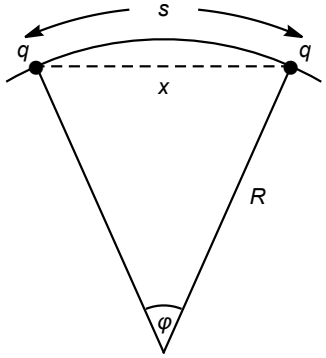

Fig. 114 Two charges q separated by a distance s along a circular contour.

$$q^2\left(\frac{1}{x}-\frac{1}{s}\right)\approx q^2\frac{s-x}{s^2}\sim\frac{q^2 s}{R^2}\,. \tag{506}$$

Next we assume a homogenous line density $1/b$ of charges along the contour screened by mobile countercharges surrounding them. The corresponding total energy difference per charge over the distance of one Debye screening length λ_D is

$$\sim\frac{1}{b}\int_0^{\lambda_D} ds\frac{q^2 s}{R^2}\sim\frac{q^2\lambda_D^2}{bR^2}\,. \tag{507}$$

Now we compare this result with the bending energy of a persistent flexible polymer in Eq. (531) of appendix B. Note that R^{-1} is the curvature and thus $R^{-2}=(\partial\vec{t}/\partial s)^2$. Hence we conclude, based on Eq. (539) also in appendix B, that the electrostatic bending stiffness is proportional to λ_D^2 and therefore

$$P_{el}\propto\frac{\lambda_B\lambda_D^2}{b^2} \tag{508}$$

(Odijk obtains the proportionality constant 1/4). Note that this is merely the electrostatic part of the total persistence length P_{tot}, i.e.

$$P_{tot}=P+P_{el}\,, \tag{509}$$

where P is the part of the total persistence length contributed not due to the above electrostatic repulsion but by other molecular interactions.

• *Forces Between Persistent Flexible Polyectrolytes in Translationally Ordered Phases*

Shape fluctuations of macromolecules have a profound effect on their interations at sufficiently elevated concentrations. Here we discuss the effect of flexibility, i.e. the effect of shape fluctuations, on the forces in hexagonally ordered DNA bundles. We shall discover that molecular flexibility leads to an effective increase of the range of the electrostatic forces.

Figure 115 shows experimental data from Podgornik et al. who have measured the repulsive force between hexagonally ordered DNA molecules in NaCl solutions under variable salt concentration as function of the perpendicular packing distance. Basically, the repulsive force decreases exponentially in two distinct regimes. At inter-helical separations less than about 30 Å the salt concentrations has no discernible effect. This is due mainly to the so called **hydration forces** - forces having to do with the structure of water layers surrounding the helix. These forces tend to be stronger than the electrostatic forces controlled by the salt concentration. This changes at larger distances where a clear concentration dependence can be observed. Here the forces decay faster when the salt concentration is larger. The question is whether or not we can construct a theory describing the force behavior in this large distance regime?

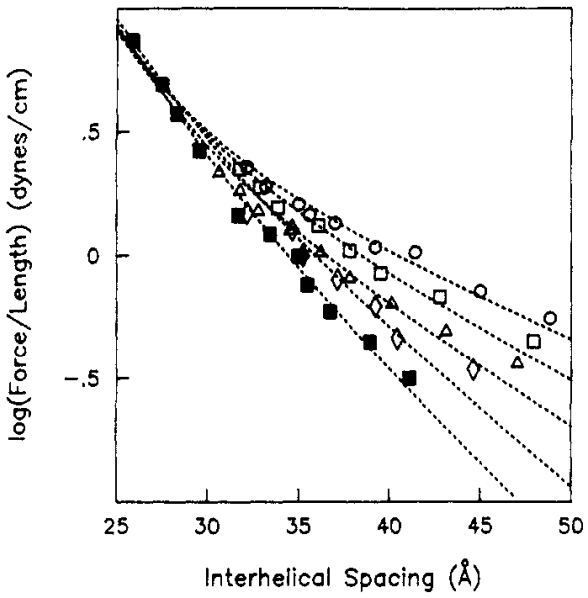

Fig. 115 Repulsion between DNA molecules in NaCl solutions. The salt concentrations are 0.2, 0.3, 0.4 0.8 and 2 M. The lines are fitted according to the theory outlined in the text. This is Fig. 4 from R. Podgornik, V. A. Parsegian *Molecular Fluctuations in the Packing of Polymeric Liquid Crystals.* Macromolecules *23*, 2265 (1990).

The approach of Podgornik and Parsegian is illustrated in Fig. 116. It is assumed that due to the hexagonal packing of the helixes every individual helix is confined to a tube of diameter R, where R is the mean inter-helical distance. Moreover, every segment of length b_{Kuhn} experiences a potential $\phi(\rho)$. In the following we use cylindrical coordinates ρ, φ and z, where z is measured along the tube axis. Expanding $\phi(\rho)$ around $\rho=R$ yields

$$\phi(\rho)=\phi(R)+\frac{1}{2}\phi''(R)x^2\,, \tag{510}$$

where $x=\rho-R$. We shall not discuss the electrostatic interaction between the DNA helices. Instead we rely on a result obtained by Podgornik and Parsegian, i.e.

$$\phi(R)=\phi_o\frac{e^{-\kappa R}}{\kappa R}\,. \tag{511}$$

Here we assume that κR is large. Hence

$$\phi''(R)\approx\kappa^2\phi(R)\,. \tag{512}$$

In the case at hand the quantity κ is the inverse Debye length. All in all this means that we consider the DNA molecule as being composed of segments of length b_{Kuhn} experiencing a harmonic potential in the radial direction from the tube's axis. The quantities x_i in Fig. 116 indicate the radial position of segment i relative to the minimum of the harmonic potential.

In order to find the free energy of the helices in this model, we employ the self-consistent field approach. As a matter of fact, it is very convenient to directly use Eq. (69). One may object that this

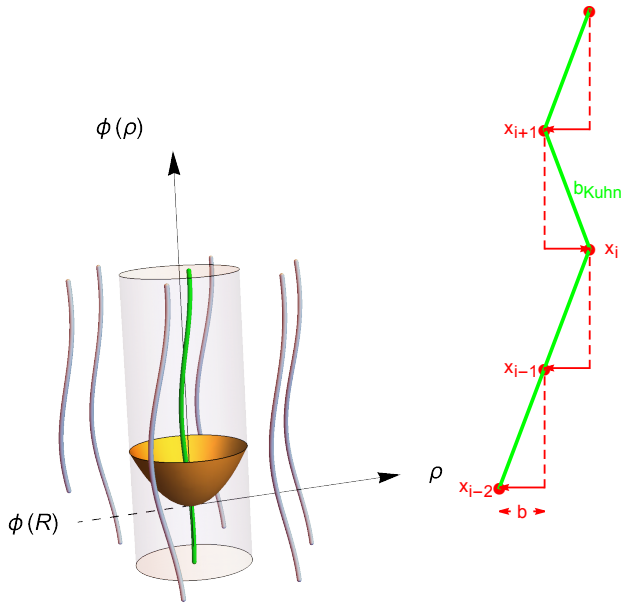

Fig. 116 Sketch of a DNA molecule (green) within an effective tube (cylinder) of radius R created by its neighbors (shown in grey) in a hexagonal array of DNA helices. Note that R is the mean separation of the helices. Each DNA segment of length b_{Kuhn} is subject to a harmonic potential $\phi(\rho)$ perpendicular to the cylinder axis illustrated by the paraboloid.

is a differential equation for one- and not three-dimensional polymers or paths in a potential $u(x)$. However, the changes necessary to upgrade our solution from one to three dimensions are minor and can be made easily at the end. Notice that the radial positions x_i of the segments, which are for the time being just x-positions relative to the potential minimum, are analogous to the arrows in Fig. 21 mapping out a conformation of a one-dimensional polymer. This means that we can use Eq. (69) as it stands and merely replace $u(x)$ by the second term in Eq. (510), i.e.

$$\left(\frac{b^2}{2}\frac{d^2}{dx^2}+\mu_o-\beta\frac{1}{2}\kappa^2\phi(R)x^2\right)\psi_o(x)=0\,. \tag{513}$$

Here $b=|x_i-x_{i-1}|$, where we assume that b is the same for every i. Now we introduce the new variable s via

$$x=\left(\frac{b^2}{\beta\kappa^2\phi(R)}\right)^{1/4}s\,. \tag{514}$$

With this substitution we obtain (513) in dimensionless form, i.e.

$$\left(\frac{d^2}{ds^2}+w-s^2\right)\tilde{\psi}_o(s)=0\,, \tag{515}$$

where

$$\mu_o=\frac{w}{2}b\kappa(\beta\phi(R))^{1/2}\,. \tag{516}$$

Equation (515) describes the one-dimensional quantum oscillator and for the ground state this means $w=1$. The total free energy of a segment b_{Kuhn} of the helix is the sum of $\phi(R)$ and $k_BT\mu_o$, i.e.

$$\Delta F(R)=\phi(R)+k_BT\mu_o=\phi(R)+\frac{1}{2}k_BTb\kappa\left(\frac{\phi(R)}{k_BT}\right)^{1/2}\,. \tag{517}$$

This is essentially equation (20) in R. Podgornik, V. A. Parsegian *Molecular Fluctuations in the Packing of Polymeric Liquid Crystals.* Macromolecules *23*, 2265 (1990). The only difference is a numerical (and for the following discussion unimportant) factor in the second term, which arises from the aforementioned reduction of the problem to one-dimension (see below).

But what is the significance of Eq. (517)? The force shown in Fig. 115 is obtained by differentiating $\Delta F(R)$ with respect to R. However, this will not alter the fact that the decay of the first term's contribution to the force is much faster in comparison to the second term, which is contributed by the shape fluctuations of the helix. The square root of $\phi(R)$ in that term essentially doubles the decay length from κ^{-1} to $2\kappa^{-1}$! Of course, changing the salt concentration changes the ionic strength and therefore κ^{-1}. Hence the different slopes of the force data for large inter-helical spacing.

Let's return to the issue of dimension. Podgornik and Parsegian use the three-dimensional version of Eq. (513). This implies that the DNA-helixes are three-dimensional random walks. The step length l (corresponding to our b) is the same in all three directions. However, it seems to this author that the direction along the tube is special. In particular $b\approx b_{Kuhn}\sqrt{\langle\theta^2\rangle}$, where $\theta(z)$ is the angle between the helix orientation and the tube's axis at point z along the tube. Since the alignment of the helices is quite pronounced, we expect $b\ll b_{Kuhn}$, with b_{Kuhn} comparable to the persistence length of DNA (about 600 Å). The 'upgrade' from one- to two dimensions means that $b^2/2$ in Eq. (513) is replaced by $b^2/4$ and the ground state value of w is not 1 but 2. Using $b^2/4$ and $w=2$ does in fact not change Eq. (517) at all.

The discussion of polyelectrolytes fills books and therefore it is best to stop at this point. However, readers interested in learning more about this important class of polymers may want to start with the following review article: M. Muthukumar *50th Anniversary Perspective: A Perspective on Polyelectrolyte Solutions* Macromolecules *50*, 9528 (2017).

7 Appendix

7.1 A: Phenomenological Models for Viscoelasticity

The Kelvin-Voigt model is only one of several simple combinations of the basic elements and, in addition, is not applicable in the full frequency range. Our next model is the so called Maxwell model (model (b)) in Fig. 50. This model arranges the two basic elements in series. Its mathematical description is

$$\sigma=\sigma_G=\sigma_\eta \qquad \gamma=\gamma_G+\gamma_\eta\,. \tag{518}$$

Using (248) and (249) we obtain

$$(b): \qquad \sigma + \frac{\eta}{G}\dot{\sigma} = \eta\dot{\gamma}. \tag{519}$$

The same ansatz as before leads to

$$G'/G = \frac{\tau_M^2\omega^2}{\tau_M^2\omega^2+1} \tag{520}$$

$$G''/G = \frac{\tau_M\omega}{\tau_M^2\omega^2+1} \tag{521}$$

$$\tan\delta = \frac{1}{\tau_M\omega}, \tag{522}$$

where $\tau_M = \eta/G$. We shall return to this model in our discussion of the chain models of Rouse and Zimm.

Yet another phenomenological model the Zener model (model (c) in Fig. 50). The mathematical description of the Zener model is slightly more complex compared to the Kelvin-Voigt or the Maxwell model. Now we have

$$\begin{aligned} \sigma &= \sigma_1 + \sigma_M \\ \sigma_M &= \sigma_2 = \sigma_\eta \\ \gamma &= \gamma_1 = \gamma_M \\ \gamma_M &= \gamma_2 + \gamma_\eta . \end{aligned}$$

The indices 1 and 2 refer to G_1 and G_2. Again we employ (248) and (249), which here leads to

$$(c): \sigma + \frac{\eta}{G_2}\dot{\sigma} = G_1\gamma + \eta\left(1+\frac{G_1}{G_2}\right)\dot{\gamma}. \tag{523}$$

As before the relation between stress and strain is linear and the above ansatz (real or complex) yields

$$G'/G_1 = \frac{\tau_2^2\omega^2/\theta+1}{\tau_2^2\omega^2+1} \tag{524}$$

$$G''/G_2 = \frac{\tau_2\omega}{\tau_2^2\omega^2+1} \tag{525}$$

$$\tan\delta = \frac{1-\theta}{\theta}\frac{\tau_2\omega}{\tau_2^2\omega^2/\theta+1}, \tag{526}$$

where $\tau_2 = \eta/G_2$ and $\theta = G_1/(G_1+G_2)$. The quantity τ_2 again describes a relaxation time. If the instantaneous strain $\gamma(t=0) = \gamma_o$ is held constant, i.e. $\dot{\gamma}(t) = 0$ for $t > 0$, then

$$\sigma(t) = \left(G_1 + G_2 e^{-t/\tau_2}\right)\gamma_o . \tag{527}$$

Question: What is the justification for $\sigma(t=0) = (G_1+G_2)\gamma_o$? (The strain occurs instantaneously at $t = 0$. The dashpot cannot follow as quickly, i.e. only the G-elements contribute to the answer.).

We briefly want to note that the maximum of $\tan\delta$ in the Zener model is at

$$\tau_2\omega_{max} = \sqrt{\theta} \tag{528}$$

and the attendant value of $\tan\delta(\omega_{max})$ is

$$\tan\delta|_{max} = \frac{1-\theta}{2\sqrt{\theta}} = \frac{1-(\tau_2\omega_{max})^2}{2\tau_2\omega_{max}} . \tag{529}$$

Let's study the low and high frequency limits of the Eqs. (524) through (526). The limit of small ω leads to the Kelvin-Voigt model (with $G_1 = G$). In the opposite limit of large ω we obtain $G' \approx G_1 + G_2$, $G'' \approx G_2/(\tau_2\omega)$, and $\tan\delta \approx (G_2/(G_1+G_2))/(\tau_2\omega)$. The special case $G_1 \ll G_2$ yields the Maxwell model in the same limit (with $G_2 = G$). Fig. 117 shows the various results of the Zener model for $G_1 = G_2 = G$. The dashed lines are the leading contributions in the above two limits. In order to gauge the value of our simple models we must relate their results to actual measurements.

Fig. 118 shows such measurements in comparison to the Zener model. Notice that the values for G_1 and G_2 follow by fitting the theoretical storage modulus to the experimental results in the respective limits at low and high frequencies. The value of $\tau_2 \approx 10^{-7}$s is obtained by adjusting the inflection point of the theoretical storage modulus to the data. Despite its simplicity the Zener model provides an overall correct qualitative description of the data.

Before we explore possible improvements of the Zener model, we should make sure that we do understand why it works the way it works. After all, the model combines three simple basic elements, i.e. two springs plus a dashpot, into a reasonable description of the mechanical properties of a complex system.

Fig. 119 shows a number of alternative combinations of the basic models, i.e. (a) (Maxwell: M) and (b) (Kelvin-Voigt: KV) depicted in Fig. 50. If we investigate the mechanical behavior of the new models, then the upper row behaves very much like the Maxwell model, i.e. $\tan\delta \sim \omega^{-1}$, whereas the lower row behaves according to the Kelvin-Voigt model, i.e. $\tan\delta \sim \omega$. None of the models reproduces the maximum of $\tan\delta$ versus ω. Only the Zener-Modell (sometimes also called Poynting-Thomson relaxation model) and its dual partner, both depicted in Fig. 120, do yield qualitative agreement with the experiment (The two models can be converted into one another via $G_1^R = G_1^K G_2^K/(G_1^K+G_2^K)$, $G_2^R = G_2^{K\,2}/(G_1^K+G_2^K)$ and $\eta^R = (G_2^K/(G_1^K+G_2^K))^2\eta^K$. The index R indicates the relaxation or Zener model, the index K indicates its dual partner.). Notice that interchanging springs and dash pots in the two models does not yield useful results or insights.

We can understand our above results as follows. At low frequencies an increase of $\tan\delta$ is observed. This means that the friction element, i.e. the dashpot, must be able to follow the excitation. This is build into the Kelvin-Voigt model, because the amplitudes in the two braches are strictly coupled. The decrease of $\tan\delta$ at high frequencies, on the other hand, requires the decoupling of the friction elements from the excitation. This is

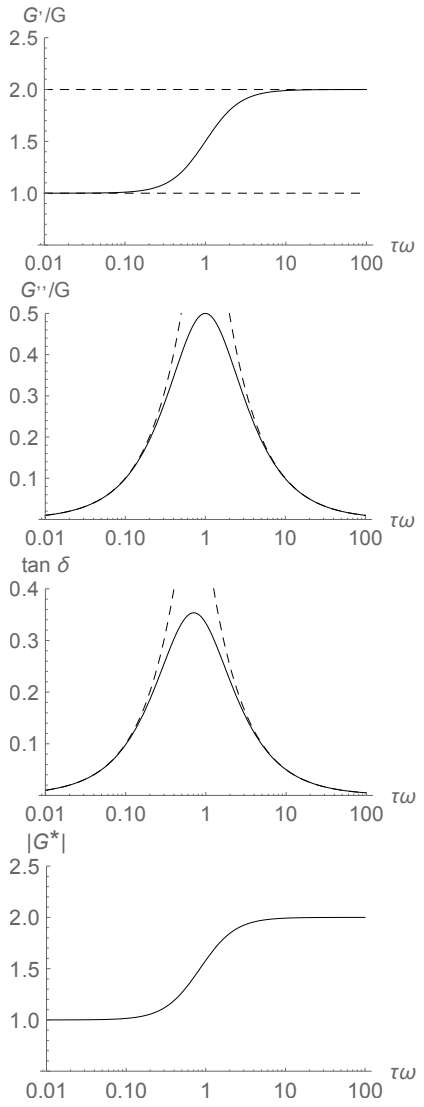

Fig. 117 Results of the Zener model.

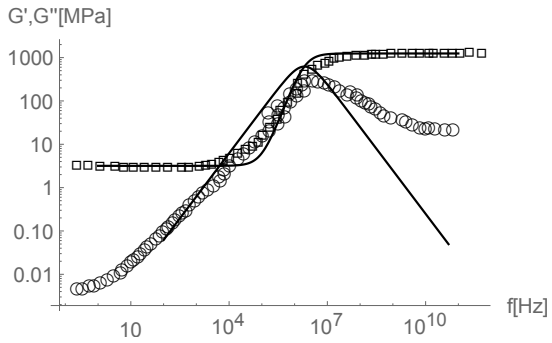

Fig. 118 Dynamic moduli of the Zener model (lines) in comparison to measured data (squares: storage modulus; circles: loss modulus) obtained for a highly cross-linked polyisoprene rubber versus strain frequency (data reproduced with the permission of Continental Reifen Deutschland). Note that the loss modulus data in this figure are the same as the ones in Fig. 74. Here the values for G_1 and G_2 are different from the values used in Fig. 74 in order to obtain better overall agreement with both moduli.

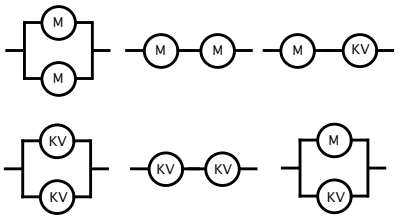

Fig. 119 Simple combination models.

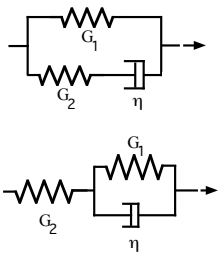

Fig. 120 Top: Zener or Poynting-Thomson relaxation model; bottom: dual partner.

build into the Maxwell model, where the spring can take over the strain from the friction element. The Zener model incorporates both behaviors.

Remark: A parameter we have mentioned is the strain amplitude. There is no amplitude dependence of the dynamic moduli predicted by the above models. This is because they are linear. Most elastomer materials contain large amounts of filler. In the case of automobile tires the fillers are carbon black and/or silica nanoparticles. The resulting materials are highly non-linear and their dynamic moduli are strongly dependent on the strain amplitude (**Payne effect**).

7.2 B: Persistence Length from Fluctuation Theory

Note that H in (449) can be expressed as an integral (continuum limit). To see this note that

$$(\vec{t}_i - \vec{t}_{i+1})^2 = 2 - 2\vec{t}_i \cdot \vec{t}_{i+1} \,. \tag{530}$$

Hence

$$H = H_o + \frac{b^2 J}{2} \sum_{i=1}^{N} \left(\frac{\vec{t}_i - \vec{t}_{i+1}}{b} \right)^2 \overset{c.l.}{=} H_o + \frac{1}{2} bJ \int_0^L ds \left(\frac{\partial \vec{t}}{\partial s} \right)^2 \,, \tag{531}$$

where $H_o = -NJ$. $c.l.$ means $N \to \infty$, $b \to 0$ while $L = Nb$. Note that bJ is a bending stiffness. The probability of a certain contour conformation is

$$p(\{\vec{t}\}) \propto \exp\left[-\beta \int_0^L ds \left\{ \frac{\lambda}{L} \vec{t}^{\,2}(s) + \frac{1}{2} bJ \left(\frac{\partial \vec{t}}{\partial s} \right)^2 \right\} \right] \tag{532}$$

($\beta = (k_B T)^{-1}$). Here λ is a Langrange multiplier due to the con-

dition

$$\frac{1}{L}\int_0^L ds\vec{t}^{\,2}(s) = 1\,, \tag{533}$$

which is the global version of the local condition $\vec{t}^{\,2}(s) = 1$. According to a general result of fluctuation theory (e.g. R. Hentschke *Statistische Mechanik* (2004); p. 228 ff)

$$\langle \hat{t}_q \cdot \hat{t}_{-q} \rangle = \frac{d-1}{2\beta}\frac{1}{\lambda + \frac{L}{2}bJq^2}\,, \tag{534}$$

where $\langle \hat{t}_q \cdot \hat{t}_{-q} \rangle$ is the Fourier transform of $\langle \vec{t}(0)\cdot\vec{t}(s)\rangle$. Note that $d-1$ distinguishes two cases: $d=3$ is a polymer in three-dimensional space and $d=2$ is a polymer in two-dimensional space. In the former case there are two fluctuating angles underlying the local orientation of $\vec{t}$, whereas in the latter case there is only one (for details see L. D. Landau, E. M. Lifshitz *Statistical Mechanics* § 127). Hence

$$\langle \vec{t}(0)\cdot\vec{t}(s)\rangle = \frac{L}{2\pi}\int_{-\infty}^{\infty}\langle \hat{t}_q \cdot \hat{t}_{-q}\rangle e^{iqs}dq = \frac{d-1}{4\beta}\left(\frac{\lambda bJ}{2L}\right)^{-1} e^{-s/P}\,, \tag{535}$$

where

$$P = \left(\frac{LbJ}{2\lambda}\right)^{1/2}. \tag{536}$$

The Lagrange multiplier follows via $\langle \vec{t}^{\,2}(0)\rangle = 1$, i.e.

$$\lambda = \frac{L(d-1)}{8\beta^2 bJ}\,. \tag{537}$$

The final result is

$$\langle \vec{t}(0)\cdot\vec{t}(s)\rangle = e^{-s/P} \tag{538}$$

with

$$P = \frac{2}{d-1}\frac{bJ}{k_BT}\,. \tag{539}$$

For $d=3$ this agrees with Eq. (40) and Eq. (452), respectively!

7.3 C: Teaching and Studying the Material in these Notes

The following listing shows the material in these notes organized into 24 lectures (1.5 hours each). This should be useful for potential lecturers. In addition, students, who wish to study the material by themselves, may be benefited by the partitioning of the course material into more easily digestible increments.

Lecture	Content	Pages
	POLYMER MICROSTRUCTURE, CLASSIFICATION, AND MASS	
L 1	Molecular Microstructure and Classification, Molecular Mass	3 - 6
L 2	Flexibility Mechanisms and Polymer Dimension	6 - 11
	EQUILIBRIUM CONFORMATION OF SINGLE CHAINS	
L 3	RIS/Transfer Matrix Approach	11 - 14
L 4	Self-Consistent Field Approach	14 - 16
L 5	Conformation Entropy, Flory's Exponent	16 - 18
L 6	The Scaling Concept	18 - 21
L 7	Scattering from Ideal Chains	21 - 24
L 8	Light Scattering and Zimm Plot	24 - 25
L 9	Scattering from Real Chains	26 - 27
	THERMODYNAMICS OF BLENDS, SOLUTIONS, AND NETWORKS	
L 10	Lattice Model for Binary Polymer Mixtures	28 - 29
L 11	Phase Separation in Polymer Mixtures and Polymers in Solution	29 - 32
L 12	Swelling of Polymer Networks	32 - 35
	POLYMER DYNAMICS	
L 13	Linear Deformation Mechanics, Ideal Fluids, Phenomenological Models of the Dynamic Moduli	35 - 44*
L 14	Time-Temperature Superposition, Shear Relaxation Modulus and Relation to Storage and Loss Modulus	44 - 47
L 15	Single Chain Dynamics: Preliminaries (friction, Brownian motion, equation of motion of the bead-spring chain with friction)	47 - 49**
L 16	Single Chain Dynamics: Rouse Model – Solution and Results	49 - 51
L 17	Single Chain Dynamics: Zimm Model – Hydrodynamic Interactions and Their Effects	51 - 55***
L 18	Polymer Entanglement	55 - 57
L 19	The Glass Process	57 - 63
	SELECTED TOPICS	
L 20	Aspects of Polymer Mechanics	63 - 68
L 21	Filler Effects	68 - 75
L 22	Liquid Crystalline Polymers	75 - 81
L 23	Reversibly Assembling Polymers	81 - 83
L 24	Polyelectrolytes	83 - 87

(*) : This lecture focusses on the straightforward introduction of Eqs. (211) and (247) and how they form the building blocks of phenomenological models of linear viscoelasticity. This means that most of the content of the two boxes *Equations and Concepts from Isotropic Elasticity* and *Equations and Concepts from Fluid Mechanics* is omitted and left as a reading assignment (or perhaps an additional lecture). Based on Eqs. (211) and (247), the Kelvin-Voigt model is discussed in relation to the damped harmonic oscillator under the influence of an external periodic force, since the latter is studied extensively in undergraduate physics. In addition, the storage and the loss modulus are introduced.

(**): including Eq. (305)

(***): There are a number of detailed calculations on these pages. For the better part they should be omitted in class. Instead one should focus on the main results and the differences between Zimm and Rouse model.